Molecular Biological Analysis of Dynamic Interactions between Influenza Viruses and Host Cells

-

Host Cell Proteomes and Viral Replication Dynamics

Dissertation

zur Erlangung des akademischen Grades

Doctor rerum naturalium
(Dr. rer. nat.)

genehmigt durch die Fakultät für für Naturwissenschaften
der Otto-von-Guericke-Universität Magdeburg

von Dipl.-Biol. Diana Vester
geb. am 14. April 1981 in Haldensleben

Gutachter:
Prof. Dr.-Ing. Udo Reichl
Prof. Dr. rer. nat. Georg Kochs

eingereicht am: 19.09.10

verteidigt am: 11.04.11

Danksagung

Die vorliegende Dissertation wurde am Lehrstuhl Bioprozesstechnik der Otto von-Guericke-Universität am Max-Planck-Institut für Dynamik komplexer technischer Systeme in Magdeburg unter der Leitung von Herrn Prof. Dr. Dr. Reichl angefertigt.

Für meine Doktorarbeit schulde ich sehr vielen Menschen einen herzlichen Dank.

Mein Dank gilt Herrn Prof. Dr. Udo Reichl für die interessante Aufgabenstellung dieser wissenschaftlichen Arbeit. Außerdem danke ich ihm für die vielfältige Unterstützung durch immerwährende Diskussionsbereitschaft, Anregungen und die gewährte wissenschaftliche Freiheit.

Herrn Prof. Dr. Georg Kochs danke ich für die freundliche Übernahme der Zweitkorrektur dieser Arbeit.

Ganz herzlich möchte ich mich bei Dr. Yvonne Genzel für ihre stets engagierte und ermutigende Betreuung meiner Doktorarbeit danken und daher viel positiven Einfluss auf die Arbeit nahm und mich in jeder Hinsicht unterstützte.

Dr. Erdmann Rapp sei für die viele Arbeit mit der MS/Protein-Identifikationen, die stete Diskussionsbereitschaft sowie bei der Hilfe der Veröffentlichung der Ergebnisse und der Diss herzlich gedankt...und natürlich seinem fleißigen Verdau-Team, speziell Kay Schallert.

Mein Dank gebührt weiterhin Antje Lagoda, Diana Hoffmann, Claudius Seitz und Marcus Hoffmann die durch ihre engagierte Forschung im Rahmen ihrer Diplomarbeiten zu einem nicht unerheblichen Teil zum Gelingen dieser Arbeit beigetragen haben. Des Weiteren möchte ich mich bei Sabine Kluge und Stefan Heldt für ihre wissenschaftlichen Beiträge zu unseren gemeinsamen Publikationen danken…und speziell Sabine, da sie mir in der letzten Phase den Rücken frei gehalten hat.

Ein besonders herzliches Dankeschön geht an alle ehemaligen und aktuellen Mitgliedern der Gruppe für die stets kollegiale und darüber hinaus freundschaftliche Atmosphäre und das dadurch sehr bereicherte Laborleben...und natürlich für den Spaß bei den vielen gemeinsamen Aktionen auch außerhalb des Laboralltags. Insbesondere möchte ich Claudia Best, Susanne König, Ilona Behrendt, Nancy Wynserski und Felicitas Hasewinkel für ihre stets gewährte Unterstützung und Hilfsbereitschaft danken. Ganz herzlich danke ich Dr. Dirk Benndorf und Dr. Timo Frensing für ihre vielen Ratschläge und Diskussionen. Dr. Katja Bettenbrock und der Systembiologie-Arbeitsgruppe sowie Dr. Dörte Gade danke ich für die Betreuung und Bereitstellung experimenteller Möglichkeiten zu Begin dieser Arbeit.

Meinen zahlreichen Zimmer-Kollegen danke ich herzlich für die hilfreichen wissenschaftlichen Diskussionen, die angenehme Atmosphäre in unserem Büro und die daraus erwachsenen Freundschaften.

Auch möchte ich mich bei meinen Freunden bedanken, die mich nicht nur tatkräftig unterstützt haben, sondern mich stets aufbauten und für die erforderliche Abwechslung sorgten.

Mein besonderer Dank gilt natürlich allen voran meinen Großeltern, meinen Eltern, meiner Schwester & dem “Zweit-liebsten Schwiegersohn” für die stetige Unterstützung während meines gesamten Studiums und meiner Promotionsphase. Danke für alles!

Meinem Lieblings-Mitdoktoranden danke ich von ganzem Herzen für seine unermüdliche Unterstützung, Rückhalt und immer währende Motivation aus der ich häufig neue Kraft schöpfte.

‚In den Wissenschaften ist viel Gewisses, sobald man sich von den Ausnahmen nicht irre machen läßt und die Probleme zu ehren weiß.’ - Johann Wolfgang von Goethe

Abstract

Influenza A viruses are important pathogens with worldwide prevalence with high morbidity and mortality rates. They are enveloped viruses within the family Orthomyxoviridae with a negative stranded segmented RNA genome that encodes for up to 11 viral proteins. Even this small set of viral proteins interacts with an array of host cell proteins and pathways, and ensures that the virus uses the host cellular machinery for many aspects of its life cycle. Throughout the past years these virus-host cell interactions were investigated in numerous studies. Viral strategies for the evasion of innate immune response, inhibition of cellular protein synthesis and permission of viral RNA and protein production were elucidated and the development of an antiviral response of host cells was uncovered. Both interaction types, host cell induced antiviral response and virus induced changes for enhanced replication, have an impact on host cell gene and protein expression patterns.

Interestingly, virus-host cell interactions have not been analyzed with respect to cell culture based influenza vaccine manufacturing processes so far. Hence, the aim of the presented work was to establish and to subsequently apply two molecular biological approaches for this objective: (I) a proteomic approach to study the global changes in cellular machinery and corresponding protein profiles and to elucidate the host cellular and virus induced events that occur upon influenza virus infection, (II) a genomic approach to study time courses and dynamics, as well as regulation of the influenza virus genome replication and transcription.

In the first part of this work, a proteomic approach was used to investigate the dynamic cellular host cell response induced by influenza virus infection in two different vaccine production cell lines, the Madin-Darby canine kidney (MDCK) and the African green monkey kidney (Vero) cell line and in a human cell reference model. The reference model was selected from three different human cell lines, which were compared for their cellular metabolism and virus yields. Finally, the lung carcinoma A549 cell line was chosen. For identification of proteins possibly involved in global host cell response mechanisms and virus-host cell interactions, quantitative two-dimensional difference gel electrophoresis (2-D DIGE) and mass spectrometry (MS) analysis were performed. In particular, host cell proteome alterations caused by infection with influenza A/Puerto Rico/34/8 (H1N1) (referred to as PR/8) virus variants showing differences in replication characteristics in the MDCK cell line were compared. Moreover, the host cell response to virus infection in Vero cells with respect to their deficiency in interferon (IFN) production and the need for virus adaptation to optimize productivity of cell lines were analyzed. Several proteins with differential abundance profiles were identified and Western blot analysis was performed for further confirmation of

selected proteins. These proteome studies revealed that proteins with changes in relative abundance are known to be involved in distinct functional classes. These included proteins participating in signal transduction, cytoskeleton remodeling, protein degradation, maintenance of metabolism, viral defense mechanisms, and especially for Vero cells, distinct forms of cellular stress responses and cell-cell interactions. It can be concluded that virus strains seem to have various abilities to control the cellular machinery of their host cells and to suppress an antiviral response, suggesting a lower induction of cellular antiviral and stress mechanisms by 'high yield strains'. Additionally, it was shown that the Vero cell line still has the ability to build-up a host cell defense state in an IFN independent manner and induced much higher stress responses compared to the MDCK cell line. The findings provide insights at the global protein level into the complexity and dynamics of virus-host cell interactions. They will improve understanding of host cell response mechanisms during influenza vaccine production and viral strategies to evade these responses and to replicate efficiently in different cell lines. Additionally, some of these proteins might also represent potential targets for improvement of cell line performance in vaccine production processes.

Another important aspect considered in the second part of this work was that the general time course of influenza virus replication in their host cells is well understood. However, much about regulation and dynamics of viral genome replication and viral transcription, especially for each of the 8 RNA segments still remains unknown. Moreover, published results were often contradictory with the consequence that different hypotheses were suggested for regulation and dynamics of viral replication. For validation and parameter estimation of an existing structured mathematical model of influenza viral replication these experimental data were not usable. Hence, due to contradictory literature data this work focused on the development of a novel reverse transcription quantitative real-time polymerase chain reaction (RT-qPCR) assay for the analysis of influenza virus transcription and replication dynamics in mammalian cell culture. The assay was based on a sequence- and polarity-specific priming reverse transcription (pspRT) used to distinguish specifically between viral genome vRNA(-), replicative intermediates cRNA(+) and viral messenger RNA (vmRNA(+)) of segments 4 (HA), 6 (NA), 7 (M) and 8 (NS) during the life cycle of influenza A PR/8 virus. Synthetic viral RNAs used as reference standards for validation and quantification were prepared for each viral RNA type and segment. Assay validation demonstrated linearity over five orders of magnitude, with a sensitivity of 1.0 – 8.9 $\times$ 10^3 of viral RNA molecules, with specificity, and repeatability and reproducibility of less than 0.8 – 3.1% coefficient of variation (CV). Dynamics of influenza PR/8 virus infection in a MDCK cell line were analyzed. In general, mainly vmRNA(+)s were synthesized during early phases of infection at an average of 0.4 hpi, followed immediately by cRNA(+) synthesis and after a short delay viral genome replication could be detected at an average of 2.5 hpi. The viral

genome vRNA(-)s were synthesized in equimolar amounts and similar dynamics whereas preferential synthesis of NS1 vmRNA(+) in early transcription phases and a delay for M1 vmRNA(+) was found. The obtained experimental results will support validation of the structured mathematical model of influenza virus replication, which provide quantitative insights in the complex intracellular events and hence also in virus-host cell interactions that take place during virus infection.

In conclusion, both approaches, proteomics and RT-qPCR, have started a new understanding of cellular processes during cell culture derived influenza vaccine production and can be used for studies on bioprocess engineering and systems biology of these bioprocesses.

Zusammenfassung

Influenza A Viren sind als Krankheitserreger aufgrund weltweiter Verbreitung und beträchtlicher Morbiditäts- und Mortalitäts-Raten von großer Bedeutung. Es handelt sich um Viren der Familie der Orthomyxoviridae. Sie besitzen ein negativ-strängiges, segmentiertes RNA-Genom, das bis zu 11 virale Proteine kodiert. Selbst diese geringe Anzahl an viralen Proteinen ermöglicht es dem Virus, durch Interaktionen mit einer Vielfalt von Proteinen der Wirtszell, die zellulären Mechanismen der Wirtzelle zu Gunsten dessen Vermehrung auszunutzen. Diese Virus-Wirtszell-Interaktionen wurden in den letzten Jahren in einer Vielzahl von Studien untersucht. Die viralen Strategien zur Überwindung der zelleigenen Immunabwehr, Unterdrückung der zellulären Proteinsynthese sowie der selektiven Durchführung der viralen RNA- und Proteinsynthese konnten so aufgeklärt werden. Ebenso ergaben diese Studien Einblicke in den Aufbau einer antiviralen Abwehr der Wirtzelle.

Interessanterweise wurden die Virus-Wirtzell-Interaktionen in Bezug auf einen Säugetier-Zellkultur-basierten Influenza-Impstoff-Produktionsprozesses bislang nicht analysiert. Daher war Ziel dieser Arbeit die Etablierung zweier molekularbiologischen Analysen und die Anwendung dieser auf den Impfstoff-Produktionsprozess: (I) einen proteomischen Ansatz zur Analyse der globalen Veränderungen der zellulären Mechanismen und Proteinprofile ausgelöst durch die Influenza-Virusinfektion und zur Aufklärung der wirtszell- und virus-induzierten Vorgänge. (II) einen genomischen Ansatz zur Analyse der zeitlichen Verläufe, Dynamiken und Regulationsmechanismen der Influenza Virus-Replikation und -Translation.

Im ersten Teil dieser Arbeit wurde eine quantitative Proteomanalyse verwendet, um die viralen Einflüsse auf die zellulären Mechanismen der Wirtszellen auf globaler Ebene in den Impfstoff-Produktionszelllinien (MDCK und Vero Zelllinie) sowie in einer humanen Referenz-Model-Zelllinie zu untersuchen. Die Auswahl eines geeigneten Referenz-Models sollte ausgehend von einem Vergleich des zellulären Stoffwechsel und der Virusproduktivität dreier humaner Zelllinien getroffen werden. Letztendlich wurde die humane Lungen-Krebszelllinie A549 als Modelsystem ausgewählt. Zur Identifikation von Proteinen, die an der generellen Wirtszellabwehr und an Virus-Wirtszell-Interaktionen beteiligt sind, wurden quantitative 2-D DIGE-Analysen zur Visualisierung regulierter Proteine und qualitative nanoHPLC-nanoESI-MS/MS-Analysen zur Identifizierung dieser Proteine durchgeführt. Insbesondere die Wirtszell-Proteomveränderungen der MDCK-Zelllinie induziert durch zwei Varianten des Influenza A/PR/8/34 (H1N1) Stamms (abgekürzt PR/8) mit unterschiedlichen Replikationsverhalten wurden verglichen. Des Weiteren wurde die Wirtszellantwort der Vero-Zelllinie in Bezug auf deren gestörtes Interferon-Produktionsystem untersucht und der

Adaptionsprozess des Virus an die Wirtzelllinie zur Virus-Produktivitäts-Steigerung analysiert. Diverse Proteine mit unterschiedlichen Regulationsprofilen wurden so in 2-D Gelen identifiziert und per Western-Blot-Analysen für einige ausgewählte Proteine deren Regulation zusätzlich verifiziert. Diese identifizierten Proteine, konnten sehr unterschiedlichen funktionellen Proteinklassen und Signalwegen zugeordnet werden, u.a. Signal-Transduktion, Proteindegradation, Cytoskelett-Komponenten, Zellstoffwechsel, viraler Abwehrmechanismus und speziell für die Vero-Zelllinie verschiedene Formen zellulärer Stressantworten und Zell-Zell-Kommunikationen. Aus den Ergebnissen lässt sich schlussfolgern, dass unterschiedliche Virus-Stämme bzw. Virus-Varianten unterschiedliche Fähigkeiten zur Kontrolle der zellulären Mechanismen der Wirtszellen bzw. zur Unterdrückung der antiviralen Abwehr besitzen. Dabei sind insbesondere Viren mit hohem Titer sog., ‚high-yield strains', am erfolgreichsten beim Unterdrücken dieser Abwehrmechanismen. Zusätzlich konnte der Aufbau einer IFN-unabhängigen Wirtszellabwehr und einer im Vergleich zu der MDCK-Zelllinie stärkeren Stressantwort in der Vero-Zelllinie gezeigt werden. Die vorliegenden Resultate geben einen Einblick in die Komplexität und Dynamik der Virus-Wirtszell-Interaktionen. Sie liefern ebenfalls ein verbessertes Verständnis der Wirtszellantwort der Influenza-Impfstoff-Produktionzelllinien, sowie der viralen Strategien die Wirtzellabwehr zu umgehen und sich effizient in verschiedenen Wirtzellen zu vermehren. Zusätzlich könnten einige dieser identifizierten Proteine potentielle Ansatzpunkte für die Verbesserung der Zelllinienproduktivität während des Impfstoff-Prozesses darstellen. Weitere experimentelle Untersuchungen zur Bestätigung und Quantifizierung dieser Annahmen sind jedoch notwendig.

Ein zweiter wichtiger Aspekt dieser Arbeit beinhaltete die Aufklärung der Dynamik und Regulation der viralen Genom-Replikation und -Transkription einzelner viraler Gen-Segmente. Im Gegensatz zum generellen Replikationszyklus sind die Dynamik und die Regulationsmechanism in der Wirtszelle weiterhin unklar. Darüber hinaus sind die meisten publizierten Studien widersprüchlich und aufgrund dessen werden sehr unterschiedliche Hypothesen zur Regulation und Dynamik der viralen Vermehrung vorgeschlagen. Zur Validierung und Parameter-Abschätzung eines strukturierten mathematischen Modells der Virusreplikation waren diese experimentellen Ergebnisse jedoch nur qualitativ von Nutzen. Daher wurde in dieser Arbeit ein neuartiger RT-qPCR Assay zur Untersuchung der Replikationsvorgänge in der Säugetier-Zellkultur entwickelt. Basierend auf einer polaritäts- und sequenz-spezifischen Umschreibung der viralen RNAs während der Reversen Transkription kann der Assay zur spezifischen Unterscheidung zwischen viraler genomischer vRNA(-), Replikations-Zwischenprodukten cRNA(+), sowie viraler Messenger-RNA vmRNA(+) der Segmente 4 (HA), 6 (NA), 7 (M) and 8 (NS) während des Influenza A PR/8 Virus-Replikationszyklus verwendet werden. Synthetische virale RNAs wurden für jedes

virale Segment und den drei jeweiligen viralen RNA-Typen hergestellt und als RNA-Referenzstandard zur Validierung und zur absoluten Quantifizierung verwendet. Die Assay-Validierung erbrachte eine Linearität von 5 Größen-Ordnungen, eine Sensitivität von mindestens $1{,}0 \times 10^3$ – $8{,}9 \times 10^3$ viralen RNA-Molekülen, eine hohe Spezifität und eine Wiederhol- und Vergleichspräzision mit einem Variationskoeffizient kleiner als 0,8 – 3,1%. Im Anschluss wurde die Dynamik der Influenza-Virusvermehrung in der MDCK-Produktionszellline untersucht. Grundsätzlich wurden in frühen Infektionsphasen (ca. 0,4 h nach Infektion) hauptsächlich vmRNA(+)s synthetisiert. Unverzüglich darauf folgte die Synthese von cRNA(+) und mit kurzer Verzögerung (ca. 2,5 h nach Infektion) die Replikation der viralen genomischen RNAs (vRNA(-)). Genom-Äquivalente (vRNA(-)) wurden in gleichen Mengen und ähnlichen Dynamiken repliziert, während unter den vmRNA(+)s eine frühe Synthese von NS1 und eine Verzögerung in der Synthese von M1 detektiert wurden. In einer Folgearbeit sollen diese experimentellen Ergebnisse zur Validierung des strukturierten mathematischen Modells der intrazellulären Influenza-Replikation eingesetzt werden. Dieses Modell soll u.a. einen quantitativen Einblick in die komplexen intrazellularen Vorgänge und daher auch in die Virus-Wirtzell-Interaktionen ermöglichen.

Zusammenfassend lässt sich sagen, das beide Anwendungen, Proteom- und RT-qPCR Assay, zu einem neuem Verständnis der Virus-Wirtzell-Interaktionen in Bezug auf den Influenza-Impstoff-Produktionsprozess geführt haben und zur weiteren Untersuchung von Bioprozessen und der Systembiologie genutzt werden können.

Table of contents

Abbreviations and symbols

2-DE	Two-dimensional gel electrophoresis
-RTfor	Gene specific forward primer uniRT
+RTrev	Gene specific reverse primer uniRT
AA	Amino acid
Amm	Ammonia
AMV-RT	Avian myeoblastosis virus reverse transcriptase
ANX	Annexin
APS	Ammonium persulfate
ATTC	American Type Culture Collection
AUC	Area under the curve
bp	Base pair
BSA	Bovine serum albumine
Bpt group	Bioprocess engineering group
BVA	Biological variation analysis
C	Celsius
CapZ	Actin-capping protein
CHAPS	3-[(3-Cholamidopropyl)dimethylammonio]-1-propanesulfonate
cDNA	Copy DNA
CG1550-PA	Tubulin-tyrosine ligase
CI	Confidence Interval
CK-5	Cytokeratin 5
CK-8	Cytokeratin 8
CMV	Cytomegalovirus
C_q	Quantification/threshold cycle
conc.	Concentration
const.	Constant
CPSF4	Cleavage and polyadenylation specific factor 4
cRNA(+)	Complementary viral RNA
CV	Coefficient of variation
DDF	Differential detergent fractionation
DIA	Difference in-gel analysis
DIGE	Difference gel electrophoresis
DMSO	Dimethylsulfoxid
DNA	Deoxyribonucleic acid
dNTP	Nucleoside triphosphate
DTT	Dithiothreitol
ds	Double strand
DSMZ	German resource centre for biological material
E	Amplification efficiency
ECACC	European Collection of Cell Cultures
E.coli	*Escherichia coli*
EDTA	Ethylenediaminetetraacetic acid
EF-1	Eukaryotic translation elongation factor 1
EFHD2	EF-hand domain family, member D2
eIF-2	Eukaryotic initiation factor 2
eIF4G1	Eukaryotic translation initiation factor 4 gamma 1
ER	Endoplasmatic reticulum
FCS	Fetal calf serum
FTCD	Formiminotransferase cyclodeaminase
g	Gram
g	Gravitational acceleration

GAPDH	Glyceraldehyde-3-phosphate dehydrogenase
GDH	Glutamate dehydrogenase
GFAP	Glial fibrillary acidic protein
Glc	Glucose
Gln	Glutamine
Glu	Glutamate
GMEM	Glasgow minimum essential medium
GRSF-1	G-rich sequence factor 1
gsp	Gene specific primer
GTPase	Guanosine triphosphatase
h	Hours
H_2O_{MP}	Ultra pure Milli-Q water
HA	Hemagglutinin
HCD	High cell density
hHRB23B	UV excision repair protein RAD23
HIV	Human immunodeficiency virus
hnRNP K	Heterogeneous nuclear ribo-nucleoprotein K
HOOK3	Golgi-associated microtubule-binding protein
HPDG	Hydroxyprostaglandin dehydrogenase 15-(NAD)
hpi	Hours post infection
hsp	Heat shock protein
HV	Hepatitis virus
ICAT	Isotope-coded affinity tagging
IEF	Isoelectric focusing
IFI-1	IFN induced protein with tetratricopeptide repeats 1
IFN	Interferon
IPG	Immobilized pH gradient
IPC	Internal positive control
ISG	IFN stimulated genes
ITGA3	Integrin alpha 3
ITGAV	Integrin alpha V
iTRAQ	Isobaric tags for relative/absolute quantification
KCIP-1	Protein kinase C inhibitor protein-1
kDa	Kilo Dalton
L	Liter
Lac	Lactate
LEPREL1	Leprecan-like 1
LOD	Limit of detection
M	Matrix protein
M	mol/L
m	Milli
μ	Micro
mA	Milliampere
MDCK	Madin-Darby canine kidney
MEM	Minimal essential medium
min	Minute
MIQE	Minimum information for publication of quantitative real-time PCR experiments
mL	Milliliter
MMLV-RT	Moloney murine leukemia virus reverse transcriptase
MnSOD	Superoxide dismutase
SDR	Short-chain dehydrogenase/ reductase
MOI	Multiplicity of infection
mRNA	Messenger RNA
MS	Mass spectrometry
MTX	Methotrexate
MW	Molecular weight

Mx	Myxovirus-resistance proteins
n	Nano
NA	Neuraminidase
NCBI	National Center for Biotechnology Information
NDRG1	N-myc downstream-regulated gene
NEP	Nuclear export signal
NF-κB	Nuclear factor kappa B
NIBSC	National Institute for Biological Standards and Control
NLS	Nuclear localisation signal
nm	Nanometer
NP	Nucleoprotein
NS	Non-structural protein
NPC	No-primer control
nt	Nucleotides
NTC	No-template control
NTP	Nucleoside triphosphate
Nuc	Nucleobindin
OD	Optical density
ORF	Open reading frame
P58IPK	Protein kinase inhibitor p58
PA	Polymerase acidic protein
PABN1	Poly(A) binding protein, nuclear 1
PA28beta	Proteasome activator hPA28 subunit beta
PABP1	Poly(A)-binding protein 1
PAGE	Polyacrylamide gel electrophoresis
PB1	Polymerase basic protein 1
PB2	Polymerase basic protein 2
PB1-F2	Polymerase basic protein 1 F2
PBS	Phosphate buffered saline
PCA	Principal component analysis
PCR	Polymerase chain reaction
PDIA3	Protein disulfide isomerase-associated 3
PFA	Paraformaldehyde
p*I*	Isoelectric point
PK	Pyruvate kinase
PKC	Protein kinase C
PKR	Protein kinase R
pmol	Pico mol
Pol II	DNA-dependent RNA polymerase II
PSMB4	Proteasome subunit beta
pspRT	Polarity-specific priming reverse transcription
PTM	Post-translational modification
PR/8	Influenza A/PR/8/34 (H1N1)
PRX	Peroxiredoxin
PVDF	Polyvinylidene fluoride
qPCR	Quantitative real-time polymerase chain reaction
R^2	Correlation coefficient
RanGAP1	RanGTPase activating protein
RB	Roller bottle
RBC	Red blood cells
RBBP4	Histone-binding protein
RFU	Relative fluorescence units
RIG-I	Retinoic acid inducible gene I
Rn	Normalized reporter
RNA	Ribonucleic acid
RNAi	RNA interference

RKI	Robert Koch Institute
rpm	Revolutions per minute
RSD	Relative standard deviation
RT	Reverse transcription
RT-PCR	Reverse transcription-polymerase chain reaction
RT-qPCR	Reverse transcription quantitative real-time polymerase chain reaction
rTth	Thermostable RT isoform of MMLV-RT
SD	Standard deviation
SDR	Short-chain dehydrogenase/ reductase
SDS	Sodium dodecyl sulfate
sec	Second
SOP	Standard operating procedure
SNP	Single nucleotide polymorphisms
ss	Single strand
TBS	Tris buffered saline
TEMED	Tetramethylethylenediamine
TFA	Trifluoracetic acid
TGF	Transforming growth factor
TGM2	Transglutaminase 2
TIM	Triosephosphate isomerase
TLR	Toll-like receptors
T_m	Melting temperature
TNF	Tumor necrosis factor
Tris	Tris(hydroxymethyl)methyl-amine
Tris-HCl	Tris(hydroxymethyl)methyl-amine hydrochloride
TTBS	Tris-Tween buffered saline
TUBA2	Tubulin alpha-2
TUBA	Tubulin alpha
U	Units
UTR	Untranslated region
uniRT	Universal reverse transcription
UV	Ultra violett
v	Volume
V	Volt
VMM	Serum-free virus maintenance medium
vmRNA(+)	Viral messenger RNA
vRNA(-)	Viral genomic RNA
vRNP	Viral ribonucleoprotein
w	Weight
W	Watt
WHO	World Health Organization

1. Introduction

Influenza A virus is an enveloped RNA virus comprising a negative sense genome with eight single stranded (ss) segments, each encoding for one or two proteins. Influenza is the causative agent of the common flu, which is a worldwide health problem leading to significant economic consequences. Studies of influenza virus biology have revealed elaborate mechanisms by which the virus interacts with its host cell and uses efficiently host cell resources for replication and suppresses concomitantly host cell defense, inducing significant cellular changes. As an answer to virus infection host cells have developed an antiviral response, which is a complex system for detection and elimination of viruses (Ludwig et al., 2006). For example, upon infection by influenza virus, host cells detect viral RNA through pathogen sensors and induce IFN release and an antiviral program (Haller et al., 2006). Simultaneously, the 11 viral proteins of influenza virus realize the viral life cycle and interfere with cellular processes. Notably, the viral non-structural protein 1 (NS1) facilitates the evasion of host cell defense through several mechanisms, including suppression of pathogenic RNA sensing and antiviral activity (Kochs et al., 2007; Krug et al., 2003), as well as cellular mRNA processing (Lamb and Krug, 2001) and protein synthesis (Lyles, 2000). Cellular immune regulatory functions of the other influenza proteins are still unknown, as their well-characterized functions only comprise distinct mechanisms such as viral entry into cells, viral RNA trafficking, replication, and transcription, or assembly of viral particles. Similarly, the role of most of the host cell factors remains unknown, and is currently being investigated (Hao et al., 2008a; Karlas et al., 2010; Koenig et al., 2010). Both interaction types, host cell induced antiviral response and virus induced changes have an impact on host cell gene expression patterns (Fornek et al., 2007). Therefore, they cause alterations in morphology, metabolic state of the cells and induce apoptosis. Whether apoptosis resulted from the inhibition of host cell gene expression, or is related to the antiviral response of the host cell or whether it is caused by viral components directly is not completely understood (Ludwig et al., 2006).

During the last years great efforts have been undertaken to reveal mechanisms of influenza-host cell interactions. Most of the previous studies on viral and host cell factors have focused on single specific interactions. With only few exceptions they have not produced more global insights into virus-host cell interactions (Baas et al., 2006; Chen et al., 2008; Fornek et al., 2007; Geiss et al., 2002). These studies have focused on basic aspects of virology, e.g. either on pathogenesis in humans (Fornek et al., 2007), discovery of novel drug targets, antiviral therapies, biomarker research (Baas et al., 2006; Geiss et al., 2001; Geiss et al., 2002), and on analysis of virulence and adaptation strategies of avian influenza virus (Chen

et al., 2008). Proteomic approaches or functional genomic tools, such as microarray based gene expression analysis have been used in these studies.

The most effective way to provide protection against influenza virus infection is through vaccination. Limitations and drawbacks of the conventional production process of influenza vaccines using embryonated chicken eggs have pushed the development of a cell culture based strategy (Genzel and Reichl, 2009). The Bioprocess Engineering (bpt) group at the Max Planck Institute Magdeburg works mainly on the establishment and optimization of integrated concepts to design and control such mammalian cell culture based influenza vaccine production processes. The continuous adherend MDCK and Vero cell lines are two promising candidates for such a production process (Genzel and Reichl, 2009). Influenza virus vaccines derived from MDCK and Vero cells have been produced and evaluated for immunogenicity, and their production has been scaled up to commercial levels (Doroshenko and Halperin, 2009; Kistner et al., 1998; Youil et al., 2004). Interestingly, cell culture based vaccine manufacturing processes have not been analyzed with respect to virus-host cell interactions so far. Although cell culture based systems have been developed successfully, limitations remain and need to be overcome, if the potential of those systems is to be fully utilized. These limitations include slow virus replication and poor virus yields of some influenza virus production strains. Limitation could be a consequence of differences in replication characteristics and a limited time-span for virus replication of infected cells due to early stress and fast induction of apoptosis (Hornickova, 1997). Therefore, a better understanding of virus-host cell interactions and viral replication mechanisms could contribute significantly to the development of methods to overcome existing bottlenecks in cell culture derived influenza vaccine manufacturing. In particular, by discovering molecular processes, which help virus strain variants to overcome host cell response or result in fast induction of stress or apoptosis in mammalian cells.

The aim of the presented work was to established and to subsequently apply two molecular biology techniques for investigating virus-host cell interactions with respect to the vaccine production process: (I) a proteomic approach to study the global changes in proteome profiles and to elucidate the host cell and virus induced events that occur during cellular processes upon viral infections, and (II) a genomic approach to study regulation and dynamics of viral genome replication and transcription. An important aspect to consider is that application of molecular biological techniques (i.e. proteome and genome analysis) to the investigation of these cellular systems is limited largely to human and mouse models due to restricted availability of constituent assay components such as antibodies, genome sequences or protein databases. Thus, first of all an appropriate human reference model cell line system for comparative investigations had to be selected. Therefore, three different adherend human cell lines were compared for cellular metabolism and virus productivity to

examine whether they are reliable and promising candidates for a human reference model, studying virus-host cell interactions. Finally, the lung carcinoma A549 cell line was chosen as a human reference model.

In the following part of the work, quantitative proteome technologies, such as 2-D DIGE coupled with nanoHPLC-nanoESI-MS/MS for protein identification were used to provide additional insights into the complexity of influenza-host cell interactions (Zhang et al., 2005). In this manner, global changes in proteome profiles can be analyzed, elucidating the events that occur during cellular processes upon viral infections. Throughout the past few years, quantitative proteomic analysis has proven in numerous publications to be a useful tool for providing important insights into protein alterations in response to influenza virus infection (Baas et al., 2006; Liu et al., 2008; Mayer et al., 2007; Shaw et al., 2008). These studies have shown, how different influenza virus strains affect host cell proteomes and how influenza virus strains may use different strategies to evade host cell response and replicate in different host cells. Furthermore, possible adaptation mechanisms of avian influenza virus or cellular factors associated with the native viral ribonucleoprotein (vRNP) and viral polymerase complexes were discovered.

A comparative proteome profiling study with the production cell lines MDCK and Vero and the human lung carcinoma cell line (A549) as a human reference model for characterization of changes in relative protein abundances after human influenza PR/8 virus infection was done. The motivation was to create a better understanding of the distinct molecular mechanisms by which some variants of influenza viruses overcome cellular immune response in mammalian cells. Therefore, early proteome alterations in MDCK cells infected with an influenza PR/8 virus strain obtained from two different suppliers were compared. Both variants showed significant differences in replication dynamics, e.g. progress of infection, induction of apoptosis in their host cells, and total amount of virus particles released as reported by Schulze-Horsel et al. (Schulze-Horsel et al., 2009).

MDCK cells are IFN competent, and the IFN response is commonly thought to be a factor strongly inhibiting virus replication. In contrast, Vero cells are deficient in IFN production. Therefore, another aspect of the proteomics part of this work was to gain a more comprehensive understanding of the complex mechanisms involved in the cellular antiviral response of Vero cells lacking an IFN system. Finally, factors relevant for adaptation of virus strains to new host cells were taken into consideration. This issue was approached experimentally by comparing Vero host cell proteome alterations in response to infection with a cell line adapted and a non-adapted influenza PR/8 virus strain. Hence, a detailed view on physiological status and cellular changes in virus producing cell lines could be obtained. Furthermore, the application of proteome profiling methods provided information about markers involved in critical host cell stress response, antiviral defense mechanisms,

metabolic changes or apoptosis induction in vaccine production cell lines.

The third part of the presented work focused on regulation and dynamics of influenza virus genome replication and transcription. Both still remain unknown. In general, the influenza A virus life cycle comprises the following steps (Lamb and Krug, 2001): The virus enters cells through receptor-mediated endocytosis. To release uncoated vRNP complexes into the cytoplasm the virus fuses with the endosomal membrane. For viral replication and transcription the vRNPs are transported into the nucleus. The synthesis of influenza virus RNA is divided into three parts, first, transcription of viral genomic RNA (vRNA(-)) into viral messenger RNA (vmRNA(+)), second, synthesis of viral complementary RNA (cRNA(+)) from genomic vRNA(-), followed by synthesis of cRNA(+) into vRNA(-) (Neumann et al., 2004). After assembly of vRNPs by association of newly synthesized vRNA(-) with nucleoproteins (NP) and viral polymerase components, these vRNPs are exported from the nucleus and incorporated into progeny virus particles followed by budding of these particles from the plasma membrane.

For a better quantitative understanding of these complex intracellular events in the life cycle of influenza virus, a mathematical model for its replication in MDCK cells with respect to the vaccine production process has been formulated (Sidorenko and Reichl, 2004). This structured mathematical model covers all steps of the virus life cycle, from attachment to viral protein synthesis, genome replication and budding in a single cell. For model establishment general information available in literature was used. Although the general time course of influenza virus replication in their host cells is well understood and described in literature, much about regulation of viral genome replication and transcription is still unknown (Cheung and Poon, 2007). In particular, for model validation and parameter estimation, i.e. dynamics and control of viral RNA synthesis, quantitative experimental data was missing. The first step in order to overcome this lack of information was the establishment of a quantification method for intracellular derived viral nucleic acids.

Several methods and studies have been described in the past for analyzing the dynamics of influenza virus replication and transcription (Kumar et al., 2008b; Ng et al., 2008; Robb et al., 2009; Uchide et al., 2002; Vreede et al., 2008). These studies have used diverse techniques, for example primer extension in combination with a vRNP reconstitution assay, semi-quantitative southern hybridization, and RT-qPCR assays. Nevertheless, most of these methods are only semi-quantitative. Often results were contradictory with the consequence that different hypotheses were suggested for regulation and dynamics of viral replication.

Due to the successful use of the RT-PCR (Chan et al., 2006b) or the RT-qPCR (Di Trani et al., 2006; Ong et al., 2007; Youil et al., 2004) for a precise determination of the number of viral copies in clinical or environmental detection assays, these techniques were selected as

an appropriate quantitative method for the application in a production process. However, standard RT-qPCR assays do not determine specifically the number of all three different influenza viral RNA types (vRNA(-), cRNA(+), vmRNA(+)) separately, which is necessary for differentiation between viral replication and transcription processes. For that purpose a method is required that targets individually the different polarities of the three viral RNA strands. Several studies have reported polarity-specific RT-PCR assays for detection of different RNA viruses such as hepatitis virus (HV) (Komurian-Pradel et al., 2004), dengue virus (Peyrefitte et al., 2003) or foot-and-mouth disease virus (Li et al., 2009). Polarity-specific priming strategies in RT-qPCR have been applied to distinguish between influenza viral transcription and vRNA(-) replication, but only for relative quantification (Kumar et al., 2008b; Ng et al., 2008). Hence, the focus of this part of the present work was on the development and validation of a RT-qPCR assay with a polarity- and sequence-specific priming strategy in RT for simultaneous determination of influenza vmRNA(+), cRNA(+) and vRNA(-). By using corresponding synthetic viral RNA reference standards an absolute quantification was achieved. The established assay was used to follow the time course of expression of four viral segments (4 (HA), 6 (NA), 7 (M) and 8 (NS)) during influenza PR/8 virus infection in MDCK cells and to assess the dynamics of viral transcription and replication of these segments.

The ability to determine the amounts of the three different types of influenza A viral RNAs (vmRNA(+), cRNA(+), vRNA(-)) during the virus life cycle in mammalian cells should facilitate mathematical modeling of the time course and the dynamics of viral transcription and replication. Based on such a model it should be possible to obtain more precise insights in basic laws of virus infection of vaccine production cells and into the interactions of viruses and host cells. Furthermore, it should also be possible to analyze effects of parameter changes on the dynamics of virus replication, to identify possible targets for molecular engineering, or to develop strategies for improving virus yields in vaccine production processes (Sidorenko and Reichl, 2004).

Overall, results from both parts of the presented work should elucidate the complex relationships between influenza viruses and the infected host cells, as well as the viral replication dynamics. Moreover, results should provide the basis for a more comprehensive understanding of the viral life cycle.

2. Background and Theory

2.1. Influenza virus

2.1.1. Classification and structure

Influenza viruses belong to the family of Orthomyxoviridae and are classified into A, B and C types, based on the antigenic differences of the internal proteins (NP and matrix protein (M)) (Lamb and Krug, 2001; Wilschut and McElhaney, 2005). They are negative sense, single stranded, enveloped RNA viruses with a segmented genome. The genomic RNAs (vRNA(-)) function as templates for messenger RNAs (vmRNA(+)) and complementary RNAs (cRNA(+)) syntheses. Both influenza A and B viruses contain 8 RNA genomic segments, whereas influenza C viruses contain only 7 RNA genomic segments. The viruses have a wide host range of birds and mammals (Webster, 1998). However, only influenza A has been responsible for influenza pandemics. The nomenclature of the different virus strains are based on the host of origin, geographic location, year of isolation, strain number and mostly the antigenic classification via their membrane glycoproteins: hemagglutinin (HA) and neuraminidase (NA) mentioned in the parenthesis, e.g. A/PR/8/34 (H1N1). There are 16 antigenic subtypes of HA (HA1-HA16) and 9 subtypes of NA (NA1-NA9) reported.

The epidemiological behavior of influenza in human population is related to the two types of antigenic variation namely ‘antigenic drift’ and ‘antigenic shift’ (Wilschut and McElhaney, 2005). ‘Antigenic drift’ involves point mutations resulting from an immune selective pressure. The changes in the antigen structure allow the virus to evade the immune system of the host. As a result, new antigenic variants (new subtypes) evolve. However, they are still related to those subtypes circulating during preceding epidemics. On the other hand, the ‘antigenic shift’ occurs much less frequently but leads to a major antigenic change. This change results from a replacement of the genomic RNA segment resulting in emergence of a potentially pandemic, influenza A virus. A new subtype virus would be antigenically distinct from earlier subtypes and could not have arisen from them by mutation. The wide host range coupled by a high mutation rate and cross species interactions generally results in the development of new virus strains, which would naturally be the major obstacle in controlling the disease by vaccination. Outbreaks of influenza disease are surveyed world-wide by the Global Influenza Surveillance Network of the World Health Organization (WHO) (WHO, 2008) and locally by each country or an European network. Their tasks are the collection of specimens, primary virus isolation and antigenic characterization.

Influenza viruses are described commonly as nearly spherical particles with a mean diameter

of 100 nm (Hay, 1998). The influenza A viral particles contain a lipid envelope, which is derived from the host cell membrane during the viral budding process. Three viral proteins, HA, NA, and matrix protein 2 (M2), are embedded in the lipid envelope (Lamb and Krug, 2001). HA and NA are spike glycoproteins and they are anchored in the lipid bilayer by short sequences of hydrophobic amino acids (AA). HA is a homotrimer, responsible for the receptor binding and membrane fusion. NA is a homotetramer whose function is to remove sialic acid groups from glycoproteins and to release the viral particle. M2 is an integral membrane homotetramer, which functions as an ion channel for the acidification of the interior of the viral particle during viral infection (Wang et al., 1994). Underneath the viral lipid envelope there is a matrix protein 1 (M1) protein layer. Inside the virus, all 8 viral RNA segments are bound to NP and to the influenza virus RNA polymerases to form vRNP complexes (Lamb and Choppin, 1983). Apart from M1, NP is the most abundant protein in the virus and it is thought to associate sequence independently with the phosphate-sugar backbone of the viral RNA. Each NP monomer interacts with approximately 20 nucleotides of the vRNA(-) (Lamb and Krug, 2001). The RNA polymerase complex is composed of three polymerase subunits (PB2, PB1, and PA). Electron micrographs of isolated vRNPs indicated that both ends of the vRNA(-) interact with each other to form a circular or supercoil structure (Cheung and Poon, 2007). The non-structural protein 2 (NS2) is present in low amounts and appears to act as a nuclear export protein for viral RNA (O'Neill et al., 1998). An illustration of influenza A virus structure is given in Figure 2.1-1.

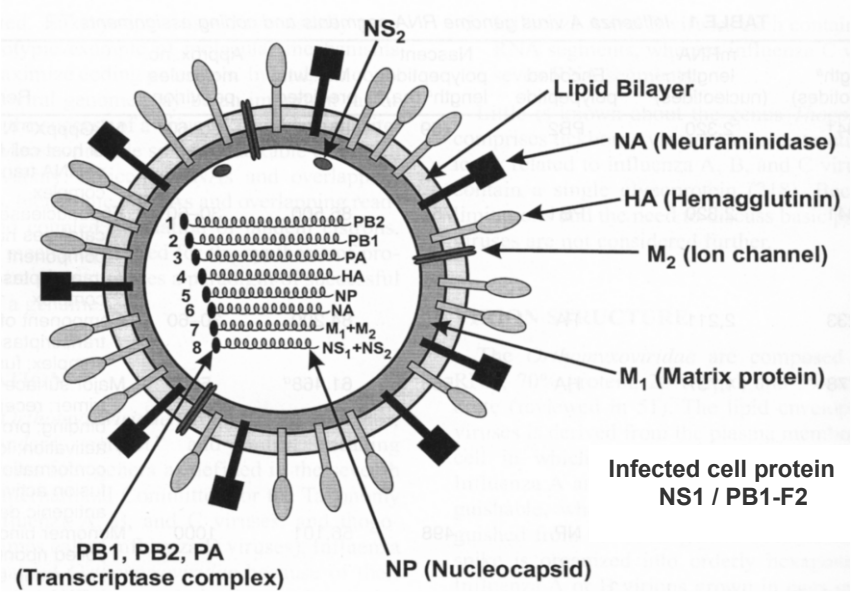

Figure 2.1-1: Structure of influenza A virus

Glycoproteins (HA, NA) are embedded in a host cell derived lipid bilayer membrane. Within the membrane the transmembrane ion channel protein M2 is located, while the structural protein M1 is underneath the bilayer. Within the core of the virus, the single stranded negative sense RNA is placed, associated with the NP and the three polymerase subunits (PB2, PB1, and PA) forming the vRNP capsid complex (Lamb and Krug, 1996).

In principle, viruses are pleomorph. Viral morphology is a genetic trait and several viral proteins (HA, NA, M1, and M2) are known to have effects on the morphology of influenza virus particles (Jin et al., 1997). Roberts et al. further demonstrated that the nature of the host cells also determines the morphology of influenza virus particles (Roberts and Compans, 1998).

The genome of the influenza A virus contains eight segments (Palese, 1977). vmRNA(+)s from segments 1 and 3 to 6 are monocistronic. vmRNA(+)s from segment 2 of some viral isolates contain an alternative open reading frame. In contrast, vmRNA(+)s derived from segments 7 or 8 can undergo alternative splicing for protein expressions (Lamb and Krug, 2001). The sizes of the viral RNA segments and the proteins encoded are summarized in Table 2.1-1. Only PB1-F2 protein from segment 2 (PB1) and NS1 protein from segment 8 (NS) are non-structural proteins.

Table 2.1-1: Viral RNA segments and coded proteins of Influenza A virus (PR/8 strain) adapted from Fields et al. (Fields et al., 2001)

Seg-ment	Size (nt)*	Protein	Poly-peptide (AA)*	Molecular weight (kDa)	Nr. of copies/ virus	Function
1	2341	PB2	759	86	30-60	RNA polymerase, cap-binding
2	2341	PB1	757	87	30-60	RNA polymerase, elongation
		PB1-F2	87	11	-	Proapoptic activity
3	2233	PA	716	84	30-60	RNA polymerase, protease, endonuclease
4	1778	HA	560	61	500	Hemagglutinin, surface glycoprotein, receptor-binding, membrane fusion
5	1565	NP	498	56	1000	Nucleoprotein, RNA binding, RNA polymerase complex, nuclear/cytoplasmic transport of viral RNA
6	1413	NA	454	50	100	Neuraminidase, surface glycoprotein, virus release
7	1027	M1	252	28	3000	Matrix protein, nuclear export, interactions with vRNPs
		M2	97	11	20-60	Matrix protein, integral membrane protein, ion channel
8	890	NS1	230	27	-	Non-structural protein, effects on cellular RNA transport, splicing, translation, IFN antagonist
		NS2	121	14	130-200	Non-structural protein, vRNP nuclear export

** nt – nucleotides; AA - amino acids*

Considering the PR/8 virus strain as an example, the influenza viral gene segments range from 890 to 2341 nucleotides in length containing approximately 20-45 non-coding nucleotides at the 3' end and 23-61 at the 5' end, depending on the segment (Steinhauer and Skehel, 2002). Usually the 13 5' terminal and 12 3' terminal nucleotides of the eight influenza A virus segments are highly conserved among all strains.

Non-coding regions that lie between the conserved promoter elements and the start or stop codons are variable in length and nucleotide composition, and their function is still unknown. Deletions, insertions, or mutations in these regions demonstrated that they are not required for viral replication or transcription (Garcia-Sastre et al., 1994; Zheng et al., 1996) but may affect these processes, possibly by interacting with NP or the polymerase complex. Furthermore, a sequence motif in the noncoding region of segment 7 is stimulating the expression of the encoded protein, whereas transcription levels remained unaffected (Enami et al., 1994). This finding suggests that the noncoding regions contain signals that affect vmRNA(+) stability or the initiation of translation (Neumann et al., 2004).

2.1.2. Influenza A virus life cycle

The influenza virus life cycle can be divided into the following stages: binding, fusion and uncoating of the influenza virus, entry of vRNPs into the nucleus, transcription and replication of the viral genome, translation of viral proteins, export of the vRNPs from the nucleus, and assembly and budding at the host cell membrane. The life cycle of influenza virus was investigated thoroughly by many groups and a number of excellent books and reviews (Flint et al., 2009; Flint et al., 2000; Hay, 1998; Lamb and Krug, 2001; Nickolson, 1998) describe the complex steps of replication in host cells. Each stage of the viral life cycle is summarized in the following. An illustration of the different stages is given in Figure 2.1-2.

Binding, fusion and uncoating of the influenza virus

Influenza viruses bind via their surface HA to sialic acid in alpha 2,3 or alpha 2,6 linkage with galactose on the host cell surface (Mochalova et al., 2003). Virus particles can be internalized by four mechanisms. Most internalization appears to be mediated by clathrin-coated pits, however internalization via caveolae, macropinocytosis, and by non-clathrin, non-caveolae pathways has also been described for influenza viruses (Matlin et al., 1981).

Uncoating of viral particles takes place in the host cell endosome. vRNPs are released from the endosome when the endosomal pH is decreased to about 5.0, which activates the viral M2 ion channels and allows protons to enter the interior of the virus particle (Chizhmakov et al., 1996). As a result, the viral M1 proteins undergo conformational changes, followed by the disruption of M1 vRNP interactions and acid-catalyzed conformational rearrangements of HA proteins. As a consequence, viral and endosomal membranes fuse and vRNPs are released into the cytoplasm (Marsh and Helenius, 1989).

Transport of vRNPs into the host cell nucleus

An unusual characteristic of the influenza virus life cycle is its dependence on the nucleus. Nucleus trafficking of the viral genome is a tightly regulated process. The eight influenza

virus genome segments are associated with four viral proteins to form vRNPs. The major viral protein in the vRNP complex is the NP, which coats the RNA. The remaining proteins PB1, PB2 and PA bind to the partially complementary ends of the viral RNA, creating a distinctive panhandle structure. The vRNPs (10-20 nm wide) rely on active import mechanism of the host cell nuclear pore complex due to the presence of nuclear localization signals (NLSs) (Cros et al., 2005). NLSs mediate their interaction with the nuclear import machinery, including the Ran guanosine triphosphatase (RanGTPase) (Deng et al., 2006a).

Influenza viral RNA transcription and replication

In general, for each of the 8 gene segments, a vRNP is assembled in the nucleus (Boulo et al., 2007). The vRNP functions in three modes (Mikulasova et al., 2000): (I) transcription, which synthesizes viral messenger RNA (vmRNA(+) from the vRNA(-) template using as primer 5' ends of cellular mRNAs containing a cap structure; (II) replication, which produces positive sense complementary RNA (cRNA(+)) and subsequently vRNA(-), both complexed with NP and the trimeric polymerase; and (III), the vRNP is exported from the nucleus into the cytoplasm and is incorporated into assembling viruses at the membrane.

Such as the mRNAs of the host cell, influenza vmRNA(+)s are capped and polyadenylated (Neumann et al., 2004). The methylated caps, however, are scavenged from host cell mRNAs and serve as primer for viral RNA synthesis, a process termed 'cap-snatching' (Krug et al., 1987). The second process allows polyadenylation of vmRNA(+)s when host cell polyadenylation has been inhibited (Amorim and Digard, 2006). Notably, early vmRNA(+) (including NP and NS1) accumulate in the cytoplasm before late vmRNA(+) (M1, HA and NS2). Both appear in varying abundances, suggesting additional control mechanisms regulating viral gene expression (Hatada et al., 1989; Shapiro et al., 1987).

The viral polymerase complex produces positive sense vmRNA(+) with host cell derived 5' methyl caps. Alternately spliced vmRNA(+) transcribed from M and NS vRNA(-) segments 7 and 8, producing the spliced vmRNA(+) for M2 and NEP/NS2, respectively, are thought to be coupled to the cellular splicing and export mechanisms (Chen and Krug, 2000). Capped vmRNA(+)s are exported selectively from the host cell nucleus through a currently unclear mechanism that may rely on components of the host cell mRNA export machinery (Engelhardt and Fodor, 2006). Polyadenylation of vmRNA(+) appears to be required for influenza vmRNA(+) export (Poon et al., 2000).

Synthesis of full length cRNA(+) requires that vRNA(-) transcription initiates without the help of a host cell methyl RNA cap as a primer (Deng et al., 2006b), and that it proceeds to the 5' end of the vRNA(-) template. Free viral NP seems to play a central role in enabling both of these features of cRNA(+) synthesis, although the molecular details of its role remain unclear (Mullin et al., 2004).

The synthesis of full-length negative strand viral RNA from a cRNA(+) template is believed to follow the same principles as the synthesis of cRNA(+) from a vRNA(-) template. The cRNA(+), complexed with viral NP, is used as template by the trimeric viral polymerase (Crow et al., 2004), and newly synthesized vRNA(-) molecules are packaged immediately with NP molecules to form vRNP complexes (Vreede et al., 2004).

Spliced and unspliced vmRNA(+) in the cytoplasm is translated by the host cell ribosomal translation machinery (Kash et al., 2006). At least eleven viral proteins are synthesized: HA, NA, PB1, PB1-F2, PB2, PA, NP, NS1, NS2, M1, and M2. In most human influenza A strains (such as PR/8), the PB1 vmRNA(+) segment is capable of producing a second protein, PB1-F2, from a short +1 open reading frame (ORF) initiated downstream of the PB1 ORF initiation codon (Chen et al., 2001). vmRNA(+) translation is believed to be enhanced by conserved 5' untranslated region (UTR) sequences that interact with the ribosomal machinery and at least one cellular RNA-binding protein, G-rich sequence factor 1 (GRSF-1), has been found to interact specifically with the viral 5' UTRs (Park et al., 1999). The viral NS1 protein and the cellular protein kinase inhibitor p58 (P58IPK) enhance viral translation indirectly by preventing the activation of the translational inhibitor protein kinase R (PKR) (Goodman et al., 2007). The viral NS1 protein has also been proposed to enhance specifically translation through interaction with host cell poly(A)-binding protein 1 (PABP1) (Burgui et al., 2003). Simultaneously, host cell protein synthesis is downregulated in influenza infection by still uncharacterized mechanisms (Kash et al., 2006).

Export of vRNP from nucleus

Influenza genomic vRNA(-) is packaged into vRNP complexes containing viral polymerase proteins and NP. As influenza vRNP complexes are too large for passive diffusion out of the nucleus, utilization of the cellular nuclear export machinery is achieved by viral adaptor proteins. M1 is critical for export of the complex from the nucleus, mediating the interaction of the vRNP complex with the viral NS2 protein, which in turn interacts with host cell CRM1/exportin-1 nuclear export protein (Boulo et al., 2007; Neumann et al., 2000).

Virus assembly and release

Influenza viruses assemble and bud from the apical plasma membrane of polarized host cells (Schmitt and Lamb, 2005). Following synthesis on membrane-bound ribosomes, the three viral integral membrane proteins, HA, NA and M2 enter the host cell endoplasmic reticulum (ER) where all three proteins are folded and HA and NA are glycosylated. HA, NA and M2 are transported to the Golgi apparatus and are directed to the virus assembly site on the apical plasma membrane via apical sorting signals (Doms et al., 1993). For a budding of infectious influenza virus particles it is essential that thus contain a full complement of the eight vRNA(-) segments. Two different models have been proposed for packaging of the

vRNPs into newly assembled virus particles. The random incorporation model proposes that there is no selection at all on which vRNPs are packaged. It is assumed that each vRNP has equal probability of being packaged, and that if enough vRNPs are packaged, a particular percentage of budding viruses will receive at least one copy of each genome segment (Enami et al., 1991). The selective incorporation model suggests that each segment contains a unique ‘packaging signal’ allowing it to act independently, with each segment being packaged selectively. There is increasing evidence for the theory of a packaging signal within the coding regions at both the 5' and 3' end of the genomic RNA (Fujii et al., 2009).

In polarized epithelial cells, assembly and budding of influenza occurs from the apical plasma membrane (Schmitt and Lamb, 2005). For efficient assembly, all viral components must accumulate at the budding site, and it is believed that the viral glycoprotein accumulation determines the site of virus assembly and budding (Nayak et al., 2004). M1 is thought to be the bridge between the envelope glycoproteins and the vRNPs for assembly (Schmitt and Lamb, 2005). Host cell factors such as polarization and the actin cytoskeleton play a critical role in determining the shape of filamentous particles (Simpson-Holley et al., 2002).

Once the viral envelope has separated from the cell membrane influenza virus particles are released actively to complete the budding process (Schmitt and Lamb, 2005). HA anchors the virus to the cell by binding to sialic acid-containing receptors on the cell surface. The enzymatic activity of the NA protein removes the sialic acid and releases the virus from the host cell. NA activity is also required to prevent the viral particles from aggregating.

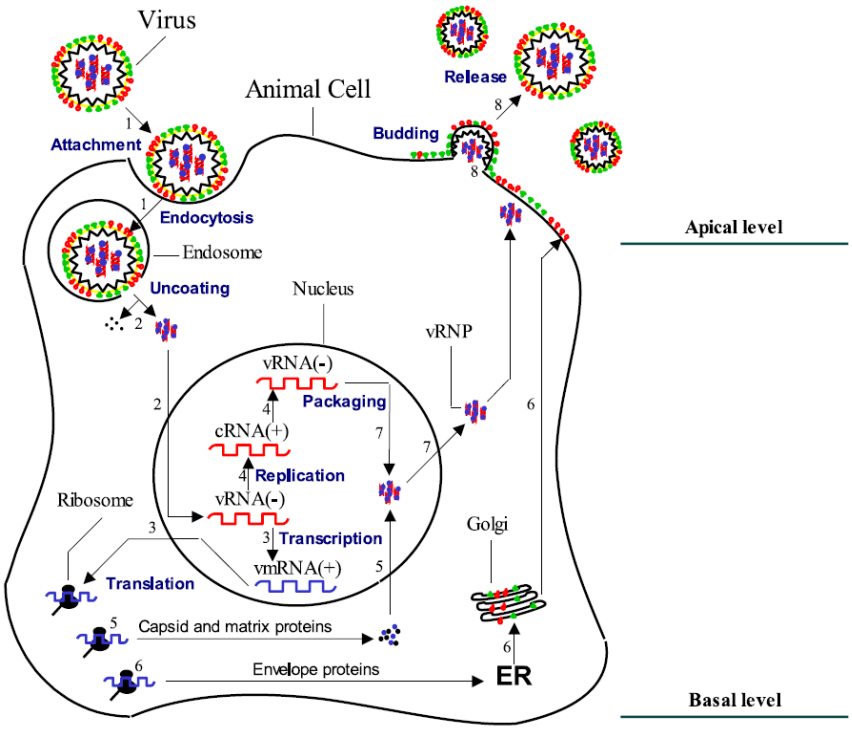

Figure 2.1-2: Influenza A virus life cycle

The virus life cycle is divided into attachment and fusion (1), followed by uncoating (2), synthesis of cRNA(+) from vRNA(-), replication of vRNA(-), transcription, translation of vmRNA(+)s to produce viral proteins (3-5), post-translational modification of viral proteins (6), assembly of viral structural components (7) and release of progeny virus (8) (Sidorenko and Reichl, 2004).

2.1.3. Influenza virus-host cell interactions

Infection of host cell with influenza virus triggers an array of host cell processes that interfere with viral replication. In the following important interactions of viral proteins with cellular factors, which either support viral replication or counteract host cell defense are described.

Replication of the virus in host cells

For replication and transcription of the influenza virus genome, not only viral factors but also host cell derived cellular factors are required (Zhang et al., 2009). Key among the functional interactions during influenza virus infection is the dependence of the virus on cellular RNA synthesis by DNA-dependent RNA polymerase II (Pol II) (Engelhardt and Fodor, 2006). The virus can alter the distribution of Pol II on cellular genes, leading to a reduction in Pol II elongation, thereby contributing to the well-known phenomenon of host cell protein synthesis shutoff, in which there is a dramatic decrease in the translation of cellular mRNAs while viral transcripts remain efficiently and selectively translated during influenza virus infection (Chan et al., 2006a). Recent functional assays and proteomics have suggested a panel of host cellular proteins, which may interact with viral polymerase and vRNP complexes (Mayer et al., 2007). NS1 protein plays a central role in these virus-host cell interactions (Kochs et al.,

2007; Krug et al., 2003). Viral NS1 protein is a nuclear, dimeric protein that is highly expressed in infected cells and has dsRNA-binding activity. Viral NS1 is also a major player in shutting down host cell protein synthesis. Therefore, it interferes with the host cell machinery, such as CPSF4 (cleavage and polyadenylation specific factor 4, 30kDa) and PABN1 (poly(A) binding protein, nuclear 1) in polyadenylation (Nemeroff et al., 1995; Qian et al., 1995). NS1 also recruits the cellular initiation factor, eIF4G1 (eukaryotic translation initiation factor 4 gamma 1), allowing for the preferential viral messengers translation (Aragon et al., 2000). A variety of intracellular signaling pathways activated by influenza, such as the Raf/MEK/ERK mitogenic kinase cascade, are in part exploited by the virus to ensure efficient replication (Ludwig et al., 2006). A number of host cell proteins, including microfilaments, G proteins, and some protein kinases, have been shown to be involved in the budding of influenza virus (Nayak et al., 2004).

Host cell innate antiviral response

The IFN induced cellular antiviral response has a primary protective function in the early stages of influenza virus infection (Garcia-Sastre, 2006). Both double strand (ds) and ssRNA, viral RNA products generated during infection, act as triggers for the production of IFN, which are recognized by two types of sensors, the transmembrane Toll-like receptors (TLR) and cytoplasmic RIG-I (retinoic acid inducible gene I)-like receptors (Garcia-Sastre, 2006). Virus-infected cells synthesize IFN and secrete it into extracellular fluid, where it binds to IFN receptors on uninfected neighboring cells. This binding, results in the induction of a cellular antiviral responses involving the upregulation of more than 100 IFN stimulated genes (ISG) (e.g. myxovirus-resistance proteins (Mx), PKR) (Ludwig et al., 2006). To establish a productive infection, influenza viruses must first overcome the IFN induced block imposed on viral replication. PKR can restrict viral replication through phosphorylation of the protein synthesis initiation factor EIF2A, resulting in a reduced translation initiation. This prevents viral replication and inhibits normal cell ribosome function, killing both the virus and the host cell if the response is active for a sufficient time. To evade the antiviral effects of PKR, influenza has evolved two strategies: (I) the virus activates a host cellular inhibitor of PKR, p58IPK, and (II) its NS1 protein blocks PKR activation (Wolff and Ludwig, 2009). The viral NS1 protein has been identified as a potent agonist of the innate antiviral signaling, both by interference with the RIG-I induction of IFN and at a later stage, by modulating processing of cellular pre-mRNA (Kash et al., 2006; Krug et al., 2003).

Influenza virus induced apoptosis

Efficient virus replication, maintenance of viral protein synthesis, shutoff of host cell protein synthesis, and production of viral particles usually leads to cytolytic death of cells at 20–40 h of infection (Julkunen et al., 2001). Influenza virus is known to induce apoptosis, in a variety

of ways, however the specific regulation mechanism still remains unclear (Ludwig et al., 2006). Currently, it is unclear whether apoptosis is a host cell defense mechanism to limit the replication and spread of virus, or a virus induced function to support viral replication. Typical host cell changes are characterized by chromatin condensation, DNA fragmentation, cell shrinking, and compartmentalization to apoptotic bodies followed by clearance of apoptotic cells by phagocytic cells (Earnshaw et al., 1999). Increased intracellular Ca^{2+} levels, elevated Fas antigen, a cell surface receptor that triggers apoptosis, and transforming growth factor (TGF)-beta levels, and activation of PKR have been associated with influenza virus induced apoptosis (Takizawa et al., 1996). In addition, IFN and enhanced PKR expression were found to potentiate influenza A virus induced apoptosis (Wolff and Ludwig, 2009). Two influenza virus proteins, NA and M1/M2 have also been suggested to regulate apoptosis. NA activates latent TGF-beta, which may then indirectly be involved in influenza virus induced apoptosis (Morris et al., 2005). In virus infected cells, the virus encodes a nonstructural protein, PB1-F2, which induces apoptosis through a mitochondrial carrier protein (adenine nucleotide translocator 1) (Chen et al., 2001).

The importance of host cell factors, which are absolutely required for influenza virus replication, have been shown in three recent studies using a novel genome wide RNA interference (RNAi) screen in mammalian cells (Hao et al., 2008a; Karlas et al., 2010; Koenig et al., 2010). These studies identified proteins, which comprise functional categories and interactions already associated with viral replication, and which were mentioned before. However, additionally host cell factors that have not previously been implicated in mediating influenza virus replication were found. Signaling molecules, including those involved in the PI3K/AKT pathway, molecules that function to regulate cytoskeletal dynamics, endosomal trafficking complex, Ca^{2+} regulation, and proteins involved in ubiquitination, phosphatase and protease activities were overrepresented, underscoring the importance of these cellular functions during influenza infection. Thus, results of these screens highlighted the importance for the analysis of virus–host cell interactions and provided new and comprehensive information on host cell determinants of replication.

Overall, knowledge of influenza virus interactions with host cells not only helps to gain important insights into viral survival and cellular defense strategies, it also uncovers novel targets for host cell factor directed antiviral therapy and provides perspectives in the mechanism of host range and virulence.

2.1.4. Regulation of the influenza virus life cycle

Influenza viral genomic RNA (vRNA(-)) is complexed, with the polymerase subunits and NP into active vRNP, which serves as a template for both viral transcription and replication (Lamb and Krug, 2001). Both, cellular and viral factors have been suggested to play crucial roles in the regulation of viral transcription and replication during infection. The mechanism for switching from viral transcription to replication however is still understood poorly. One hypothesis is a control or switching mechanism to regulate the polymerase transcription and viral genome replication activity (Biswas et al., 1998). This hypothesis suggests that a sufficient amount of soluble NP in the nucleus, which is not associated with vRNPs, is required to switch from viral transcription to replication. Recently, Vreede et al. demonstrated that there may be no switch, regulating the initiation of RNA synthesis and proposed a model, suggesting that nascent cRNA(+) is degraded by host cell nucleases unless it is stabilized by newly synthesized viral RNA polymerase and NP (Vreede et al., 2004). Additional hypotheses are, that different concentrations of initiating nucleoside triphosphate (NTP) are required for viral replication and transcription (Vreede et al., 2008) as well as a regulatory function for the NS2 protein (Robb et al., 2009). Another study proposed a regulatory role of segment-specific non-coding sequences of influenza virus on viral RNA synthesis, whereas heterologous viral RNA segments with identical non-coding sequences stimulated viral RNA replication (Ng et al., 2008). Furthermore, host cell signaling pathways (e.g. nuclear factor kappa B (NF-κB)) might be involved in influenza virus replication and could regulate differentially influenza virus RNA synthesis (Kumar et al., 2008b). In the following the first two hypotheses are explained in more detail:

Switching mechanism hypothesis

The switching mechanism hypothesis supposes that in later infection phases viral RNA synthesis is switched from viral transcription mode to replication mode (Biswas et al., 1998). NP was identified as a prime candidate for a switching molecule based on several temperature-sensitive NP mutants defective in replication and RNA binding (Medcalf et al., 1999). Biochemical studies suggested that free NP is required for the synthesis of full-length transcripts (Shapiro and Krug, 1988). It was proposed that mechanistically interaction of NP with the polymerase (polymerase modification) (Mena et al., 1999) or with the promoter element of the template RNA (template modification) (Fodor et al., 1994) alters the mode of transcriptional initiation.

Stabilization hypothesis

The stabilization model suggests that there is no switch regulating the initiation of RNA synthesis (Vreede et al., 2004). It was shown that in the presence of preexisting viral RNA polymerase and NP, influenza A virus synthesizes both vmRNA(+) (transcription) and

cRNA(+) (replication) early in infection. vmRNA(+) is protected from normal cellular degradative processes by the presence of a 5′ cap and a 3′ poly(A) tail, whereas nascent cRNA(+) is presumably rapidly degraded by host cell nucleases. The transition to a replicative phase occurs when cRNA(+) is protected by the specific binding of RNA polymerase (assembled from newly synthesized PB1, PB2, and PA) to the cRNA(+) promoter (Gonzalez and Ortin, 1999). The cRNA(+)-polymerase promoter complex then serves as a nucleation point for binding of free newly synthesized NP, leading to the formation of active and stable vRNPs suitable for replicative vRNA(-) synthesis.

Time course and dynamics of influenza virus replication

Besides regulation, time course and dynamics of replication of the different viral RNA segments are not understood entirely. General estimations are as follows. It is suggested that the relative abundance of specific vmRNA(+) and vRNA(-) are controlled throughout infection (Lamb and Krug, 2001). In general, synthesis of vmRNA(+)s starts early after infection and reaches a maximum rate at about 2.5 hours post infection (hpi) (Shapiro and Krug, 1988). Synthesis of viral cRNA(+)s begins not until vmRNA transcription, but maximum synthesis rates of NS1 cRNA(+) is reached at about 1.5 hpi before maximum vmRNA(+) synthesis rate (Shapiro et al., 1987).

Immediately after infection, primary viral transcription occurs (Hay, 1998). At this stage, all eight vmRNA(+)s are synthesized in equimolar amounts. This is followed by the second viral transcription stage. The second viral transcription stage can be further subdivided into early and late phases. In the early phase of the second viral transcription, NS1 and NP vRNA(-) are synthesized preferentially. As a consequence, NS1 and NP are the predominant viral proteins in infected cells at this stage (Hay et al., 1977). It is possible that NP is required for viral replication and transcription of viral RNA. NS1 might be required for the regulation of cellular gene expression. During the late phase, vRNA(-)s are synthesized in equivalent amounts, as required for progeny virus genome. At this stage, the NS1 protein is synthesized in a reduced level. In contrast, HA, NA, and M1 vmRNA(+)s are synthesized preferentially (Smith and Hay, 1982). In contrast to other viral proteins polymerases occurred proportionally low. They are required in only catalytic amounts.

Viral protein synthesis seems to be primarily regulated on the transcription and not on the translation level. Since, the synthesized amount of viral protein is proportional to the amount of vmRNA(+) (Hatada et al., 1989). Additionally, viral gene expression could be regulated through sequence differences of the segments, which is also supposed for the non-coding regions of the highly conserved areas (Zheng et al., 1996).

2.1.5. Influenza virus vaccine production

The most effective way to provide protection against influenza infections is through vaccination. Human vaccines against influenza have been available for almost 60 years (Audsley and Tannock, 2008). Viral vaccines are typically categorized into live (attenuated) and dead vaccines. Live (attenuated) vaccines comprises all vaccines containing infectious, replicating virus while dead vaccines only contain virus particles, which have been chemically inactivated or viral components (e.g. whole virus, split virus and subvirus vaccines). Live human influenza vaccines containing cold-adapted influenza viruses were developed more than three decades ago (Wareing and Tannock, 2001). Influenza viruses can be attenuated by adapting them to replicate at lower temperatures (25–33°C). Then these cold-adapted virus strains are re-assorted with selected epidemic strains, which donate the gene segments encoding HA and NA. Live vaccines are given usually orally or nasally mimicking the natural route of infection and much lower doses of virus are required for vaccination (e.g. FluMist®, MedImmune Vaccines, Inc., USA). Alternatively, recent advancements in reverse genetics now make it possible to generate influenza viruses entirely from cloned plasmid DNA by cotransfection of appropriate cells with 8 or 12 plasmids encoding the influenza virus sense RNA and/or vmRNA(+). This technology could enable the routine and rapid generation of strains for either inactivated or live attenuated influenza vaccines (Subbarao and Katz, 2004).

Current human vaccines are usually trivalent and contain inactivated representative influenza A H1N1, H3N2 and influenza B surface antigens. Vaccine strains are re-evaluated each year by the WHO. Traditionally, the majority of viruses used for inactivated vaccines are still prepared by growth in the allantoic cavity of embryonated chicken eggs. Allantoic virus is purified, concentrated and inactivated. Since the 1970s, most influenza A seed strains used for vaccine production have been prepared by genetic reassortment using the surface glycoproteins of wild type strains chosen by the WHO experts and an PR/8 or PR/8-like master strain as a backbone. The use of this high-growth phenotype of the laboratory strain is believed to reduce the possibility of extraneous infectious agent contamination (Kilbourne et al., 1971).

Throughout the past decade, efforts towards mammalian cell culture derived vaccines were started (Kistner et al., 1998). The first inactivated human influenza vaccine derived from cell culture grown virus have been granted for seasonal vaccination (Optaflu® by Novartis-Behring, Germany) (Doroshenko and Halperin, 2009). Other vaccine candidates are under development or in clinical trials. The main reason for the establishment of cell culture derived vaccines is the improved flexibility and scalability compared to production in eggs in case of pandemics. Some other drawbacks associated with the use of eggs are poor growth of some reassortant vaccine strains in eggs (Audsley and Tannock, 2008), and that vaccines can

contain traces of potentially reactogenic endotoxins, formaldehyde or egg proteins (Wright and Webster, 2001). Additionally, egg growth often selects variants that differ in their glycosylation patterns from the original clinical isolates.

The suitability of a number of cell lines for the growth of influenza viruses has been investigated and some are currently used in manufacturing processes. Cell lines under investigations are conventional, continuous cell lines growing adherently, e.g. MDCK, Vero or a proprietary MDCK 33016 suspension cell line (Novartis Vaccines, Basel, Switzerland) (Genzel and Reichl, 2009). Additionally, there are so-called designer cell lines, e.g. PER.C6® (Crucell, The Netherlands) (Pau et al., 2001), AGE1.CR® (ProBiogen, Berlin, Germany) (Lohr et al., 2009) and EBx™ (Vivalis, Nantes, France) (Pearson, 2007) established. These cell lines were derived from human or animal cells and transformed by viral or cellular immortalizing genes or oncogenes (Genzel and Reichl, 2009). In the following, two promising cell line candidates will be described in more detail.

The MDCK cell line was derived from the kidney of a healthy female cocker spaniel in 1958 (Gaush et al., 1966; Madin and Darby, 1958). This cell line has been studied extensively as it provides an excellent model for the study of kidney and epithelial development (Simmons, 1982). It has been used for influenza virus titer determination via plaque and $TCID_{50}$ assay and is used commonly for the clinical isolation of influenza (Gaush and Smith, 1968). Different MDCK cell lines can be obtained from cell culture collections such as the American-Type Culture Collection (ATCC; e.g. CCL34) or European Collection of Cell Culture (ECACCs; e.g. 841211903). Additionally, other MDCK cell lines with unknown origin are used. Therefore, care must be taken when comparing experimental results from the literature. The MDCK cell line is a well studied vaccine production candidate, which is known to support successfully influenza growth since many years (Genzel et al., 2004; Tree et al., 2001) and many companies are currently considering MDCK cells for vaccine manufacturing. Besides vaccine production this cell line is also of interest for seed virus isolation (high growth reassortant) as well as for reverse genetic approaches (Murakami et al., 2008; Wang and Duke, 2007).

The Vero cell line was derived from kidney fibroblasts from an African green monkey and has been used for the production of polio and rabies vaccine for more than twenty years (Montagnon et al., 1981). It has been recommended by the WHO for influenza vaccine production and is such as the MDCK cell line discussed for isolation of seed virus and reverse genetic approaches (Nicolson et al., 2005). Different Vero cell lines are available at the cell culture collections and described in the literature (mostly used: ECACC, e.g. 88020401; ATCC, e.g. CCL-81).The Vero cell line contains a genetic lesion in the IFN locus and therefore is deficient in IFN production (Diaz et al., 1988). IFN is implicated in apoptosis

induction and in the cellular immune response after viral infection. As a result of IFN deficiency the cells seem to be extremely permissive to viral infection. Therefore, the Vero cell line is used widely to produce virus and vaccine stocks (Montagnon and Vincent-Falquet, 1998), to perform IFN bioassays and to study virus-host cell interactions (Chew et al., 2009; Kistner et al., 1998; Rourou et al., 2009). Surprisingly, initial studies indicated that influenza viruses grew poorly in Vero cells (Lau and Scholtissek, 1995). Improvements in yields were later obtained by the addition of trypsin to the cultures and a traditional cell line adaptation process by passaging the virus strain several times in the cells (Govorkova et al., 1995).

Influenza virus vaccines derived from MDCK and Vero cell lines have been produced and evaluated for immunogenicity, and their production has been scaled up to commercial levels (Doroshenko and Halperin, 2009; Kistner et al., 1998; Youil et al., 2004).

Although cell culture based systems have been developed successfully, limitations remain that need to be overcome, if the potential of those systems is to be utilized fully. These limitations include slow virus replication and poor virus yields of some influenza virus seed strains, e.g. as a consequence of a limited time-span for virus replication of infected cells due to early stress and fast induction of apoptosis (Hornickova, 1997). A better understanding of molecular mechanisms involved could contribute significantly to the development of methods to overcome existing bottlenecks in cell culture derived influenza vaccine manufacturing. In particular in molecular mechanisms, which help virus variants to overcome host cell defence or result in fast induction of stress or apoptosis in mammalian cells.

2.2. Proteomic approach

2.2.1. General overview

Two-dimensional gel electrophoresis (2-DE) is a powerful, high-resolution method to separate a complex mixture of peptides and proteins (O'Farrell, 1975). Each dimension of the procedure assesses successively two distinct fundamental characteristics of proteins: their isoelectric point (p*I*) value during isoelectric focusing (IEF) and their molecular weight (MW) during sodium dodecyl sulfate polyacrylamide gel electrophoresis (SDS-PAGE). As a result, the protein content of any sample is resolved throughout the gel in the form of an average of 1000–2500 spots corresponding to about 300–1000 proteins.

2-DE was described by Klose and O'Farrell in 1975 and has since been developed further (Klose, 1975; O'Farrell, 1975). The introduction of an immobilized pH gradient (IPG) for the IEF separation has resulted in improved reproducibility and has become the reference method for 2-DE (Bjellqvist et al., 1982). At all stages, 2-DE has undergone several modifications, including polypeptide solubilization, the use of wider or narrower IPG strips, strip equilibration between both dimensions and gel quality for the second-dimension separation, that have improved the quality of the results obtained (Goerg et al., 2004). Additionally, advances in staining techniques have challenged the traditional Coomassie brilliant blue or silver staining methods, which can be replaced by fluorescent staining using dyes such as SyproRuby. These allow reliable quantitative assessment of separated proteins with high sensitivity and high dynamic range (Yan et al., 2000). Finally, the development of bioinformatic tools (Appel et al., 1997) and various MS techniques have complemented the gel-based proteomics approach to offer reliable gel-to-gel comparison and protein identification capabilities. Despite advances of non-gel based proteomic technologies, including liquid chromatography coupled with tandem MS (LC-MS/MS) and tagging strategies such as ICAT (isotope-coded affinity tagging) or iTRAQ (isobaric tags for relative/absolute quantification), 2-DE remains the most important and widespread method of the current proteomic techniques (Patton et al., 2002; Wu et al., 2006).

Over the past several years tremendous progress in developing proteomics technologies for global protein post-translational modifications (PTMs) analysis has been made (Farley and Link, 2009). PTMs are enzymatic, covalent chemical modifications of proteins that occur typically after the translation of mRNAs. These modifications are relevant because they can potentially change a proteins physical or chemical properties, activity, localization, or stability. Some PTMs can be added and removed as a mechanism for reversibly controlling protein function and cell signaling. More than 300 different types of PTMs have been described, many of which are known to have pivotal roles in cellular physiology and disease.

Fluorescent stain and immuno-based methods, modification-specific enrichment techniques combined with advanced MS/MS methods have revealed a surprisingly large extent of PTMs in proteins (Hoffman et al., 2008; Zhao and Jensen, 2009). Recent developments have resulted in techniques used for the analysis of PTM using chemical proteomics (Tate, 2008). The key unifying step is the generation of a protein labeled with a small chemical tag at the site of PTM. A highly selective chemical reaction, termed a biorthogonal ligation, is then performed between the chemical tag and a capture reagent to introduce one or more secondary label(s). Secondary labels enable detection, manipulation and enrichment of proteins bearing a specific PTM (Tate, 2008). The methodology for the initial introduction of the chemical tag is tailored to the PTM of interest, exploiting either *in vivo* metabolic labeling with a tagged analogue of the PTM or selective (post-lysis) modification of a PTM by chemical or enzymatic means. Secondary labels enable detection, manipulation and enrichment of proteins bearing a specific PTM (Tate, 2008).

Advantages of 2-DE

2-DE can be applied to almost any type of protein-containing sample, including eukaryotic tissue and derived extracts, cells and organelles, biological fluids, prokaryotic organisms and plants. However, adequate sample preparation according to the specific aim of the proposed study is of great importance (Shaw and Riederer, 2003).

Because of its high resolving power and its large sample loading capacity, 2-DE allows several hundred proteins to be displayed simultaneously on a single gel, yielding a direct and global view of a sample proteome at a given time point. Additionally, 2-DE can demonstrate changes in relative abundance of visualized proteins and can separate protein isoforms, variants and PTMs. Quantitative proteomics can be achieved by assessing differences in protein abundance across gels using related software. Once detected, proteins in individual spots can be identified by MS (Carrette et al., 2006).

Limitations of 2-DE

However, 2-DE still has several limitations. First, the number of samples that can be run simultaneously is limited by the duration of the procedure (about 5 days) and the equipment available. Second, despite maximum precautions, there will be some degree of gel-to-gel and run-to-run variability in the expression of the same protein set. Finally, some proteins may escape the capabilities of conventional 2-DE for several reasons, including poor solubility (membrane proteins, aggregates), an extreme p*I* or exceeding the upper or lower MW size limits (Van den Bergh et al., 2003). One of the main disadvantages is the inability to visualize low-copy-number proteins when highly abundant gene products are present (Corthals et al., 2000). Although approximately 10000–30000 proteins are present in the proteome of a cell (even more in tissue), only between 1000 and 2000 of the most abundant

proteins can be visualized on a single gel (Carrette et al., 2006). Enrichment of such low abundant proteins is a preanalytical step that should be considered seriously. Various prefractionation methods have been developed, including specific cell or microorganism cultures, laser capture microdissection, fluorescence-activated cell sorting of antibody-bound cells, differential centrifugation or detergent extraction of organelles, and reversed-phase high-performance liquid or affinity chromatography (Ahmed and Rice, 2005; Michelsen and von Hagen, 2009).

2.2.2. Two-dimensional difference gel electrophoresis (2-D DIGE)

The limitations of 2-DE i.e. lack of sensitivity and reproducibility, or quantitative capacities of existing labeling reagents, has limited the use of this technique as a quantitative tool. 2-D DIGE builds on this technique by adding a highly accurate quantitative dimension (Unlu et al., 1997). 2-D DIGE enables multiple protein extracts to be separated on the same 2-DE gel. This is made possible by individual labeling of each extract using spectrally resolvable, size and charge-matched fluorescent cyanine dyes known as CyDye DIGE fluors (Cy2, Cy3 and Cy5) (Unlu et al., 1997; Zhou et al., 2002). The linearity, sensitivity, and wide dynamic range (3.6 orders of magnitude) of these fluorescent cyanine dyes have made 2-D DIGE into a quantitative technique. The detection limit of proteins using Cy2 is 0.075 ng, using Cy3 is 0.025 ng, and using Cy5 is 0.025 ng (Marouga et al., 2005). Compared with silver staining (sensitivity: 1 ng) these dyes are clearly more sensitive.

2-D DIGE involves the use of a internal reference standard, which comprises equal amounts of protein from each biological sample in the experiment (Alban et al., 2003). Including the internal standard on each gel in the experiment with the individual biological samples means that the abundance of each protein spot on a gel can be measured relative (i.e. as a ratio) to its corresponding spot in the internal standard present on the same gel.

Quantitative gel and proteome alteration analysis can be done with commercial available software tools, i.e. DeCyder 2D Differential Analysis software (GE-Healthcare). Image analysis consists of the following processes: spot detection, background subtraction, in-gel normalization, gel artifact removal, gel-to-gel matching, statistical analysis. The software automatically detects, matches, and analyzes protein spots in multiplexed fluorescent images. It contains two analysis modules, one for difference in-gel analysis (DIA), and one for biological variation analysis (BVA). The DIA module uses proprietary algorithms to detect overlapping, differently colored images within the same gel. It automatically and objectively performs background subtraction, quantification, normalization, and preliminary spot matching. The BVA module then matches images between the different gels of an experimental series, looking for consistent differences between samples across all gels being

compared. It then applies statistics to associate a level of confidence and generates a list of statistically significant differences, based on user-specified threshold parameters.

The co-separation of different samples in combination with an image analysis implementing an internal standard by the 2-D DIGE technique has the ability to reduce substantially the effects of gel-to-gel variation on the quantification of a protein spot (Gade et al., 2003). Therefore, the confidence that a difference in fluorescence intensity between two samples is due to biological rather than experimental variation has increased (Van den Bergh et al., 2003). The high variability of standard 2-DE also means there is a need to run several replicate gels for the generation of statistically confident results. The high precision and reproducibility of 2-D DIGE means that biological replicates can replace gel replicates requiring fewer gels for more accurate results (Shaw et al., 2003).

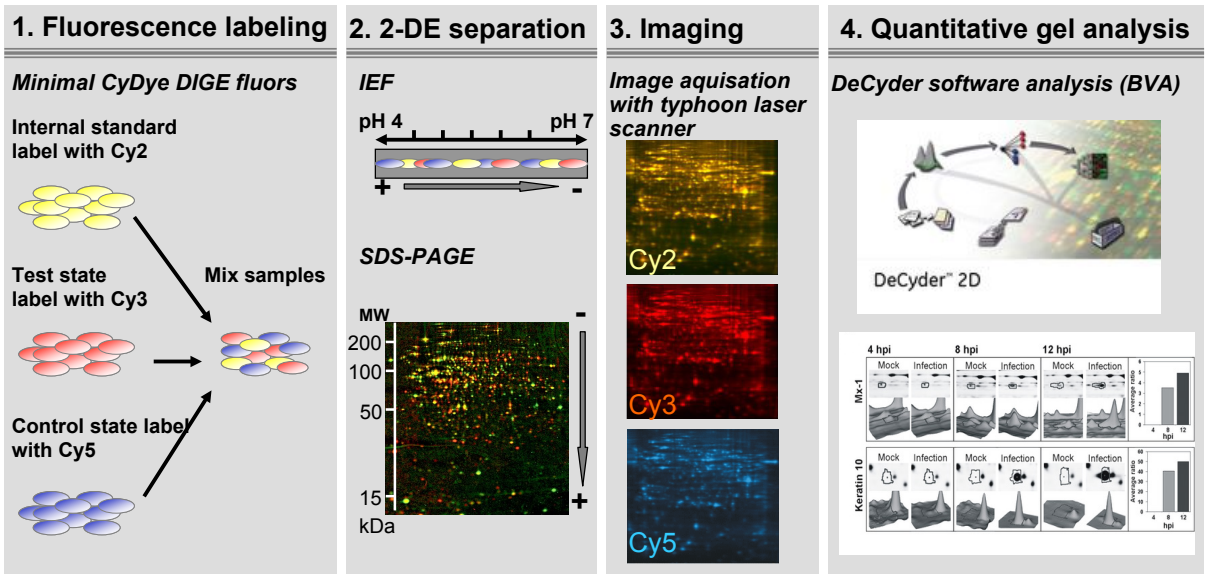

Figure 2.2-1: Overview of the 2-D DIGE technique

2-D DIGE technique enables quantification with statistical confidence for 2-DE gel experiments, where thousands of fluorescence-labeled proteins are resolved by charge/pI (using IEF) and apparent MW (using SDS-PAGE).

Many of the limitations of 2-DE have been overcome by 2-D DIGE, making it an ideal technique for comparison of different protein samples. However, 2-D DIGE still has several limitations. One of the main disadvantages is as before the inability to visualize low-copy-number proteins, limitations in the number and the types of protein that can be visualized.

2.2.3. Viral proteomics: virus-host cell interactions

Virus-host cell interactions reflect the balance of host cell defenses and virus virulence mechanisms. Advances in proteomic technologies now allow to compare protein content between complex biologic systems ranging from cells to animals and clinical samples (Viswanathan and Fruh, 2007). Thus, it is now possible to characterize virus-host cell

interactions from a global proteomic view. Most reports to date focus on cataloging protein content of viruses and identifying virulence associated proteins or proteomic alterations in host cells using mostly clinical samples or mouse models. A more in-depth understanding of virus-host cell interactions has the potential to improve the mechanistic understanding of pathogenicity and virulence, thereby defining novel therapeutic and vaccine targets. Additionally, proteomic characterization of the host cell response can provide virus specific host cell biomarkers for rapid pathogen detection and infectious diseases and characterization in biomedical research (Zhang et al., 2005).

There have been many studies using microarrays to profile cellular changes at the transcription level in response to viral infection or individual viral protein synthesis (Kellam, 2001). For example, Geiss et al. monitored the expression level of thousands of host cell mRNAs by microarray studies of human cell lines (HeLa, A549) in response to NS1 mutant influenza viruses or active and inactive influenza virus infection (Geiss et al., 2001; Geiss et al., 2002). They reported differential expression of up to 300 host cell mRNAs. Several genes involved in protein synthesis, transcriptional regulation, and cytokine signaling were induced by influenza virus replication. Deletion of the viral NS1 gene increased the number and magnitude of expression of cellular genes implicated in the IFN, NF-κB, and other antiviral pathways. However, there is also a need to determine changes at the protein level, in part because changes observed in mRNA abundance do not always correspond to changes at the protein level (Tian et al., 2004). Additionally, many viral proteins affect protein turnover without affecting the transcription rate of the protein, e.g. by promoting or interfering with polyubiquitination (Shackelford and Pagano, 2005). Virus induced changes in the cellular proteome have been assessed by comparing protein profiles before and after viral infection by proteomics techniques. 2-DE has been used to study host cell interactions by determining changes in the cellular proteome upon infection by several different viruses, where protein spots that differed before and after infection were excised and identified by MS (Maxwell and Frappier, 2007). Alfonso et al. used 2-DE to examine changes in Vero cells after infection with african swine fever virus. They identified 12 induced cellular proteins, which included redox related proteins, nucleoside diphosphate kinases, heat shock proteins and apolipoproteins (Alfonso et al., 2004). Brasier et al. reported changes in 24 nuclear proteins upon infection with respiratory syncytial virus. Such as the above-described viruses, these proteins included heat shock proteins and redox stress related proteins (Brasier et al., 2004). 2-DE analysis was also used to determine the effects of HBV replication on host cell-protein synthesis (Tong et al., 2008). 66 spots were identified as differentially abundant proteins involved in the retinol metabolism pathway, calcium ion-binding proteins, and proteins associated with protein degradation pathways. Liu et al. analyzed human cell lines infected with avian H9N2 influenza virus and possible adaptation mechanisms of avian influenza virus

(Liu et al., 2008). They described abundance changes of proteins involved in particular cellular functions, including cytoskeleton components, components of RNA-processing pathways, and regulators of cellular metabolism. Baas et al. used a macaque animal model infected with influenza A virus, combining functional non-gel based proteomic approaches and mRNA microarrays (Baas et al., 2006). In addition, the authors described the establishment of an animal model for influenza infection and biomarker profiling as an early prognostics tool for infection.

In summary, all these approaches focused on the pathogenesis in humans, discovery of novel drug targets, antiviral therapies and biomarker research in the biomedical investigation field. However, cell culture based influenza vaccine manufacturing processes have so far not been analyzed with respect to virus-host cell interactions on the proteome level.

2.2.4. Cell culture engineering using proteomic approaches

Mammalian cell culture is important for the production of biopharmaceuticals, i.e. therapeutic proteins, monoclonal antibodies or vaccines (Genzel and Reichl, 2009; Walsh, 2006). Great efforts have been made in the last ten years to identify genes and pathways to increase productivity of cell culture, to identify metabolic bottlenecks, to understand mechanism of protein synthesis, to develop better nutrients and media formulation, to reduce apoptosis and to increase growth rate. With the proteomics technology thorough high throughput studies of changes at protein levels related to product yields in different cultivation conditions and studies to establish functional relationships between cellular machinery and productivity are possible (Kuystermans et al., 2007). Proteomics in combination with cell engineering strategies provides a better understanding of cellular behavior of mammalian cells used for bioprocesses.

Some early studies using proteomic techniques to understand cellular mechanisms of product synthesis, apoptosis, cell proliferation and the influence of the physicochemical environment have been reported (Griffin et al., 2007; Gupta and Lee, 2007). A proteomic comparison of CHO cells was made between a productive recombinant clone selected at high methotrexate (MTX) concentration and clones of intermediate and low productivities (Hayduk and Lee, 2005). The authors noted a fourfold increase in actin-capping protein (CapZ). Due to similarities between CapZ and cytochalasin D, they hypothesized that the addition of cytochalasin D might result in enhanced productivity and product secretion. In combination with MTX gene amplification, the addition of cytochalasin D resulted in a 52- to 150-fold increase in recombinant protein productivity. Transcriptional profiling of apoptotic pathways in batch and fed-batch CHO cultures (Wong et al., 2006a) revealed that during periods of high viability, most pro-apoptotic signaling genes were down-regulated. However,

upon loss in viability, several early pro-apoptotic signaling genes were up-regulated. At later stages of viability loss, late proapoptotic effector genes such as caspases and DNases were up-regulated. These findings resulted in the development of cell lines, which are apoptosis resistant (Wong et al., 2006b). A transcriptomic and proteomic analysis of NS0 cells grown at different densities in perfusion culture has identified a total of 47 genes and 53 proteins that were regulated at high cell density (Krampe et al., 2008). Specifically, it was found that up-regulation of gene expressions and protein syntheses involved in energy metabolism, antiapoptosis, and cell cycle checkpoints ensured cell survival in high cell density (HCD) populations. Overall, they suggested that the balance among several factors involved in energy metabolism might be essential for fine tuning the cells choice between survival and apoptosis, leaning towards the side of apoptosis at HCD. Kumar et al. used 2-D DIGE to show that suspension adapted CHO-K1 cells respond to low culture temperature (31°C) by differential regulation of 201 proteins following the temperature shift (Kumar et al., 2008a). Their results indicate a number of key regulatory proteins and pathways (e.g. growth regulation, translation (eukaryotic initiation factor 4A), apoptosis (importin-α), cytoskeleton (vimentin) and glycoprotein quality control (alpha glucosidase 2)) that are involved in modulating the response to hypothermia.

Hence, proteomics data connected with the tremendous amounts of bioprocess data provide insights into the regulatory networks within the cell under bioprocess conditions and how to manipulate them to increase overall productivity.

2.3. Quantitative real-time PCR (qPCR) approach

2.3.1. General overview

The introduction of qPCR has changed dramatically the field of quantitative nucleic acid and gene expression analysis. This new technique is a refinement of the original PCR developed by Mullis et al. in 1985 (Saiki et al., 1985). By PCR essentially any DNA sequence present in a complex sample can be amplified in a cyclic process to generate a large number of identical copies. This made it possible, e.g. to manipulate DNA for cloning purposes, genetic engineering, and sequencing. However, the conventional PCR method had some limitations. By first amplifying the DNA sequence and then analyzing the end product, quantification was difficult since the PCR amplificates the same product amount independent of the initial template amount. This limitation was resolved in 1992 by the development of qPCR (Higuchi et al., 1992).

qPCR quantitates the initial amount of the template specifically, sensitively and reproducibly, and is the preferred alternative to other forms of quantitative PCR that detect the amount of final amplified product at the endpoint (Arya et al., 2005; Bustin and Nolan, 2004). Endpoint quantification can be affected by inhibitors, poorly optimized reaction conditions or saturation effects by inhibitory PCR by-products and ds amplicons. qPCR monitors the fluorescence emitted during the reaction as an indicator of amplicon production during each PCR cycle (i.e. in real-time). qPCR quantification eliminates post-PCR processing of PCR products (necessary in conventional PCR). This helps to increase throughput and reduces carryover contamination. In comparison to conventional PCR, qPCR also offers a much wider dynamic range of up to 1000-fold (compared to 107-fold in conventional PCR) with a wide range of ratios that can be assayed with equal sensitivity and specificity. The qPCR system is based on the detection and quantification of a fluorescent reporter (Wilhelm and Pingoud, 2003). This signal increases in direct proportion to the amount of PCR product in a reaction. By recording the amount of fluorescence emission at each cycle, it is possible to monitor the PCR reaction during exponential phase, where the first significant increase in the amount of PCR product correlates to the initial amount of target template. The higher the starting copy number of the nucleic acid target, the sooner a significant increase in fluorescence is observed. A significant increase in fluorescence above the baseline measured during 3-15 cycles indicates detection of accumulated PCR product. A fixed fluorescence threshold is set significantly above the baseline. The parameter C_q (threshold cycle) is defined as the cycle number at which the fluorescence emission exceeds the fixed threshold (Figure 2.3-1).

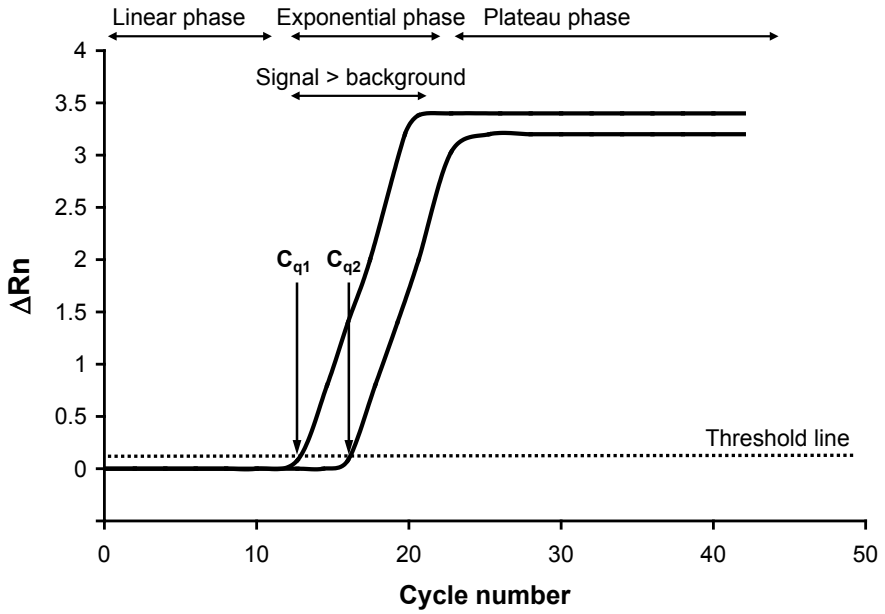

Figure 2.3-1: PCR amplification curve

The PCR amplification curve displays the accumulation of fluorescent emission at each reaction cycle. The curve can be divided into three different phases: linear, exponential and plateau phase. Data from these phases are important for calculating background signal, cycle threshold (C_q), and amplification efficiency. Picture adapted from Kubista et al. (Kubista et al., 2006).

There are three main fluorescence-monitoring systems for DNA amplification (Wittwer et al., 1997): (I) hydrolysis probes, (II) hybridizing probes and (III) DNA-binding agents. Hydrolysis probes include TaqMan probes, molecular beacons and scorpions. They use the fluorogenic 5' exonuclease activity of Taq polymerase to measure the amount of target sequences in cDNA samples. DNA binding dye chemistry quantitates the amplicon production (including non-specific amplification and primer-dimer complex) by the use of a non-sequence specific fluorescent intercalating agent (SYBR-green I). SYBR green I is a fluorogenic minor groove binding dye that exhibits little fluorescence when in solution but emits a strong fluorescent signal upon binding to dsDNA (Morrison et al., 1998).

The threshold cycle or the C_q value is the cycle at which the first significant increase in ΔRn (normalized reporter) is detected. ΔRn is the difference between Rn+ (Rn value of a reaction containing all components - sample of interest) and Rn- (Rn value detected in no-template-control (NTC)-baseline value). It is the ΔRn plotted against cycle numbers that produces the amplification curves and gives the C_q value. The exponential growth phase provides the most useful information about the reaction. The slope of the log-linear phase reflects the amplification efficiency (E). E can be calculated by the formula:

$$E = 10^{(-1/slope)} - 1 \qquad \textit{(Equation 1)}$$

The efficiency of the PCR should be 90 - 100% (-3.6 > slope > -3.1). A number of variables can affect PCR efficiency (Bustin and Nolan, 2004; Wong and Medrano, 2005). These factors include length of the amplicon, secondary structure and primer quality. For the slope to be an indicator of real amplification (rather than signal drift), there has to be an inflection point. This is the point on the growth curve when the log-linear phase begins. A C_q value of 40 or higher means no amplification and this value cannot be included in the calculations.

There are different approaches to quantitate the amount of template (Livak and Schmittgen, 2001). (I) The absolute standard curve method determines the input copy number of the transcript of interest, usually by relating the PCR signal to a standard curve. In this method, a standard curve is first constructed from RNA of known concentration. This curve is then used as a reference standard for extrapolating quantitative information for RNA targets of unknown concentrations. (II) Relative gene expression comparisons (relative standard method) use an endogenous/internal control, which is more abundant and remains constant, in proportion to total RNA. This method is also named comparative threshold method ($2^{-\Delta\Delta Ct}$). By using an invariant endogenous control as an active reference, quantification of an RNA target can be normalized for differences in the amount of total RNA. The most commonly used controls are 18S RNA, GAPDH (glyceraldehyde-3-phosphate dehydrogenase) and β-actin. The issue of the choice of a normalizer has been reviewed by Suzuki et al. (Suzuki et al., 2000). For the use of GAPDH as a normalizer it has been shown that its expression may be upregulated in proliferating cells too (Bustin, 2000). Therefore, GAPDH has to be used with caution.

Melting curve analysis

Melting curves represent the temperature dependence of the fluorescence. They are recorded subsequent to the amplification of the target sequence by PCR (Wilhelm and Pingoud, 2003). The detection can be performed either with dsDNA-specific dyes, e.g. SYBR Green I or with sequence-specific probes. Melting curves are used for genotyping of insertion/deletion polymorphisms and of single nucleotide polymorphisms (SNPs) (Maas et al., 2003), DNA methylation detection, for product characterization and specificity verification (Ririe et al., 1997). In melting curves, the signal decreases gradually as a result of a temperature-dependent quench and more abruptly at a certain temperature because of the melting of the products. The melting temperature (T_m) is defined as the temperature at which the deepest decrease of signal occurs. This can be identified conveniently as the peak value in the negative derivative of the melting curve. Additionally, the area under the curve (AUC) of the peaks is proportional to the amount of product. Therefore, melting curves may be used for quantifications with internal standardization when T_m values of sample and competitor products are significantly different. With SYBR Green I, the amplification of the correct target sequence can be confirmed. In most cases, nonspecific products have different lengths and therefore deviating melting temperatures (Ririe et al., 1997).

2.3.2. qPCR for RNA quantification

RNA gene quantification has been constrained by the lack of fast, reliable and accurate methods. Northern blotting has been used for quantification, however it can require a large amount of total RNA and is time-consuming. The advent of PCR and the combination of RT and qPCR led quickly to the use of RT-qPCR for RNA/mRNA quantification (Bustin, 2000).

Reverse transcription

Sample acquisition and purification of the RNA mark the initial step of every RT-qPCR. Isolation of total cellular RNA can be accomplished using a number of methods, such as solution-based (e.g. guanidinium thiocyanate-phenol-chloroform or alkaline extraction) and solid-phase/column-based protocols (e.g. silica matrices, anion-exchange material, magnetic bead based nucleic acid purification) (Tan and Yiap, 2009). Generally, successful RNA extraction requires four important steps: effective disruption of cells or tissue; denaturation of nucleoprotein complexes; inactivation of nucleases, e.g. RNase removal. The target RNA should be free of contaminants including protein, carbohydrate, lipids, or other nucleic acid. Quality and also integrity of the isolated RNA will directly affect the results of all succeeding scientific research (Tan and Yiap, 2009).

The initial step in RT-qPCR is the production of a single strand complementary DNA copy (cDNA) of the RNA through the action of the retroviral enzyme, reverse transcriptase (RT). Two main types of enzyme are commercially available: Moloney murine leukemia virus (MMLV-RT) and avian myeoblastosis virus (AMV-RT) (Gerard et al., 1997). Additionally, a thermostable RT isoform of the MMLV-RT exists (rTth). An oligonucleotide primer is required to initiate cDNA synthesis. This oligonucleotide primer anneals to the RNA, and the cDNA is extended towards the 5' end of the RNA through the RNA-dependent DNA polymerase activity of the RT. Primer can be either gene specific or nonspecific, both have advantages and disadvantages (Resuehr and Spiess, 2003). Random hexamer primer contains all possible nucleotide combinations of a 6-base oligonucleotide and bind to all RNAs present. Similarly, oligonucleotides consisting solely of deoxythymidine residues (Oligo-dT) anneal to the polyadenylated 3' tail found on most mRNAs. RT reactions primed by random hexamers and Oligo-dT primer maximize the number of genes that can be assayed from a small RNA sample. Alternatively, a gene specific primer can be used for the RT reaction. For some rare genes the use of sequence-specific primer increases specificity and decreases background. Notably, with gene specific primer, a separate RT reaction must be carried out for each gene of interest. The RT step is the source of most of the variability in a RT-qPCR experiment. The RT enzyme is sensitive to salts, alcohols or phenol remaining from the RNA isolation. Inter- and intraassay variabilities are therefore common for RT reactions. Additionally, it cannot be assumed that different reactions have the same RT efficiency. If one can minimize the

nonspecificity and variability in this step, then the reliability of the subsequent quantification will be increased.

Use of standard RNA molecules for absolute quantification

To obtain high precision in RT and qPCR a highly defined standard curve for absolute quantification is needed (Kubista et al., 2006). The common approach is to co-amplify a standard, either in the same or separate tube. A wide range of DNA and RNA standards have been reported (Bustin, 2000; Livak and Schmittgen, 2001). It is accepted generally that DNA standards are not an optimal choice because they do not compensate for the inherent variability in the RT step. Endogenous RNA standards or internal standards (β-actin or GAPDH) and synthetic RNAs have both been used as amplification standards. Internal standards show problems of widely differing abundance, different amplification primer, and the fact that their expression is sensitive to some experimental treatments. External standard RNAs are an improvement over endogenous standard RNAs because their levels can be controlled, however they are not homologous to the sequence of interest and are likely to have differing amplification efficiencies. A homologous synthetic RNA standard can be defined as an *in vitro* transcribed synthetic RNA that shares the same primer binding sites as the native RNA. These RNA standards are the most suitable for two reasons: (I) useable to control the variability during the RT step and (II) RNA standards have the same or very similar RT and PCR efficiencies. For *in vitro* transcription DNA dependent RNA polymerases of bacteriophage origin with different promoters (SP6, T7, T3) are used to transcribe RNA from a DNA template (Milligan et al., 1987). Synthetic RNA standards are created generally from the entire native gene, cloned into a plasmid containing an RNA polymerase promoter (SP6, T7) suitable for *in vitro* transcription (Pokrovskaya and Gurevich, 1994). An optimized protocol, which avoids labor-intensive cloning procedure was reported by Fronhoffs et al. (Fronhoffs et al., 2002) to create PCR templates containing a T7 promoter gene sequence for *in vitro* transcription.

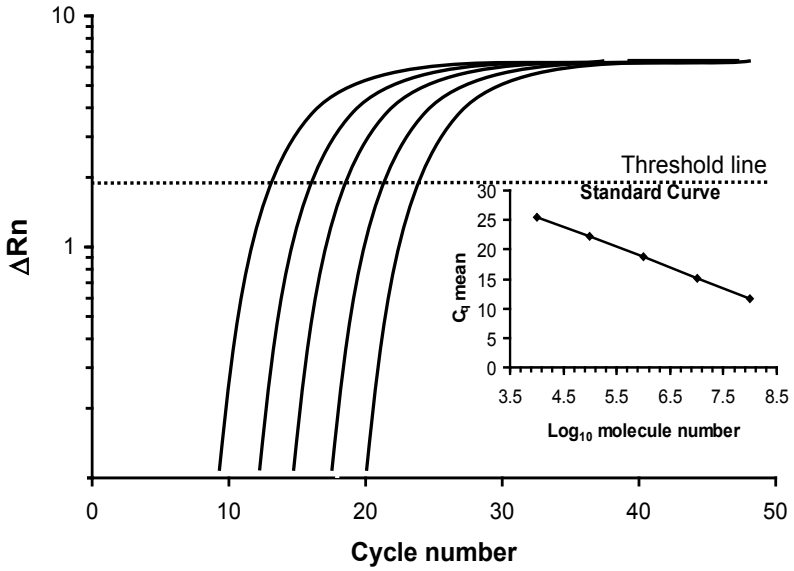

Figure 2.3-2: qPCR standard curve

qPCR amplification curves in logarithmic scale for five standard samples. Crossing points with threshold line are the C_q values. The C_q values are plotted vs. the logarithm of the initial number of template copies in the standard samples. Picture adapted from Kubista et al. *(Kubista* et al.*, 2006).*

2.3.3. The MIQE guidelines for qPCR

Currently, a lack of census exists on how best to perform and interpret qPCR assays. The 'Minimum Information for Publication of Quantitative Real-Time PCR Experiments' (MIQE) guidelines were published by Bustin et al. in 2009 to help ensure the integrity, consistency and transparency and reliability of results (Bustin et al., 2009). MIQE described the minimum information necessary for evaluating and validating qPCR assays. Following these guidelines encourages better experimental practice, allowing more reliable and unequivocal interpretation of qPCR results. Therefore, these guidelines were carefully attended for the present qPCR assay.

MIQE guidelines reviewed a number of key issues of qPCR assay validation:

Analytical sensitivity refers to the minimum number of copies in a sample that can be measured accurately with an assay. Here, sensitivity is expressed as the limit of detection (LOD), which is the concentration that can be detected with reasonable certainty (95% probability is used commonly) with a given analytical procedure.

Accuracy refers to the difference between experimentally measured and actual concentrations, presented as fold changes or copy number estimates.

Repeatability (short-term precision or intraassay variance) refers to the precision and robustness of the assay with the same samples repeatedly analyzed in the same assay. It may be expressed as the standard deviation (SD) for the C_q variance. Alternatively, the SD or the CV for copy number or concentration variance may be used.

Reproducibility (long-term precision or interassay variance) refers to the variation in results between runs or between different laboratories and is typically expressed as the SD or CV of copy numbers or concentrations.

Precision. There are many explanations for variation in qPCR results, including temperature differences affecting the completion of annealing and/or denaturation, concentration differences introduced by pipetting errors, and stochastic variation. Precision in qPCR typically varies with concentration, decreasing with the copy number. Ideally, intraassay variation (repeatability) should be displayed in figures as SD error bars or as confidence interval (99%, CI) on standard curves with replicate samples. CVs should not be used with C_q but can be used to express the variance in copy numbers or concentrations.

Linear dynamic range. The dynamic range over which a reaction is linear (the highest to the lowest quantifiable copy number established by means of a standard curve) must be described. The dynamic range should cover at least 3 orders of magnitude and ideally should extend to 5 or 6 $\log_{10}$ concentrations. Correlation coefficients (R^2) must be reported and CIs should be provided through the entire linear dynamic range.

2.3.4. qPCR in virology

Especially in the field of molecular diagnostics and pathogen detection, qPCR-based assays have become a widely accepted tool in the recent past (Espy et al., 2006). It has provided major contributions, e.g. an increase in sensitivity over conventional PCR, the ability to confirm the amplification product and to quantitate the target concentration. Furthermore, nucleotide sequence analysis of the amplification products has facilitated epidemiological studies of infectious disease outbreaks, and the monitoring of therapeutic response, in particular with viruses, which mutate at high frequency (Ratcliff et al., 2007). Viral load and antiviral resistance or subtyping assays are now part of monitoring infections by human immunodeficiency virus (HIV), HV, cytomegalovirus (CMV) or influenza virus (Ellis and Zambon, 2002). Fluorogenic PCR-based methods using TaqMan PCR technology, have been described for the detection and identification of influenza A and B viruses. In these assays, primer/probe sets targeting the M gene of influenza A and B viruses (Schweiger et al., 2000), or the M gene of influenza A and the HA gene of influenza B (van Elden et al., 2001), were designed to differentiate influenza A and B viruses. In the first of these studies, specific primer/probe sets were also selected to identify HA (H1 and H3) and NA (N1 and N2) subtypes. Moreover, besides diagnosis general virology studies have been reported monitoring the levels of specific gene activity as a result of growth under manipulated conditions. Altered viral entry or replication, caused by the modification of target tissues, can also be monitored using qPCR and can be used to link between virus replication and the expression of cellular genes (Mackay et al., 2002).

2.3.5. Analysis of influenza replication dynamics through differential quantification of influenza viral RNA types

The general mechanism of influenza virus replication in their host cells is well understood, however much about regulation of viral genome replication and transcription especially for each of the 8 RNA segments still remains unknown. For a better quantitative understanding of these complex intracellular events taking place during influenza virus life cycle, i.e. time course and control of viral RNA synthesis, quantitative experimental data are indispensable.

In many studies molecular methods such as RT-PCR (Chan et al., 2006b) or RT-qPCR techniques (Di Trani et al., 2006; Ong et al., 2007; Youil et al., 2004) have been used successfully for precise quantitative determination of the number of influenza viral copies in clinical or environmental detection assays as stated above. For example, Youil et al. compared MDCK and Vero cell lines for their ability to propagate type A and type B cold-adapted and wild type influenza viruses (Youil et al., 2004). The growth of these viruses has been measured as plaque forming units (via plaque assay) as well as viral particle formation (RT-qPCR assay) to assess the suitability of these cell lines to support the development of live attenuated influenza vaccines.

However, the standard detection RT-PCR assays do not distinguish between cRNA(+) and vRNA(-) emerging during viral genome replication or vmRNA(+) emerging during viral transcription. Hence, there are not suitable to study the time course and dynamics of viral RNA synthesis. Moreover, these detection assays used only one or two segments, e.g. M, HA or NA for detection of influenza virus. For specific determination of the number of all three different influenza viral RNA types (vRNA(-), cRNA(+), vmRNA(+)) separately a method is required that targets individually the different polarities of the viral RNA strands. Several studies have reported polarity-specific RT-PCR assays for detection of different RNA viruses such as HV (Komurian-Pradel et al., 2004), dengue virus (Peyrefitte et al., 2003) or foot-and-mouth disease virus (Li et al., 2009). Polarity-specific priming strategies to distinguish between influenza virus transcription and replication were also described before (Kumar et al., 2008b; Ng et al., 2008; Uchide et al., 2002). In one study (Kumar et al., 2008b) the authors reported the identification of a specific step of the viral life cycle that is influenced by NF-κB signaling, by using two known NF-κB inhibitors and a variety of influenza virus-specific assays (qPCR). For differential quantification they used sense specific primer during RT and gene specific primer for each of the 8 RNA segments during qPCR. The viral RNA levels, expressed as C_q values, were normalized by the RNA levels of reference genes (GAPDH). They have shown that NF-κB inhibitors decreased specifically (I) the level of vRNA(-) in virus-infected cells and (II) the level of RNA transcription from the cRNA(+) promoter. Additionally, they have provided evidence that the NF-κB molecule p65 is responsible for the

differential regulation of vRNA(-) synthesis. Ng et al. studied the role of segment-specific non-coding sequences of influenza A virus on viral RNA synthesis (Ng et al., 2008). RT-qPCR assays specific for the vRNA(-) and vmRNA(+) of NA, NS and PB2 segments were developed. For differential quantification they used oligo-dT_{20} or viral RNA specific primer during RT and gene specific primer during qPCR. They used serially diluted plasmids containing the corresponding sequences as standard controls. Recombinant viruses, with the NS segment-specific non-coding sequences replaced by the corresponding sequences of the NA segment, were characterized. The NS and NA vRNA(-) levels in cells infected with these mutants were much higher than those of the wild type, whereas the NS and NA vmRNA(+) levels of the mutants were comparable to the wild-type levels. In conclusion, their results showed that the segment specific regions have roles in controlling viral transcription and replication. Southern hybridization reported by Uchide et al. (Uchide et al., 2002) showed the quantification of specific PCR products for HA vRNA(-) and c/mRNA(+) (amplified by using polarity-specific primer) in cell culture and proved the lack of HA RNAs in mock infected cells in the absence of virus. A RT-PCR/Southern blot assay was used for monitoring influenza virus production and to evaluate the effect of antiviral agent on influenza virus genome replication and transcription steps. However, the mentioned studies used either a semi-quantitative southern hybridization technique only for HA (Uchide et al., 2002) or RT-qPCR assays, where viral copy numbers were determined by normalization to reference genes (Kumar et al., 2008b) or by viral DNA standards (Ng et al., 2008), representing only relative quantification techniques. Beside these PCR approaches primer extension assays were used widely to compare viral RNA type levels in cells infected with influenza virus (Robb et al., 2009; Vreede et al., 2008). In brief, autoradiographic analysis of extended cDNAs resulted in three radiolabeled bands of the expected sizes for vRNA(-), cRNA(+) and vmRNA(+). With this technique Vreede et al. studied the mechanisms regulating the synthesis of mRNA(+), cRNA(+), and vRNA(-) by the influenza A virus RNA-dependent RNA polymerase (Vreede et al., 2008). They showed that *de novo* synthesis of cRNA(+) *in vitro* was more sensitive to the concentrations of ATP, CTP, and GTP than capped-primer-dependent synthesis of mRNA(+). A model was presented, which shows *de novo* initiation of influenza virus cRNA(+) synthesis occurred at a vRNA(-) template residue by binding of the related NTP. Moreover, Robb et al. proposed a role for the NS2 protein in the regulation of viral transcription and replication that is independent of its vRNP export function by using vRNP reconstitution and primer extension assays (Robb et al., 2009).

In summary, these studies used diverse techniques and most of the results are contradictory. Therefore, different hypothesis are suggested to describe dynamics of viral replication. Hence, it is still not clear whether at all the relative viral RNA amounts are regulated during the viral life cycle

3. Materials and Methods

3.1. Equipment, materials and chemicals

A complete list of chemicals, equipment and materials is given in the Appendix in Table A-D.

3.2. Cell culture and virological methods

Liquid handling was done under a laminar flow box using autoclaved or sterile filtered solutions, sterile plastic material or autoclaved glass ware and sterile media. Cell lines were cultured at 37°C, 5% CO_2 and with saturated humidity.

3.2.1. Cultivation/passaging methods

Cells were grown in corresponding media (Table B-1-4, Appendix) in static cultures (passaged every 4–7 days, when confluent). Static cultures were inoculated with corresponding cell numbers and cell growth media volume for about 4-7 days. When fully confluent, the cells were washed three times with phosphate-buffered saline (PBS - NaCl (8.00 g/L), KCl (0.20 g/L), KH_2PO_4 (0.20 g/L), Na_2HPO_4 (1.15 g/L) in H_2O_{MP}), and were detached by exposure to trypsin solution (0.05% trypsin / 0.02% EDTA in PBS) for 20 min at 37°C. The trypsin activity was stopped by addition of an equal volume of cell growth media to the trypsin/cell solution. Cell solution was transferred into new static culture vessel with fresh cell growth media. Simultaneously, a sterility test was prepared by addition of about 2.5 mL cell solution per casein peptone soy peptone medium (CASO: 30 g/L CASO in H_2O_{MP}) flask and incubation at 37°C. Sterility is confirmed after a minimum of 14 days of incubation with negative result. Inoculation cell densities, used culture vessels and corresponding media and trypsin volume are summarized in Table 3.2-1.

Table 3.2-1: Summary of conditions for cell lines used

Cell line	Inoculation cell density (cells/mL)	Vessel/media volume (mL)	Trypsin/EDTA volume (mL)
A549	4.0×10^4	T175/100, T75/50, T25/20	5, 3, 1
HepG2	3.2×10^5	T175/100, T75/50, T25/20	5, 3, 1
NCI-N87	$3.0 – 4.0 \times 10^5$	T175/100, T75/50, T25/20	5, 3, 1
MDCK	$1.0 – 2.0 \times 10^5$	RB*/250, T25/20, 6 cm dish/10	10, 1
Vero	2.0×10^5	T25/20	1

** RB – roller bottle*

3.2.2. Freezing/storage of cells

Cells were stored as master cell bank over long periods in cryo tubes in liquid nitrogen (-135°C). For that purpose, confluent grown cells were processed as described in the

passaging method part before. After centrifugation (500 × *g*, 5 min) the pellet was dissolved in special cryo medium (corresponding cell growth medium and 10% dimethyl sulfoxide (DMSO)) to cell densities of 2-4 × 10^6 cells/mL. Cryo cell solution was subdivided in 1.5 mL cryo tubes and frozen for 2 h at -20°C and subsequently at -80°C overnight. For final long-term storage aliquots were transferred into liquid nitrogen. For re-cultivation cells were quickly unfrozen in a 37°C water bath and suspended in pre-warmed cell growth medium. After centrifugation (500 × *g*, 5 min) cells were dissolved additionally in fresh pre-warmed cell growth medium to remove DMSO, transferred into cell culture vessels and cultured under standard procedures. After 1 day cells were washed with PBS and fresh medium was added.

3.2.3. Cell concentration

Determination of cell concentration was done according to standard operation procedures (SOP Nr. Z/01; Nr. G/21; Appendix F). Therefore, medium was aspirated and cells were washed three-times with PBS. Next, cells were incubated with trypsin solution for detachment such as described in section 3.2.1. The trypsin activity was stopped by addition of an equal volume of cell growth media to the trypsin/cell solution. The density of this cell suspension prior to seeding/infection was determined either manually by counting under the microscope using a hemacytometer or automatically using a ViCell XR counting device (Beckman-Coulter, Krefeld/Germany).

3.2.4. Basic extracellular metabolites

Off-line measurement of basic extracellular metabolites i.e. glucose, lactate, glutamine, ammonia and glutamate was done using the Bioprofile 100 Plus (Nova Biomedical, Rödermark, Germany) (SOP Nr. A/02; Appendix F). Dilution series of standards of each metabolite used for quantification were measured minimum in triplicate. Standard measurements were performed before and after each series of measurement. Measuring ranges and relative standard deviations of the method (RSD in %) are shown in Table 3.2-2 (Genzel and Reichl, 2007).

Table 3.2-2: Validation results for a Bioprofile 100 Plus

	Glucose	Lactate	Glutamine	Glutamate	Ammonia
Concentration (mM)	1.1 – 41.1	2.3 – 27.0	0.2 – 2.6	0.2 – 2.6	0.2 – 5.2
RSD (%)	1.3	1.5	1.2	1.6	1.5

Molar yield-coefficients $Y_{Lac/Gluc}$ and $Y_{Amm/Gln}$ were calculated with the concentrations of the respective metabolites at different time points with the following equation:

$$Y_{P/S} = \frac{P_{t_n} - P_{t_0}}{S_{t_0} - S_{t_n}} \qquad \textit{(Equation 2)}$$

$Y_{P/S}$ = *molar yield-coefficient*

P_{t_n} = *product concentration [mmol·L^{-1}] at time point n h*

P_{t_0} = *product concentration [mmol·L^{-1}] at time point 0 h*

S_{t_0} = *substrate concentration [mmol·L^{-1}] at time point 0 h*

S_{t_n} = *substrate concentration [mmol·L^{-1}] at time point n h*

3.2.5. Virus infection

Cells were grown in static cultures with corresponding media (Table B-1-4, Appendix) to confluence level. Growth medium was withdrawn and cells were washed three-times with PBS before adding a serum-free virus maintenance medium (VMM) (Table B-1-4, Appendix). For multi-cycle infection of cells, trypsin (Invitrogen, 500 U/mL) was added to supernatants at a final activity of 500 U/T175, 250 U/T75 and 50 U/6 cm dish. A summary of characteristic parameters is shown in Table 3.2-3. Infection for proteome analysis was done without trypsin addition to the medium to prevent proteolytic degradation during protein extraction. Virus seed was added at the corresponding multiplicity of infection (MOI) based on infectious virus particle concentration determined as tissue-culture infectious dose ($TCID_{50}$/mL) (Mahy and Kangro, 1996) on cell concentrations summarized in Table 3.2-3 for the respective experiments. For viral RNA quantification experiments an additional 1h incubation step at 4°C was performed for synchronization of infection. Subsequently, cells were washed again with PBS to remove unbound virus particles and fresh VMM was added. Infections were carried out for desired periods under identical conditions as during cell growth. As untreated control mock infections were performed, simulating the procedure for virus infection without virus addition. Therefore, control and virus infection were processed identically.

Table 3.2-3: Summary of infection conditions used

Approach		Vessel/ media volume (mL)	VMM	Cell concentration at time of infection (cells/mL)	Virus strain
Cell culture	**A549**	T75/50	F12K/MEM	2.1×10^5	A/PR/8/34-RKI *
		T175/100	F12K/MEM	4.3×10^5	A/PR/8/34-RKI *
	HepG2	T75/50	MEM/RPMI	5.2×10^5	A/PR/8/34-RKI *
		T175/100	MEM/RPMI	4.4×10^5	A/PR/8/34-RKI *
	NCI-N87	T75/50	RPMI/MEM	3.5×10^5 - 2.4×10^5	A/PR/8/34-RKI *
		T175/100	RPMI/MEM	2.8×10^5 - 3.5×10^5	A/PR/8/34-RKI *
Proteomics	**A549**	T25/20	F12K	2.0×10^5	A/PR/8/34-RKI *
	MDCK	T25/20	GMEM	5.0×10^5	A/PR/8/34-RKI *
		T25/20	GMEM	7.0×10^5	A/PR/8/34-NIBSC #
	Vero	T25/20	GMEM	3.2×10^5	A/PR/8/34-RKI *
		T25/20	GMEM	3.2×10^5	A/PR/8/34-RKI-Vero ad. x
qPCR	**MDCK**	6 cm dish/10	GMEM	1.2×10^6	A/PR/8/34-RKI *
		RB/250	GMEM	5.6×10^5	A/PR/8/34-RKI *

** RKI - Robert Koch Institute (Berlin, Germany), # NIBSC - National Institute for Biological Standards and Control (Hertfordshire, UK), x Vero ad. – virus adaptation to Vero cells over 5 passages*

3.2.6. Virus quantification

Hemagglutination assay

Hemagglutination assay was done according to SOP (Nr. V/05; Appendix F). Titration of influenza virus by hemagglutination is based on the method described by Mahy and Kangro (Mahy and Kangro, 1996). For each sample (100 µL), two serial 1:2 dilutions were made in round-bottomed 96-well microtiter plates containing 100 µL PBS. To each well 100 µL of a red blood cell (RBC) solution (2×10^7 RBC/mL; RBC diluted 1:2 with alsevers solution (20.5 g/L glucose, 8.0 g/L sodium citrate, 0.55 g/L citric acid, 4.2 g/L NaCl in H_2O_{MP})) was added and incubated for 60–90 min at room temperature. The last dilution showing complete hemagglutination was taken as the end point and was expressed as log HA units per test volume (100 µL). An internal standard was used to compensate fluctuations caused by the varying quality of RBC. The assay was validated with a dilution error for standard HA test: ± 0.3 log HA units/ 100 µL. From HA units, total virus particle concentrations or virus yields were calculated based on the assumption that at the last dilution of virus showing complete agglutination, the ratio of RBC and virus particles is equivalent:

$$\textit{Total virus particle concentration [virions/mL]} = c_{RBC} \times 10^{(\log HA/100\mu L)} \qquad \textit{(Equation 3)}$$

The detection limit was 0.3 log HA units/100 µL corresponding to about 2.0×10^7 virions/mL.

Active virus titration- $TCID_{50}$ assay

Active virus titration ($TCID_{50}$) (Mahy and Kangro, 1996) was done according to SOP (Nr. V/08; Appendix F). Confluent grown MDCK cells in a 96-well plate and a 10-fold serial dilutions of the culture supernatants were prepared in VMM with addition of gentamycin (1% v/v). Prior to inoculation, the MDCK cells were washed three-times with 100 µL PBS per well. To each well, 100 µL of the diluted culture supernatants was added for inoculation (eight replicates per dilution). After 1 day cultivation, 100 µL of VMM with gentamycin was added to each well, and the plate was incubated subsequently for another day. The plate was washed once with PBS and 100 µL of ice-cold acetone solution (80%) was added to each well for fixation (30 min, 0°C). Then the plate was washed three-times with PBS before addition of the primary antibody (40 µL per well of a 1:5 dilution (PBS): equine influenza A anti-goat produced in goat (nanoTools, Teningen, Germany)). After 60-min incubation (37°C) the plate was washed three-times with PBS and the secondary antibody (40 µL per well of a 1:500 dilution with PBS; Molecular Probes) was added. The plate was washed three-times with PBS after 60 min incubation (37°C) and a final volume of 100 µL PBS was added before fluorescence microscopy. The titers of infectivity were calculated from eight replicates according to the method of Spearman-Kärber (Mahy and Kangro, 1996). The quantification limit was 3.2×10^2 infectious virus particles/mL with an error of ±0.3 log.

3.2.7. Propidium iodide staining of cell nucleus

For propidium iodide staining of the cell nucleus the cells were cultured until confluence in 96-well plates (flat bottom) and washed twice with PBS. Digitonin (1 mg/mL in DMSO; Sigma-Aldrich) was used for permeabilisation of the cells. For fixation 1% paraformaldehyde (PFA) was used. After 2 h incubation at 4°C cells were washed three-times with PBS. RNAs were digested by addition of RNAse A (final concentration 1 mg/mL) for 30 min at 37°C. Cells were covered with propidium iodide (1 mg/mL in H_2O_{MP}; 1.5 mM; Sigma-Aldrich) for 1-5 min. Fluorescence-stained cells were examined with a laser scanning microscope 510 (Carl Zeiss AG, Jena, Germany) using an absorption maximum of 535 nm and an fluorescence emission maximum of 617 nm (Schulze-Horsel et al., 2009).

3.3. Methods for protein analysis

3.3.1. Protein extraction

Whole cell proteins were extracted at selected hpi according to Vester et al. (Vester et al., 2009). At each time point the medium was aspirated, cells were washed twice with 250 mM sucrose buffer and 1 mL of 2-D DIGE-compatible lysis buffer (7 M urea, 2 M thiourea, 4% 3-[(3-Cholamidopropyl)dimethylammonio]-1-propanesulfonate (CHAPS), 30 mM Tris, pH 8.5 – 9.0) was added for chemical lysis. After complete lysis protein samples were sonicated for additional mechanical extraction on ice with 2 × 10 s bursts with the Sonotrode SonoPuls (Bandelin Electronic, Berlin, Germany) and incubated for 30 min at room temperature. Removal of cell debris, DNA and membranes by centrifugation (36 000 × *g*, 30 min, 20°C) yielded a soluble protein fraction. The protein content was determined using the Bradford assay (Bradford, 1976). After extraction, proteins were used for a multiplexed proteome analysis by the 2-D DIGE method (Gade et al., 2003).

3.3.2. Protein labeling

Minimal CyDye labeling (GE Healthcare, München, Germany) was performed at a ratio of 50 µg of protein to 200 pmol of Cy3 (mock infection, control state), Cy5 (infection, test state) or Cy2 (internal standard, pool of the two samples). Non-specific labeling was excluded by additional dye swap experiments to allow labeling of each sample with Cy3 and Cy5. Labeling was performed according to the manufacturer's protocol. Briefly, labeled samples were vortexed and incubated on ice for 30 min in the dark. The reaction was quenched by addition of 1 µL of 10 mM lysine, vortexed, and incubated on ice for further 10 min in the dark. Labeled samples were pooled and an equal volume of '2 × lysis' buffer (7 M urea, 2 M thiourea, 1% CHAPS, 1% carrier ampholytes pH 3-10 (GE Healthcare) and 1% dithiothreitol (DTT)) was added as well as a rehydration buffer (6 M urea, 2 M thiourea, 1% CHAPS, 0.5%

carrier ampholytes pH 3-10 (GE Healthcare) and 0.4% DTT) to a final volume of 450 µL. The total protein amount on each gel was about 150 µg. Individually, up to 250 µg unlabeled protein mix was loaded additionally to the labeled protein mix for protein identification.

3.3.3. Protein separation by 2-DE

IEF was carried out using the IPGphor system (GE Healthcare) and commercial 24-cm long IPG strips (pH 4-7, linear, GE Healthcare). The following settings and conditions for active rehydration of the IPG strips, sample entry and IEF were modified compared to Goerg et al. (Goerg et al., 2000): constant temperature at 20°C, (1) 30 V for 7 h, (2) 60 V for 6 h, (3) 200 V for 1 h, (4) 1000 V for 1 h, (5) a gradient to 8000 V for 0.5 h and (6) 8000 V for 8h, resulting in a total of about 65000 Vh. Moist filter papers were put between the electrodes and the IPG gel after completion of step (3). After IEF the IPG strips were equilibrated for 15 min in equilibration buffer (6 M urea, 30% glycerol, 2% SDS, 0.05 M Tris-HCl, pH 8.8, 0.01% bromphenol blue) supplemented with 1% DTT. A second equilibration step of 15 min with the same equilibration buffer, supplemented with 2.5% iodacetamide, was carried out subsequently. SDS-PAGE was done according to the method of Laemmli (Laemmli, 1970) using the Ettan Dalt II system (GE Healthcare). Gels (375 mM Tris-HCl, 0.1% SDS and 10% acrylamide) were poured between low-fluorescent glass plates, of which one plate was treated with bind-silane (Sigma-Aldrich, Taufkirchen, Germany). Twelve parallel gels were run at 25°C (running buffer: 25 mM Tris, 192 mM glycine and 0.1% SDS). The IPG strips were sealed with 0.5% agarose in SDS running buffer on top of the gels. Electrophoresis was conducted overnight at 2 W/gel and was stopped when the bromophenol blue marker reached the end of the gels.

3.3.4. Image acquisition and analysis

Cy2-, Cy3- and Cy5-labeled protein images were produced by excitation of gels at 488, 532 and 633 nm, and emission at 520, 590 and 680 nm, respectively, using the Typhoon Variable Mode Imager 9400 (GE Healthcare). Gels were scanned directly between the low-fluorescent glass plates with a resolution of 100 µm and a standard pixel volume of 60 000-80 000 for all scans. Determination of protein abundance and statistics based on 2-D DIGE were carried out with the DeCyder 2D software package (version 6.04.11, GE Healthcare) as described before (Gade et al., 2003). Briefly, spot detection was used to merge Cy3 with Cy2, and Cy5 with Cy2, and the volume ratio data for each pair was obtained by normalizing the merged gel. This was identical to the volume ratio (Cy3:Cy2 and Cy5:Cy2) of each gel, which was labeled with Cy2 as the internal standard. The average ratio of abundance was calculated for each spot after all Cy2, Cy3, and Cy5 images were correlated. To assess biological variation three individual infection experiments were carried out and a minimum of four gel replicates were used for inter-gel matching performed with the BVA mode. Analysis for significance

using a Student's t-test was done for those proteins found to be different in mock infection and infection samples. Only protein spots showing a high-significance ($p < 0.001$) and at least a 1.7-fold difference in abundance (ratio of mean normalized spot volume of mock versus infected samples) were considered as up- or down-regulated. These protein spots of interest were selected for identification by MS.

3.3.5. Protein identification by nanoHPLC-nanoESI-MS/MS

After separation, protein spots were picked from 2-D DIGE gels using an Ettan spot picker (GE-Healthcare). The proteins were digested with porcine trypsin in gel and identified by nanoHPLC-nanoESI-MS/MS. Fully automated online pre-concentration and separation of the tryptic digested samples was performed using a set of capillary- and nanoHPLC instruments of the Agilent 1100 Series (Agilent, Waldbronn, Germany) operated in series. Mass spectrometric detection was carried out by online coupling nanoHPLC with a QSTAR XL (QqTOF) mass spectrometer (Applied Biosystems/MDS/Sciex, Darmstadt, Germany) operated in MS and MS/MS mode. The instrument was equipped with an online nano-electrospray ion source (NanoSpray II Source) and upgraded with a heated interface. Data interpretation of acquired ESI-MS/MS peptide spectra was performed via automatic database search of product-ion spectra using MASCOT (Perkins et al., 1999) (version 2.2, Matrix Science, London, UK). For final protein confirmation at least two product-ion spectra of different peptides of each identified protein were verified manually. A detailed description of the procedure for identification of the proteins is given in the Appendix (section E). Special handling precautions were used to minimize human keratin contamination, e.g. working particle and dust-free (handling, equipment, chemicals). Additionally, during spot picking, tryptic digestions and MS handling steps several negative controls were conducted.

3.3.6. Western blot analysis

Equal amounts of protein extracts were diluted in SDS sample buffer (250 mM Tris-Cl, pH 6.8; 40% glycerol; 8% SDS; 0.01% bromophenol blue; 10% β-mercaptoethanol) and heated at 95°C for 5 min. Subsequently, proteins were separated by SDS-PAGE (SDS-10%) and electrotransferred to polyvinylidene fluoride (PVDF)-membranes (Milipore, Schwalbach/Ts., Germany) using a wet-blot blotting system (BioRad, Hercules, CA, USA) according to standard protocols (Laemmli, 1970). The membranes were blocked with Tris buffered saline (TBS), containing 0.05% Tween-20 (TTBS) and 5% nonfat dry milk for 1 h at room temperature. Primary antibodies against NS1, actin and Mx1 (Santa Cruz biotechnology, Santa Cruz, CA, USA/Cell signaling, Leiden, Netherlands) were diluted in TTBS containing either 5% nonfat dry milk or 5% BSA in experimentally optimized final dilutions. Membranes were incubated with primary antibody dilutions over night at 4°C. Prior to the addition of secondary antibodies membranes were washed three-times with TTBS. Secondary

antibodies (peroxidase-conjugated donkey anti-rabbit or peroxidase-conjugated donkey anti-mouse, Jackson Immuno Research Laboratories, Suffolk, UK) were added at experimentally determined optimal dilutions ranging from 1:10000 to 1:30000 diluted in TTBS containing 5% nonfat dry milk powder. After incubation for 1 h, blots were washed three-times with TTBS. Blots were developed with 1.5 mL of SuperSignal West Dura Extended Duration Substrate (Thermo Scientific, Waltham, MA, USA). Bands were detected with a Chemolumineszenz Imager CHEMOCAM (INTAS, Göttingen, Germany) detection system. Band intensities were normalized to ERK2 (Santa Cruz biotechnology) as a loading control and quantified using the Gel Pro Analyzer Software (Media Cybernetics, Bethesda, MD, USA).

A typical workflow for the whole proteomic/2-D DIGE approach is shown in Figure 3.3-1.

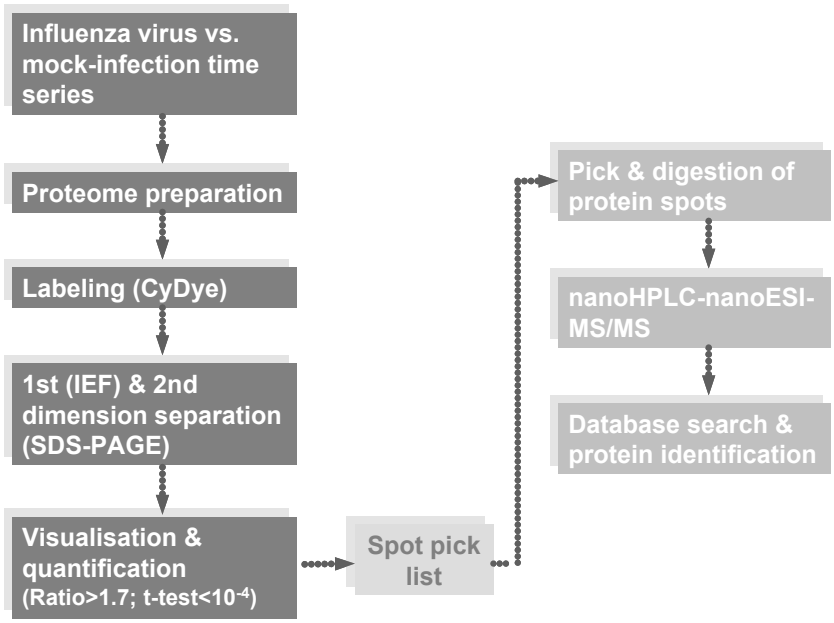

Figure 3.3-1 Workflow for the proteomic/2-D DIGE approach

Proteome difference abundance analysis and protein identification steps including protein extraction, CyDye labeling, IEF using IPG strips, SDS-PAGE, fluorescence scanning, image analysis with the Decyder 2D software package, and automated excision and identification via nanoHPLC-nanoESI-MS/MS of differentially abundant spots.

3.4. Analytical methods for nucleic acid quantification

3.4.1. Extraction of total cellular RNA from cells

Infection was performed under standard conditions (6 cm dishes, influenza A PR/8-RKI, MOI= 6, 4°C step; section 3.2.5). RNA was extracted at selected hpi. Following the removal of supernatant, cells were washed with PBS and total cellular RNA was extracted from cells with NucleoSpin RNA II (Macherey-Nagel, Düren, Germany). At first, lysis buffer RA1 was added directly to the infected cells, which were collected with a cell scraper. The rest of the extraction protocol was done according to the instructions of the manufacturer.

3.4.2. Synthetic viral RNA reference standards

Synthetic viral RNAs used as reference standards for the validation and quantification procedure were prepared for each viral RNA type (vRNA(-), cRNA(+), vmRNA(+)) for the viral segments 4 (HA), 6 (NA), 7 (M) and 8 (NS)). The QIAamp Viral RNA Mini kit (Qiagen, Hilden, Germany) was used to extract vRNA(-) from 280 µL supernatant of infected MDCK cells at 72 hpi. Infection was performed under standard conditions (influenza A PR/8-RKI, MOI= 6) (section 3.2.5). Extraction protocol was done according to the instructions of the manufacturer. Universal RT (uniRT) was carried out using Superscript II RT (Invitrogen, Carlsbad, CA, USA) and the primer Uni12 (M) (Chan et al., 2006b) (Table C-2, Appendix), which is complementary to the conserved 12 nucleotides of the 3' end of all influenza A virus RNA segments. Briefly, 10 µL of the RNA preparation was mixed with 1 µL of 15 pmol Uni12 (M) and 2 µL of 12.5 mM dNTP to a total volume of 13 µL. The mixture was incubated for 5 min at 65°C. After a cooling step to 4°C, 5 µL 5 × firststrand buffer, 4 µL 25 mM MgCl2, 2 µL 0.1 M DTT and 1 µL Superscript II RT (50 U/µL) were added. RT reaction was carried out at 42°C for 60 min and was terminated by heating at 70°C for 5 min. A negative control with either water as template or without primer addition was handled in parallel with each reaction. The cDNAs obtained were used for primer extension PCR to create templates containing a T7 promoter gene sequence for *in vitro* transcription of synthetic viral RNAs (Fronhoffs et al., 2002). In brief, a T7 phage polymerase promoter sequence (21 nt) was added to the 5' end of the corresponding primer, summarized in Table C-2 (Appendix), in conventional PCR assays for full-length amplification. Resulting PCR products were *in vitro* transcribed using the TranscriptAid T7 High Yield Transcription Kit (Fermentas, St. Leon-Rot, Germany) including DNase digestions following the manufacture's protocol. Alternatively, the PCR products were cloned by standard procedure in pGEM-T Easy vectors (Qiagen, Hilden, Germany) according to manufactures instructions. The RNA transcript was purified using the 'clean-up of RNA from the reaction mixtures' protocol of the NucleoSpin RNA II kit (Macherey-Nagel). Purity was verified by electrophoresis on formaldehyde gels and concentration was determined by spectrophotometry. The amount of RNA transcripts was converted to molecular copies based on the molecular weight of the corresponding base pair.

$$n_{(molecule)} = \frac{m_{(template)} \cdot N_A}{k \cdot N_{(base)} \cdot 10^9} \qquad \textit{(Equation 4)}$$

$n_{(molecule)}$	*number of molecules*
$m_{(template)}$	*template [ng]*
N_A	*Avogadro constant: $6.022 \cdot 10^{23}$ [mol^{-1}]*
k	*average mass of base pair [ssDNA 325 Da/bp] or base respectively [ssDNA 325 Da/base; ssDNA 340 Da/base]*
$N_{(base)}$	*number of bases of used molecules*

3.4.3. Reverse transcription quantitative real-time polymerase chain reaction (RT-qPCR) assay

Polarity-specific priming reverse transcription (pspRT)

A separate quantitative pspRT step with total cellular RNA extracts, together with the corresponding RNA standard curve (10-fold dilution series prepared with synthetic viral RNA reference standards) was performed using the protocol described above (uniRT), but using only 4 µL RNA template instead of 10 µL. To initiate the cDNA synthesis from the vRNA(-), a gene specific forward primer (-RTfor) of the corresponding viral segment was used (Figure 3.4-1). Accordingly, a gene specific reverse primer (+RTrev) of the corresponding viral segment was used to initiate synthesis from the positive stranded viral RNAs (vRNA(+) = vmRNA(+) and cRNA(+)), whereas a conventional Oligo-dT primer with 5' T additions (Oligo-dT) served for the synthesis of vmRNA(+) (Table C-3, Appendix). Finally, the molecule number of cRNA(+)s was determined by calculating the vRNA(+) minus the vmRNA(+).

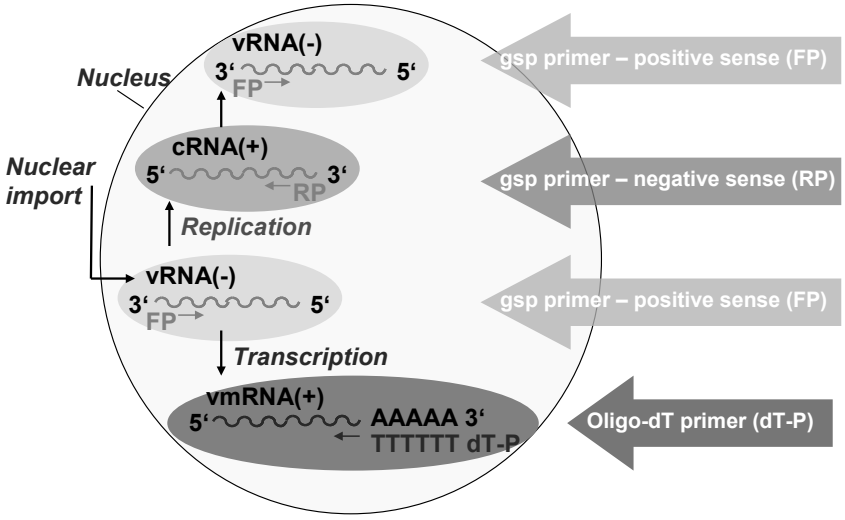

Figure 3.4-1: Polarity- and gene specific priming strategy during pspRT

Differentiation between the three viral RNA types (vRNA(-), cRNA(+), vmRNA(+)) synthesized in the nucleus. FP - forward primer, RP - reverse primer, dT-P - Oligo-dT primer, gsp - gene specific primer.

Quantitative real-time PCR (qPCR)

The qPCR step was performed using the qPCR Core kit for SYBR green I QGS (Eurogentec, Köln, Germany) on an iCycler iQ (Biorad, Hercules, CA, USA) using software version v.3.1.7050 in 96-well format. Briefly, qPCR reaction components were set-up in triplicate according to the manufacturer's instruction and were supplemented with 1 µL viral cDNA from the pspRT step and 18 pmol of corresponding forward and reverse real-time primer (Table C-3, Appendix) in a 25 µL reaction volume. Standard cycling conditions were 95°C for 5 min, followed by 40 cycles of 95°C for 15 s, 58-62°C for 15 s, 72°C for 1 min and an additional melting curve analysis (65°C, 10 s, 60 cycles, 0.5°C temperature rise steps) was

carried out. For primer-annealing 58°C for segment 4 (HA) and 7 (M) and 62°C for segment 6 (NA) and 8 (NS) were used. A negative control with water as sample was included in each run. The quantity of all three viral RNA molecules of the four viral segments was determined using the corresponding synthetic viral RNA standard curve, processed in parallel. Specificity of the PCR products was monitored with melting curve analysis. A typical workflow for the RT-qPCR assay is shown in Figure 3.4-2. Especially for vmRNA(+) of segment 7 and 8, only the vmRNA(+) splice variants of M1 and NS1 were detected, due to the choice of PCR primer binding sites (Table C-3, Appendix) at the viral segments. The total average number of RNA molecules per cell was obtained taking into account the dilutions made during cDNA synthesis and qPCR and the total number of cells used for RNA extraction.

$$c_{RNA} = \frac{V_{(RNA-E)} \cdot V_{(RT-total)}}{V_{(cDNA)} \cdot V_{(RNA-RT)}} \cdot cell\ count^{-1} \cdot 10^{\frac{Cq-b}{a}} \qquad \textit{(Equation 5)}$$

c_{RNA}	*intracellular RNA concentration [molecules/cell]*
$V_{(RNA-E)}$	*elution volume of RNA extraction [µL]*
$V_{(RT-total)}$	*total volume of RT reaction [µL]*
$V_{(RNA-RT)}$	*RNA extract volume used for RT reaction [µL]*
$V_{(cDNA)}$	*cDNA volume used for qPCR reaction [µL]*
C_q	*quantification cycle*
b	*ordinate intercept of regression curve*
a	*slope of regression curve*
cell count	*total cell number*

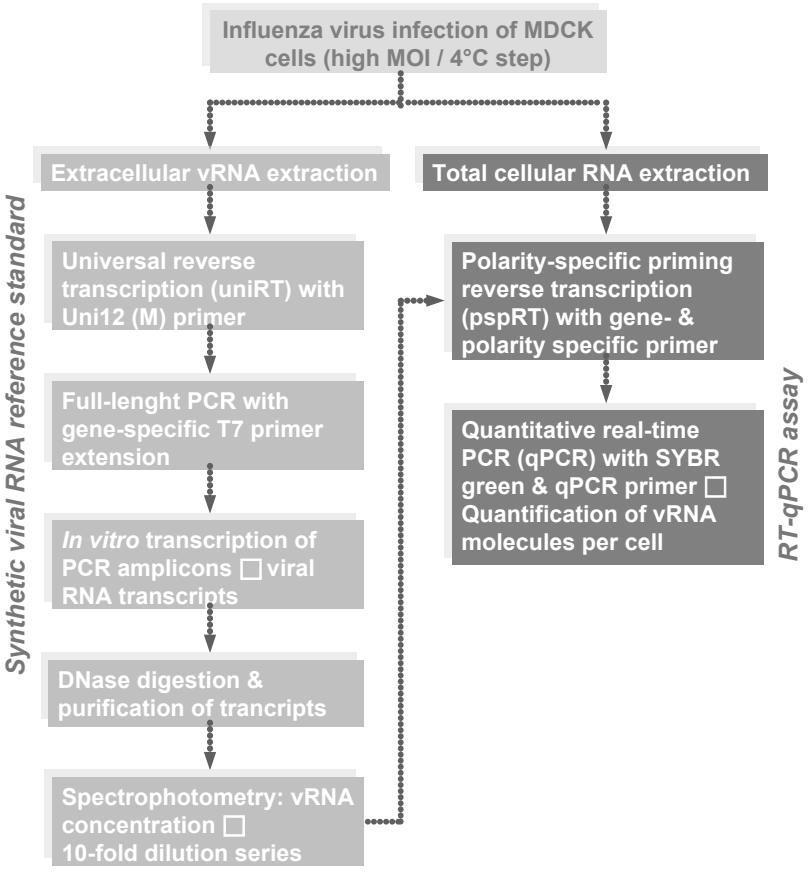

Figure 3.4-2: Workflow for the RT-qPCR assay

3.4.4. Validation procedure for the RT-qPCR assay

A polarity and sequence-specific standard curve was generated by 10-fold serial dilution of synthetic viral RNA reference standards (vRNA(-), cRNA(+), vmRNA(+) of viral segments 4 (HA), 6 (NA), 7 (M) and 8 (NS)). Regression analysis including calculation of standard curve slopes and intercepts (quantification cycle C_q versus log viral RNA quantity), amplification efficiencies E and linearity of the assay was done. Standard curve estimations were also used to confirm sensitivity (LOD), repeatability (intraassay variation) and reproducibility (interassay variation) of the assay.

Specificity and sensitivity

Specificity of the assay was assessed by processing NTCs during pspRT and qPCR and no-primer controls (NPCs) or exchange of polarity-specific primer during pspRT. Additionally, uninfected total cellular RNA extracts were tested and melting curve analysis of PCR products was done to exclude unspecific products or primer dimer synthesis. Finally, specificity of the assay was confirmed by direct sequencing of full-length PCR products used for production of reference standards as well as PCR products of qPCR. Serial dilutions in the range of 1.0×10^{0} – 1.0×10^{-7} ng/µL RNA of the viral reference standards were used in triplicate to determine sensitivity of the assay. For calculation of the corresponding number of RNA molecules a cDNA reference standard curve was processed in parallel in qPCR.

Repeatability/Reproducibility

Serial dilutions within a range of 1.0×10^{0} – 1.0×10^{-5} ng/µL RNA of the corresponding viral RNA reference standards were used to determine the repeatability and reproducibility of the assay. CV for evaluation of the repeatability was calculated by testing three technical replicates of dilution series in the same RT-qPCR assay. To estimate the reproducibility, dilution series were analyzed in independent triplicates in three different RT-qPCR assays.

$$CV = 100 \cdot \frac{SD}{\bar{x}} \qquad \textit{(Equation 6)}$$

CV *coefficient of variation [%]*
SD *standard deviation*
$\bar{x}$ *mean value*

Linear Regression analysis of validation data

Assay reproducibility studies were also used for checking the requirements for a linear regression analysis by several statistical tests, i.e. the normality of the distributions of residuals using the David test (David et al., 1954), and the homogeneity of variances with the F-test. The Grubb's test was used to detect outliers. Using linear regression a partial regression line was calculated, which describes the best linear relationship between the $\log_{10}$

RNA molecule concentrations and the estimated C_q values. After determination of the standard errors the individual predicted values were transformed into CIs (level of significance P=99%) around the corresponding observed C_q values. This analysis of variance was used to test whether the relationship between observed and expected RNA molecule concentrations is significant and therefore reliable.

Validation of total cellular RNA extraction

The validation procedure was extended to the total cellular RNA extraction from MDCK cells (section 3.4.1) by normalization to the cell reference genes β-actin and GAPDH (Gropp et al., 2006). Linearity tests of a serial dilution of MDCK cell lysates before application to extraction columns were performed. CV for evaluation of the reproducibility of total cellular RNA extraction was calculated by testing five technical replicates. The RT-qPCR assay was performed using the protocol described above (section 3.4.3) using primer for the corresponding cell reference genes β-actin and GAPDH (Appendix C, Table C-1). For calculation of the corresponding number of RNA molecules a cDNA reference standard curve was processed in parallel in qPCR.

3.4.5. Linear regression analysis of RT-qPCR data

Viral RNA molecule numbers during the life cycle of influenza virus obtained by the RT-qPCR assay were analyzed by linear regression to quantify onset of production, production rates and time delay between start of infection and start of production of specific viral segment or viral RNA type. The analysis was done by Stefan Heldt (bpt group MPI Magdeburg) as a supporting work (Vester et al., 2010). Raw data were transformed by taking the $\log_{10}$ of the viral RNA molecule copy numbers. Analysis focused on two phases: a delay time in which the number of viral RNA molecules was constant or decreased only slightly in case of vRNA(-) and a phase of exponential increase, i.e. production of viral RNAs. Both phases were fitted separately to obtain the corresponding parameters. A parallel line to the abscissa

$$y = p1 \qquad \text{(Equation 7)}$$

approximated the delay phase. Whereas, the production of RNA corresponded to a straight line in the transformed data set and was, thus, fitted with a linear polynomial function

$$y = p2x + p3 \qquad \text{(Equation 8)}$$

For regression analysis a linear least-squares method implemented in the Curve Fitting Toolbox (ver 1.2.2) in Matlab R2008b (The MathWorks, Inc., Natick, MA, USA) was used. To assess the goodness of fit for this type of method R^2 values and non–simultaneous prediction bounds for the parameters (95%, CI) were calculated. Three methods are considered for

estimation of these bounds: the calculation by intersecting confidence bands, by first–order propagation of variance and the application of Fieller's theorem (Carter et al., 1991; Schwartz and Gelb, 1984). The intersection of both regression lines was used to calculate the time delay Δt [h] between infection and production of a specific segment.

3.4.6. Determination of extracellular influenza viral RNA in cell culture supernatant by RT-qPCR

A typical workflow for the determination of extracellular influenza viral RNA in cell culture supernatant by RT-qPCR is shown in Figure 3.4-3. The QIAamp Viral RNA Mini kit (Qiagen; section 3.4.2) was used to extract influenza genomic vRNA(-) from 280 µL cell culture supernatant of infected MDCK cells (RB, without 4°C step; MOI=1; influenza A PR/8-RKI virus; section 3.2.5) with 60 µL elution volume. Extraction protocol was done according to the instructions of the manufacturer. Synthetic viral RNA used as reference standard for quantification was produced as described in section 3.4.2. A polarity and sequence-specific standard curve was generated by serial dilution of synthetic viral RNA reference standard vRNA(-) of viral segment 7 (M) 1.0 x 10^{-1} – 1.0 x 10^{-6} ng/µL vRNA(-). A separate RT step with extracellular viral RNA extracts, together with the corresponding RNA standard curve was performed using the protocol described above (section 3.4.2), but using random hexamer primer instead of Uni12 (M) primer. The qPCR step was performed as described before (section 3.4.2) using 1 µL cDNA from the RT step and 18 pmol of corresponding forward and reverse primer of segment 7 (M) (Table C-4, Appendix) in a 25 µL reaction volume. Standard cycling conditions were 95°C for 5 min, followed by 40 cycles of 95°C for 15 s, 60°C for 1 min and an additional melting curve analysis (65°C, 10 s, 60 cycles, 0.5°C temperature rise) was carried out. The total average number of virus particles per mL was obtained taking into account dilutions made during cDNA synthesis and qPCR, total volume of cell culture supernatant used for RNA extraction and the assumption that every virus particle contains every RNA segment only once.

$$c_{Virus} = \frac{V_{(RNA-E)} \cdot V_{(RT-total)}}{V_{(cDNA)} \cdot V_{(RNA-RT)}} \cdot V_{(sample)}{}^{-1} \cdot 10^{\frac{Cq-b}{a}} \qquad \textit{(Equation 9)}$$

c_{Virus}	*viral particle titer [virions/mL]*
$V_{(RNA-E)}$	*elution volume of RNA extraction [µL]*
$V_{(RT-total)}$	*total volume of RT reaction [µL]*
$V_{(RNA-RT)}$	*RNA extract volume used for RT reaction [µL]*
$V_{(cDNA)}$	*cDNA volume used for qPCR reaction [µL]*
$V_{(sample)}$	*total volume of supernatant sample [mL]*
C_q	*quantification cycle*
b	*ordinate intercept of regression curve*
a	*slope of regression curve*

For verification of the quantification efficiency of the RT-qPCR, results were compared to data of a HA assay for conventional virus quantification. HA titers were determined as described above (section 3.2.6). Titers are reported conventionally as log HA units per test volume (log HA units/100µL). For better comparability of both, RT-qPCR and HA data, results of the HA assay were converted to virions per mL (total virus particles concentration) by Equation 3 (section 3.2.6).

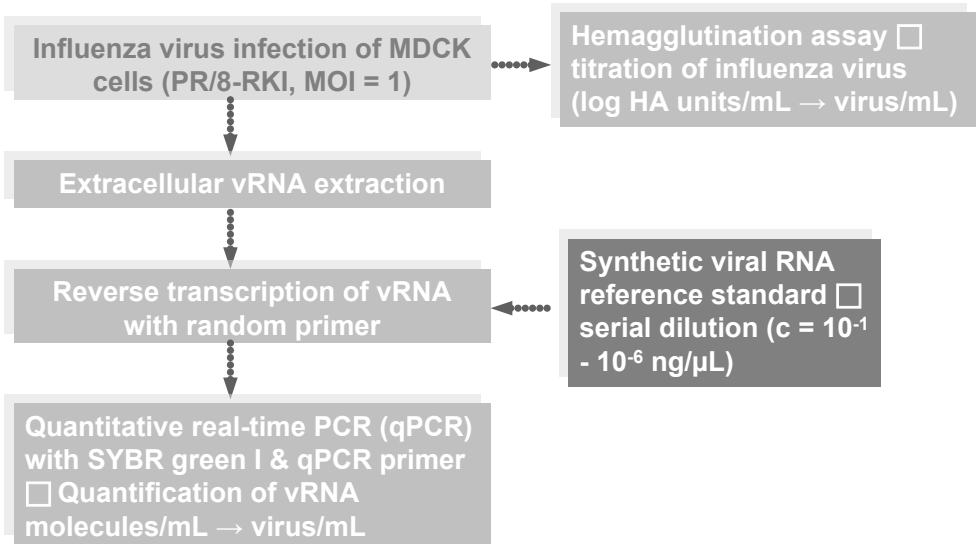

Figure 3.4-3: Workflow for determination of extracellular influenza viral RNA in cell culture supernatant by RT-qPCR vs. determination of virus particles concentration by conventional virus quantification (HA assay)

For validation of the extracellular influenza viral RNA extraction step, regression analysis including calculation of standard curve slopes and intercepts (quantification cycle C_q versus log extracellular viral RNA quantity) and confirmation of linearity and sensitivity of the extraction step was done.

For determination of linearity and sensitivity, three independent serial dilutions (concentrated, 1:2, 1:10, 1:100, 1: 1000, 1:10000) of the influenza PR/8-RKI seed virus ($TCID_{50}$ 3.5×10^7 virions/mL) were prepared for application to extraction columns. Extraction protocol was done according to the instructions of the manufacturer (section 3.4.2; QIAamp Viral RNA Mini kit, Qiagen). For determination of extracellular viral RNA quantity a standard curve was generated by serial dilution of synthetic viral RNA reference standard vRNA(-) of viral segment 7 (M) 1.0×10^0 – 1.0×10^{-8} ng/µL vRNA(-). Afterwards, the RT-qPCR assay was performed using the protocol described above in this section.

4. Results

4.1. Selection of a human cell line as model for the proteomic approach

There is an increasing need for a better understanding of the intracellular, molecular mechanisms during cell culture based influenza vaccine production processes. Several non-human cell lines, i.e. MDCK or Vero, are potential candidates for successful vaccine production (Genzel and Reichl, 2009). However, application of molecular techniques (i.e. proteome/genome analysis) to investigate these cellular systems is restricted, as most of the antibodies, microarrays, etc. commercially available are limited to human or mouse models. Another problem is that the associated genomes have only been sequenced partially. Although some non-human proteins could be identified by MS with the aid of homology analysis (Fullekrug et al., 2006), numerous MS/MS data of proteins cannot be interpreted. The problem may be solved to some extend with the study of a human infection model.

For this reason, metabolism and virus yield of three different human cell lines was compared to select such a model system. Therefore, a gastric carcinoma cell line (NCI-N87), a hepatocellular carcinoma cell line (HepG2) and a lung carcinoma cell line (A549) were cultivated and infected, to examine whether they are suitable for studying virus-host cell interactions and signal transduction mechanisms. Experiments on cell metabolism during cell growth and virus infection in different media and on effects of different infection parameters, e.g. trypsin concentration and MOI were carried out. This characterization was essential to have optimal growth conditions and a stable and well adapted infection system related to the MDCK and Vero cell system.

However, as it transpired finally in this work, concerns have proven themselves as unsubstantiated. Both MDCK and Vero host cell proteins could be identified in the following proteome study by MS with the aid of homology analysis. Nevertheless, HepG2 and A549 cells could be used as reference models in additional infection experiments in recent signal transduction studies of the molecular biology subgroup of the bpt group of the MPI Magdeburg and can continue to be used.

4.1.1. Characteristics and morphology of three human cell lines

The human lung carcinoma continuous cell line, A549, was first described by Giard et al. in 1973 (Giard et al., 1973) and further characterized by Lieber et al. (Lieber et al., 1976). A549 cells were derived through explant culture of lung carcinoma tissue from a 58-year-old man.

The A549 cell line was grown as a monolayer culture with a doubling time described in literature of about 48 h in log phase growth (Lieber et al., 1976). The cells were epithelial in morphology and contain numerous, small cytoplasmic granules readily seen by inverted light microscopy (Figure 4.1-1B). A549 cells showed comparable cell growth performance, confluence levels and cell morphology to MDCK and Vero cells (Figure 4.1-1).

NCI-N87 is a gastric carcinoma cell line derived in 1976 by Park et al. (Park et al., 1990) established from a liver metastasis of a gastric carcinoma from an American male. The well differentiated adherent cell line NCI-N87 grew as islands/compact colonies of tightly cohesive epithelial morphology and formed coherent monolayers (Figure 4.1-1A) with a doubling time of about 47 h in log phase growth. NCI-N78 cells did grow to confluency.

HepG2 is an immortalized cell line, which was derived from the liver tissue of a 15 year old male with a well differentiated hepatocellular carcinoma (Aden et al., 1979). These cells were epithelial in morphology (Figure 4.1-1). The cell line grew as a monolayer culture with a doubling time of about 50-60 h in log phase growth. HepG2 cells showed nearly confluent levels only when seed at high cell concentrations.

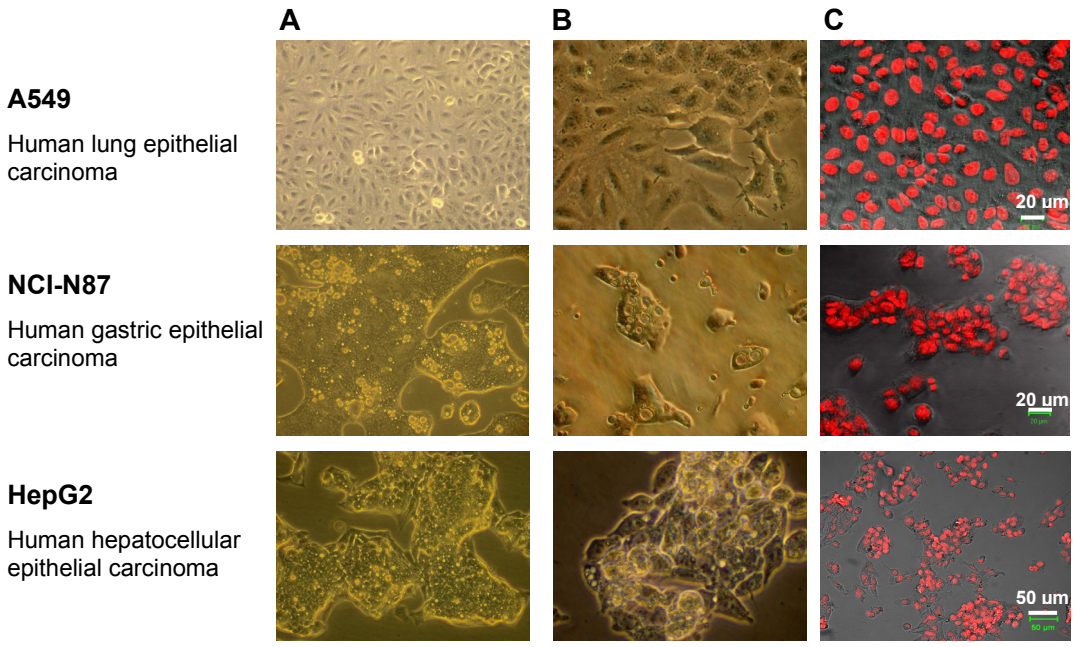

Figure 4.1-1 Cell morphology during cell growth phase of A549, NCI-N87 and HepG2 cell lines

(A) After 4/7/6 days cell growth, respectively and (B) zoom in on detail, observed with inverted light microscope without staining; (C) Laser scan microscopic picture of nuclei stained with propidium iodide (red). Scale bars (white) are only shown in (C).

4.1.2. Cellular metabolism during cell growth and virus infection phase

For analysis and optimization of cell growth and virus infection of A549, NCI-N87 and HepG2 cells, experiments in T175-flasks were carried out in triplicate (mean values are given). The metabolite concentrations of glucose, lactate, glutamine, glutamate and ammonia in two

different media were compared to follow the carbon and energy metabolism as well as to identify media limitations and growth inhibition effects. Each medium for the three cell lines was either recommended by ATCC or by various publications (Barnard et al., 1988; Chailler and Menard, 2005; Keskinen et al., 1999). During infection phase (influenza PR/8 virus strain obtained from the RKI, Berlin, Germany; referred to as PR/8-RKI ;MOI = 1) the HA titers and cell concentrations were compared to investigate whether a special VMM was needed for influenza virus production. Starting cell concentrations are specified in Table 3.2-1 (section 3.2.1) and virus infection conditions in Table 3.2-3 (section 3.2.5).

A549 cell line

The metabolic profiles for glucose uptake and lactate release of A549 cells indicated a glucose consumption of 7.68 mM F12K / 5.56 mM MEM^{A549} over the cultivation time and of 10.25 mM F12K / 4.89 mM MEM^{A549} over the infection time, while 15.04 mM F12K / 11.44 mM MEM^{A549} and 15.37 mM F12K / 7.46 mM MEM^{A549} lactate were released, respectively (Figure 4.1-2 A). This leads to an overall molar yield lactate/glucose $Y_{lac/gluc}$ = 1.96 F12K / $Y_{lac/gluc}$ = 2.06 MEM^{A549} for cell growth and $Y_{lac/gluc}$ = 1.5 F12K / $Y_{lac/gluc}$ = 1.53 MEM^{A549} for infection phase (Table 4.1-2). A549 cells consumed 1.67 mM F12K / 2.17 mM MEM^{A549} glutamine while the ammonia level reached 1.62 mM F12K / 1.90 mM MEM^{A549} after 120 h of cultivation (Figure 4.1-2B). Whereas 1.41 mM F12K / 1.56 mM MEM^{A549} glutamine consumption and 1.81 mM F12K / 1.91 mM MEM^{A549} ammonia release were observed during 96 h infection phase (Figure 4.1-2B). Overall molar yield ammonia/glutamine was $Y_{amm/gln}$ = 0.97 F12K / $Y_{amm/gln}$ = 0.88 MEM^{A549} for cell growth and $Y_{amm/gln}$ = 1.29 F12K / $Y_{amm/gln}$ = 1.23 MEM^{A549} for the infection phase (Table 4.1-2). The metabolic profiles of glutamate indicated, for both cell growth and infection phase, a release of 0.47 mM F12K / 0.35 mM MEM^{A549} or 0.58 mM F12K / 0.79 mM MEM^{A549}, respectively (Figure 4.1-2C).

Parallel to the metabolite profiles the virus release was monitored in HA units of the cell culture supernatant of A549 cells (Figure 4.1-2C). At about 12 hpi F12K / 36 hpi MEM^{A549} virus could be detected. Maximum virus yield of 1.4 log HA/100 µL was reached at 72 hpi for F12K and 1.55 log HA/100 µL was reached at 84 hpi for MEM^{A549}. This corresponds to approximately 1411 F12K / 1562 MEM^{A549} viral particles per cell (Table 4.1-3) based on the cell concentration at time of infection (Table 4.1-1) calculated by Equation 3 (section 3.2.6). During time course of infection, a clear increase in viable and dead cells in the supernatant could be observed at 40 hpi with a final concentration of dead cells of approximately 1.0 x 10^5 cells/mL F12K / 1.6 x 10^5 cells/mL MEM^{A549} at 96 hpi (Figure 4.1-2D).

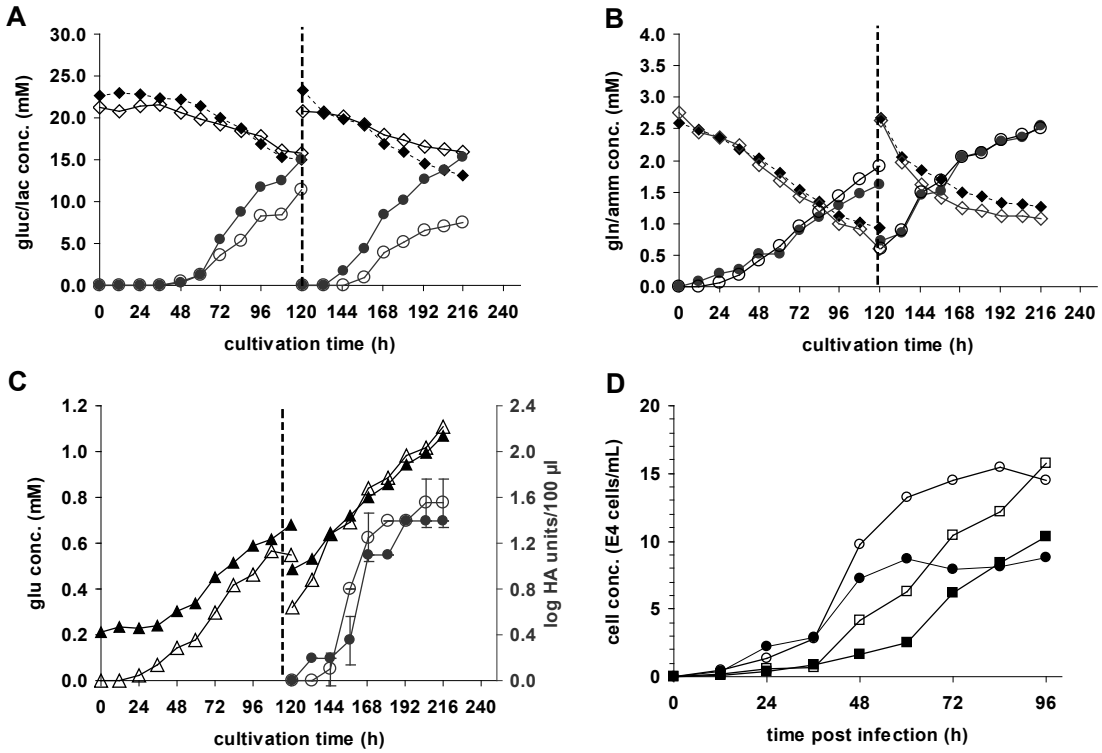

Figure 4.1-2: Cellular metabolism during cell growth (0-120 h) and virus infection (120-240 h) of the A549 cell line

Comparison of (A) glucose (gluc-◆) and lactate (lac-●) concentration, (B) glutamine (gln-◆) and ammonia (amm-●) concentration, (C) glutamate (glu-▲) concentration and HA-values (●)(± SD of triplicates) and (D) concentration of viable (●) and dead (■) cells in supernatant in A549 cultures in 2 different media (F12K-full symbols; MEM^{A549}-empty symbols). Cells were cultured in T175-flasks in triplicate (mean values are given), infected with influenza PR/8-RKI virus, MOI=1, trypsin 500 U/flask. At time of infection medium exchange to VMM was performed (vertical line).

NCI-N87 cell line

The metabolic profiles for glucose uptake and lactate release were compared for both media in NCI-N87 cells (Figure 4.1-3; Table 4.1-1). From 4.82 mM RPMI$^{NCI-N87}$ / 5.33 mM MEM$^{NCI-N87}$ total glucose consumed 10.04 mM RPMI$^{NCI-N87}$ / 11.21 mM MEM$^{NCI-N87}$ lactate was produced during cell growth (144 h), resulting in an overall molar yield of $Y_{lac/gluc}$ = 2.08 RPMI$^{NCI-N87}$ / $Y_{lac/gluc}$ = 2.1 MEM$^{NCI-N87}$ (Table 4.1-2). During virus infection 8.72 mM RPMI$^{NCI-N87}$ / 6.36 mM MEM$^{NCI-N87}$ glucose were metabolized to 19.07 mM RPMI$^{NCI-N87}$ / 13.06 mM MEM$^{NCI-N87}$ lactate (96 h), corresponding to $Y_{lac/gluc}$ = 2.19 RPMI$^{NCI-N87}$ / $Y_{lac/gluc}$ = 2.05 MEM$^{NCI-N87}$. Degradation and uptake of 0.99 mM RPMI$^{NCI-N87}$ / 1.48 mM MEM$^{NCI-N87}$ glutamine resulted in 1.36 mM RPMI$^{NCI-N87}$ / 1.58 mM MEM$^{NCI-N87}$ ammonia during cell growth, resulting in an overall molar yield of $Y_{amm/gln}$ = 1.27 RPMI$^{NCI-N87}$ / $Y_{amm/gln}$ = 1.07 MEM$^{NCI-N87}$ (Table 4.1-2). During virus infection still 0.52 mM RPMI$^{NCI-N87}$ / 1.23 mM MEM$^{NCI-N87}$ glutamine was used and led to 1.02 mM RPMI$^{NCI-N87}$ / 1.44 mM MEM$^{NCI-N87}$ ammonia production, thus $Y_{amm/gln}$ = 1.95 RPMI$^{NCI-N87}$ / $Y_{amm/gln}$ = 1.17 MEM$^{NCI-N87}$ (Table 4.1-2). The metabolic profiles of glutamate indicated, for both cell growth and infection

phase, a release of 0.32 mM RPMI$^{NCI-N87}$ / 0.34 mM MEM$^{NCI-N87}$ or 0.50 mM RPMI$^{NCI-N87}$ / 0.70 mM MEM$^{NCI-N87}$, respectively (Figure 4.1-3C).

Parallel to the metabolite profiles the virus release was monitored in HA units of the cell culture supernatant of NCI-N87 cells (Figure 4.1-3C). At about 24 hpi RPMI$^{NCI-N87}$ / 24 hpi MEM$^{NCI-N87}$ a significant increase in virus titer could be detected. Maximum virus yield of 1.1 log HA/100 µL was reached at 24 hpi for RPMI$^{NCI-N87}$ and 1.1 log HA/100 µL was reached at 36 hpi for MEM$^{NCI-N87}$. This corresponds to approximately 709 RPMI$^{NCI-N87}$ / 567 MEM$^{NCI-N87}$ viral particles per cell (Table 4.1-3) based on the cell concentration at time of infection (Table 4.1-1) calculated by Equation 3 (section 3.2.6). During time course of infection, a clear increase in dead cells in the supernatant could be observed at 20 hpi with a final concentration of dead cells of approximately 1.3 x 10^5 cells/mL RPMI$^{NCI-N87}$ / MEM$^{NCI-N87}$ at 84 hpi (Figure 4.1-2D). Viable cell concentration in the supernatant first increased until 36 hpi with maximum cell numbers of 1.7 x 10^5 cells/mL RPMI$^{NCI-N87}$ and then decreased consistently (Figure 4.1-2D).

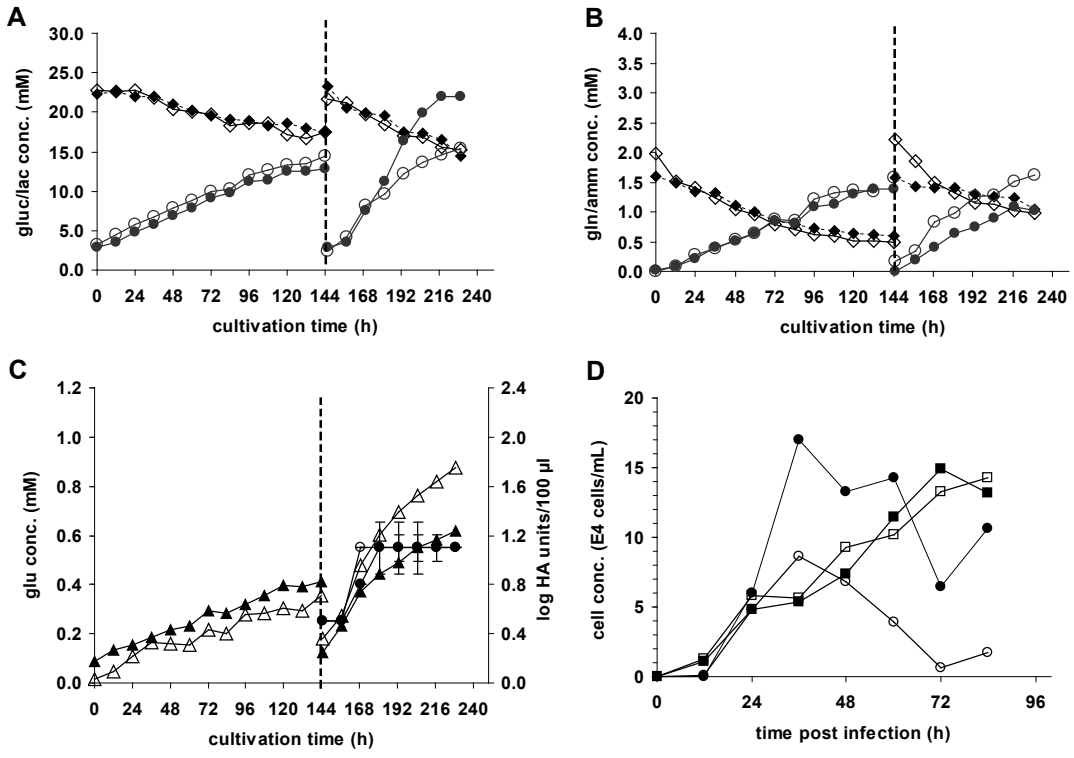

Figure 4.1-3: Cellular metabolism during cell growth (0-144 h) and virus infection (144-240 h) of the NCI-N87 cell line

Comparison of (A) glucose (gluc-◆) and lactate (lac-●) concentration, (B) glutamine (gln-◆) and ammonia (amm-●) concentration, (C) glutamate (glu-▲) concentration and HA-values (●)(± SD of triplicates) and (D) concentration of viable (●) and dead (■) cells in supernatant in NCI-N87 cultures in 2 different media (RPMI$^{NCI-N87}$-full symbols; MEM$^{NCI-N87}$-empty symbols). Cells were cultured in T175-flasks in triplicate (mean values are given), infected with influenza PR/8-RKI virus, MOI=1, trypsin 500 U/flask. At time of infection medium exchange to VMM was performed (vertical line).

HepG2 cell line

The metabolic profiles for glucose uptake and lactate release were compared for both media in HepG2 cells (Figure 4.1-4; Table 4.1-1). From 11.44 mM MEM^{HepG2} / 9.35 mM $RPMI^{HepG2}$ total glucose consumed 29.04 mM MEM^{HepG2} / 23.97 mM $RPMI^{HepG2}$ lactate was produced during cell growth (144 h), resulting in an overall molar yield of $Y_{lac/gluc}$ = 2.54 MEM^{HepG2} / $Y_{lac/gluc}$ = 2.56 $RPMI^{HepG2}$ (Table 4.1-2). During virus infection 8.90 mM MEM^{HepG2} / 8.96 mM $RPMI^{HepG2}$ glucose were metabolized to 22.89 mM MEM^{HepG2} / 22.21 mM $RPMI^{HepG2}$ lactate (96 h), corresponding to $Y_{lac/gluc}$ = 2.57 MEM^{HepG2} / $Y_{lac/gluc}$ = 2.48 $RPMI^{HepG2}$ (Table 4.1-2). Degradation and uptake of 1.57 mM MEM^{HepG2} / 1.39 mM $RPMI^{HepG2}$ glutamine resulted in 1.28 mM MEM^{HepG2} / 1.59 mM $RPMI^{HepG2}$ ammonia during cell growth, resulting in an overall molar yield of $Y_{amm/gln}$ = 0.81 MEM^{HepG2} / $Y_{amm/gln}$ = 1.15 $RPMI^{HepG2}$ (Table 4.1-2). During virus infection still 0.65 mM MEM^{HepG2} / 0.76 mM $RPMI^{HepG2}$ glutamine was used and led to 1.10 mM MEM^{HepG2} / 1.32 mM $RPMI^{HepG2}$ ammonia production, thus $Y_{amm/gln}$ = 1.69 MEM^{HepG2} / $Y_{amm/gln}$ = 1.75 $RPMI^{HepG2}$ (Table 4.1-2). The metabolic profiles of glutamate indicated no release during cell growth phase and a release of 0.85 mM MEM^{HepG2} / 0.70 mM $RPMI^{HepG2}$ during the infection phase (Figure 4.1-4C).

Parallel to the metabolite profiles the virus release was monitored in HA units of the cell culture supernatant of HepG2 cells (Figure 4.1-4C). At about 24 hpi MEM^{HepG2} / 24 hpi $RPMI^{HepG2}$ a significant increase in virus titer could be detected. Maximum virus yield of 1.85 log HA/100 µL was reached at 72 hpi for MEM^{HepG2} and 1.7 log HA/100 µL was reached at 60 hpi for $RPMI^{HepG2}$. This corresponds to approximately 1892 MEM^{HepG2} / 1739 $RPMI^{HepG2}$ viral particles per cell (Table 4.1-3) based on the cell concentration at time of infection (Table 4.1-1) calculated by Equation 3 (section 3.2.6). During time course of infection, a clear increase in dead and viable cells in the supernatant with a maximum cell concentration of about 1.5 x 10^5 cells/mL MEM^{HepG2} / $RPMI^{HepG2}$ at 48 hpi for dead cells and about 9 x 10^4 cells/mL MEM^{HepG2} at 36 hpi for viable cells (Figure 4.1-2D) could be observed. Afterwards a clear decrease of cell concentration in the supernatant could be detected.

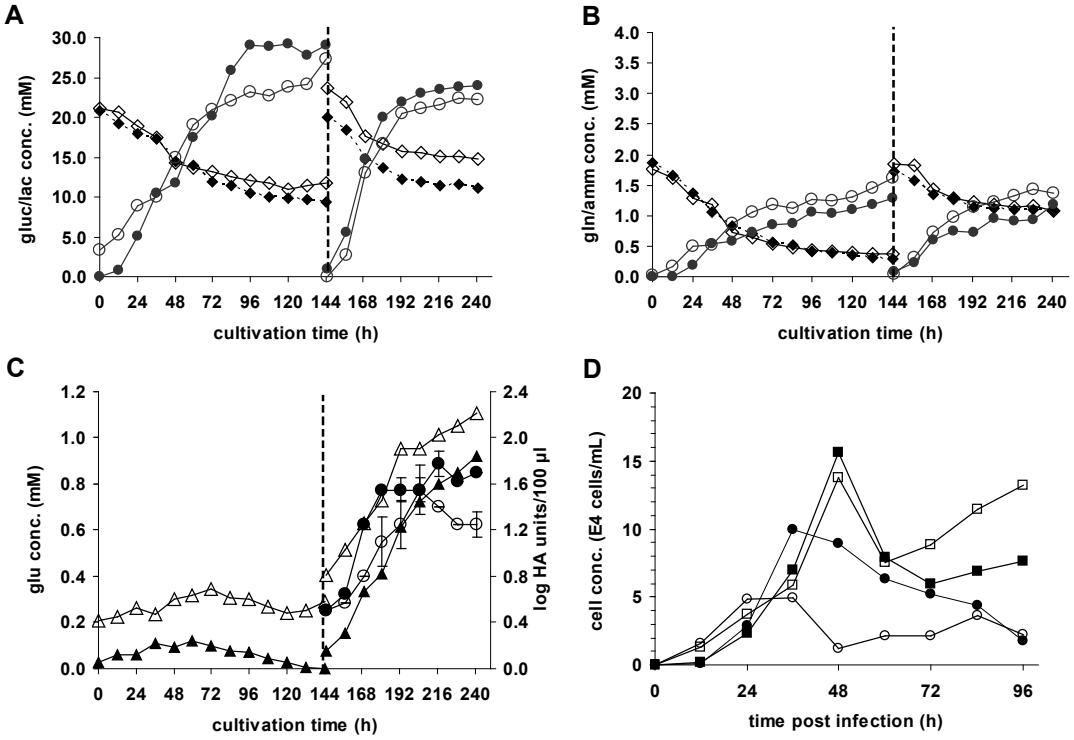

Figure 4.1-4: Cellular metabolism during cell growth (0-144 h) and virus infection (144- 240 h) of the HepG2 cell line

Comparison of (A) glucose (gluc-◆) and lactate (lac-●) concentration, (B) glutamine (gln-◆) and ammonia (amm-●) concentration, (C) glutamate (glu-▲) concentration and HA-values (●)(± SD of triplicates) and (D) concentration of viable (●) and dead (■) cells in supernatant in HepG2 cultures in 2 different media (MEM^{HepG2}-full symbols; $RPMI^{HepG2}$-empty symbols). Cells were cultured in T175-flasks in triplicate (mean values are given), infected with influenza PR/8-RKI virus, MOI=1, trypsin 500 U/flask. At time of infection medium exchange to VMM was performed (vertical line).

Table 4.1-1: Comparison of growth parameters and differences in initial and final total metabolite concentrations (Δ values) of human cell lines

		A549		**NCI-N87**		**HepG2**	
		F12K	MEM^{A659}	$RPMI^{NCI-N87}$	$MEM^{NCI-N87}$	MEM^{HepG2}	$RPMI^{HepG2}$
Initial cell conc.	Cell growth	0.4	0.4	3.0	4.0	3.2	3.2
(x 10^5 cells/mL)	Virus infection	4.3	4.3	3.5	3.5	4.4	4.4
Cultivation time	Cell growth	120	120	144	144	144	144
(h)	Virus infection	96	96	96	96	96	96
Metabolite concentrations [a, b]							
Δ glucose	Cell growth	-7.68	-5.56	-4.82	-5.33	-11.44	-9.35
(mM)	Virus infection	-10.25	-4.89	-8.72	-6.36	-8.90	-8.96
Δ lactate	Cell growth	15.04	11.44	10.04	11.21	29.04	23.97
(mM)	Virus infection	15.37	7.46	19.07	13.06	22.89	22.21
Δ glutamine	Cell growth	-1.67	-2.17	-0.99	-1.48	-1.57	-1.39
(mM)	Virus infection	-1.41	-1.56	-0.52	-1.23	-0.65	-0.79
Δ ammonia	Cell growth	1.62	1.90	1.36	1.58	1.28	1.59
(mM)	Virus infection	1.81	1.91	1.02	1.44	1.10	1.32
Δ glutamate	Cell growth	0.47	0.35	0.32	0.34	0.00	0.08
(mM)	Virus infection	0.58	0.79	0.50	0.70	0.85	0.70

[a] *Δ values were calculated by dividing the corresponding metabolite concentration at the start and the end of cultivation and infection phase*

[b] *Negative Δ values indicate that substrate is consumed, positive values that metabolite is released*

Table 4.1-2: Comparison of metabolite yields during cell growth and infection of human cell lines

Metabolite yields [a)]	**A549**		**NCI-N87**		**HepG2**	
	F12K	MEM^{A659}	$RPMI^{NCI-N87}$	$MEM^{NCI-N87}$	MEM^{HepG2}	$RPMI^{HepG2}$
Cell growth $Y_{lac/gluc}$	1.96	2.06	2.08	2.10	2.54	2.56
Virus infection $Y_{lac/gluc}$	1.50	1.53	2.19	2.05	2.57	2.48
Cell growth $Y_{amm/gln}$	0.97	0.88	1.37	1.07	0.81	1.15
Virus infection $Y_{amm/gln}$	1.29	1.23	1.95	1.17	1.69	1.75

[a)] *Calculation of yields (Y) were done as described in section 3.2.4 (Equation 2)*

Table 4.1-3: Comparison of max. HA titers and cell specific virus yields of different human cell lines

	A549		**NCI-N87**		**HepG2**	
	F12K	MEM^{A659}	$RPMI^{NCI-N87}$	$MEM^{NCI-N87}$	MEM^{HepG2}	$RPMI^{HepG2}$
Max. HA titer (log HA/100 µL)	1.40	1.55	1.10	1.10	1.85	1.70
Cell specific virus yield [a)]	1411	1562	709	567	1892	1739

[a)] *Calculation of cell specific virus yields were done as described in section 3.2.6 (Equation 3) divided by the cell concentration at time of infection (Table 4.1-1)*

In summary, no significant differences in initial and final concentration of metabolites (Δ values) were observed comparing the two media of the three human cell lines. HepG2 showed higher amounts of consumed and released metabolites, indicating a higher overall glycolytic activity (Table 4.1-1). Glutamate release was always coupled to virus replication in the human cell lines (Table 4.1-1). Neither ammonia nor lactate concentrations reached inhibiting concentration for cell growth in both media (Table 4.1-1). For cell cultivation HepG2 and NCI-N87 cells had to be seeded at high cell concentration since most of the seeded cells did not attached to the T-flaks surface and died fastly (Table 4.1-1). Additionally, although using this high seeding cell concentrations, HepG2 and NCI-N87 cells did not grow to confluency at all. Lowest maximum HA titers were observed for NCI-N87 cells (Table 4.1-3).

4.1.3. Effect of different infection parameters on virus yield

The effect of MOI in combination with different VMM and trypsin addition was tested for influenza PR/8-RKI virus infection. Additionally, the cell specific infective virus particle concentration was determined by $TCID_{50}$ assay. Studies were carried out in T75-flasks. Starting cell numbers (Table 3.2-1; section 3.2.1) and virus infection conditions (Table 4.1-1; section 3.2.5) were as specified before. Variations from MOI 0.1 to 1.5 were compared by HA titers for both VMM. Since especially proteome analysis must be done without proteases to avoid protein degradation, experiments focused on infection conditions without trypsin addition. Therefore, infection with (250 U/flask) and without trypsin was compared by HA titers, glutamate release and cell concentrations in supernatant for one VMM and a fixed MOI of 1.

A549 cell line

No influence on maximum HA titers was observed for variations in MOI during A549 cell culture infection for both media (Figure 4.1-6A, B). Finally, all infections reached the same maximum titer of about 2.0 log HA unit/100 µL only at different time points. Thus, the MOI had an effect on virus growth dynamics but not on final yields. The lower the MOI the longer the lag phase before HA titers were detectable and increased.

Testing the effect of trypsin addition during infection of A549 cells revealed highest virus titers of 1.9 HA units/100 µL at 60 hpi with trypsin. Without trypsin activation, virus replication was delayed and lower HA titers of 1.1 HA units/100 µL were reached at 84 hpi compared to infection with trypsin (Figure 4.1-6A). This delay was also reflected in the released amounts of glutamate without trypsin activation (Figure 4.1-6A). No significant differences could be observed for the cell concentrations in the supernatant (Figure 4.1-6B).

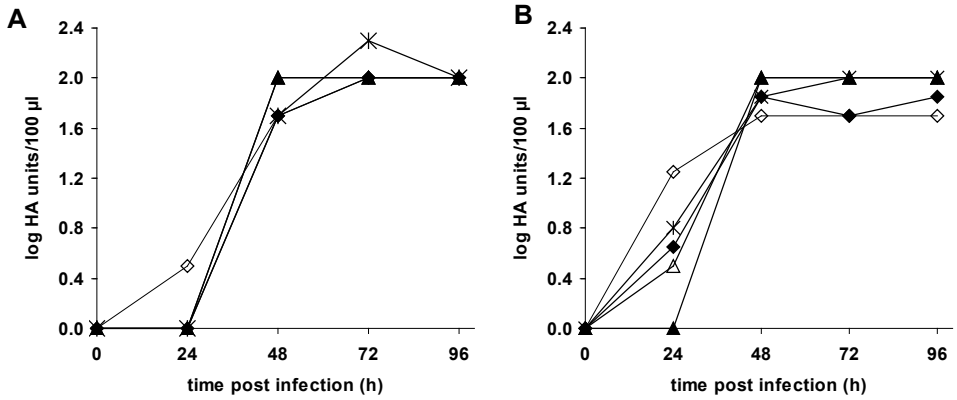

Figure 4.1-5: Effect of MOI on virus yields of the A549 cell line
Infection with influenza PR/8-RKI virus in (A) F12K and (B) MEM^{A549} VMM (T75-flasks; after 120 h growth ; trypsin: 250 U/flask) with different MOI (1.5-◇, 1.0-, 0.5-◆, 0.25-△, 0.1-▲).*

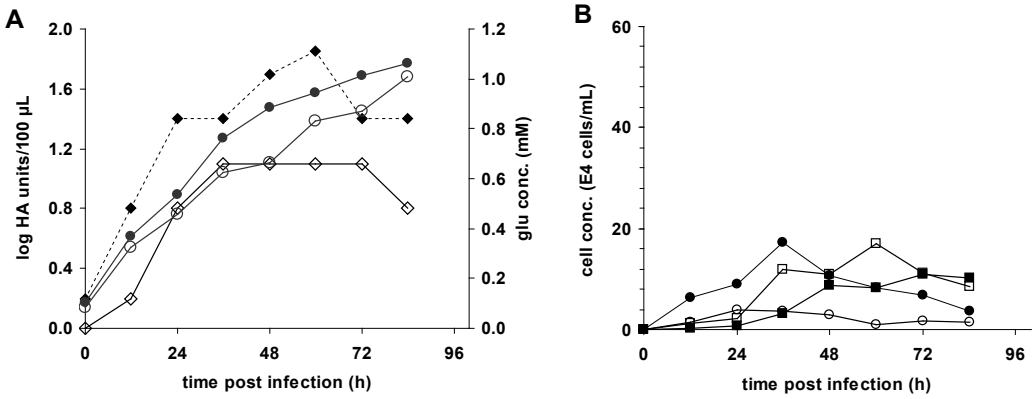

Figure 4.1-6: Effect of trypsin addition on virus yields of the A549 cell line
Infection with (250 U/flask) (full symbols) or without (empty symbols) trypsin supplementation to F12K VMM. Cells were infected after 120 h growth with influenza PR/8-RKI virus with MOI=1 in T75-flasks. (A) glutamate (glu-●) concentration and HA-values (◆) and (B) concentration for viable (●) and dead (■) cells in supernatant of A549 cultures are shown.

NCI-N87 cell line

For variations in MOI during NCI-N87 cell culture infection an influence on maximum HA titers was observed for both media (Figure 4.1-7A, B). As before a maximum HA titer of 1.2 log HA unit/100 µL was reached when using MOI in the range 1.5-1.0. The lower the MOI the lower the maximum HA titers reached, showing a possible MOI-dependency for this cell line.

Testing the effect of trypsin addition during infection of NCI-N87 cells revealed highest virus titers of 1.2 HA units/100 µL with trypsin at 96 hpi. Without trypsin activation, virus replication was delayed and similar HA titers of 1.1 HA units/100 µL were reached compared to infection with trypsin (Figure 4.1-8A). This almost identical time course was also reflected in similar glutamate release dynamics (Figure 4.1-8A). No significant differences could be observed for the cell concentrations in the supernatant (Figure 4.1-8B).

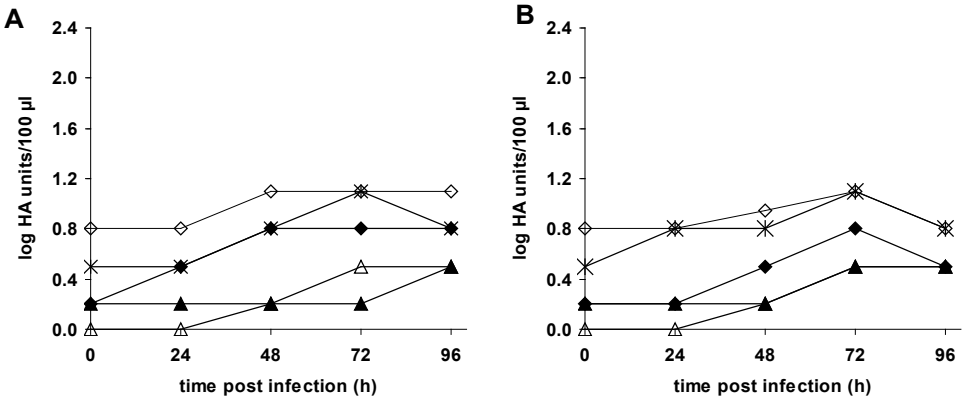

Figure 4.1-7: Effect of MOI on virus yields of the NCI-N87 cell line
Infection with influenza PR/8-RKI virus in T75-flasks after 144 h of cultivation in (A) RPMI$^{NCI-N87}$ and (B) MEM$^{NCI-N87}$ VMM (trypsin: 250 U/flask) with different MOI (1.5-◇, 1.0-, 0.5-◆, 0.25-△, 0.1-▲).*

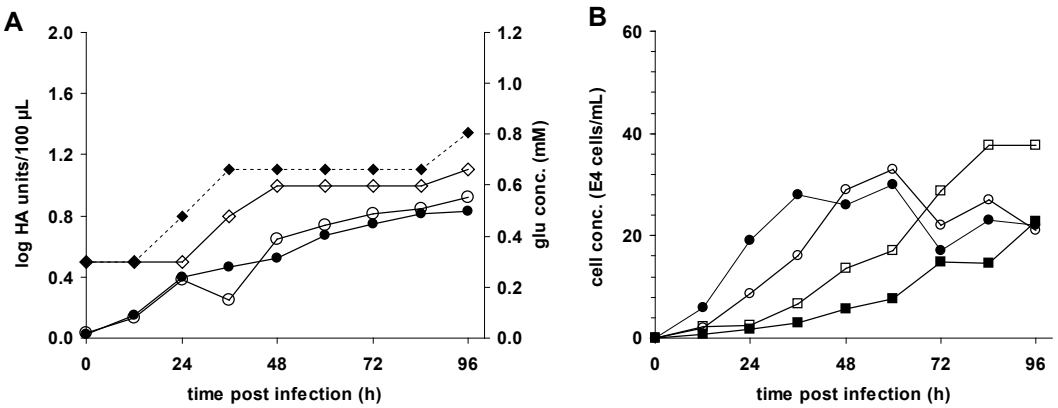

Figure 4.1-8: Effect of trypsin addition on virus yields of the NCI-N87 cell line
Infection with (250 U/flask) (full symbols) or without (empty symbols) trypsin supplementation to RPMI$^{NCI-N87}$ VMM. Cells were infected after 144 h growth with influenza PR/8-RKI virus with MOI=1 in T75-flasks. (A) glutamate (glu-●) concentration and HA-values (◆) and (B) concentration for viable (●) and dead (■) cells in supernatant of NCI-N87 cultures are shown.

HepG2 cell line

For variations in MOI during HepG2 cell culture infection no influence on maximum HA titers was observed for both media (Figure 4.1-9A, B). Finally, all infections reached the same maximum titer of about 2.3 log HA unit/100 µL only at different time points. Thus, the MOI had an effect on virus growth dynamics but not on final yields. The lower the MOI the longer the lag phase before maximum HA titers were detectable and increased.

Testing the effect of trypsin addition during infection of HepG2 cells revealed highest virus titers of 1.9 HA units/100 µL with trypsin at 72 hpi. Without trypsin activation, virus replication was delayed by 12 h, however maximum HA titers of 1.4 HA units/100 µL reached similar levels (Figure 4.1-10A). This delay was also reflected in the released amounts of glutamate without trypsin activation (Figure 4.1-10A). No significant differences could be observed for the cell concentrations in the supernatant (Figure 4.1-10B).

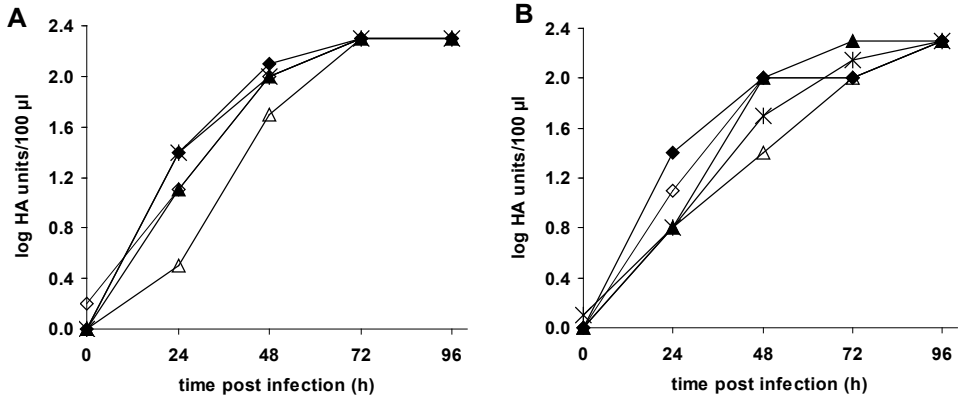

Figure 4.1-9: Effect of MOI on virus yields of the HepG2 cell line
Infection with influenza PR/8-RKI virus in T75-flasks after 144 h of cultivation in (A) MEM^{HepG2} and (B) RPMI^{HepG2} VMM (trypsin: 250 U/flask) with different MOI (1.5-◇, 1.0-, 0.5-◆, 0.25-△, 0.1-▲).*

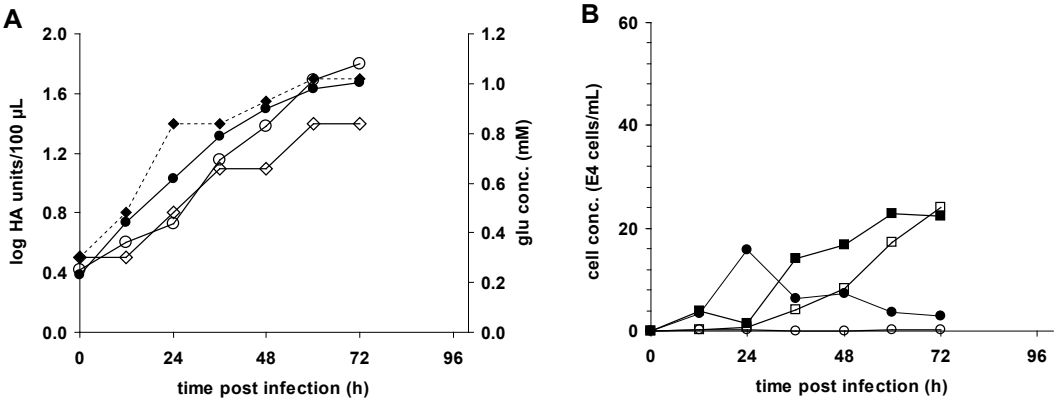

Figure 4.1-10: Effect of trypsin addition on virus yields of the HepG2 cell line
Infection with (250 U/flask) (full symbols) or without (empty symbols) trypsin supplementation to MEM^{HepG2} VMM. Cells were infected after 144 h growth with influenza PR/8-RKI virus with MOI=1 in T75-flasks. (A) glutamate (glu-●) concentration and HA-values (◆) and (B) concentration for viable (●) and dead (■) cells in supernatant of HepG2 cultures are shown.

Cell line specific infective virus particle concentration was determined by $TCID_{50}$ assay (section 3.2.6) to verify the stability of the produced active virus particles (Figure 4.1-11). The maximum number of active virus particles was reached at 24 hpi for HepG2 cells ($10^{7.6}$ virions/mL), at 48 hpi for A549 cells ($10^{7.5}$ virions/mL). Afterwards the virus activity decreased within the next 48 h by about 1 log step for HepG2 cells and within the last 24 hpi by half log step for A549 cells. Only very low active virus particle titers of about $10^{5.9}$ virions/mL were observed for NCI-N87 cells, showing no significant increase in titers compared to the starting concentration.

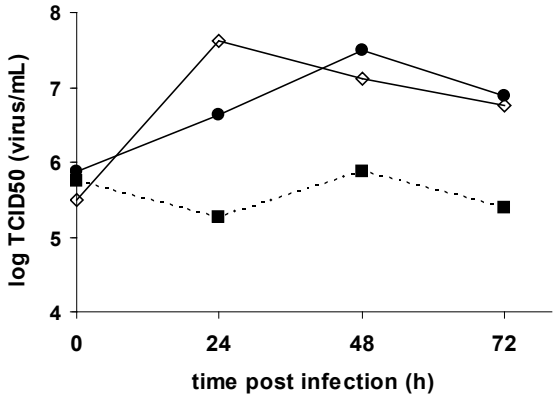

Figure 4.1-11: Cell line specific infective virus particle titers ($TCID_{50}$)
Infection of A549 cells in F12K (●), NCI-N87 cells in $RPMI^{NCI\text{-}N87}$ (■) and HepG2 cells in MEM^{HepG2} (◇) VMM (with 250 U/flask trypsin) with influenza PR/8-RKI virus (MOI=1 in T75-flasks).

In summary, no influence of MOI on maximum HA titers were observed for A549 and HepG2 cells for both media. Only NCI-N87 cells showed MOI-dependency. As before, lowest maximum HA titers were observed for NCI-N87 cells. HA titers were lower without trypsin addition, however viral replication could be detected. Glutamate release was always coupled to virus replication in all three human cell lines. Maximum active virus particle concentrations ($TCID_{50}$) were reached before maximum HA titers, except for NCI-N87 cells.

Overall, metabolism and virus yield screening of three human cell lines demonstrated that only A549 and HepG2 cells are promising candidates as a human cell reference model. Finally, on the basis of these data, A549 cells were selected for proteomic approaches, because they showed (I) comparable cell growth performance and cell morphology to MDCK and Vero cells, (II) comparatively high virus titer (HA, $TCID_{50}$) and virus replication even without trypsin addition and (III) lower metabolic activity and growth in uncomplex media.

4.2. Proteome alterations in human influenza A virus infected mammalian cell lines

4.2.1. Infection kinetics and proteome alterations in A549 and MDCK cells infected with influenza A PR/8-RKI

For a better understanding of virus-host cell interactions the changes in relative protein abundances caused by human influenza virus infection in MDCK and in A549 cells were examined at different time points during the infection (Vester et al., 2009). MDCK cells are used widely and are considered candidates for influenza virus vaccine production processes (Brands et al., 1999; Genzel and Reichl, 2007; Tree et al., 2001). As discussed under 4.1 A549 cells were selected for a comparison of influenza virus infection in a human cell line. Under standardized conditions relevant for vaccine production (Genzel et al., 2004) the PR/8-RKI virus variant was used to infect MDCK and A549 cells. To ensure a direct infection of all cells (single step infection) a MOI of 6 was used. Successful influenza virus infection was verified by measuring virus titers in the cell culture supernatant using the HA assay (Figure 4.2-1; section 3.2.6).

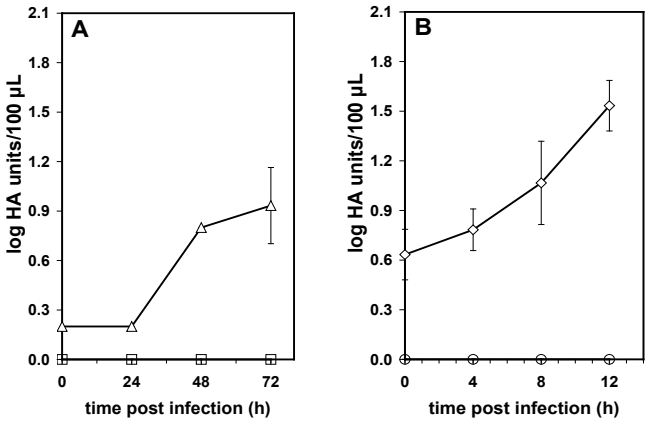

Figure 4.2-1: Virus titers (HA) for influenza PR/8-RKI virus infected (A) A549 cells and (B) MDCK cells

Infection kinetics of (A) A549 cells infected with PR/8-RKI virus (Δ) and mock infection (□)and (B) of MDCK cells infected with PR/8-RKI virus (◊) and mock infection (o) (T-flasks, without trypsin addition, MOI = 6). Symbols represent mean values ± SD of three independent experiments.

Influenza virus infected MDCK cells started to produce virus particles at about 4 to 6 hpi whereas in infected A549 cells virus production did not start until 24 hpi (Figure 4.2-1). Due to this result, different protein extraction time points were chosen to display the different dynamics in virus replication and also the resulting protein abundance changes during early infection phases. As the aim was to look for the proteome response of the infected cells early time points post infection were of interest. It was thus not necessary to reach maximum HA values or maximum virus yields as shown during the experiments. Later infection events

have not been considered. Proteins were extracted 4, 8 and 12 hpi for MDCK cells and at 24, 48 and 72 hpi for A549 cells, respectively. Proteome response was analyzed only from attached cells. Influenza virus replication comprises typical steps starting with attachment of virus to the host cell and internalization by endocytosis. Viral RNA genome replication and translation occurs in the nucleus leading to assembly of vRNP complexes in the cytoplasm and release of viral particles by budding (Sidorenko and Reichl, 2004). Time series of HA displayed significant differences in virus replication dynamics depending on cell line, from early and maximum virus production phase to the beginning of virus induced apoptosis, which was also reported by Schulze-Horsel et al. (Schulze-Horsel et al., 2009).

The proteome profiles of MDCK and A549 cells were examined by 2-D DIGE (see section 3.3), resolving a range of about 1200 protein spots for MDCK cells and about 1050 protein spots for A549 cells on individual gels. When comparing mock infected against influenza virus infected labeling a total number of only 8 differentially abundant spots in the protein profile were found for each cell line at different time points post infection. A set of representative 2-D DIGE gels is shown in Figure 4.2-2A for A549 cells at 72 hpi and in Figure 4.2-2B for MDCK cells at 12 hpi (altered proteins labeled serially with numbers).

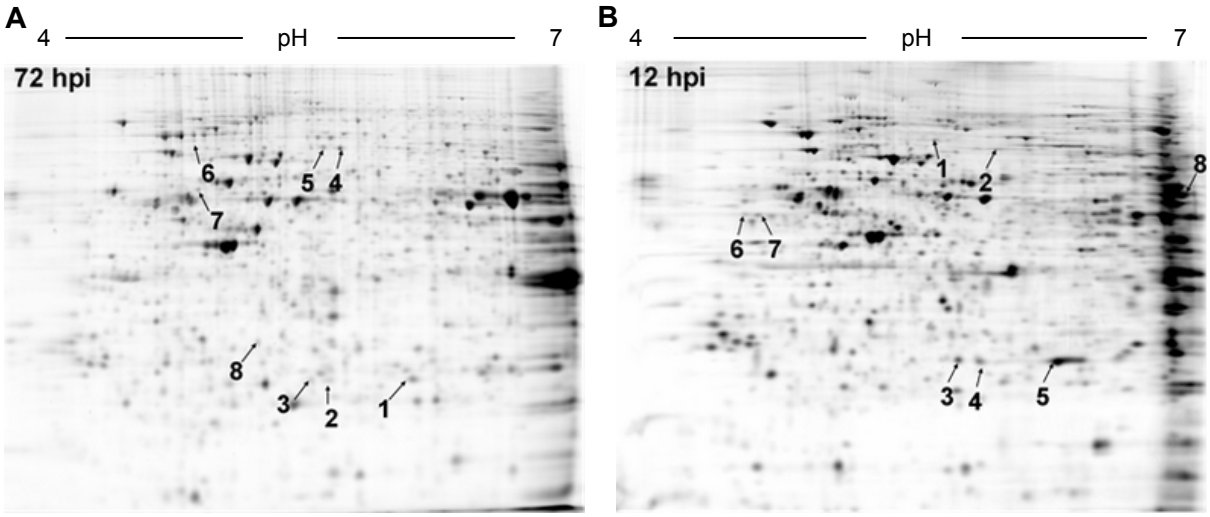

Figure 4.2-2: Representative 2-D DIGE gels of the proteome response of PR/8-RKI infected (A) A549 cells and (B) MDCK cells

Total protein extracts (Cy2-labeled proteins) resolved by 2-D DIGE (24 cm; pH 4-7; 10% SDS-PAGE) from 72 hpi (A549) and 12 hpi (MDCK).

Identified proteins are listed in Table 4.2-1 for A549 cells and in Table 4.2-2 for MDCK cells. Every protein spot was identified by at least two peptides using nanoHPLC-nanoESI-MS/MS (section 3.3.5). Identified proteins fulfill relevant functions in diverse biological processes such as stress response through molecular chaperones or proteolysis, mRNA translation, influenza virus induced signal transduction and as cytoskeleton components.

Table 4.2-1: Proteins identified as being differentially abundant in A549 cells infected with influenza PR/8-RKI virus variant compared to mock infected cells

Spot ID[a)]	NCBI no[b)]	Protein description	MASCOT scores Matched peptides [c)]	MASCOT scores Mowse score [d)]	Protein function
1	662841	Heat shock protein 27 (HSP27)	4	182	Chaperone/apoptosis
2	31542939	Hydroxyprostaglandin dehydrogenase 15-(NAD) (HPDG)	9	290	Prostaglandin inactivation
3	40354192	Keratin 10	8	398	Cytoskeleton protein
4	188901	IFN induced Mx protein (MxA)	16	501	Signal transduction (IFN induced)
5	188901	IFN induced Mx protein (MxA)	11	367	Signal transduction (IFN induced)
6	39777597	Transglutaminase 2 isoform a (TGM2)	14	451	Signal transduction/apoptosis
7	189308	Nucleobindin (Nuc)	7	357	Signaling, apoptosis
8	1008915	Proteasome activator hPA28 subunit beta (PA28beta)	8	243	Ubiquitin pathway (IFN induced)

a) *Spot ID represents the number on the 2-DE gels (Figure 4.2-2A)*
b) *Accession numbers according to the NCBInr database.*
c) *Number of peptides identified by MS/MS given by MASCOT*
d) *Mowse score is -10 x log(p), where p is the probability that the observed match is a random event. Based on the NCBInr database using the MASCOT searching program as MS/MS data. Scores greater than 53 are significant (p < 0.05)*

Table 4.2-2: Proteins identified as being differentially abundant in MDCK cells infected with influenza PR/8-RKI virus variant compared to mock infected cells

Spot ID[a)]	NCBI no[b)]	Protein description	MASCOT scores Matched peptides[c)]	MASCOT scores Mowse score[d)]	Protein function
1	73969443	Ran GTPase-activating protein 1 (RanGAP1)[e)]	4	91	mRNA processing/export
2	50978856	Myxovirus resistance protein (Mx1)	5	156	Signal transduction (IFN induced)
3	61740600	Keratin 10	20	620	Cytoskeleton protein
4	61740600	Keratin 10	8	303	Cytoskeleton protein
5	61740600	Keratin 10	9	358	Cytoskeleton protein
6	73974634	N-myc downstream regulated gene 1 (NDRG1)[e)]	4	77	Cell signaling
7	73974634	N-myc downstream regulated gene 1 (NDRG1)[e)]	4	131	Cell signaling
8	57096100	Eukaryotic translation elongation factor 1 (EF-1)[e)]	2	101	Protein synthesis

a) *Spot ID represents the number on the 2-DE gels (Figure 4.2-2B)*
b) *Accession numbers according to the NCBInr database.*
c) *Number of peptides identified by MS/MS given by MASCOT*
d) *Mowse score is -10 x log(p), where p is the probability that the observed match is a random event. Based on the NCBInr database using the MASCOT searching program as MS/MS data. Scores greater than 53 are significant (p < 0.05)*
e) *Predicted protein; derived from annotated genome sequence (NW_876264) using gene prediction method (GNOMON)*

The differentially abundant protein patterns of both cell lines showed no overlap except for two proteins. These two proteins are the myxovirus resistance protein (Mx1, spot 2, Table 4.2-2) in MDCK cells, named IFN induced Mx protein in human cells (MxA, spots 4 and 5, Table 4.2-1) and keratin 10 (MDCK: spots 3, 4 and 5, Table 4.2-2; A549: spot 3,Table 4.2-1).

The fact that various proteins (e.g. NDRG1, MxA, keratin 10) are identified in more than one spot on the gel indicates that some regulated proteins had PTM or several kinds of cleavages. PTMs can be hypothesized for protein spots with the same molecular weight but different p*I* (Goerg et al., 2004). This can be assumed for NDRG1 (spot 6 and 7, Figure 4.2-2B) in MDCK cells, which are reported to be phosphorylated (Olsen et al., 2006). However, PTMs have not been described for MxA proteins (spot 4 and 5, Figure 4.2-2A) in A549 cells so far and this shift in p*I* can therefore not be explained (Haller et al., 2009). Compared to their corresponding molecular weight and p*I* the three keratin 10 spots identified in infected MDCK cells (spot 3, 4 and 5, Figure 4.2-2B) showed varying locations in the corresponding gels. This could indicate several kinds of cleavage products or fragmentations (Liu et al., 2008).

The 16 identified proteins showed high variability of relative protein abundance over time indicating dynamic changes in the host cell proteomes in response to influenza virus infection. Interestingly, all of these proteins were up-regulated and none were down-regulated during influenza virus infection (Figure 4.2-3).

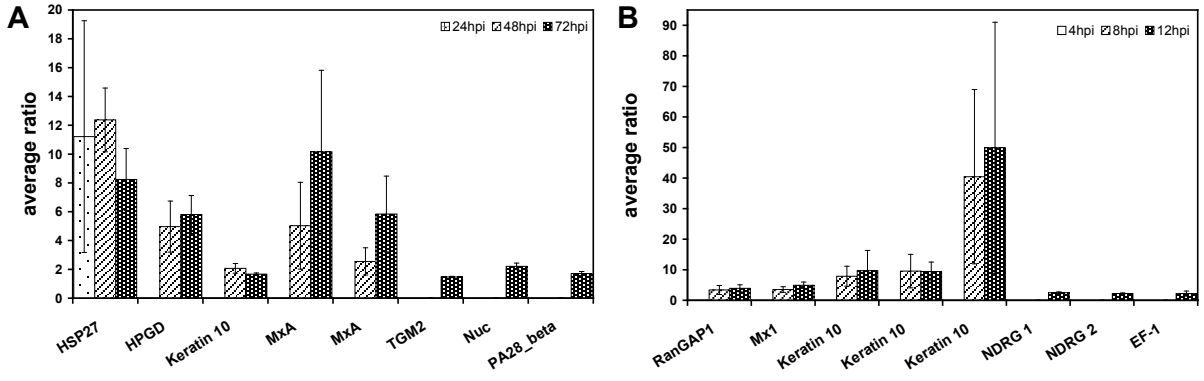

Figure 4.2-3: Quantitative data of proteome alterations of influenza PR/8-RKI infected A549 cells and MDCK cells

Average ratios of relative protein abundance of influenza PR/8-RKI virus infected (A) A549 cells and (B) MDCK cells against mock infected cells. Bar charts represent average ratios of the spot volumes (mean values ± SD of three independent experiments).

The diagram of Figure 4.2-3 shows that none of the identified proteins was differentially abundant at the earliest time point post infection at 4 hpi in MDCK cells. Only one protein (HSP27, spot 1, Figure 4.2-2A) in A549 cells was found to be regulated at all three time points (Figure 4.2-4A). This was unexpected with respect to the infection kinetics (Figure

4.2-1) showing an increase in HA at the same time point. The first extraction time points were chosen to represent early events in intracellular virus replication and virus release. Most of the identified proteins were not regulated significantly until the second extraction time point, which correlates to an increased production of viruses (Figure 4.2-1) measured by HA assay. Number and ratio of differentially abundant proteins increased at the third time point (Figure 4.2-3). In MDCK cells three proteins (NDRG1, EF-1) appeared to be up-regulated only at the last extraction time point after 12 hpi (spot 6, 7 and 8, Figure 4.2-3B). TGM2, nucleobindin and PA28-beta (spot 6, 7 and 8, Figure 4.2-3A) were regulated only at the last extraction time point in A549 cells, representing proteome changes at a very late stage of influenza virus infection. MDCK cells showed a wide dynamic range of protein abundance changes with an average ratio spanning from two-fold up to 50-fold for spot 5 (keratin 10) at 12 hpi (Figure 4.2-4B). Whereas for A549 cells only a range from about two-fold up to 12-fold was found (Figure 4.2-3A).

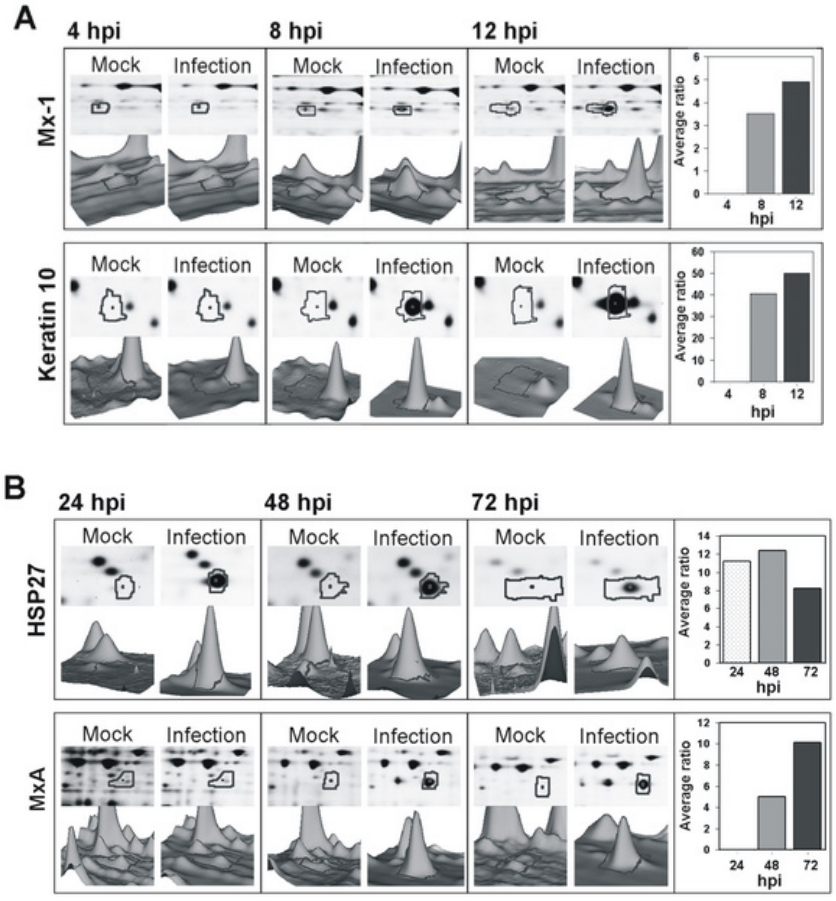

Figure 4.2-4: Selected altered abundant protein spots of proteome response in PR/8-RKI infected (A) MDCK cells and (B) A549 cells

Enlarged region of the respective 2-D DIGE map and the corresponding spot volume, showing a three dimensional view of representative altered abundant proteins during influenza PR/8-RKI virus infection. Bar charts represent average ratios of the spot volumes.

4.2.2. Infection kinetics and proteome alterations in MDCK cells infected with different influenza A PR/8 virus variants

A comparison of virus variants of the PR/8 strain by Schulze-Horsel et al. (Schulze-Horsel et al., 2009) obtained from two different suppliers (NIBSC, RKI) showed clear differences in maximum virus titers ($TCID_{50}$ and HA) and virus replication dynamics. In particular, induction of apoptosis and average life-time of infected MDCK cells were correlated with virus yields. To obtain further insights into the biological mechanisms of these differences, proteome data on MDCK cell infections with a virus variant obtained from RKI described in the previous study (see section 4.2.1) and referred to as 'data on PR/8-RKI variant' (Vester et al., 2009) are compared in the following to the PR/8-NIBSC variant (Vester et al., 2010).

High virus titers at the start of infection reflect the high MOI of 6 used for the infection (Figure 4.2-5;4.2-1) as well as the lower $TCID_{50}$ of the PR/8-NIBSC seed virus compared to the PR/8-RKI seed virus (data not shown). During infection with PR/8-NIBSC increase in virus titers could be seen 4 hpi, which was the same as described for PR/8-RKI virus (Figure 4.2-1) (Vester et al., 2009). The concentration of total virus particles increased over time from 1.5 to 2.0 log HA units/100µL at 12 hpi for MDCK cells infected with PR/8-NIBSC virus (Figure 4.2-5) and from 0.7 to 1.6 log HA units/100µL infected with PR/8-RKI (Figure 4.2-1). These differences in virus yields in comparison to previously described yields (Schulze-Horsel et al., 2009) could be due the early investigation time points and to the lack of trypsin in the virus growth medium used in this study. Flow cytometric monitoring of influenza virus infectivity was used for verification of infection in MDCK cells (Schulze-Horsel et al., 2009) and showed that 90% of the cells were infected at 6 hpi using PR/8-RKI / -NIBSC virus (data not shown).

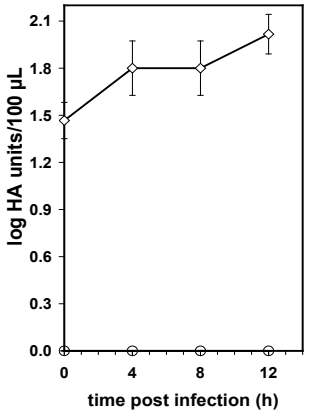

Figure 4.2-5: Virus titers (HA) for influenza PR/8-NIBSC virus infected MDCK cells

Infection kinetics of MDCK cells infected with PR/8-NIBSC (◊) and mock infection (o) (T-flasks, without trypsin addition, MOI = 6). Symbols represent mean values ± SD of three independent experiments.

Proteome alteration profiles at early time points post infection of PR/8-NIBSC infected MDCK cells were compared with mock infected MDCK cells using 2-D DIGE technology (see section 3.3). A representative 2-D DIGE gel of the proteome response at 12 hpi is shown in Figure 4.2-6A. The analysis with the BVA module of the DeCyder 2D software detected about 1440 ± 178 protein spots in total. Among them, 36 protein spots revealed changes in the relative abundance with statistical significance (± 1.7- fold change in relative abundance, $p < 0.001$) and are labeled serially with numbers in Figure 4.2-6A. Some characteristic proteins showing consistent abundance changes were selected as examples, and are displayed in Figure 4.2-6B in enlarged form. Comparison of the proteome profiles showed that infection with the two virus variants resulted in significant differences in the total number of regulated proteins. The PR/8-NIBSC virus variant caused the highest abundance changes while PR/8-RKI showed only 8 changes (Figure 4.2-2). Furthermore, PR/8-NIBSC induced an earlier perturbation of the proteome profile.

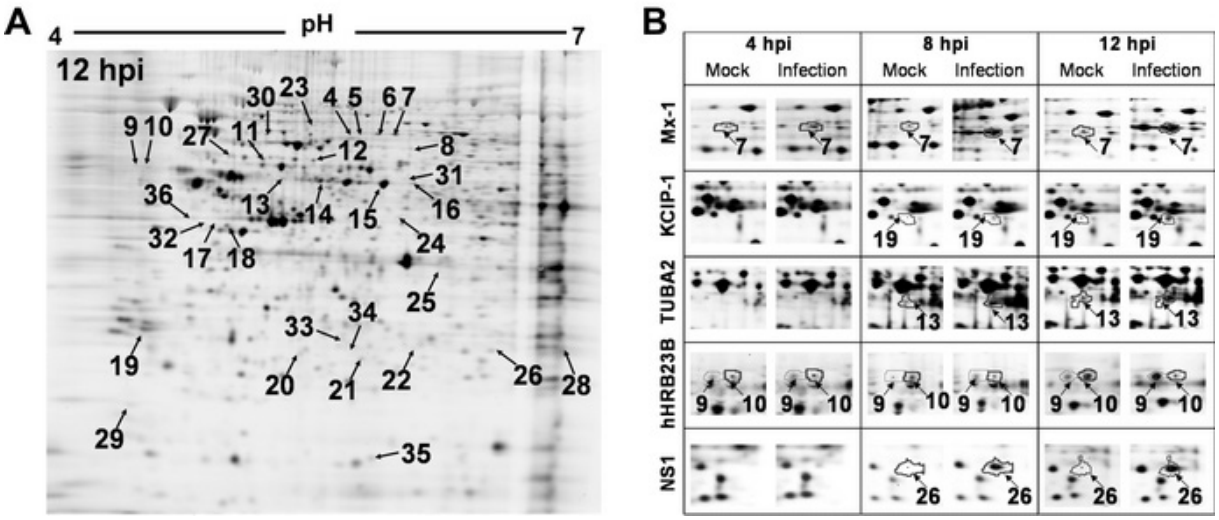

Figure 4.2-6: Representative 2-D DIGE gel of the proteome response and enlarged region of selected altered abundant proteins in PR/8-NIBSC infected MDCK cells

(A) Total protein extract (Cy2-labeled proteins) resolved by 2-D DIGE (24 cm; pH 4-7; 10% SDS-PAGE) of influenza PR/8-NIBSC virus variant infected MDCK cells at 12 hpi. (B) Enlarged regions of the respective 2-D DIGE gel region of selected altered abundant proteins (Mx1, spot 7; KCIP-1, spot 19; TUBA2, spot 13; hHRB23B, spots 9 and 10; NS1, spot 26).

Application of IPG strips with a broader pH range (pH 3–11) was tested before, but did not show any additional regulated protein spots (data not shown) is this particular case. As a result, whole proteome analysis was done with low range pH strips (pH 4-7) in the interest of improved separation efficiency.

The PR/8-RKI variant resulted in only up-regulated proteins (Figure 4.2-3), whereas the PR/8-NIBSC variants showed variability in the dynamics of relative protein abundance, resulting in 12 protein spots with decreased and 24 protein spots with increased abundance

levels displayed in Figure 4.2-7. More precisely, 3 protein spots were found to be differentially abundant at the earliest time points investigated at 4 hpi. However, the majority of the identified protein spots were not regulated significantly until 8 hpi and showed increased regulation levels only 12 hpi. Additionally, 10 protein spots appeared to be regulated only at the last extraction time point at 12 hpi.

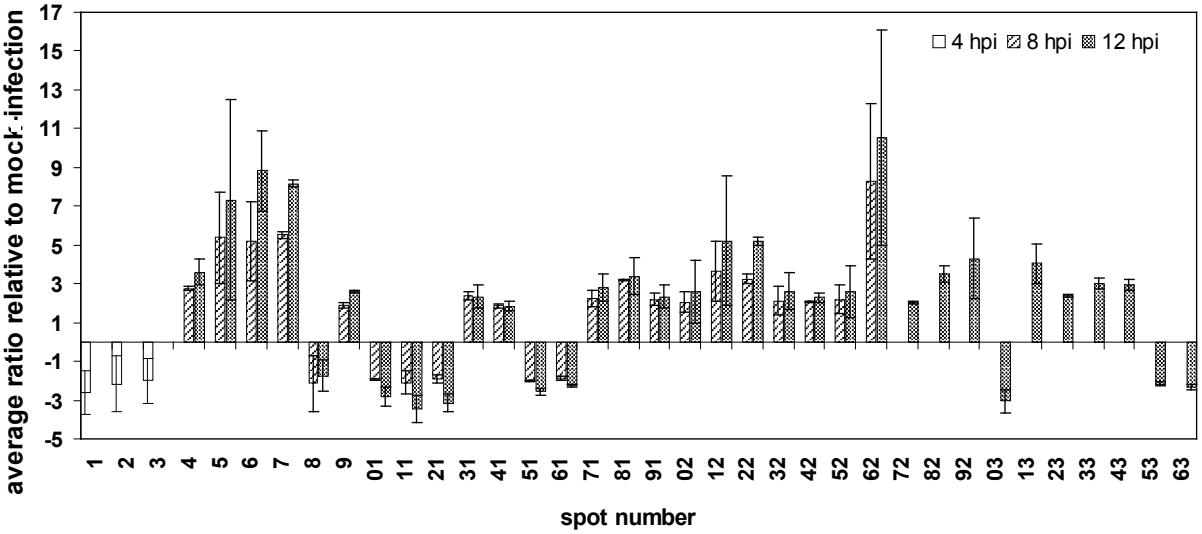

Figure 4.2-7: Quantitative data of proteome alterations of PR/8-NIBSC infected MDCK cells
Average ratios of relative protein abundance of infected against mock infected MDCK cells (influenza PR/8-NIBSC virus variant) at 4, 8 and 12 hpi. Bar charts represent average ratios of the spot volumes (mean values ± SD of three independent experiments).

All protein spots showing altered abundance levels were excised from the gel and in-gel digested with trypsin, followed by nanoHPLC-nanoESI-MS/MS analysis (section 3.3.5). Out of these 36 proteins analyzed 32 were identified unambiguously through their peptide fragmentation mass fingerprints using MASCOT and protein databases. Figure 4.2-8 shows an example of the nanoHPLC-nanoESI-MS/MS analysis results of a selected spot. The 32 identified proteins are summarized in Table 4.2-3, numbered according to Figure 4.2-6. These proteins act in diverse biological processes such as influenza virus induced signal transduction, cytoskeleton and microtubule remodeling, vesicle transport, proteolysis or DNA transport and repair. In comparison to the PR/8-RKI variant proteins for signal transduction, cytoskeleton remodeling and transport mechanisms were additionally affected by infection.

Table 4.2-3: Proteins identified as being differentially abundant in MDCK cells infected with influenza PR/8-NIBSC virus variant compared to mock infected cells

Spot ID[a)]	NCBI no[b)]	Protein description	MASCOT scores			Protein function
			Matched peptides[c)]	Mowse score[d)]	Sequ. cov (%)	
1	229552	Albumin	25	1083	42	Transport/cargo
2	229552	Albumin	25	1136	40	Transport/cargo
3	229552	Albumin	28	1349	43	Transport/cargo

4	50978856	Myxovirus resistance protein 1 (Mx1)	8	258	11	Signal transduction (IFN induced)
5	50978856	Myxovirus resistance protein 1 (Mx1)	6	169	9	Signal transduction (IFN induced)
6	50978856	Myxovirus resistance protein 1 (Mx1)	14	484	22	Signal transduction (IFN induced)
7	50978856	Myxovirus resistance protein 1 (Mx1)	11	508	15	Signal transduction (IFN induced)
8	61740600	Keratin 10	9	297	14	Cytoskeleton component
9	57094213	UV excision repair protein RAD23 (hHRB23B) [e)]	7	268	15	Protein degradation
10	57094213	UV excision repair protein RAD23 (hHRB23B) [e)]	2	90	4	Protein degradation
11	73946455	Heterogeneous nuclear ribo-nucleoprotein K (hnRNP K) [e)]	10	396	17	Nucleic acid transport
12	73946449	Heterogeneous nuclear ribo-nucleoprotein K (hnRNP K) [e)]	8	373	19	Nucleic acid transport
13	73996516	Tubulin alpha-2 (TUBA2) [e)]	4	171	7	Cytoskeleton component
14	73996455	Cytokeratin 8 (CK-8)	18	933	35	Cytoskeleton component
15	73996455	Cytokeratin 8 (CK-8)	22	998	37	Cytoskeleton component
16	73996455	Cytokeratin 8 (CK-8)	18	873	30	Cytoskeleton component
17	73958059	Beta-actin [e)]	5	212	14	Cytoskeleton component
18	61740600	Keratin 10	12	674	20	Cytoskeleton component
19	73992048	Protein kinase C inhibitor protein-1 (KCIP-1) [e)]	5	285	20	Signal transduction
20	73981584	Proteasome subunit beta(PSMB4)[e]	3	175	9	Protein degradation
21	61740600	Keratin 10	8	322	12	Cytoskeleton component
22	73996314	Cytokeratin 5 (CK-5)	11	555	13	Cytoskeleton component
23	73949168	F-box protein, helicase, 18 [e)]	22	912	35	DNA replication/repair
24	61740600	Keratin 10	4	118	5	Cytoskeleton component
25	73946797	Annexin A1 (ANXA1) [e)]	5	176	17	Vesicle transport
26	8486133	Non-structural protein 1 (NS1)	3	119	13	Influenza viral protein
27	73946455	Heterogeneous nuclear ribo-nucleoprotein K (hnRNP K) [e)]	6	239	13	Nucleic acid transport
28	57106546	Triosephosphate isomerase (TIM)[e]	2	140	8	Metabolism/glycolysis
30	73969353	Tubulin-tyrosine ligase (CG1550-PA) [e)]	6	192	10	Cytoskeleton modification
31	73952424	Interferon-induced protein with tetratricopeptide repeats 1 [e)]	4	161	9	Zn-dependent protease
32	73958059	Beta-actin [e)]	3	116	7	Cytoskeleton component
33	61740600	Keratin 10	13	518	19	Cytoskeleton component

a) *Spot ID represents the number on the 2-D DIGE gels (Figure 4.2-6)*

b) *Accession numbers according to the NCBInr database*

c) *Number of peptides identified by LC-MS/MS given by MASCOT*

d) *Mowse score is -10 x log(p), where p is the probability that the observed match is a random event. Based on the NCBInr database using the MASCOT searching program as LC-MS/MS data. Scores greater than 53 are considered significant ($p < 0.05$)*

e) *Predicted protein; derived from annotated genome sequence (NW_876264) using gene prediction method (GNOMON)*

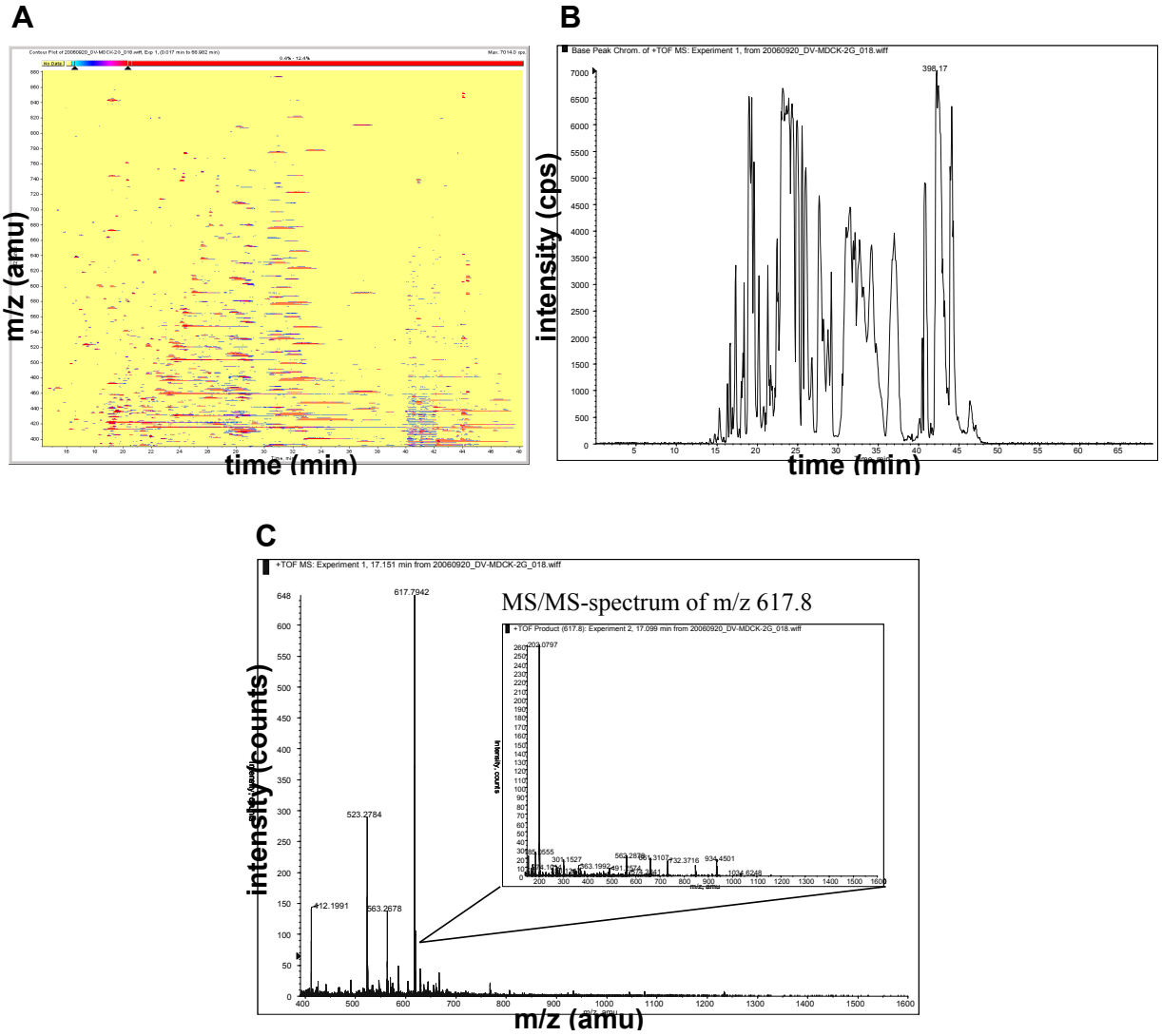

Figure 4.2-8: nanoHPLC-nanoESI-MS/MS results of spot 28 (PR/8-NIBSC infected MDCK cell) after in-gel digestion

Representative spectra of a spot from the PR/8-NIBSC infection in MDCK cells separated by nanoHPLC-nanoESI-MS/MS. (A) Contour plot (x-axis: retention-time / y-axis: m/z) of the tryptic digested spot 28, (B) base peak chromatogram of the reversed phase (C18) separation of the tryptic peptides of spot 28, (C) MS spectrum at time point 17.15 min of the chromatographic separation showing the fragmentation pattern (MS/MS fragment ion spectrum) of the precursor ion at m/z 617.8. The protein spot was identified as TIM (spot 28; Table 4.2-3) by searching the NCBInr database.

4.2.3. Infection kinetics and proteome alterations in Vero cells infected with influenza A PR/8 virus

Besides the MDCK cell line, an alternative vaccine production cell line with specific characteristics has been used to determine the effects of viral replication on proteome profiles (Vester et al., 2010). The Vero cell line used is deficient in IFN expression (Govorkova et al., 1995) and previous studies reported the common method of passaging of influenza virus for several times as a need to obtain higher yields with faster replication dynamics (Ozaki et al., 2004). To get insights into complex mechanism involved in the cellular immune response of these cells lacking an IFN system or mechanisms relevant for adaptation of virus strains, proteome alterations of Vero cells in response to infection with a cell line adapted and a non-adapted human PR/8 strain were analyzed (Vester et al., 2010).

For Vero cells infected with cell line adapted PR/8-RKI-Vero virus, HA titer did not increase significantly until 24 hpi and reached maximum titers of 1.6 log HA units/100µL at about 72 hpi (Figure 4.2-9). Due to this result, compared to MDCK cells later protein extraction time points were chosen to display the different dynamics in virus replication and also the resulting protein abundance changes. In the observed sampling time no virus particle release could be detected for Vero cells infected with non-adapted virus (Figure 4.2-9). Differences in the HA at 0 hpi were due to different $TCID_{50}$ values of the two seed viruses.

Flow cytometric monitoring of influenza A virus infectivity (Schulze-Horsel et al., 2009) was used for verification of infection in Vero cells and showed that 95% of the cells were infected at 20 hpi using the PR/8-RKI-Vero strain (data not shown).

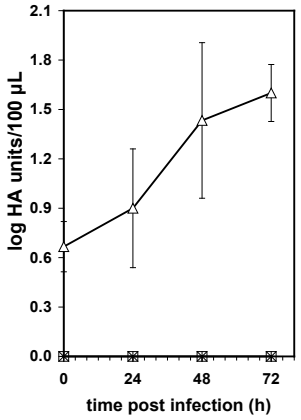

Figure 4.2-9: Virus titers (HA) for influenza PR/8-RKI-Vero virus infected Vero cells

Infection kinetics of Vero cell infected with cell line adapted PR/8-RKI-Vero virus (∆) and non-adapted PR/8-RKI virus (∗) and mock infection (□)(T-flasks, without trypsin addition, MOI = 6). Symbols represent mean values ± SD of three independent experiments.

The proteome profiles of Vero cells at different time points of infection with both, a cell line adapted influenza virus and a non-adapted virus were compared. After 2-DE separation (section 3.3) a total number of 1635 ± 66 protein spots were detected. A set of representative gels of the proteome profiles of Vero cells at the corresponding time points post infection are shown in Figure 4.2-10A-C for cell line adapted virus infection. The analysis revealed changes in abundance of 55 proteins, (infection versus mock infection, spot volume ratios ± 1.7- fold change in relative abundance, $p < 0.001$) in response to infection with the cell line adapted virus (Figure 4.2-11A). 24 proteins were down- and 31 proteins were up-regulated (Figure 4.2-11A).

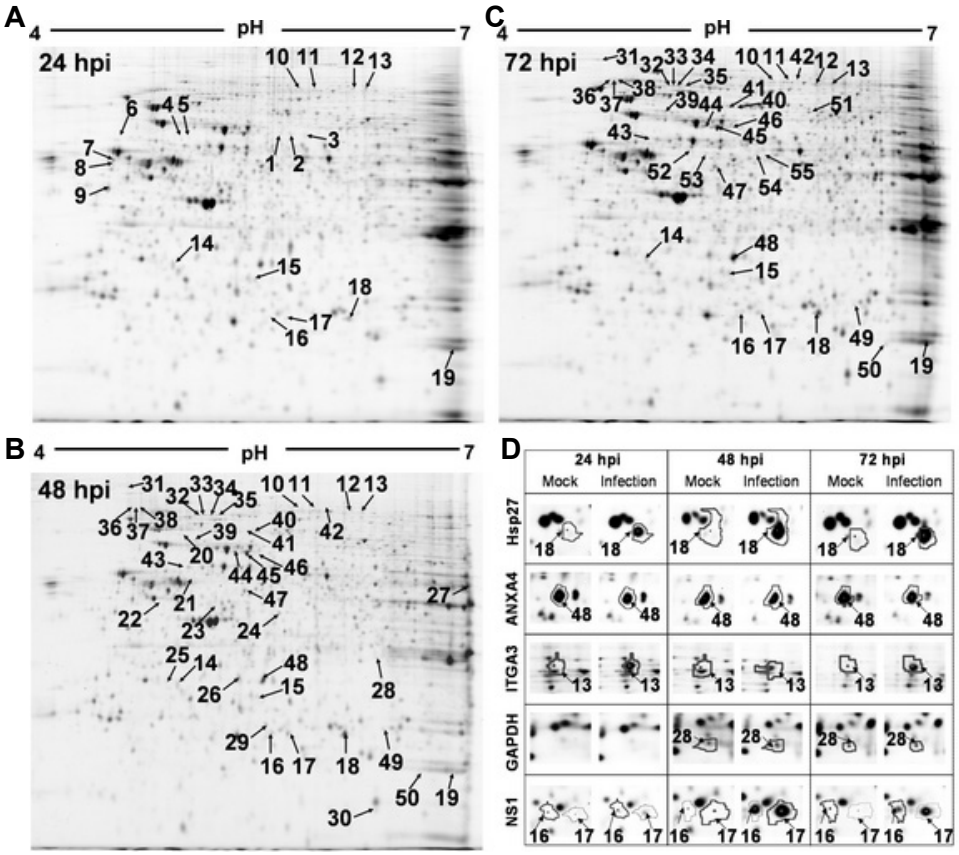

Figure 4.2-10: Representative 2-D DIGE gels of the proteome response and enlarged regions of selected altered abundant proteins in PR/8-RKI-Vero infected Vero cells

Total protein extracts (Cy2-labeled proteins) resolved by 2-D DIGE (24 cm; pH 4-7; 10% SDS-PAGE) of cell line adapted PR/8-RKI-Vero infected Vero cells at (A) 24, (B) 48 and (C) 72 hpi. (D) Enlarged regions of the respective 2-D DIGE gel region of selected altered abundant proteins (HSP27, spot 18; ANXA4, spot 48; ITGA3, spot 13; GAPDH, spot 28; NS1, spots 16 and 17).

Representative regulated proteins differed not only with respect to the extent of changes in abundance, but also in the time course of these changes as displayed in 4.2-10D (enlarged region of representative gel map). At the first infection time point (24 hpi) differences were identified for only 20 proteins (Figure 4.2-11A). The most pronounced changes of the proteome were observed at 48 hpi, with 41 altered abundant proteins. Towards the end of

the infection with cell line adapted virus (72 hpi) relative abundance changes decreased slightly to 34 regulated proteins.

In contrast, infection with the non-adapted virus led to a total of only five regulated proteins (4.2-11B). Two proteins were up- and three down-regulated. Protein spots 2-5 (4.2-11B) were also found to be regulated by the cell line adapted virus (spots 10-13, Table 4.2-4).

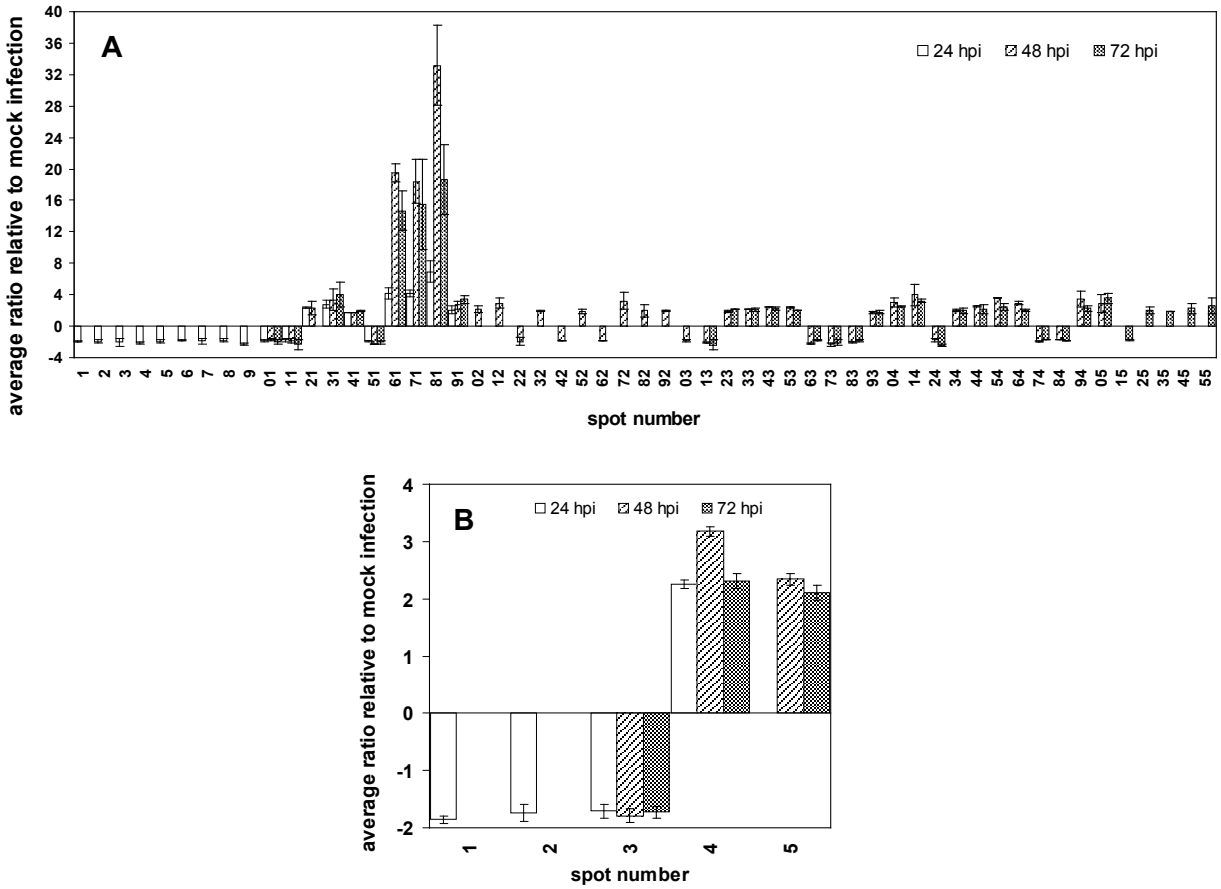

Figure 4.2-11: Quantitative data of proteome alterations of (A) cell line adapted PR/8-RKI-Vero and (B) non-adapted PR/8-RKI infected Vero cells

Average ratios of relative protein abundance of infected against mock infected Vero cells at 24, 48 and 72 hpi.(B) spot numbers in brackets correspond to spot numbers of (A). Bar charts represent average ratios of the spot volumes (mean values ± SD of three independent experiments).

Following to spot picking and tryptic digestion, protein identification was carried out by nanoHPLC-nanoESI-MS/MS analysis (section 3.3.5). 50 out of 55 protein spots selected for the cell line adapted virus infection were identified (Table 4.2-4). The identified proteins included cell interaction or cell adhesion factors, members of the cytoskeleton and intermediate filament system, proteins involved in maintenance of the intracellular redox state or glycolytic metabolism, as well as stress response proteins comprising protein folding and anti-apoptosis associated proteins. The small set of identified proteins altered due to infection with non-adapted virus is listed in Table 4.2-5 and included one type of protein, Integrin alpha 3 (ITGA3).

Table 4.2-4: Proteins identified as being differentially abundant in Vero cells infected with cell line adapted influenza PR/8-RKI-Vero virus compared to mock infected cells

Spot ID[a)]	NCBI no[b)]	Protein description	MASCOT scores			Protein function
			Matched peptides[c)]	Mowse score[d)]	Sequ. cov (%)	
2	229552	Albumin	14	550	23	Transport/cargo
4	109115262	Keratin 10	13	610	20	Cytoskeleton component
5	109115262	Keratin 10	15	861	22	Cytoskeleton component
7	109096460	Tubulin, alpha (TUBA) [e)]	5	229	11	Cytoskeleton component
8	109102035	Histone-binding protein (RBBP4)[e)]	10	525	21	Chromatin remodeling
9	75075845	Vimentin	20	932	36	Intermediate filament
10	109114294	Integrin alpha 3 (ITGA3) [e)]	9	257	12	Cell adhesion/interaction
11	109114294	Integrin alpha 3 (ITGA3) [e)]	6	169	6	Cell adhesion/interaction
12	109114294	Integrin alpha 3 (ITGA3) [e)]	6	161	6	Cell adhesion/interaction
13	109114294	Integrin alpha 3 (ITGA3) [e)]	9	257	12	Cell adhesion/interaction
14	114554262	EF-hand domain family, member D2 (EFHD2) [e)]	12	597	27	Ca^{2+} signal modulators
16	8486133	Non-structural protein 1 (NS1)	5	339	23	Influenza viral protein
17	8486133	Non-structural protein 1 (NS1)	9	464	36	Influenza viral protein
18	109066218	Heat shock protein 27kDa	15	196	52	Chaperone/apoptosis
19	109003875	Peroxiredoxin (PRX) [e)]	12	202	49	Oxidative stress
20	109086287	Golgi-associated microtubule-binding protein (HOOK3) [e)]	5	179	6	Microtubule-binding protein
21	109096823	Keratin 1	27	1279	32	Cytoskeleton component
22	109095369	Enolase 2 [e)]	9	386	20	Metabolism/glycolysis
23	109096855	Keratin 8	8	395	15	Cytoskeleton component
24	109087525	N-myc downstream regulated gene 1 (NDRG1) [e)]	5	199	14	Signaling/apoptosis
25	114554262	EF-hand domain family, member D2 (EFHD2) [e)]	12	524	46	Ca^{2+} signal modulators
26	114577902	Annexin IV (ANXA4) [e)]	18	777	47	Vesicle transport
27	109081748	Pyruvate kinase (PK) [e)]	23	645	48	Metabolism/glycolysis
28	109095230	Glyceraldehyde-3-phosphate dehydrogenase (GAPDH) [e)]	3	63	14	Metabolism/glycolysis
29	90082004	Unnamed protein product	7	286	25	Chaperone/stress response
31	114667194	Hypothetical protein [e)]	5	212	3	Intermediate filament
32	114649455	Heat shock protein 105kD [e)]	14	577	12	Chaperone/ER stress
33	114649455	Heat shock protein 105kD [e)]	16	717	15	Chaperone/ER stress
34	114649455	Heat shock protein 105kD [e)]	12	581	12	Chaperone/ER stress
35	114649455	Heat shock protein 105kD [e)]	17	822	16	Chaperone/ER stress
36	109100308	Integrin alpha V (ITGAV) [e)]	10	181	9	Cell adhesion/interaction
37	109100308	Integrin alpha V (ITGAV) [e)]	12	593	10	Cell adhesion/interaction
38	109100308	Integrin alpha V (ITGAV) [e)]	16	272	18	Cell adhesion/interaction
39	109100069	Dynein 1 [e)]	9	176	12	Cytoplasmic intermediate chain
40	109053865	Leprecan-like 1 (LEPREL1) [e)]	12	314	21	Collagen biosynthesis
41	109071319	Heat shock protein 90kDa [e)]	5	146	9	Chaperone/viral gene expression
42	109114294	Integrin alpha 3 (ITGA3) [e)]	6	178	6	Cell adhesion/interaction

43	109111923	Heterogeneous nuclear ribo-nucleoprotein K (hnRNP K) [e]	13	590	27	Nucleic acid transport
44	109070524	Heat shock protein 70kDa [e]	10	265	15	Chaperone/nuclear transport
45	109070524	Heat shock protein 70kDa [e]	30	416	24	Chaperone/nuclear transport
46	109070524	Heat shock protein 70kDa [e]	18	899	17	Chaperone/nuclear transport
47	55846684	Glial fibrillary acidic protein (GFAF	23	1262	45	Intermediate filament
48	114577902	Annexin IV (ANXA4) [e]	21	994	55	Vesicle transport
49	109114613	Short-chain dehydrogenase/ reductase (SDR) [e]	5	178	19	Oxidoreductase
50	74136169	Superoxide dismutase (MnSOD)	3	68	16	Oxidative stress
51	109072274	Villin 2 (Ezrin) [e]	18	636	17	Cytoskeleton organization/signaling
52	109043586	Nuclear receptor co-repressor/ HDAC3 complex subunit [e]	6	266	21	Transcription regulation
53	109065595	Chaperonin containing TCP1 [e]	14	404	30	Chaperone/protein folding
54	114684889	Formiminotransferase cyclodeaminase (FTCD) [e]	10	364	17	Amino acid metabolism
55	109080868	Protein disulfide isomerase-associated 3 (PDIA3) [e]	7	186	13	ER - glycoprotein folding

[a] *Spot ID represents the number on the 2-D DIGE gels (Figure 4.2-10)*
[b] *Accession numbers according to the NCBInr database*
[c] *Number of peptides identified by LC-MS/MS given by MASCOT*
[d] *Mowse score is -10 x log(p), where p is the probability that the observed match is a random event. Based on the NCBInr database using the MASCOT searching program as LC-MS/MS data. Scores greater than 53 are considered significant ($p < 0.05$)*
[e] *Predicted protein; derived from annotated genome sequence (NW_001122895) using gene prediction method (GNOMON)*

Table 4.2-5: Proteins identified as being differentially abundant in Vero cells infected with non-adapted influenza PR/8-RKI virus compared to mock infected cells

Spot ID[a]	NCBI no[b]	Protein description	MASCOT scores			Protein function
			Matched peptides[c]	Mowse score[d]	Sequ. cov (%)	
1	109114294	Integrin alpha 3 (ITGA3) [e]	3	80	3	Cell adhesion/interaction
2	109114294	Integrin alpha 3 (ITGA3) [e]	5	105	6	Cell adhesion/interaction
3	109114294	Integrin alpha 3 (ITGA3) [e]	6	80	6	Cell adhesion/interaction
4	109114294	Integrin alpha 3 (ITGA3) [e]	9	257	12	Cell adhesion/interaction
5	109114294	Integrin alpha 3 (ITGA3) [e]	6	161	7	Cell adhesion/interaction

[a] *Spot ID represents the number of the diagram of quantitative protein abundance (Figure 4.2-11)*
[b] *Accession numbers according to the NCBInr database*
[c] *Number of peptides identified by LC-MS/MS given by MASCOT*
[d] *Mowse score is -10 x log(p), where p is the probability that the observed match is a random event. Based on the NCBInr database using the MASCOT searching program as LC-MS/MS data. Scores greater than 53 are considered significant ($p < 0.05$)*
[e] *Predicted protein; derived from annotated genome sequence (NW_001122895) using gene prediction method (GNOMON)*

4.2.4. Western blot verification

To validate data obtained from 2-D DIGE, Western blot analysis (section 3.3.6) was performed for 3 proteins showing consistent and clear abundance changes after PR/8-NIBSC and PR/8-RKI virus infection in MDCK cells. Proteins chosen were involved in different cellular processes, e.g. actin, a cytoskeleton component and Mx1, a protein involved in the antiviral response. Additionally, the viral NS1 protein found abundantly in PR/8-NIBSC infected MDCK cells was monitored over the time course of infection. Western blot analysis confirmed the differential abundance for all of these proteins (Figure 4.2-12). The protein expression profile of two selected differentially abundant proteins was further confirmed by RT-qPCR (Seitz et al., 2010). Here, the determination of the mRNA transcript level of the viral NS1 and Mx1 in MDCK cells infected with both PR/8-NIBSC and PR/8-RKI virus variants further supported results obtained by proteome data.

Western blots were also carried out for proteins of Vero cells infected with PR/8-RKI-Vero. Therefore, the time course of the viral NS1 regulatory protein and Mx1, an IFN induced antiviral response protein as a negative control for IFN deficiency of Vero cells were analyzed. Consistent with the observations in 2-D DIGE analysis, NS1 was found to be up-regulated and no Mx1 protein could be detected, due to the absence of IFN (Figure 4.2-12).

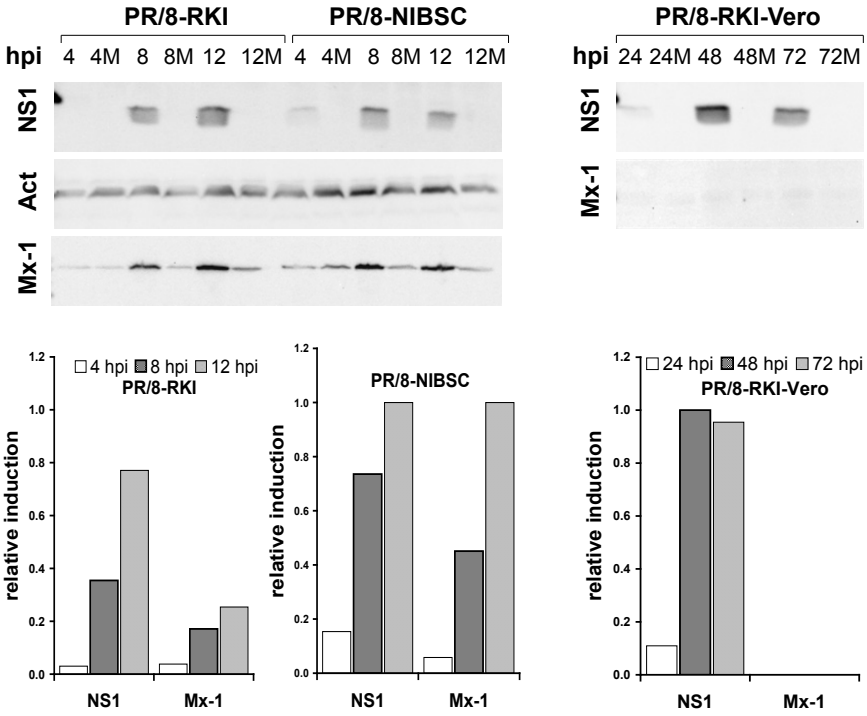

Figure 4.2-12: Western blot analysis of representative altered abundant proteins

Influenza PR/8-RKI and PR/8-NIBSC virus infected MDCK cells and influenza PR/8-RKI-Vero virus infected Vero cells. Protein profiles of viral NS1, actin and Mx1 are shown for infected and mock infected (M) MDCK cells and viral NS1 and Mx1 for infected and mock infected (M) Vero cells. After densitometric analysis, signal intensity was normalized to ERK2. Bar charts show relative induction of normalized densitometric values of some representative proteins.

4.3. RT-qPCR assay for the analysis of human influenza A virus transcription and replication dynamics

4.3.1. Development of a RT-qPCR assay

To verify the existing mathematical model on influenza virus replication and to better understand virus replication dynamics during vaccine production an assay system able to distinguish specifically between viral genome vRNA(-), replicative intermediates cRNA(+) and viral messenger RNA (vmRNA(+)) of segments 4 (HA), 6 (NA), 7 (M) and 8 (NS) during the life cycle of influenza virus was needed. Hence, a RT-qPCR assay was developed for the analysis of influenza A virus transcription and replication dynamics in MDCK cells (Vester et al., 2010).

As a first step for assay development an optimal RNA extraction method was established. Consequently, 4 different extraction protocols were compared, including (I) Trizol extraction method (Invitrogen), (II) the QIAamp Viral RNA Mini Spin Kit (Qiagen), (III) RTP DNA/RNA Virus Mini Kit (Invitek) and (IV) NucleoSpin RNA II (Macherey-Nagel). Due to laborious and time-consuming handling steps the Trizol method was inapplicable and the RTP DNA/RNA Virus Mini Kit showed no linear correlation after serial dilution of viral RNA and both methods were therefore excluded after first tests (data not shown). Based on good linearity and sensitivity results (data not shown) the QIAamp Viral RNA Mini Kit was used to extract vRNA(-) from supernatant of infected cells and the NucleoSpin RNA II Kit for extraction of total cellular RNA of cells by applying a direct lysis on culture dish (section 3.4.1).

Accurate transcript quantification using RT and qPCR depends on the construction of standard curves. To date, different approaches for the development of standard curves include the use of plasmid clones containing the cDNA of interest as a template or constitutively expressed genes, such as β-actin and 16S ribosomal RNA. In contrast, external RNA standards used to obtain a standard curve offering some important advantages by processing samples and RNA standards in parallel and therefore with the same efficiency and conditions. Hence, for the RT-qPCR assay the production of synthetic viral RNAs used as reference standards for validation and quantification was established for each influenza viral RNA type and segment. For uniRT Uni12 (M) primer were selected from the complementary sequence to the conserved viral RNA-termini. Previous studies performed with Uni12 (M) primer (Chan et al., 2006b; Hoffmann et al., 2001) showed that they were applicable to all subtypes of influenza A virus to ensure an optimal and broad application range. Uni 12 (M) primer were used to generate a full-length cDNAs of each segment and viral RNA type followed by conventional PCR with gene specific primer for amplification of full-length PCR products (Figure 4.3-1). Here, modified primer pairs (Table C-2, Appendix)

from sequences described previously (Chan et al., 2006b) were used for amplification of the full-length segments of influenza A virus. Due to difficulties with long cDNAs and PCR products and probably secondary RNA structures it was not possible so far to produce full-length products of segment 1 (PB2), 2 (PB1) and 3 (PA). PCR products of segment 4 (HA), 6 (NA), 7 (M) and 8 (NS) were chosen for further analysis and were identified accurately using agarose gel electrophoresis, representative shown for segment 6 (NA) and 8 (NS) (Figure 4.3-2A). Synthetic viral RNA synthesis by *in vitro* transcription of viral cDNA, based on an optimized protocol described by Frohnhoffs *et al*., was applied (Fronhoffs et al., 2002). This protocol avoids labor intensive cloning procedure and create templates containing a T7 promoter gene sequence for *in vitro* transcription of these standard viral RNAs (Figure 4.3-1). *In vitro* transcribed RNAs were identified accurately using formaldehyde gel electrophoresis representative shown for segment 6 (NA) and 8 (NS) (Figure 4.3-2B). The viral RNA reference standards have the advantage that both, standard viral RNA and unknown viral RNA sample undergo the same pspRT and qPCR conditions (Bustin et al., 2009).

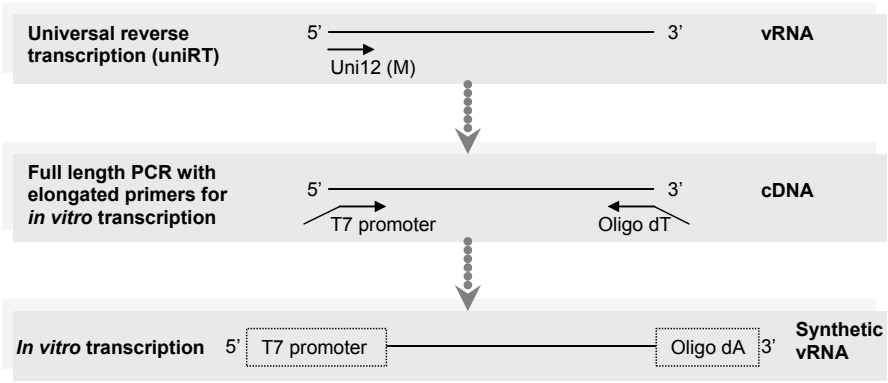

Figure 4.3-1: Scheme of in vitro transcribed viral RNA reference standards for vmRNA(+) synthesis

Primer pairs were elongated at the 5'-end of the 5'-primer with T7-promoter (5'-T7), and at the 5'-end of the 3'-primer with Oligo-dT (3'-Oligo-dT). Synthesis of cRNA was performed by in vitro transcription with T7 RNA polymerase.

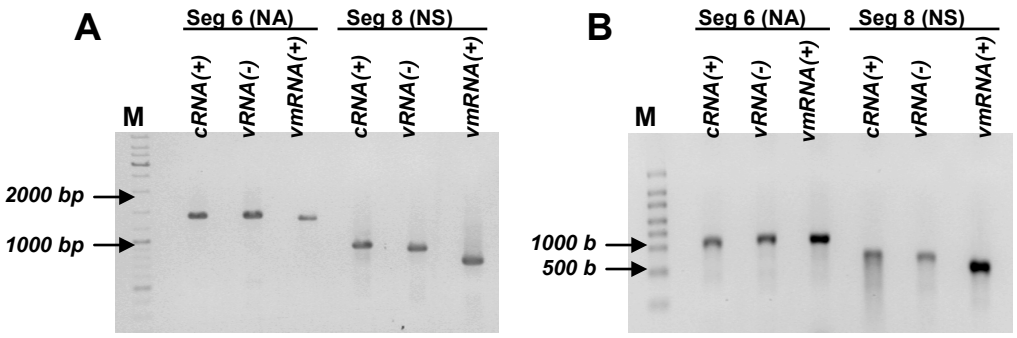

Figure 4.3-2: Quality control of viral RNA reference standards of segment 6 (NA) and 8 (NS)

(A) Agarose gel electrophoresis of full-length PCR products and (B) formaldehyde gel electrophoresis of in vitro transcribed RNA standards of cRNA(+), vRNA(-), vmRNA(+) of segment 6 (NA) and 8 (NS). M: GeneRuler DNA Ladder (Fermentas) (A); M: RiboRuler High Range RNA Ladder (Fermentas) (B).

A polarity-specific priming strategy during RT was established to distinguish in a total cellular RNA mixture between the three types of viral RNAs (vmRNA(+), cRNA(+) and vRNA(-)) and synthesize these specifically (section 3.4.3). Through the construction of gene specific sense (-RTfor), antisense (+RTrev) and the use of Oligo-dT primer (Table C-2 Appendix) for the four viral segments, the cDNA synthesis of the different viral types could be initiated separately based on their different polarities.

As a first step in building up a qPCR platform based on SYBR green I detection, single dilution series of the polarity-specific reverse-transcribed synthetic RNA standards were amplified (section 3.4.3). A representative qPCR amplification curve and the resulting standard curve is shown for the vmRNA(+) of segment 7 (M) in Figure 4.3-3. Primer sets for qPCR were designed particularly producing only short amplification products of each segment to prevent mismatching and false-amplification (Bustin and Nolan, 2004) (Table C-3, Appendix). The fluorescence emitted from SYBR green I bound to dsDNA, which is proportional to the amount of amplified DNA, was measured at the end of the annealing phase of each PCR cycle. The log-linear phase of the amplification reaction can easily be detected. Quantification of viral RNA is achieved by extrapolation of fluorescence signals from test samples against the synthetic RNA reference standard curves, which represent the initial copy numbers for a defined fluorescence signal.

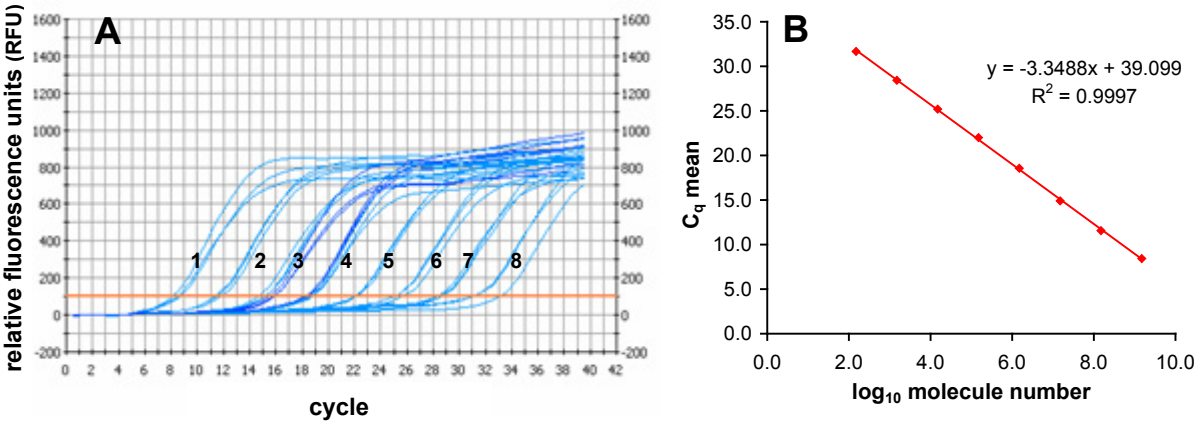

Figure 4.3-3: RT-qPCR amplification curve and standard curve of vmRNA(+) reference standard of segment 7 (M)

(A) Amplification curves of descending 10-fold dilution of synthetic vmRNA(+) reference standard of segment 7 (M) in triplicate. (B) Obtained standard curve by plotting C_q values vs. the logarithm of initial molecule number of the corresponding synthetic RNA reference.

High quality data needed for high precision and reliability of the assay were obtained by optimizing pspRT and qPCR conditions (Bustin et al., 2009). Optimization included design and selection of optimal primer combinations and concentrations, temperature and duration time of pspRT synthesis and annealing and extension of PCR, type of RT enzyme and concentration of Mg^{2+} (optimization data not shown; optimal conditions, section 3.4.2/3.4.3).

4.3.2. Validation of the RT-qPCR assay

For assay validation standard curves were generated in triplicates by serial dilution of viral RNA reference standards of viral segments 4 (HA), 6 (NA), 7 (M) and 8 (NS) (section 3.4.4).

Specificity and sensitivity of the assay

Sequence analysis of the PCR products of all viral segments used, confirmed the accurate amplification of the respective viral segments (data not shown). Additionally, for assay specificity verification a melting curve analysis was used to identify different reaction products, including nonspecific products and primer-dimers (Ririe et al., 1997). Melting curves were generated after completion of amplification by increasing the temperature in small steps and monitoring the fluorescent signal at each step. As the dsDNA in the reaction denatured, fluorescence decreased rapidly and significantly. A plot of the negative first derivative of the change in fluorescence (-dF/dT, rate of change of fluorescence) vs. temperature has distinct peaks that correspond to the T_m of each product. Representative melting curves are shown for vRNA(-) of segment 6 (NA) and 8 (NS) with T_m values of 85.5°C and 86.9°C, respectively in Figure 4.3-4. Analysis of all corresponding qPCR products showed no unspecific products or primer dimer synthesis.

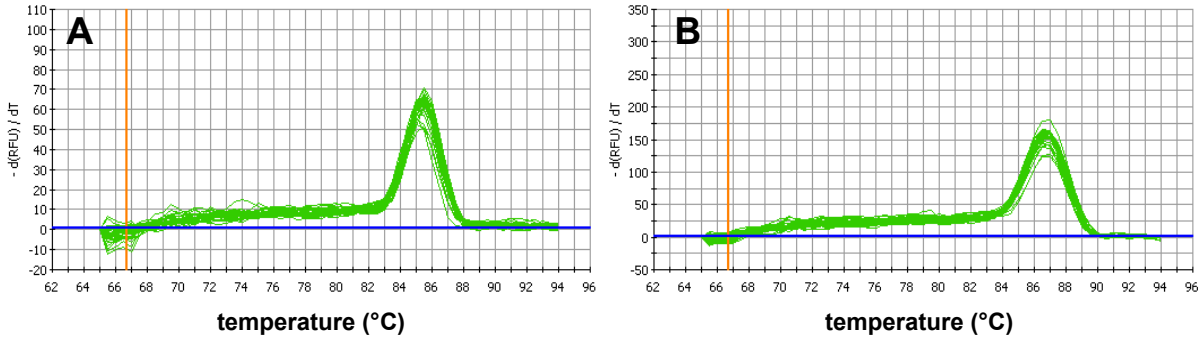

Figure 4.3-4: Melting curve analysis of PCR products of vRNA(-) of segment (A) 6 (NA) and (B) 8 (NS)
After completion of amplification, melting curves were generated by increasing temperature and monitoring fluorescent signal. As dsDNA denatured, fluorescence signal decreased. The negative first derivative of change in fluorescence (-dF/dT) was plotted as a function of temperature.

No cross reactivity was detected with RNA extracts from uninfected cells or by the use of a complementary polarity-specific primer during pspRT (data not shown).

According to the 'MIQE guidelines for qPCR' (Bustin et al., 2009), NTCs with high C_q can be ignored if the C_q for the lowest concentration tested is at least 5 C_q values lower than the C_q of the NTC. C_q of positive tested NTC were in the range of about 33 - 34. Using this guideline the lowest concentration of detected viral RNA molecules was in the range of a C_q of about 28, which corresponds to 1.0 x 10^3 – 8.5 x 10^3 RNA molecules for all viral RNA reference standards tested. Linearity was shown for a minimum of five orders of magnitude. The precise working range of the respective viral RNA type and segment is listed in Table 4.3-1.

Table 4.3-1: Validation results of the RT-qPCR assay

Parameter	Segment 4 (HA)			Segment 6 (NA)		
	vRNA(-)	cRNA(+)	vmRNA(+)	vRNA(-)	cRNA(+)	vmRNA(+)
Sensitivity (LOD) (× 10^3 mol)	5.6	5.5	5.7	5.1	5.1	5.3
Linear range (× 10^3-10^7 mol)	5.6	5.5	5.7	5.1	5.1	5.3
CV repeatability C_q (%)	< 2.3	< 0.8	< 1.7	< 1.3	< 1.4	< 1.4
CV reproducibility C_q (%)	< 1.6	< 1.6	< 2.8	< 1.7	< 2.6	< 1.4
Linear Regression						
Slope	-3.41	-3.41	-3.53	-3.42	-3.25	-3.33
Intercept	41.21	41.16	41.62	38.18	38.54	38.17
Amplification efficiency (E%)	96	96	92	96	103	100
R^2	0.995	0.996	0.995	0.999	0.997	0.995
Standard deviation of the method (SD)	0.48	0.45	0.33	0.19	0.31	0.13
	Segment 7 (M)			**Segment 8 (NS)**		
	vRNA(-)	cRNA(+)	vmRNA(+)	vRNA(-)	cRNA(+)	vmRNA(+)
Sensitivity (LOD) (× 10^3 mol)	8.2	7.9	1.0	8.5	7.7	6.6
Linear range (× 10^3-10^7 mol)	8.2	7.9	1.0	8.5	7.7	6.6
CV repeatability C_q (%)	< 1.8	< 2.0	< 1.5	< 2.3	< 2.0	< 1.5
CV reproducibility C_q (%)	< 3.1	< 3.0	< 2.5	< 1.7	< 2.3	< 2.8
Linear Regression						
Slope	-3.73	-3.64	-3.45	-3.35	-3.60	-3.45
Intercept	42.31	42.00	45.6	39.77	40.34	39.29
Amplification efficiency (E%)	85	88	92	99	90	95
R^2	0.995	0.993	0.989	0.997	0.996	0.999
Standard deviation of the method (SD)	0.34	0.18	0.55	0.09	0.14	0.12

Serial dilution series of different synthetic viral RNA reference standards for quantification of vRNA(-), cRNA(+), vmRNA(+) of viral segments 4 (HA), 6 (NA), 7 (M) and 8 (NS) were used.

Repeatability/reproducibility of the assay

The mean values of the CV of the repeatability (intraassay variation) of the C_q values for the linear range of the assay were < 2.3% for segment 4 (HA), < 1.4% for segment 6 (NA), < 2.0% for segment 7 (M) and < 2.3% for segment 8 (NS) when measuring triplicates (Table 4.3-1). The mean values of the CV of the reproducibility (interassay variation) of the C_q values were < 2.8% for segment 4 (HA), < 2.6% for segment 6 (NA), < 3.1% for segment 7 (M) and < 2.7% for segment 8 (NS) when measuring three independent viral RNA reference standard curves. Overall, results confirmed good repeatability and reproducibility of the RT-qPCR method for high and low copy numbers of viral RNAs (Table 4.3-1).

Linear Regression analysis of assay validation data

All tested viral RNA reference standard curves met the criteria for applying linear regression analysis within the calibration range. All residuals of the calibrations curves showed normal distributions within homogeneous variances. No outliers were detected. Representative regression curves of the synthetic viral RNA reference standard of vRNA(-), cRNA(+) and vmRNA(+) of segment 8 (NS) are shown in Figure 4.3-5. Results are summarized in Table 4.3-1. SD in a range of 0.12 – 0.48 (1 – 4% standard error) of the calibration range demonstrated precise regression results. Regression models seemed to fit the data well, and R^2 showed strong linear correlations (>0.98). Overall amplification efficiency (Equation 1) was between 85% and 103% depending on the viral segment and viral RNA type (Table 4.3-1).

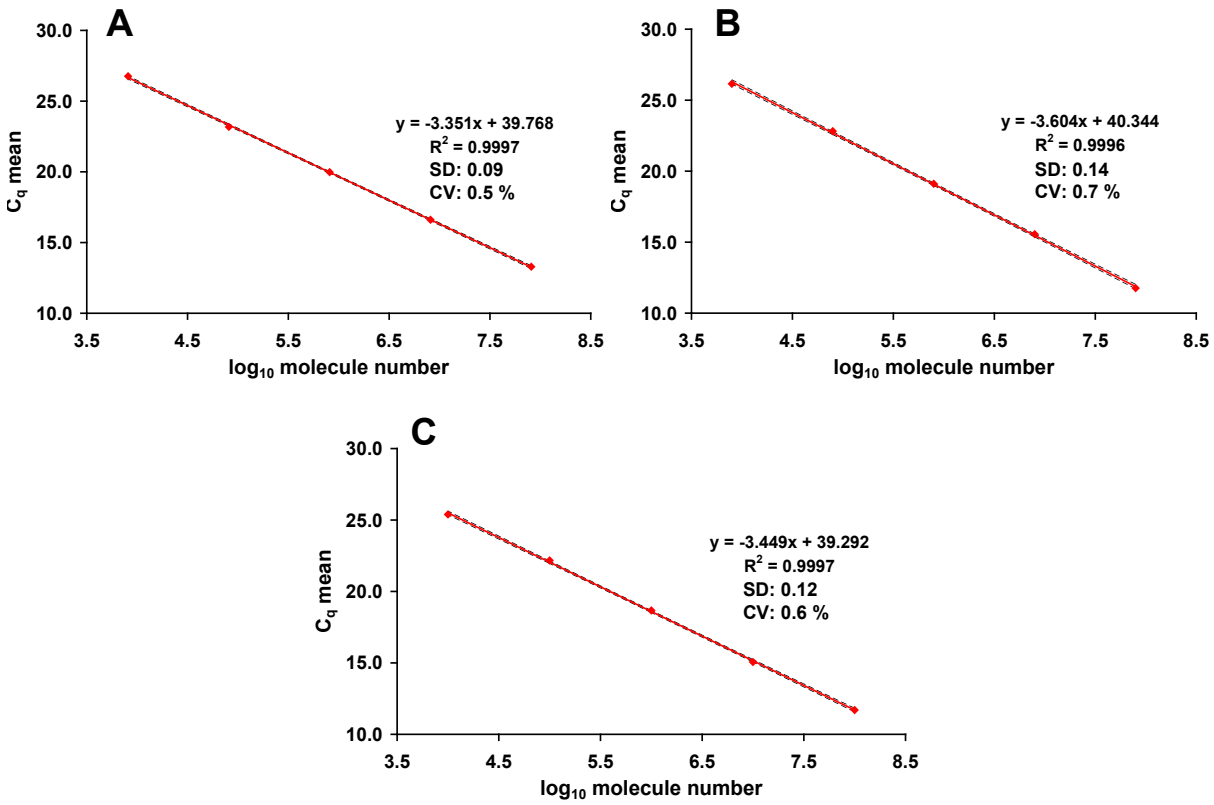

Figure 4.3-5: Regression curves of the synthetic viral RNA reference standards of segment 8 (NS)

Regression curve (red line) of vRNA(-) (A), cRNA(+) (B) and vmRNA(+) (C) of segment 8 (NS) obtained by plotting log_{10} molecule number against the C_q value with corresponding CI (99%) (dashed black lines), SD and CV.

Validation of total cellular RNA extraction

The validation procedure of the established assay was extended to the initial step of total cellular RNA extraction from the cells (section 3.4.1) by normalization to the cell reference genes β-actin and GAPDH (Figure 4.3-6) (Gropp et al., 2006). Linearity and reproducibility tests of a serial dilution of MDCK cell lysates before application to extraction columns and fivefold repetition of the procedure were done. Results showed linearity to 2.4 x 10^1 RNA molecules for β-actin and 1.7 x 10^1 RNA molecules for GAPDH and a CV of 3-5% for β-actin and 3-6% for GAPDH (Figure 4.3-7).

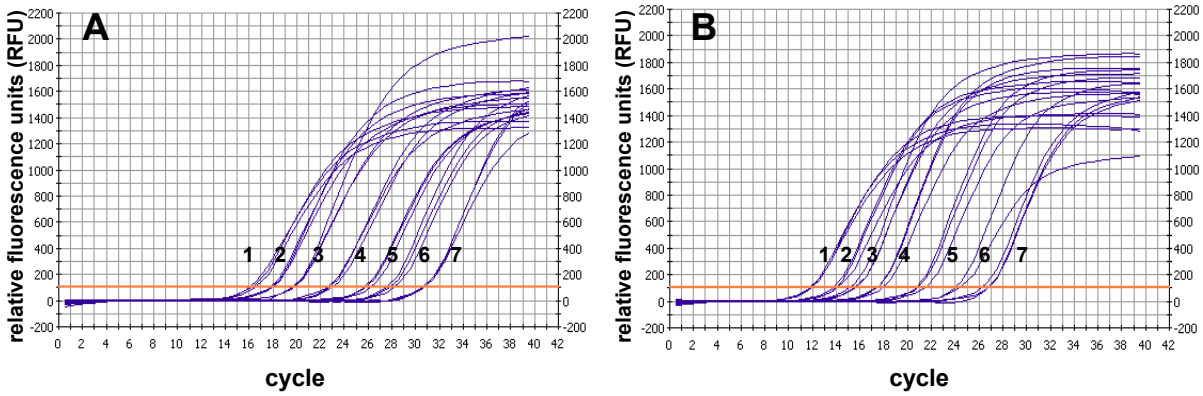

Figure 4.3-6: RT-qPCR amplification curves of (A) β-actin and (B) GAPDH

Descending 10-fold dilution of total cellular RNA extracts used in triplicate as template for RT-qPCR for quantification of the reference genes (A) β-actin and (B) GAPDH.

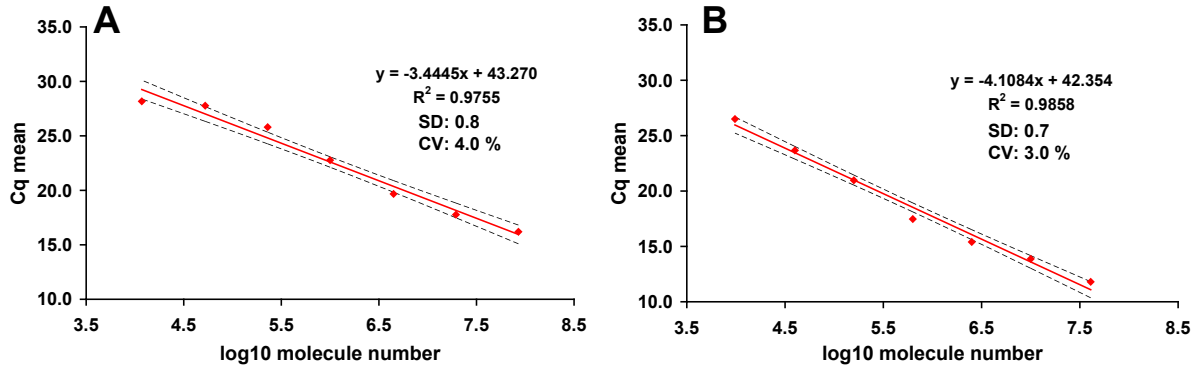

Figure 4.3-7: Regression curves of RNA serial dilution series of (A) β-actin and (B) GAPDH

Regression curves (red line) obtained by the RT-qPCR amplifications above (Figure 4.3-6) by plotting log_{10} molecule number against the C_q value with corresponding CI (99%) (dashed black lines), SD and CV.

In summary, RT-qPCR assay validation demonstrated linearity over five orders of magnitude, with a sensitivity of 1.0 × 10^3 – 8.9 × 10^3 of viral RNA molecules, specificity, repeatability and reproducibility of less than 0.8 – 3.1% CV (Table 4.3-1). Therefore, this RT-qPCR assay appeared to be suitable for the analysis of human influenza A virus replication dynamics.

4.3.3. Analysis of human influenza A virus replication dynamics

The general time course of influenza virus replication in their host cells is well understood, however much about regulation of viral genome replication and viral transcription, especially for the different viral RNA segments still remains unknown. Hence, total cellular RNA from MDCK cells infected with influenza virus A PR/8-RKI at a MOI of 6 was extracted at 30 min intervals for the first 4 hpi. Subsequently, one hour intervals were used. Time courses of transcription and replication of the viral segments 4 (HA), 6 (NA), 7 (M) and 8 (NS) were determined by RT-qPCR assay specific for vmRNA(+), cRNA(+) and vRNA(-) (section 3.4.3). The time courses are shown in Figure 4.3-8.

Transcription of vmRNA(+) (Figure 4.3-8A) started at an average of 0.4 hpi for viral segments 4 (HA), 6 (NA) and 8 (NS1) and about 1.0 hpi for segment 7 (M1). Start point was also confirmed by linear regression analysis (Δt, Table 4.3-2). The average number of vmRNA(+) per cell of all segments increased rapidly within the first 5 hpi. Only segment 6 (NA) showed a slightly slower synthesis rate (p_2 = 0.66, Table 4.3-2) compared to the other segments (average p_2 = 0.9, Table 4.3-2). Afterwards, the average number of vmRNA(+) per cell of all segments remained at high levels (2300 – 6400 molecules per cell) until about 12 hpi. A 3-fold decrease in the number of vmRNA(+) per cell was visible for segments 4 (HA), 6 (NA) and 8 (NS1). In contrast, the number of vmRNA(+) per cell of segment 7 (M1) dropped only by a factor of 1.5.

Synthesis of replicative intermediates cRNA(+) (Figure 4.3-8B) started immediately after the transcription of vmRNA(+) on average at an average of 0.3 – 0.9 hpi for viral segments 4 (HA), 6 (NA) and 7 (M), which was also confirmed by linear regression analysis (Δt, Table 4.3-2). The average number of cRNA(+) per cell increased rapidly for the next 5 h and remained at high levels with only a slight decrease after 12 hpi. Maximum average numbers in the range 2100 - 4300 cRNA(+) molecules per cell were achieved. Only synthesis of cRNA(+) of segment 8 (NS) was slightly different. Increase started about half an hour earlier compared to the other cRNA(+) molecules, but reached only half of the average number of the other cRNA(+) per cell (maximum about 1200 per cell). Interestingly, vmRNA(+) and cRNA(+) synthesis showed the same time courses for segment 8 (NS).

In contrast to the other two RNA types, the vRNA(-) (Figure 4.3-8C) of the four analyzed segments were synthesized in equimolar amounts with similar dynamics, also confirmed by linear regression analysis (Δt 2.09-2.85, Table 4.3-2, Figure 4.3-10). Results showed that both, cRNA(+) and vmRNA(+) were produced with an approximately 1.6 – 1.7-fold higher rate compared to vRNA(-) (p_2, Figure 4.3-10). However, only net increases were taken into account not considering vRNA(-)s already packed and released at this time point. Corresponding to the high MOI used for infection (MOI=6) about 53 – 87 vRNA(-) molecules

per cell were detected during the first hour after the 'cold infection' at 4°C (Matlin et al., 1981). The total amount of these genome equivalents decreased at an average of 2.5 hpi (average Δ*t*, Table 4.3-2, Figure 4.3-10) and then increased rapidly until 7 hpi. Afterwards the average number of vRNA(-) molecules remained at high levels (about 3500 - 5300 per cell) until the last extraction time point at 24 hpi. The delay between the initiation of active replication of the vRNA(-) (average Δ*t* 2.5 hpi) and the increase of the number of their precursor molecules (cRNA(+)) was about 1.9 h (average Δ*t* 0.6 hpi).

For comparison, the release of total number of influenza virus particles was monitored by a conventional HA assay (section 3.2.6). Virus titer in the supernatant started to increase 6 hpi. A high number of virus particles were released into the supernatant for the following 6 h until virus replication ceased, and a maximum virus titer of 2.7 log HA units/100µL was obtained at the last extraction time point (24 hpi). Interestingly, the onset of maximum virus particle release (HA titer, Figure 4.3-8) correlated with the maximum concentration of all viral RNA types at about 6 hpi. Afterwards, a characteristic drop in the concentration of the three RNA types of all viral segments was visible at about 8 hpi (Figure 4.3-8).

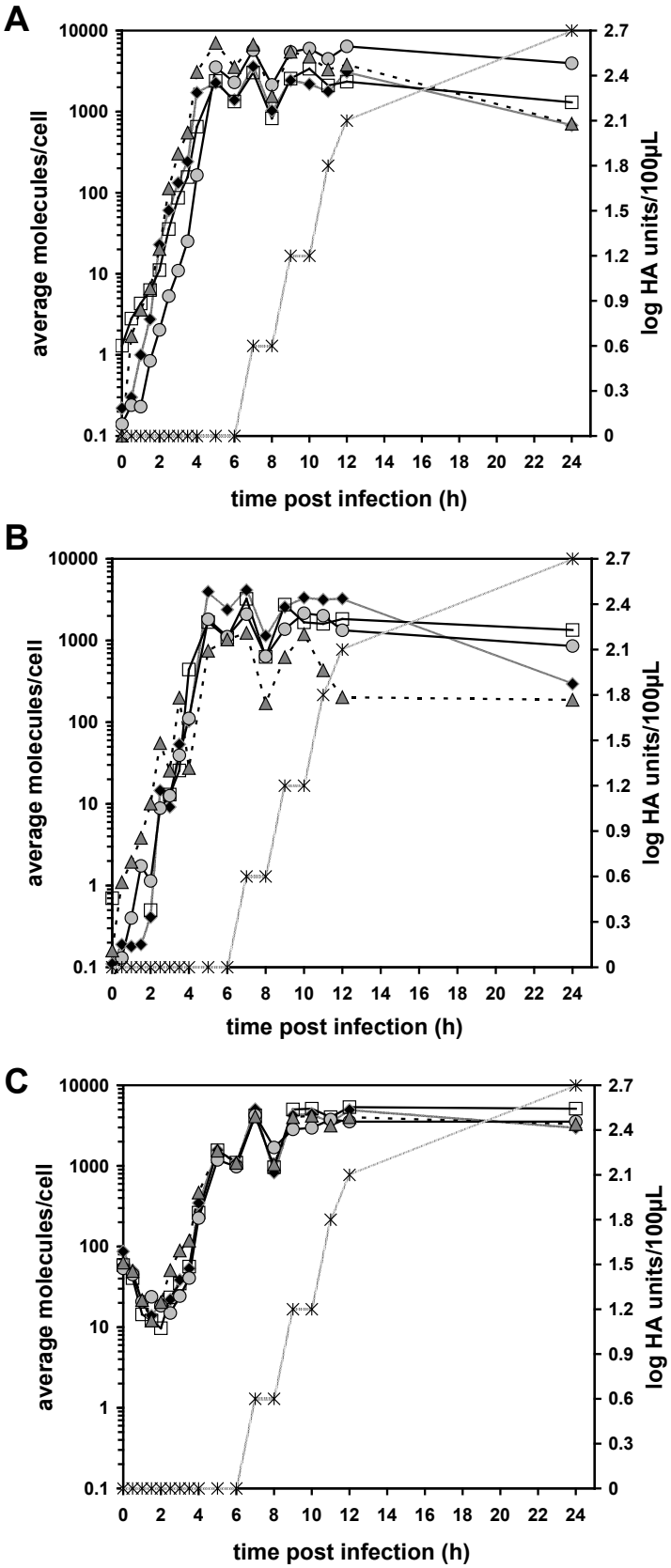

Figure 4.3-8: Time course of vmRNA(+) (A), cRNA(+) (B) and vRNA(-) (C) synthesis for segments 4 (HA), 6 (NA), 7 (M) and 8 (NS) during influenza PR/8-RKI virus infection in MDCK cells

Viral segments 4 (HA-◆), 6 (NA-□), 7 (M-●) and 8 (NS-▲) in PR/8-RKI infected (MOI=6) MDCK cells. Average molecules per cells were determined by RT-qPCR assay with corresponding synthetic viral RNA reference standard curves. Total virus particles (*) in the supernatant expressed as log HA units per test volume (log HA units/100µL) plotted in each graph.

Time courses of the ratio of vmRNA(+)s to viral genome equivalents vRNA(-) (vmRNA(+) / vRNA(-)) are shown in Figure 4.3-9, to reflect the viral replication level and its activity. The kinetics of vRNA(-) replication and the ratios indicated that the replication of the viral genome started after a short delay at 2 hpi and reached a peak between 3.5 - 4 hpi for segment 4 (HA), 6 (NA) and 8 (NS) and 5 hpi for segment 7 (M). Overall, however, the time courses of viral transcription and replication of all segments followed the same dynamics.

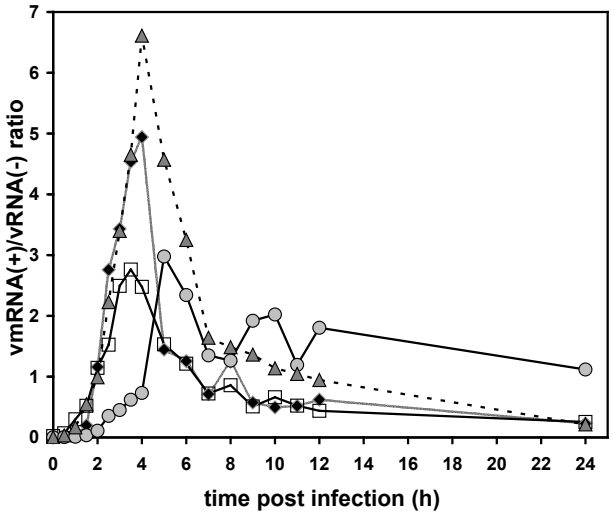

Figure 4.3-9: Time course of vmRNA(+) molecules to viral genome molecules vRNA(-) for segments 4 (HA), 6 (NA), 7 (M) and 8 (NS) during influenza PR/8-RKI virus infection in MDCK cells

Ratios of vmRNA(+)/vRNA(-) of viral segments 4 (HA-◆), 6 (NA-□), 7 (M-●) and 8 (NS-▲) during the first 24 hpi in PR/8-RKI infected (MOI=6) MDCK cells.

For statistical verification of obtained viral segment molecule numbers a linear regression analysis was done by Stefan Heldt (bpt group, MPI Magdeburg) as supporting work (Vester et al., 2010). The mathematical analysis aims at elucidating the onset of production and the production rates of the different viral RNA types. RNA production rates (regression parameter p_2) and its respective 95% confidence bounds were obtained by fitting a linear polynomial to the exponential increase of viral RNA molecule number. The time delays Δt were calculated as the intersection of this regression line with a parallel line to the abscissa, which was fitted during the initial delay phase. Error bars of Δt for all four viral RNAs are based on Fieller's theorem. The respective bars for vmRNA(+)s and cRNA(+)s were calculated by intersecting confidence bands neglecting p_1 uncertainty. Table 4.3-2 shows the obtained regression parameters and Figure 4.3-10 the RNA production rates p_2 and the calculated time delays Δt.

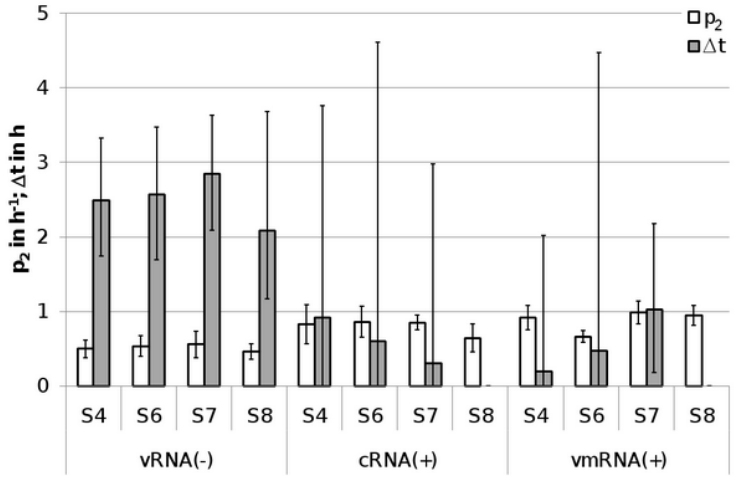

Figure 4.3-10: Statistical verification through linear regression analysis of the time course data of four viral segments during influenza PR/8-RKI virus infection in MDCK cells

Statistical analysis of the time courses of viral segments (4 (HA), 6 (NA), 7 (M) and 8 (NS)) during PR/8-RKI infection in MDCK cells. Regression parameters p_2 (□) and respective 95% confidence bounds obtained by fitting a linear polynomial to the exponential increase of viral RNA molecule copy number. Time delay Δt (■) calculated as intersection of the regression line with a parallel line to the abscissa fitted during initial delay phase. Error bars of Δt based on confidence interval (CI) of p_2 from Table 4.3-2.

Table 4.3-2: Parameters, 95% confidence intervals (CI) and R^2 values for linear regression analysis of time course of four viral segments during influenza PR/8-RKI virus infection in MDCK cells

		Base line		**Exponential phase**					**Δ*t* [h]**
		p_1	± (95%)	p_2 [h^{-1}]	±(95%)	p_3	± (95%)	R^2	
vRNA(-)	**S4 (HA)**	1.51	0.23	0.50	0.12	0.26	0.49	0.94	2.49
	S6 (NA)	1.41	0.26	0.54	0.14	0.03	0.61	0.94	2.57
	S7 (M)	1.44	0.17	0.56	0.18	-0.15	0.83	0.93	2.85
	S8 (NS)	1.49	0.30	0.46	0.10	0.53	0.42	0.94	2.09
cRNA(+)	**S4 (HA)**	-0.71	0.25	0.83	0.26	-1.47	1.11	0.89	0.92
	S6 (NA)	-0.85	1.91	0.86	0.21	-1.37	0.58	0.92	0.60
	S7 (M)	-1.02	1.71	0.85	0.10	-1.28	0.28	0.98	0.31
	S8 (NS)	-0.80	*	0.65	0.19	-0.40	0.52	0.89	*
vmRNA(+)	**S4 (HA)**	-0.59	0.86	0.92	0.17	-0.78	0.48	0.96	0.20
	S6 (NA)	0.28	2.12	0.66	0.07	-0.04	0.21	0.98	0.48
	S7 (M)	-0.70	0.32	0.99	0.16	-1.72	0.48	0.98	1.02
	S8 (NS)	-1.00	*	0.95	0.13	-0.53	0.36	0.97	*

** Number of initial sampling points of the respective RNA did not allow fitting of base line and calculation of Δt.*

In summary, the qPCR assay was shown to be important for determining essential features of intracellular events and dynamics of the life cycle of influenza virus in MDCK cell culture.

4.3.4. Determination of extracellular influenza viral RNA in cell culture supernatant by RT-qPCR

A slightly modified RT-qPCR assay (section 3.4.6), to complement existing conventional virus quantification methods (e.g. HA assay) was established to measure titers of influenza virus in cell culture supernatants of infected MDCK cells. For characterization of the RT-qPCR assay the important step of extracellular viral RNA extraction was validated for determination of the dynamic range and sensitivity of this step. For verification of feasibility in mammalian cell culture a cross-validation with a conventional HA assay for influenza virus quantification was done by following the time course of influenza PR/8-RKI virus infection in MDCK cells. The conventional HA assay detects the total number of virus particles by hemagglutination based on the agglutination of RBC with the viral surface proteins expressed as log HA units/100µL. Whereas the RT-qPCR assay detects the total number of vRNA(-) of segment 7 (M), which can be converted into virus particle concentrations using the assumption that every virus particle contains every RNA segment only once. Both assays detect infectious and non-infectious virus particles. For better comparability of both data, results were converted to virus particles per mL (Equation 3 and 9).

The validation procedure of the extracellular influenza viral RNA extraction step (section 3.4.6) was done with three serial dilutions of PR/8-RKI seed virus ($TCID_{50}$ 3.5×10^7 virions/mL) before application to extraction columns. Quantification was done by RT-qPCR with the protocol described in section 3.4.6 using the synthetic RNA reference standard for vRNA(-) of segment 7 (M). The extracellular viral RNA extraction showed linearity over four orders of magnitude and a confirmed sensitivity (LOD) to 1.7×10^4 viral RNA molecules corresponding to 1.1×10^{-5} ng of viral RNA (Figure 4.3-11).

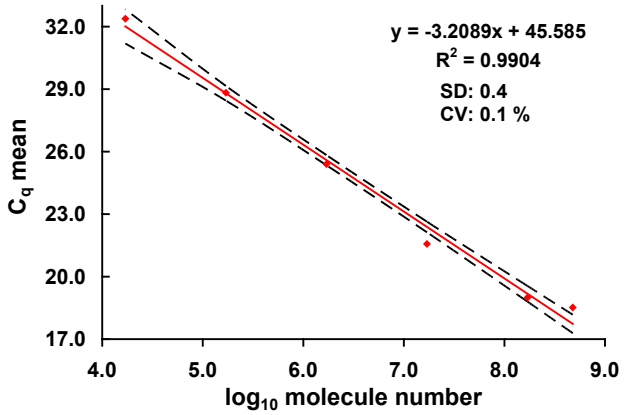

Figure 4.3-11: Regression curve of three dilution series of influenza A PR/8-RKI seed virus used for extracellular RNA extraction obtained by RT-qPCR of segment 7 (M)

Regression curves (red line) obtained by the RT-qPCR of segment 7 (M) by plotting log_{10} molecule number against the C_q value with corresponding CI (99%) (dashed black lines), SD and CV.

Following the time course of influenza PR/8-RKI virus infection in MDCK cells both methods, HA and RT-qPCR assay showed comparable dynamics of influenza virus particle concentrations (Figure 4.3-12). Both assays detected almost identical maximum virus concentrations of about 50 hpi. Nevertheless, both quantification methods showed variations of virus particle concentration at the beginning (about 6 – 18 hpi) and the end (about 50 – 77 hpi) of influenza virus infection. At these time points the HA assay detected lower or higher virus titers, respectively, compared to RT-qPCR results. Variations in the beginning accounted for the low virus particle concentration at this time of infection and the low LOD of 2.0 x 10^7 virions/mL of the HA assay. Whereas the minimal virus concentration detected by the RT-qPCR assay was 1.47 x 10^6 virions/mL corresponding theoretically to log HA units -1.13. Through the use of synthetic viral RNA reference standard curves (segment 7 (M) vRNA(-)) for quantification, the sensitivity of the assay could be estimated which was equated with the last dilution step. Hence, the effective minimal virus concentrations that could be detected in this time course was approximately 5.0 x 10^3 virions/mL, which was much lower than the real minimum virus concentration detected during this experiment.

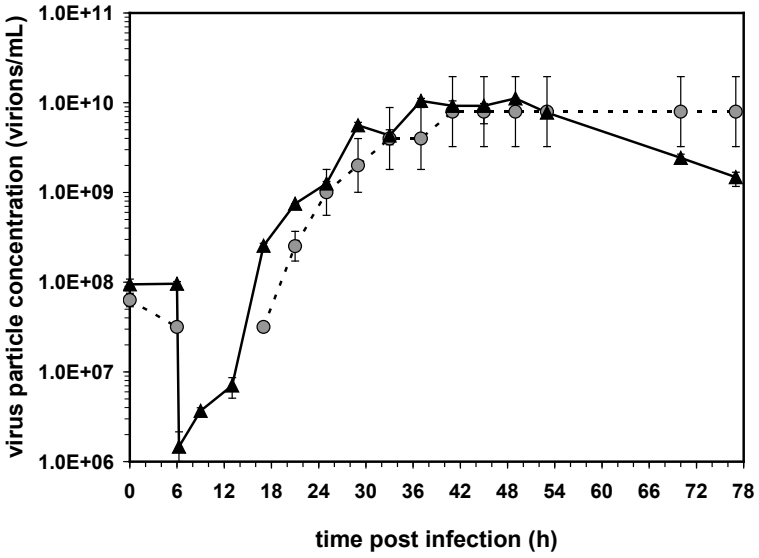

Figure 4.3-12: Virus particle concentration in cell culture supernatant of influenza PR/8-RKI (MOI=1) virus infected MDCK cells determined by RT-qPCR and HA assay

Virus titers in the cell culture supernatant determined by RT-qPCR assay (▲) with extracellular viral RNA of viral segment 7 (M) quantified with corresponding synthetic viral RNA reference standard curves expressed as virions/mL (mean values ± SD of three intraassay replicates). Virus titers in the cell culture supernatant determined by HA assay (●) expressed as virions/mL (± SD of the method).

In conclusion, the RT-qPCR assay offers improvements over the conventional HA quantification method for measuring influenza virus concentration in the cell culture supernatant of infected MDCK cells due to lower detection limits.

5. Discussion

5.1. Selection of a human cell line as model for the proteomic approach

Application of molecular techniques (i.e. proteome and genome analysis) to the investigation of mammalian cell systems is limited largely to human and mouse models due to restricted availability of constituent assay components such as antibodies, genome sequences or protein databases. For this reason, three different human cell lines were compared to select such a model system: a gastric carcinoma cell line (NCI-N87), a hepatocellular carcinoma cell line (HepG2) and a lung carcinoma cell line (A549). Cellular metabolism and the effect of different infection parameters (MOI, trypsin, media) were characterized with respect to growth behavior and influenza virus yield of three different human cell lines. This characterization was essential to have optimal growth conditions and a stable and well adapted infection system related to the MDCK and Vero cell system.

A549 cells reportedly support viral pathogens and were used in a wide range of viral infection studies, i.e. for influenza virus (Nyman et al., 2000). In contrast, NCI-N87 cells were used in a wide range of studies of the regulation of digestive functions in the context of gastric physiology and pathology (Basque et al., 2001; Chailler and Menard, 2005), but was never before used in influenza virus infection studies. HepG2 cells have a model chromosome number of 55 and are not tumorgenic in nude mice (Aden et al., 1979). HepG2 cells secret a variety of major plasma proteins; e.g., albumin, transferrin and plasminogen (Knowles et al., 1980). They have been grown successfully in large scale cultivation systems. HepG2 cell line was shown to be highly permissive for influenza virus (Ollier et al., 2004). Cells expressed plasmin, a trypsin-like protease known to activate HA of influenza virus that is thus present potentially in the supernatant of HepG2 cell cultures. This protease could enable these cells to support the replication of influenza viruses even without the addition of trypsin. Keskinen et al. showed that HepG2 cells are extremely poor IFN producers and they also exhibit a very weakly antiviral response, which could account for impaired ability to eradicate viral infection (Keskinen et al., 1999).

It is well known that growth and survival of mammalian cells in culture depends on the availability of nutrients, the characteristics of the cell culture surface (for adherent cells), the accumulation of cytotoxic metabolites, and the oxygen supply (Quesney et al., 2003). Therefore, it is necessary to examine the nutrient consumption and metabolite production of cells by following the metabolic profiles and yields to prevent their depletion and to limit the production of cytotoxic metabolites, which could cause poor growth characteristics or cell

death. The energy necessary for growth and cell survival is provided by several metabolic pathways including the glycolysis, the citric acid cycle and the respiratory chain. Genetic variances, which are characteristic for continuous cell lines affect the metabolism of cell lines (Haegstroem, 2000). Such variances cause high substrate consumptions with poor energy efficiency and accumulation of toxic waste products, i.e. lactate and ammonia in culture supernatant (Hassell et al., 1991). Glucose used as main carbon source is oxidized mainly in glycolysis to pyruvate and then to lactate. This results in an acidification of culture media and growth inhibition when lactate increases over 40 mM (Glacken et al., 1986). By using the molar yield-coefficient $Y_{Lac/Gluc}$ characterization of growth behavior of cells and their metabolism is possible. Theoretically, 2 mol lactate can be generated from 1 mol glucose when out of the C_6-chain of glucose 2 C_3-chains are formed (yield-coefficient $Y_{Lac/Gluc}$ = 1). Glutamine metabolism often is the main energy source of cells (30-50% cellular energy) with 2 main pathways: the transaminase pathway and the glutamate dehydrogenase (GDH) pathway (Haegstroem, 2000). In both pathways the carbon body is integrated in the citric acid cycle via α-ketoglutarate. For the evaluation of growth behavior in relation to glutamine metabolism the yield-coefficient $Y_{Amm/Gln}$ can be used. From the GDH-pathway 2 mol ammonia can be produced from 1 mol glutamine, this leads to $Y_{Amm/Gln}$ > 1. Ammonia concentrations of >2-10 mM are typically inhibiting cell growth (Glacken et al., 1986).

Glucose and glutamine concentration were not a limiting factor in the cell growth or infection phase for the three human cell lines, as residual glucose concentration was about 10 mM and culture residual glutamine concentration was about 0.5 mM. The consumption of glucose and glutamine results in the accumulation of toxic metabolites such as lactate and ammonia. The maximum lactate concentration measured under the experimental conditions used (about 15 mM for A549 and NCI-N87 cells; about 30 mM for HepG2 cells) was below levels considered toxic for animal cell cultures described by Hassell et al. (Hassell et al., 1991). Also ammonia was produced at non-toxic concentrations (about 2.0 mM A549 cells; 1.4 mM NCI-N87 cells; 1.5 mM HepG2 cells).

Considering the overall molar yields for lactate and glucose $Y_{lac/gluc}$ a comparatively high level and inefficient use of glucose was found (e.g. on average 1.5 – 2.6). Thus, probably most of the glucose went directly into lactate production, which seems to be typically for continuous cell lines as it is often reported in literature (Haegstroem, 2000). The $Y_{lac/gluc}$ molar yields of more than 2, found for HepG2 could not be explained by glucose metabolism in glycolysis. Typically, $Y_{amm/gln}$ molar yields for the cell growth phase were in the range of about 1. So it seems that, in particular in this phase, the glutamine metabolism mainly took place over the transaminase pathway, whereas in most of the infection phases the cells were using both the transaminase and glutamine dehydrogenase pathway (yield factor >1.2) or ammonia was produced from other AA.

Although glutamine is the most relevant AA in cell culture, it is important to consider the metabolism of other AAs such as glutamate. Consumption of AAs could be explained by their integration in peptides during protein synthesis. A minimal consumption of glutamate was seen for HepG2 cells at the end of the cell growth phase. Interestingly, A549 and NCI-N78 cells showed a release of glutamate into media during the entire cell growth phase indicating that glutamine was transformed into glutamate or underwent deamination. When comparing the glutamate profiles after infection it could be seen that glutamate was released in parallel to the increase in virus titer. Infected cells go into apoptosis, thus membranes of mitochondria are permeabilized and destabilized, later the cells lyse as they release viruses. Thus, the increase in glutamate in the medium during infection may represent the release of the intracellular glutamate pool, as discussed previously by Genzel et al. (Genzel et al., 2006). Nevertheless, there must be additional processes or events to explain the glutamate levels found, since the intracellular glutamate pool is not big enough to make such effects possible. Overall, with the exception of glutamate no significant influence of virus infection on the measured metabolism could be seen. From some media only slightly higher lactate release was measured during infection phase.

For infection studies cell lines should grow fast to high cell concentrations in order to provide enough host cells for virus production. With A549 and HepG2 cell concentrations of 4.3-5.4 × 10^5 cells/mL were obtained and confluence was achieved after 4 days of cultivation. Both cell lines showed similar morphology and growth characteristics compared to MDCK cells. In contrast, NCI-N87 cells showed much lower cell concentrations. Cells grew more in compact colonies or cell clumps rather than to confluent monolayers.

Comparison of the virus yields of the human cell lines in this study showed that A549 and HepG2 cells were capable of efficient virus amplification with maximum titers of about 2.0 or 2.3 HA units/100 µL, respectively. Much lower maximum titers of about 1.2 HA units/100 µL were obtained with NCI-N87 cells. With respect to maximum HA titers, A549 and HepG2 cells showed to be candidate model cell lines to Vero or MDCK cells achieving HA titers in the range 2.5-3.3 for influenza PR/8 virus (Genzel and Reichl, 2009). Determination of cell specific virus yields showed that human cell lines released about 1500 (A549 cells), 1800 (HepG2 cells) and 700 (NCI-N87 cells) viruses. However, compared to MDCK cells, from which up to 12000 virus particles per cell with influenza PR/8 virus can be released, these viral yields are very low.

Trypsin addition did have a low effect on maximum HA titers of influenza virus in all three cell lines. However, the effect on virus replication dynamics was much more pronounced. Trypsin addition resulted in faster replication. However, even without trypsin an infection occurred but with lower maximum virus titers. This delay was also described by Tree et al. showing that without trypsin the maximum virus titer was reached later than with trypsin added at time of

infection for influenza A/PR8/34 virus in MDCK cells (Tree et al., 2001). Similar results were also reported for infections in avian suspension designer cells AGE1.CR (Lohr et al., 2009). Keskinen et al. reported that especially HepG2 cells support the replication of influenza viruses even without the addition of trypsin (Keskinen et al., 1999), which was also confirmed by this study (Figure 4.1-10). For other cell lines, i.e. PER.C6 and Vero, it is reported that replication requires trypsin addition (Govorkova et al., 1995; Pau et al., 2001). Additionally, it could be seen that MOI had no influence on the obtained maximum HA titer for the HepG2 and A549 cell lines tested, indicating that this parameter is not critical for the infection process. As expected, the time point of detectable HA increase was shifted with decrease in MOI. This relationship was also described by Rimmelzwaan et al. for influenza A/Neth/18/94 virus in MDCK cells (Rimmelzwaan et al., 1998). The lower the MOI was set, the later the increase of HA was observed. This delay appears to be a function of the number of influenza virus particles used for infection. In contrast to A549 and HepG2 cell lines, NCI-N87 cells showed slightly lower titers when using low MOI. A similar effect was also reported by Hao et al. (Hao et al., 2008b). They found that influenza virus replication of respiratory dendritic cells increased with increasing MOIs. In contrast, evaluation of HEK-293 as a suitable expression platform for the production of influenza virus vaccine indicated that at high MOI, the number of viable virus producing cells was reduced shortly after the infection and resulted in lower virus yields (Le Ru et al., 2010). They suggested an early induced apoptosis before efficient virus production could have taken place. Additionally, MOI-dependency was also shown before to be not only cell line specific but also virus strain specific (Merten, 2002).

Virus replication also depends on metabolism of cells and inhibiting media compounds. For influenza virus, is it well known that high ammonia chloride concentrations (20 mM) prevent the HA mediated fusion of the viral envelope with endosomes thus preventing the release of the viral genome into the cytoplasm of the host cell (Cruz et al., 1999). Low ammonia concentrations are thus crucial during the first hours of the infection cycle. In this study with a maximum ammonia concentration of less than 1.5 mM at the end of the cell growth phase and less than 2.5 mM after virus replication, an inhibition was not likely.

In summary, each human cell line supports the replication of influenza A virus. Dynamics but not necessarily maximum titers differ with the MOI, different media or trypsin addition does not have or have only slightly an effect on maximum HA titers. Overall, metabolism and virus yield screening of the three human cell lines demonstrated that only A549 and HepG2 cells are promising candidates as a human cell reference model. Finally, on the basis of these data, A549 cells were selected for proteomic approaches, because they showed (I) comparable cell growth performance and cell morphology to MDCK and Vero cells, (II) comparatively high virus titer (HA, $TCID_{50}$) and virus replication even without trypsin addition and (III) lower metabolic activity and growth in uncomplex media.

5.2. Proteome alterations in human influenza A virus infected mammalian cell lines

Proteome alterations of A549, MDCK and Vero cells infected with different variants of the influenza PR/8 virus strains were profiled and a set of differentially abundant proteins were identified. These proteins are involved in diverse biological processes. The different pathways and their interdependency, as well as some interesting proteins are discussed in the following.

5.2.1. Functional significance of altered abundant proteins in A549 and MDCK cells infected with influenza A PR/8-RKI

Cytoskeleton protein

Alterations in keratin abundance with a wide dynamic range and high regulation level (up to 50-fold up-regulation compared to mock infected cells, Figure 4.2-3) were identified in both infected cell lines. Keratin 10 belongs to the type I cytokeratin family, which are heteropolymeric structural proteins and components of intermediate filaments. The data support a role in the mechanisms and regulation of gene expression of the cytoskeleton system during influenza virus infection, which was described repeatedly (Arcangeletti et al., 2008; Arcangeletti et al., 1997; Avalos et al., 1997). Interactions of cytokeratin with influenza virus were also shown in a recent proteome study of avian virus infected AGS cells (Liu et al., 2008). Arcangeletti et al. reported that various cytoskeleton networks, which are involved in the replication and expression of influenza virus, may also act as a regulator in virus induced signaling (Arcangeletti et al., 1997). This was supported by the demonstration that influenza viral NP and M1 proteins are associated to cytoskeleton elements (Avalos et al., 1997). The mechanism and regulation of gene expression by transporting and positioning of mRNAs seems to be the same as described for actin (Miralles and Visa, 2006). For this purpose cytoskeleton components acquire a high affinity for nucleic acids, when they are cleaved into subunits by proteases. This could explain the appearance of PTMs such as fragmentation as observed for protein spot 3, 4, 5 (Figure 4.2-2), and indicate a modification step induced by influenza virus infection rather than an increased protein synthesis (Badock et al., 2001). In addition, general morphological changes of infected cells with specific alterations of the cytoskeleton have been shown (Arcangeletti et al., 1997). Moreover, the transport of various viruses or viral components between nucleus and cell periphery seems to be regulated by the cytoskeleton, this may for instance facilitate an efficient spread of progeny virus particles, as observed for vaccinia virus (Cudmore et al., 1995).

Protein synthesis and degradation

During influenza virus infection protein synthesis is maintained at high levels and a switch from cellular to viral protein synthesis occurs despite the presence of high levels of functional cellular mRNAs in the cytoplasm of infected cells (Chan et al., 2006a). So it is not surprising that eukaryotic translation elongation factor 1 (EF-1, spot 8, Table 4.2-2) was found to be differentially abundant in MDCK cells. The up-regulation of EF-1 is already described in microarray studies on HeLa cells infected with influenza virus (Geiss et al., 2001). EF-1 is responsible for the enzymatic delivery of aminoacyl tRNAs to the ribosome. Regarding the translational control by influenza virus it is known that suppression of the eukaryotic initiation factor 2 (eIF-2) is used for selective translation of influenza virus vmRNA(+)s (Katze et al., 1986). Furthermore, interactions of EF-1 with HIV proteins are described, representing possible interaction platforms for influenza virus as well. Accordingly, EF-1 stimulates the binding of Pol II to HIV-1 TAR RNA and the release of viral HIV RNA from polysomes, permitting RNA to be packaged into viruses (Cimarelli and Luban, 1999).

Another protein of interest induced by influenza virus is Ran GTPase-activating protein 1 (RanGAP1, spot 1, Table 4.2-2). O'Neill et al. reported a role of RanGAP1 as a transport factor in nuclear import of influenza A vRNPs (O'Neill et al., 1995). On the other hand microarray studies of Geiss et al. in influenza virus infected HeLa cells reported a down-regulation of RanGAP1 genes (Geiss et al., 2001). The authors suggested a correlation with the viral NS1 in inhibiting mRNA polyadenylation, splicing and export of cellular mRNAs within the nucleus. RanGAP1 is a homodimeric 65-kD polypeptide that induces specifically the GTPase activity of Ran, representing a key regulator of the Ran GTP/GDP cycle. Ran is a Ras-related, mainly nuclear protein, which induces regulatory pathways involved in mitosis, nucleus import of proteins with NLS, pre-mRNA processing and nucleus export (Bischoff et al., 1995).

High abundance was also identified for proteasome activator hPA28 subunit beta (PA28_beta, spot 8, Table 4.2-1), a member of the protein degradation pathway regulated by viral replication at late time of infection in A549 cells. Similar results were shown by Geiss et al., who described enhanced mRNA levels of PA28_beta in microarray analysis of influenza virus infected HeLa cells (Geiss et al., 2001). The proteasome pathway plays a central role in degradation of intracellular proteins and is critical for diverse cellular functions. For cellular immune responses, it may represent an important pathway affected by influenza virus replication (Coux et al., 1996). In cellular immune response the modified IFN induced proteasome variant, the immunoproteasome, is the major source for the generation of viral antigens (Sijts et al., 2002). As shown by Shin *et al*., the immuno-proteasome is regulated by HCV induced innate cellular immune response (Shin et al., 2007).

Signal transduction, stress response and apoptosis

Proteins with different levels of abundance involved in signal transduction, stress response and apoptosis were found in MDCK and A549 cells. The identified proteins included a well-known IFN induced protein, an obviously upregulated myxovirus resistance protein (Mx1, spot 2, Table 4.2-2, Figure 4.2-2) or IFN induced Mx protein (MxA, spot 4 and 5, Table 4.2-1, Figure 4.2-2). Determination of the mRNA transcript level of Mx1 by RT-qPCR also showed a higher expression level in infected MDCK cells (Seitz et al., 2010). Geiss et al. reported a significant induction of Mx genes during a microarray analysis in A549 cells in response to infection with wild type and mutant influenza A virus (Geiss et al., 2002). This was also shown in a macaque infection study using specific oligonucleotide arrays, and non-gel based proteomics (Baas et al., 2006). In contrast, a proteome study on the cellular response to avian influenza virus in a human gastric cell line did not detect Mx proteins (Liu et al., 2008). These proteins belong to the class of dynamin-like large GTPases known to be involved in intracellular vesicle trafficking and organelle homeostasis. Mx proteins are key components of the antiviral state in many species (Haller et al., 2007b). They show antiviral activity against a wide range of RNA viruses, including influenza viruses. In principle, Mx proteins detect viral infection by sensing nucleocapsid-like structures. Viral components are trapped and sorted to locations where they become unavailable for the generation of new viral particles (Haller et al., 2007a). The virus is inhibited at an early stage in its life cycle, soon after host cell entry and before genome amplification.

Another protein up-regulated during progress of infection of MDCK cells was the N-myc downstream-regulated gene 1 (NDRG1, spot 6 and 7, Table 4.2-2), which belongs to the alpha/beta hydrolase superfamily. To our knowledge it has not been described before that NDRG1 to be altered in the presence of influenza virus. A relation to infections was only shown for HV in yeast-two hybrid assays, which reported NDRG1 interaction with viral proteins (Ahn et al., 2004). NDRG1 is a 43 kDa protein and highly conserved among multi-cellular organisms. It is a predominantly cytosolic protein expressed ubiquitously in tissues in response to cellular stress signals. NDRG1 induces stress mechanisms involved in cellular differentiation, proliferation and growth arrest, tumor progression or heavy metal accumulation, hypoxia and DNA damage response (Ellen et al., 2008). Stein et al. reported a regulation of NDRG1 by the p53 protein, which is essential for the induction of apoptosis and which is involved in the IFN response in influenza virus infected cells (Stein et al., 2004). These findings indicate the role of NDRG1 as a mediator of apoptosis.

Heat shock proteins (hsp) are synthesized in response to a wide variety of stressful stimuli, including viral infections with the biological purpose of rendering the host cells to be resistant to further and more severe stress (Ciocca et al., 1993). It has been reported that hsps inhibit the replication of a variety of RNA viruses as well as influenza virus (Watanabe et al., 2006).

On the other hand, many viruses utilize specific hsps for their replication. Interactions of influenza virus and hsps are reported by modulating hsp activity or as an influenza virus M1 protein binding factor involved in the virus life cycle (Liang et al., 2007). This study observed the most consistent accumulation of heat shock protein 27 (HSP27, spot 1, Table 4.2-1) in response to influenza A virus infection of human A549 cells, also described for avian influenza virus H9N2 infection (Liu et al., 2008). HSP27 is an important small hsp (27 kDa) that functions as a molecular chaperone in human cells. Besides its putative role in thermotolerance, it is of special clinical interest, because of an association with other viral infections, e.g. adenovirus and HV (Ciocca et al., 1993) or its contribution to cellular intrinsic immunity against HIV (Liang et al., 2007). Recent data indicate a role in signal transduction pathways of several cell regulators (e.g. tumor necrosis factor (TNF) alpha, interleukin 1, protein kinase C (PKC)), which affect HSP27 phosphorylation (Ciocca et al., 1993).

For A549 cells, significant differences were detected in protein levels of a catabolic enzyme, the hydroxyprostaglandin dehydrogenase 15-(NAD) (HPDG, spot 2, Table 4.2-1). Investigations describing major alteration during influenza virus infections have so far not been reported for this protein. A prostaglandin synthase was found to be regulated during the microarray analysis of A549 cells in response to influenza virus infection (Geiss et al., 2002). HPDG controls the biological activity of prostaglandin by converting it into an inactive keto-metabolite. Apparently, HPDG interacts with cyclooxygenase-2 to control the cellular levels of prostaglandins (Tai et al., 2006). Tai et al. reported that prostaglandins are indeed an important regulator of immune responses affecting cytokine production (Tai et al., 2006). They also mentioned a significant role in cancer, inflammation and reproduction processes. Preclinical studies reported a therapeutic efficacy of prostaglandins against influenza virus (Bernasconi et al., 2005) by inhibition of virus induced inflammatory reactions and virus replication in pulmonary cells. Due to these facts it seems possible that HPDG is involved in the specific induction of the inactivation of prostaglandins by influenza virus to overcome host cell induced virus defense mechanisms.

The induction of cellular proteins correlated directly to apoptosis was not observed for A549 cells until 72 hpi, the latest time point of infection analyzed. One of these altered proteins is transglutaminase 2 (TGM2, spot 6, Table 4.2-1), which is an inducible transamidating acyltransferase that catalyzes Ca^{2+}-dependent protein modifications. Similar to mRNAs coding for Mx and prostaglandin synthase it was found to be regulated in influenza virus infected A549 cells (Geiss et al., 2002). TGM2 is reported to act in transmembrane signaling and cell surface adhesion processes as well as having a general protective and stabilizing role in cells and tissues. TGM2 is well-characterized, involved in intracellular signaling (induced by TGFbeta, NF-κB and AP for cellular defense), apoptosis and regulation of the cytoskeleton network (Fesus and Piacentini, 2002). It is induced in cells undergoing

apoptosis. TGM2 interacts with mitochondria, shifting them to a higher polarized state and an altered redox status (Fesus and Piacentini, 2002). Recently, a growing number of viral and cellular proteins has been found to be modified by TGM2, suggesting a novel function in viral pathogenesis (Jeon and Kim, 2006).

Nucleobindin (Nuc, spot 7, Table 4.2-1), also induced during the late infection phase of A549 cells, is a class Ca^{2+}-binding protein containing an EF-hand motif that has multiple functions. To our knowledge, a study reporting Nuc altered in the presence of influenza virus has not been described before. The 55-kDa, hydrophilic Nuc shows features of a secretory protein (Ballif et al., 1996) and also of a transcription factor through the leucine zipper regions (Valencia et al., 2008). It is highly abundant in the Golgi region and could play a key role in Ca^{2+} homeostasis within the cis-Golgi network. Additionally, it interacts with multiple binding partners, including cyclooxygenases and hydroxyprostaglandin synthase, engaged as a potential regulator (Ballif et al., 1996). Nuc was first identified by its binding to laddered DNA during apoptosis in mouse cell lines and is reported to promote autoimmunity and apoptosis in mice (Ballif et al., 1996). However, despite its great importance in various signaling pathways, understanding of the regulation of its biological functions remains limited. Probably, Nuc is related to influenza virus infection via its presence in the Golgi network during modification steps of virus proteins or it plays a role in apoptosis triggered by the virus in late phase of infection.

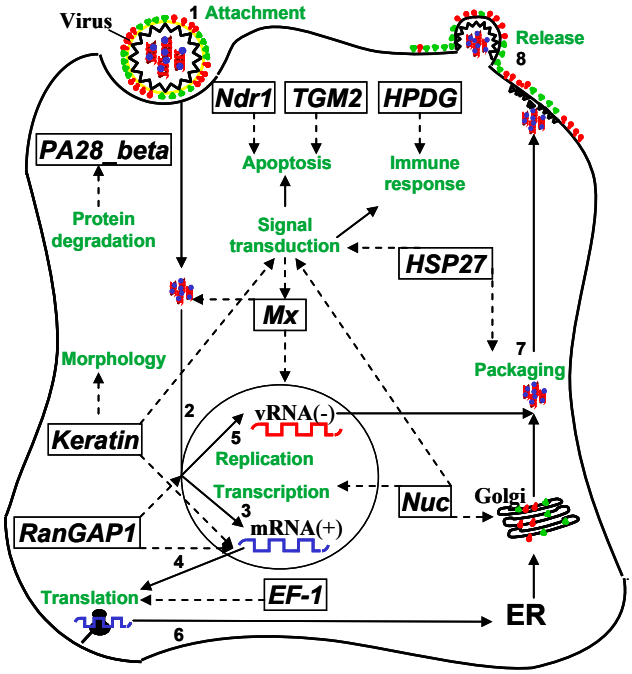

Figure 5.2-1: Possible involvement of identified proteins in host cell response during influenza A virus infection

Different steps of the replication cycle of influenza A virus are signed by numbers and continuous lines, corresponding to published literature (Sidorenko and Reichl, 2004). Dotted arrows indicate hypothetical interactions of the proteins (abbreviations framed).

5.2.2. Virus-host cell interactions in A549 and MDCK cells infected with influenza A PR/8-RKI virus

It is well known that 2-DE is limited to the identification of high abundant proteins (Olsen et al., 2006). As expected, low abundant regulatory proteins e.g. transcription factors and kinases, could not be found to differ in abundance during the infection cycle in the present study since they were all below the LOD of current 2-DE technology (Corthals et al., 2000). Moreover, no influenza A virus proteins (including viral membrane proteins) could be identified within the analyzed protein samples of PR/8-RKI infected A549 and MDCK cells. This could be due to solubilization, strip internalization or separation problems known for basic proteins (Shaw and Riederer, 2003) or due to high-abundant proteins masking lower abundant viral proteins (Corthals et al., 2000). Determination of the mRNA transcript level of the viral NS1 by RT-qPCR for example showed a low expression level of the PR/8-RKI variant (Seitz et al., 2010), accounting also for the absence in this study.

Results of the 2-D DIGE analysis suggested clearly that the proteome cellular network of infected MDCK cells was not affected significantly until 8 hpi (Figure 4.2-3), whereas virus production already started at 4 hpi (Figure 4.2-1). Possible involvements of the identified proteins during intracellular influenza virus life-cycle in A549 and MDCK cells are shown in Figure 5.2-1. Enhanced inductions of RanGAP1, a protein responsible for mRNA transport in the nucleus, as well as the emergence of keratin 10 cleaving products responsible for transport and positioning of mRNAs were found (Figure 5.2-1). These findings indicated an early perturbation of the host cell protein synthesis machinery, to allow for an enhanced virus protein synthesis. The induction of Mx1 (Figure 4.2-4B) is of particular interest, because it is involved in the early host cell defense mechanism induced by IFN. This signal transduction mediator is related to a larger set of proteins, involved in IFN stimulated host cell defense that should have been affected but could not be identified by 2-DE in this study. However, MDCK cell stress response to influenza virus infection was not observed until 12 hpi when first abundance changes of NDRG1 occurred, a protein, which is essential for the induction of cellular stress mechanisms and apoptosis (Figure 5.2-1).

In contrast to MDCK cells the proteome abundance changes in response to influenza virus infection of A549 cells are quite different. Data did not show an extensively affected cellular protein synthesis, which is causing possibly the delayed virus production (Figure 4.2-1). Of particular interest is the up-regulation of HPDG, which suggests a specific inactivation of prostaglandins by influenza virus to overcome host cell induced virus defense mechanisms (Figure 5.2-1) The opposite to this pathway is the host cell immune response reflected by changes in abundance of MxA (Figure 4.2-4A). Furthermore, influenza virus replication is correlated with a strong accumulation of HSP27 (Figure 4.2-4A), a protein with stress

protection function. Whether this is induced directly by the virus or part of the immune response of the host cell is not clear. In the latest infection phase (72 hpi) an enhanced stress response is suggested by induction of TGM2 (signal transduction), Nuc (transcription factor) and PA28-beta (protein degradation) (Figure 4.2-3A). These proteins indicate an increased level of apoptosis.

In summary, greater evidence of enhanced induction of apoptosis and cell stress response was detected for A549 cells compared to MDCK cells, which could be due to the significant longer infection times. In contrast to that, proteome changes for MDCK cells indicated an early, virus induced perturbation of protein synthesis and antiviral response mechanisms. This suggests that proteins involved in antiviral response mechanism in mammalian cells induced by Mx proteins could be a promising target for engineering high producer cell lines for vaccine production. Turning off Mx activity could result in a delayed cellular immune response to viral infection. This would results in extended virus production phases and higher virus yields. This suggestion was also supported by a study of Koerner et al., which shows a dramatically higher susceptibility to influenza virus infection in mice fibroblast and *in vivo* in mice lacking Mx genes (Koerner et al., 2007). Unfortunately, recent studies reported that in MDCK cells Mx proteins did not showed an anti-influenza activity, which correlates to a lack of IFN induced antiviral activity (Seitz et al., 2010). However, other proteins identified in this study might also represent potential targets for improvement of cell line performance in vaccine production. For example, NDRG1 a known apoptosis inducer could be a target to reduce or delay the onset of apoptosis and prolonging the viability of host cells leading also to longer virus production phases. Similar effects were reported for overexpression of an anti-apoptotic protein bcl-2 known to suppress the mitochondrial apoptotic pathway in diverse cellular systems (Kuystermans et al., 2007). Overexpression of bcl-2 resulted in an improved robustness to nutrient deprivation and toxin exposure, including longer survival in intensified culture systems (Tey and Al-Rubeai, 2004).

5.2.3. Functional significance of altered abundant proteins in MDCK cells infected with influenza A PR/8-NIBSC virus

Signal transduction

The proteins identified included several well-known IFN induced proteins, which are involved in signal transduction processes. Apparent up-regulation of different isoforms of myxovirus resistance protein 1 (Mx1, spots 4-7, Table 4.2-3), PKC inhibitor protein-1 (KCIP-1, spot 19, Table 4.2-3) and IFN induced protein with tetratricopeptide repeats 1 (IFI-1, spot 31, Table 4.2-3) could be observed. Mx proteins are believed to counteract influenza virus infection by interfering in different steps of the virus replication cycle (Haller et al., 2007a). Influenza virus

entry requires PKC activity and this is believed to be stimulated upon the binding of virus to cellular receptors (Hoffmann et al., 2008). In support of this, PKC inhibitors have been shown to inhibit influenza virus replication (Hoffmann et al., 2008). Thus, the pathways associated with these IFN induced and up-regulated proteins are indicating an early establishment of an antiviral state in MDCK cells infected with the PR/8-NIBSC virus variant. This finding is consistent with the previous proteome study of influenza PR/8-RKI virus (Vester et al., 2009). However, in this previous study only one isoform of Mx1 and no other IFN induced proteins were reported to be up-regulated.

Cytoskeleton proteins

Significant differences between infected and mock infected cells were detected in protein levels of several cytoskeletal network proteins, e.g. keratin 10 (spot 8, 18, 21, 24, 33, Table 4.2-3), cytokeratin 8 (CK-8, spots 14-16, Table 4.2-3), cytokeratin 5 (CK-5, spot 22, Table 4.2-3), beta-actin (spot 17, 32, Table 4.2-3), tubulin alpha-2 (TUBA2, spot 13, Table 4.2-3) and tubulin-tyrosine ligase (CG1550-PA, spot 30, Table 4.2-3). Most of these protein spots were up-regulated and only one isoform of keratin 10 (spot 8, Figure 4.2-6A), one isoform of cytokeratin 8 (spot 15, 16, Figure 4.2-6A) and the tubulin remodeling protein (spot 30, Figure 4.2-6A) were down-regulated significantly during PR/8-NIBSC infection. Various controls and special handling precautions were used to avoid and check for human keratin contamination (data not shown). Similar results for changes in cytokeratin levels during influenza virus replication were also shown for the PR/8-RKI variant in MDCK cells reported in this work before (see section 4.2.1) and for avian virus infected AGS cells (Liu et al., 2008). The host cell cytoskeletal network is involved in the transport of viral components in the cell, in particularly during the stages of virus entry and virus budding (Radtke et al., 2006). It has been shown that influenza virus requires an intact actin cytoskeleton for entry (Sun and Whittaker, 2007), and it has been hypothesized that interactions between the cytoskeleton and lipid rafts facilitate budding of virus particles (Simpson-Holley et al., 2002). Several studies have also indicated that cytoskeletal proteins such as tubulin and actin are involved in regulation of viral gene expression (Arcangeletti et al., 1997). Furthermore, an association of influenza viral NP and M proteins with cytoskeletal elements has been reported (Avalos et al., 1997), and actin and tubulin were both identified as proteins that interact with influenza vRNP complexes (Mayer et al., 2007).

Protein degradation

For the UV excision repair protein RAD23 (hHRB23B, spots 9-10, Table 4.2-3) two differentially abundant isoforms were observed. Probably, both spots correspond to different levels of an inactive and an active form with spot 9 up-regulated and spot 10 down-regulated (Figure 4.2-7). The two spots with different p*I* but same molecular weight were identified

clearly as the same protein, suggesting PTMs. RAD23 belongs to a family of adaptor molecules with affinity for both the proteasome and ubiquitinylated proteins. It is assumed that RAD23 shuttles the ubiquitinylated proteins to the proteasome for destruction, and therefore has an important role during protein degradation (Schauber et al., 1998). Consistent with these findings higher abundance levels of the proteasome subunit beta (PSMB4, spot 20, Table 4.2-3) were found in response to influenza virus infection. Both proteins have central roles in degradation of intracellular proteins and are critical for diverse cellular functions (Coux et al., 1996; Schauber et al., 1998). Therefore, their change in abundance levels may indicate to an important pathway affected by influenza virus replication and suggesting an enhanced stress response during PR/8-NIBSC virus infection.

Others

An important characteristic of PR/8-NIBSC virus infection was the high induction of the viral NS1 (spot 26, Table 4.2-3) at 8 hpi and its further increased abundance at 12 hpi (Figure 4.2-7). The NS1 protein is encoded by viral RNA segment 8. It binds dsRNA and forms dimers *in vivo*, and has been suggested to perform several important accessory functions for optimal replication of the virus in its host cell (Hale et al., 2008). Importantly, the NS1 protein represses the host cell antiviral response by multiple mechanisms. These mechanisms include the inhibition of the IFN inducible dsRNA activated kinase PKR and the blocking of IFN production (Kochs et al., 2007). However, NS1 has multiple functions, which may contribute additionally towards efficient virus replication, including a temporal regulation of viral RNA synthesis, control of vmRNA(+) splicing, enhancement of viral vmRNA(+) translation, regulation of virus particle morphogenesis and suppression of apoptosis (Hale et al., 2008). Interestingly, the NS1 protein was not detected during PR/8-RKI infections suggesting different capacities of different virus variants to suppress the host cell response (Krug et al., 2003).

Noteworthy, three isoforms of albumin were found with an increased abundance level in mock infected MDCK cells (spots 1-3, Table 4.2-3) but only at early extraction time points. Albumin is a common plasma protein and a typical component of serum-containing cell culture media. Epithelial MDCK cells perform endocytosis and take up plasma proteins with their cargo for further use (e.g. cholesterol carrying low density lipoproteins, fatty acid carrying albumin, iron carrying transferrin, etc.) (Simionescu et al., 2002). Albumin, acting as a transport or cargo protein for some important substrates such as fatty acids etc., was found only at low level in infected cells. This might indicate either lower permeability for albumin, consumption of stored or attached albumin in infected cells or competition of albumin with the virus for endosomes.

Another protein of interest induced by PR/8-NIBSC virus is annexin A1 (ANXA1, spot 25, Table 4.2-3). Annexins are calcium-dependent phospholipid-binding proteins and are proposed to act as scaffolding proteins at certain membrane domains. ANXA1 has been shown to prevent fusion of raft-associated vesicles (Derry et al., 2007). Interestingly, ANXA2, which interacts with A1, has the opposite effect and is required for the apical transport of raft-associated vesicles (Jacob et al., 2004). Since influenza virus also buds from raft domains this indicates a potential regulatory role of ANXA1 (Derry et al., 2007).

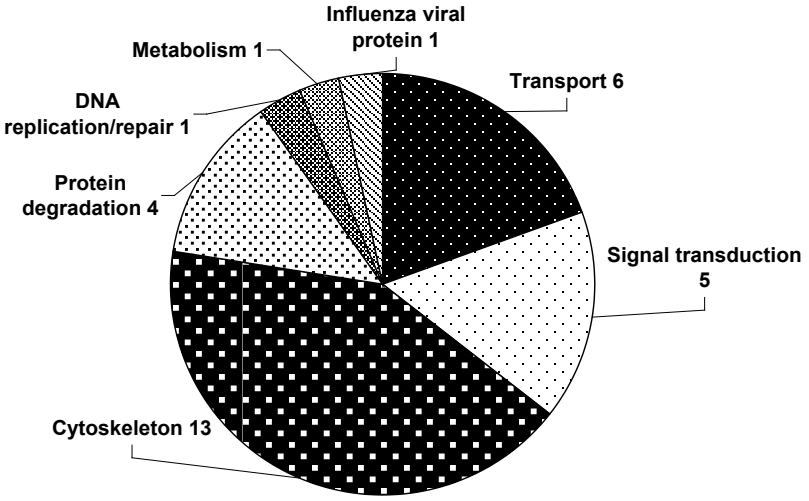

Figure 5.2-2: Functional classification of the identified proteins regulated after PR/8-NIBSC infection in MDCK cells. Number of identified proteins is indicated, respectively.

5.2.4. Differences in virus-host cell interactions in MDCK cells infected with influenza A PR/8-NIBSC and PR/8-RKI virus

Early cellular proteome alterations in MDCK cells after infection with two influenza PR/8 virus variants with differences in replication characteristics were compared. Analysis of proteome data showed that infection with the virus variants resulted in significant differences in the total number of regulated proteins. The PR/8-NIBSC virus variant caused the highest abundance changes with 36 regulated proteins while PR/8-RKI showed only 8 changes. Furthermore, PR/8-NIBSC induced an earlier perturbation of the proteome profile. Additionally, PR/8-NIBSC infections seem to induce a stronger IFN stimulated host cell response than PR/8-RKI. As a result three well-known IFN induced proteins (Mx1, KCIP1, IFI-1, Figure 4.2-7) are up-regulated significantly. Moreover, three additional isoforms of Mx1 occurred, indicative for PTMs marking different regulation states, were identified after infection with PR/8-NIBSC. Identification of an inhibitor of PKC, i.e. KCIP1 could be another possible hint on increasing overall productivity of the vaccine production process. As stated before influenza virus entry requires PKC activity (Hoffmann et al., 2008). Hence, treatment with PKC inhibitor significantly reduces viral replication (Hoffmann et al., 2008). In contrast, activation of PKC

leads to enhanced virus production in cell culture. These opposing effects strongly support a role for PKC activity in influenza virus replication and may serve as a target for antiviral drugs. This means that compounds that result in increased virus titers may be beneficial for boosting the production of cell culture grown influenza virus vaccines.

An enhanced stress response after PR/8-NIBSC infection is also suggested from the finding that several proteins responsible for protein degradation were induced. Most interesting was the significant higher abundance of the viral NS1 protein during PR/8-NIBSC infection. This regulatory viral protein is essential for the virus to prevent the establishment of a cellular antiviral state. Higher induction of the antiviral state despite higher NS1 abundance could indicate different capacities of different NS1 variants to counteract and suppress the host cell response (Krug et al., 2003). In contrast, the NS1 protein was not detected during PR/8-RKI infections. A possible explanation for such differences was reported in recent studies, which showed that the AA at position 55 of NS1 affects virus growth positively in MDCK cells (Murakami et al., 2008). They suggested that a Lys-to-Glu substitution is responsible for the enhanced type of IFN antagonistic property of NS1, leading to high growth in MDCK cells. Interestingly, the PR/8-RKI strain showed the same NS1 mutation in recent sequencing experiments (data not shown). Two possible explanations are proposed: (I) Substitution may enhance the productivity of this protein in this cell line, via its increased interaction with host cell molecules, such as chaperones, which can precisely hold and rapidly transport NS1. (II) Substitution may increase the intrinsic IFN antagonism of NS1 via a higher affinity for host cell mRNAs, resulting in the enhanced inhibition of IFN gene expression.

It is known that influenza viruses take advantage or interfere with the antiviral host cell response for efficient replication (Hale et al., 2008; Iannello et al., 2006; Ludwig et al., 2006). Additionally, different virus strains have significant differences in their capabilities to induce or suppress the establishment of an antiviral state (Hayman et al., 2006). Obviously, such differences between strains and subtypes can be correlated with replication efficiency and form the biological basis for the different replication characteristics of PR/8-NIBSC and PR/8-RKI investigated in this study. Due to the high relevance of such findings for yields in vaccine manufacturing these differences should be further investigated and additional strains incorporated in a more comprehensive study. For example, comparing different high and low yield strains could reveal different strategies to escape the host cell antiviral response due to their strain specific virulence and replication mode. Understanding of these differences in viral strategies could help to find a general cell engineering procedure for suppression of antiviral response and improvement of virus yields.

5.2.5. Functional significance of altered abundant proteins in Vero cells infected with influenza A PR/8 virus

Cell-cell interactions

The largest group of functional related proteins that were differentially abundant in Vero cells infected with cell line adapted but also with non-adapted virus was found to be involved in cell-cell interactions. These proteins include different isoforms of ITGA3 (spots 10-13, 42, Table 4.2-4; spots 1-5, Table 4.2-5) and for cell line adapted virus infections additionally different isoforms of integrin alpha V (ITGA5, spots 36-38, Table 4.2-4) were either up- or down-regulated (Figure 4.2-11). Integrins are heterodimeric cell adhesion molecules that link the extracellular matrix to the cytoskeleton (van der Flier and Sonnenberg, 2001). Additionally, they act as receptors that organize the cytoskeleton, integrins play an important role in controlling various steps in the signaling pathways, which regulate processes as diverse as proliferation, differentiation, apoptosis, and cell migration. Integrins are receptor molecules for the extracellular matrix such as fibronectin, collagen, and laminin, which act as a potent regulator of cell growth, differentiation, and gene expression. Ligand binding or aggregation of integrin receptors also initiates a number of metabolic changes (van der Flier and Sonnenberg, 2001). In some instances activation of transcription factors and induction of gene expression have been demonstrated (Lafrenie and Yamada, 1996). Most interesting is the fact that integrins can protect cells from apoptosis during influenza virus infection by a co-operation with TNF-alpha signaling (Richter and Topham, 2007).

Heat shock proteins

Another large functionally related group of most consistently up-regulated proteins in infected Vero cells (Figure 4.2-11A) contained 4 different kinds of hsp, including HSP 27kDa (spot 18, Table 4.2-4), HSP 105kDa (spots 32-35, Table 4.2-4), HSP 90kDa (spot 41, Table 4.2-4) and HSP 70kDa (spots 44-46, Table 4.2-4). Mammalian cells have developed response networks, which detect and control diverse forms of stress. One of these responses, known as heat shock response is a universal mechanism necessary for cell survival under a variety of unfavorable conditions such as virus infections (Santoro, 2000). These heat shock proteins serve as cellular chaperones, participating in protein synthesis and transport through various cellular compartments. Virus infection of mammalian cells often results in induction of hsp synthesis. Interactions between stress proteins and viral components have been described at different stages of the viral life cycle and a possible role in the control of virus replication and morphogenesis is discussed (Santoro, 1996). However, for example HSP90 is an abundant, house-keeping protein, essential for viability of eukaryotic cells. It interacts with the PB2 subunit of the viral RNA polymerase and is suggested to have an important role in viral gene expression (Naito et al., 2007). HSP70 was identified as an influenza virus M1

protein binding factor involved in the virus life cycle. It may play a role within the nuclear transport of vRNP complexes (Watanabe et al., 2006). For HSP27 recent data indicate a role in signal transduction pathways of several cell regulators (e.g. TNF-alpha, interleukin 1, PKC) (Ciocca et al., 1993).

Metabolism/glycolysis

For some of the identified proteins it is not clear if their functions are either associated with response to influenza virus infection or in virus replication cycle (Shaw et al., 2008). However, some of these proteins have further roles in addition to their known basic functions. For example, different proteins involved in the glycolytic pathway were found to be regulated (pyruvate kinase, spot 27; GAPDH, spot 28; enolase 2, spot 22; Table 4.2-4). Enolase in addition to tubulin, has been reported to stimulate transcription of the Sendai virus genome (Ogino et al., 2001). A role in RNA virus transcription has been proposed for GAPDH. Phosphorylated forms of GAPDH have been shown to bind to the genomic cis-acting RNA of human parainfluenza virus type 3 (Choudhary et al., 2000). *In vitro* data indicate that GAPDH has a negative regulatory role in transcription of this virus depending on its phosphorylation (Choudhary et al., 2000). However, it is not clear whether these glycolytic activities are required during infection or whether these are alternative new functions for these well-known proteins, or if it is just a stress response of metabolism.

Oxidative stress response

Finally, it was found that influenza virus infections induce a number of different enzymes involved in the maintenance of the redox state of cells. Influenza virus infections have been shown previously to induce the formation of reactive oxygen species, which cause oxidative stress and may play a role in inflammatory response (Choi et al., 1996). 2-D DIGE has identified peroxiredoxin (PRX, spot 19, Table 4.2-4), superoxide dismutase (MnSOD, spot 50, Table 4.2-4) and an oxidoreductase (SDR, spot 49, Table 4.2-4) as being up-regulated by influenza virus infection in Vero cells. Besides their obvious redox functions, different roles have also been identified for these proteins in apoptosis and transcription in cells (Choi et al., 1996).

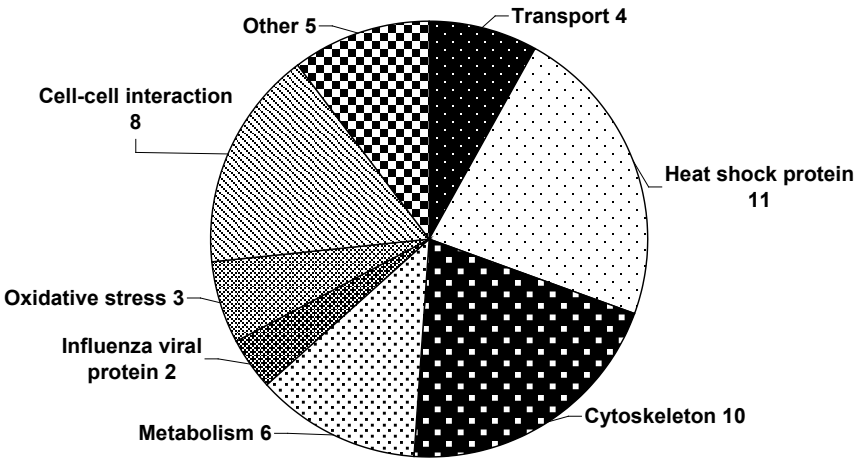

Figure 5.2-3: Functional classification of the identified proteins regulated after PR/8-RKI-Vero infection in Vero cells. Number of identified proteins is indicated, respectively.

5.2.6. Virus-host cell interactions in IFN deficient Vero cells infected with influenza A PR/8 virus and influenza virus adaptation mechanisms

It is reported that Vero cells, in addition to their inability to produce IFN, are also defective in their ability to induce ISGs. However, Vero cells have the ability to induce an antiviral state in an IFN independent manner (Chew et al., 2009). The existing antiviral signaling pathways in Vero cells is known to be atypical and do not rely on classical antiviral signaling pathways such as in MDCK cells. Whether this can explain the permissive nature of Vero cells to viral infections (Kistner et al., 1998) has to be further elucidated and the exact mechanisms characterized. In agreement with this, the present proteome study did not show regulation of any IFN stimulated proteins for example Mx proteins etc. as identified in infected MDCK cells. Therefore, no clear suggestions concerning the specific role of the HSP27 kDa protein and other identified proteins associated with signal transduction pathways in establishment of an antiviral state can be made. On the other hand, the significant higher abundance of the viral NS1 protein seems to indicate a high viral activity to suppress antiviral mechanisms involved in Vero host cell response. However, it is unlikely that the regulatory activity of IFN pathways is involved during virus replication in Vero cells. On the other hand NS1 could also be involved in an anti-apoptotic effect in this cell line as reported by Zhirnov et al. (Zhirnov et al., 2002). They proposed a concept that apoptosis is induced in Vero cells by alternative IFN independent pathways not used in MDCK and that they may restrain an anti-apoptotic program by the NS1 directed down-regulation of NF-κB. Enhancement of this anti-apoptotic effect by additional knockdown of NF-κB could be used to reduce or delay the onset of apoptosis and prolonging the viability of Vero cells is suggested to be a possible successful cell engineering strategy. Another study suggested that specific accumulation of NS1 in the nucleus may contribute to efficient viral replication in Vero cells due to control of vmRNA(+)

synthesis (Ozaki and Kida, 2007). The Lys-to-Glu substitution in NS1 detected in the PR/8-RKI strain (data not shown) was reported not to mediate viral growth enhancement in Vero cells, which was for example found in MDCK cells (Murakami et al., 2008). Another strategy to increase cell viability and productivity, which could also be a possible Vero cell engineering target is the hsp70 kDA. Since transfection of NS0 myeloma fusion partner cells with hsp70 kDA gene resulted in higher hybridoma yield by improving cellular resistance to apoptosis (Lasunskaia et al., 2003).

Furthermore, the signaling pathway induced by integrin receptors is of interest because it might represent early virus recognition events or responses to virus particle entry. Both functions could display the first line of defense against incoming pathogens. This hypothesis is also supported by results obtained for non-adapted virus infection, which also resulted in regulation of 5 isoforms of integrin alpha 3 (Figure 4.2-11B). The absence of virus particle release after infection with non-adapted viruses indicated a lack of essential properties for successful viral replication, however virus particles could still attach to or enter their host cells. Therefore, this integrin mediated signaling via extracellular matrix interactions is possibly a first virus recognition signal acting as cell to cell communication pathway substituting IFN signaling.

In future studies, mechanisms of virus adaptation to production cell lines have to be further investigated. It is still not clear whether viruses undergo a natural selection process or changes in the genome sequence of viral proteins (e.g. HA or NS1) play a crucial role during adaptation. Notably, passaged viruses adapt to their host cell through mutation in the receptor binding site of the viral HA gene (Connor et al., 1994; Gambaryan et al., 1999; Mochalova et al., 2003). In particular for HA, the most abundant surface protein, changes in the glycosylation pattern seem to play an important role in the adaptability (Diaz et al., 1988; Ozaki et al., 2004; Schwarzer et al., 2009).

5.3. RT-qPCR assay for the analysis of human influenza A virus transcription and replication dynamics

The general time course of influenza virus replication in their host cells is well-understood, however much about regulation of viral genome replication and vmRNA(+) transcription still remains unknown (Cheung and Poon, 2007). The ability to determine quantitatively the amounts of the three different types of influenza A viral RNAs occurring during virus life cycle in mammalian cells will facilitate the study and modeling of the time course and dynamics of viral transcription and replication. Several studies have been described in the past for analyzing virus dynamics (Kumar et al., 2008b; Ng et al., 2008; Robb et al., 2009; Uchide et al., 2002; Vreede et al., 2008). These studies used diverse techniques, for example primer extension and vRNP reconstitution assays or semi-quantitative southern hybridization and RT-qPCR assays. Nevertheless, most of the results are contradictory and therefore different hypothesis were suggested for regulation and dynamics of viral replication.

Here, a RT-qPCR assay based on synthetic viral RNA reference standards, a pspRT and a qPCR was established and optimized (Vester et al., 2010). The assay was used to distinguish specifically between and to quantitatively determine the average number of molecules per cell for vRNA(-), cRNA(+), vmRNA(+) of viral segments 4 (HA), 6 (NA), 7 (M) and 8 (NS) during the life cycle of influenza virus.

5.3.1. Development and validation of the RT-qPCR assay

For validation of molecular techniques such as qPCR, i.e. in terms of the MIQE guidelines (Bustin et al., 2009), the full determination of assay performance characteristics, e.g. efficiency, specificity, linear dynamic range, LOD and precision are required. These parameters must be thoughtful considered for qPCR assays to ensure its precision, correct interpretation, reliability and relevance (Freeman et al., 1999).

Successful synthesis and amplification by the qPCR method relies on the specificities of the designed primer. The study aimed at the establishment of either (I) full length cDNAs or (II) PCR products due to the choice of primer binding sites at conserved regions of the viral segments, to assess the different polarities of the three types of viral RNAs during the RT step or (III) to amplify only short gene specific PCR products during the qPCR step. All primer were carefully designed and optimized for theses different application areas and requirements. Since the assay was validated for infection with influenza PR/8 virus strain, when using other virus subtypes only new real-time primer need to be adapted and optimized. Most of the pspRT primer, the universal primer Uni12 (M) and the primer for full-length PCR products will not need an optimization due to the choice of primer binding sites at

conserved regions of the viral segments. Moreover, the PR/8 strain was chosen due to its high relevance as a backbone for genetic reassortment for the annual seed virus generation in vaccine production for H1N1 viruses (Kilbourne et al., 1971).

To obtain high precision in pspRT and qPCR a highly defined calibration curve was needed (Kubista et al., 2006). Therefore, validation and quantification procedures were done with 12 synthetic viral RNA reference standards according to each of the four viral segments and the three viral RNA types to be measured. An optimized protocol, which avoids labor-intensive cloning procedures (Fronhoffs et al., 2002), was used to create templates containing a T7 promoter gene sequence for *in vitro* transcription of these standard viral RNAs. The viral RNA reference standards have the advantage that both, standard viral RNA and unknown viral RNA samples, undergo same pspRT and qPCR conditions (Bustin et al., 2009).

Another aspect to obtain high precision and reliability of the assay was the optimization of pspRT and qPCR conditions (Bustin et al., 2009). Optimization included the design and selection of optimal primer combinations and concentrations, the temperature and duration time of pspRT synthesis and annealing and extension of PCR, the type of RT enzyme and the concentration of Mg^{2+} (data not shown).

As demonstrated, the synthesis and amplification in all calibration curves was linear over a wide range of input copies, with good sensitivity, precision, repeatability and reproducibility (Table 4.3-1). Regarding specificity, although the SYBR Green I dye can bind indiscriminately to any dsDNA (Arya et al., 2005), monitoring of the qPCR reaction products by melting curve analysis showed that the assay was specific for the respective segment and viral RNA type. Additionally, clearly different C_q values were obtained for all negative and complementary controls and sequencing of the amplicons confirmed the specificity of the assay. Results indicate that the assay has a good repeatability and reproducibility, as shown by low CV values of less than 0.8 – 3.1% within and between qPCR assays. In terms of sensitivity, the smallest amount of viral RNA detected reliably, was about 1.0×10^3 – 8.9×10^3 viral RNA molecules. Compared to conventional RT-qPCR assays used for diagnostic procedures (Di Trani et al., 2006) the sensitivity determined was lower. In contrast to these diagnostic assays the LOD was defined as a precaution due to the complex priming strategies and occasional emerging low rate of incorrect strand detection. LOD was not based on linear regression analysis (Bustin et al., 2009). Nevertheless, sensitivity of the assay established is adequate as quantification is based on a high number of infected cells cultured in parallel, and usefulness is demonstrated clearly in the time courses obtained for infection studies.

Further improvement of sensitivity and specificity by modifying the complex RT strategy would facilitate interpretation of experimental results and parameter estimation for

mathematical modeling. Options for improvement of sensitivity and specificity might be, for example, to perform the pspRT reaction at higher temperature to reduce secondary structures inducing self priming of the RNA, to reduce the comparatively high concentration of target RNA templates or to reduce or to eliminate the possible carry-over of active RT enzymes and RT primer (Bustin and Nolan, 2004). Other studies reported the use of tagged RT primer with non-viral and viral-specific sequences, which can be amplified during PCR with primer corresponding to the tag-sequence and viral-specific primer (Craggs et al., 2001).

Another advent could be the inclusion of an internal positive control (IPC) to monitor false negative results due to PCR failure caused by expired reagents, poor technique, equipment failure or presence of enzyme inhibitors. IPC could also help to determine RNA extraction efficiency. Practically, an IPC could be added to each sample before the extraction step (Di Trani et al., 2006). It consists of a second target sequence, represented by a rodent RNA for example, unrelated to the sequence to be detected and available in commercial kits. Adding the IPC before influenza virus RNA extraction would allows monitoring of the whole process from extraction to RT-qPCR.

A recent publication, published after completion of this work suggested low specificity of the developed RT-qPCR assay (Kawakami et al., 2011). They recommended a method which is based on RT using tagged primers to add a 'tag' sequence at the 5' end and a hot-start method. Nevertheless, validation procedure for specificity determination of this publication was done with 10^9 copies of synthetic viral vRNA, cRNA, and mRNA of segment 5 (NS) of A/WSN/33 virus (WSN;H1N1) generated by reverse genetics. This means, validation was done with a segment, a virus and a measuring range or viral RNA concentration not used in this work. Especially the high RNA copy number is not matching our measuring range which ends at about 10^7 viral copies and which was validated for specifity in our work. Notwithstanding, these findings have to be considered when using the RT-qPCR assay.

5.3.2. Human influenza A virus replication dynamics

The validated RT-qPCR assay was evaluated finally by following the time course of influenza PR/8-RKI virus infection in MDCK cells for four viral segments. It is accepted widely that the replication and transcription of the influenza viral genome is a selective process (Smith and Hay, 1982). In infected cells, the synthesis of each vmRNA(+) molecule is known to vary over the time course of infection, also shown by this study. Predominantly, transcription of vmRNA(+) in early phases of virus infection was detected (Figure 4.3-8A), which was reported before (Cheung and Poon, 2007). Moreover, these studies also described the preferential synthesis of NS1 vmRNA(+) and a delay for M1 vmRNA(+) correlated with the synthesis rates of the corresponding proteins (Hay et al., 1977). Findings that NS1 is a

predominant viral protein in infected cells in early phases of infection are in agreement with its function in the control of cellular mRNA synthesis and cellular signal transduction (Hale et al., 2008). The same applies also to the viral M1 protein, which is synthesized preferentially during later stages of infection, in agreement with its function as a translocation-factor and regulator of vRNPs nuclear export (Lamb and Krug, 2001). Except for M1, the amounts of vmRNA(+) decreased 3-fold during late phase of infection, this could be due to shut down of vmRNA(+) synthesis (Shapiro et al., 1987) and degradation of vmRNA(+) molecules.

With a short delay in the middle at an average of 0.3-0.9 hpi after onset of viral transcription first cRNA(+) molecules could be detected followed by the synthesis of vRNA(-) genome equivalents at an average of 2.5 hpi (Figure 4.3-8C). As described before (Hatada et al., 1989), cRNA(+)s were synthesized nearly simultaneously and in equimolar amounts for viral segments 4 (HA), 6 (NA) and 7 (M). Only synthesis of cRNA(+) of segment 8 (NS) was slightly different.

Interestingly, about 53 – 87 vRNA(-) molecules per cell were detected at time of infection (Figure 4.3-8C) although viral genome replication could not have taken place. This could be due to the ’cold infection’ step at 4°C, which allows virus particles to attach to the cell membrane but not to enter due to inhibition of endocytosis (Shapiro and Krug, 1988). Obviously, the genomes of virus particles attached were also detected by the assay and the decrease in the number of vRNA(-) per cell until 2.5 hpi could allow determining detachment kinetics. As infection was performed at a MOI of 6, the comparatively high number of vRNA(-) per cell reflects attachment of non-infectious virus particles, which enter the cells but do not have the ability to reproduce and are finally degraded (Marcus et al., 2009).

Another characteristic during the time course of infection observed for all viral RNA types is a drop in the number of viral molecules per cell of all segments at about 8 hpi. This drop was also identified in other infection experiment (data not shown) and seems to be correlated to the strong increase in HA activity 6 hpi, and therefore the onset of virus budding and release. This correlation could be referring to a short interruption of viral RNA synthesis due to a bottleneck in use of cellular resources or in molecules required for virus replication. The budding of a high number of virus particles including their genome copies could however only explain a drop in vRNA(-) genome equivalents but not for their precursor cRNA(+) or vmRNA(+). Accordingly, putting both hypothesis together, high budding and release activities could refer to high genome replication rates and this could lead to a shortage of resources for the synthesis of cRNA(+) and vmRNA(+).

Overall, it has to be considered that the HA assay underestimates the release of virus particles due to its low sensitivity and high standard error. Hence, budding and release of virus particle could have been started much earlier than expected by the HA titers and

genome copies (vRNA(-)) were continuously assembled into viral particles and released. Consequently, this could lead to an underestimation of the synthesis rate of vRNA(+) due to a balance in synthesis, assembly and release of vRNA(-) genome copies. This could also account for the much lower synthesis rates of vRNA(-) (on average of 0.5) compared to the synthesis rates of cRNA(+) and vmRNA(+) (p_2 0.8 and 0.9, respectively) in the beginning of infection.

The ratios of vmRNA(+) molecules to viral genome molecules vRNA(-) (Figure 4.3-9), reflecting the viral replication level and its activity reached a peak at 3.5 - 4 hpi of viral segment 4 (HA), 6 (NA) and 8 (NS). The similar time course of the ratios indicated that the dynamic pattern of viral replication and transcription is similar. The fact that segment 7 (M) showed a peak after a time lag of 1 h (at about 5 hpi) is most likely due to its delay in vmRNA(+) transcription.

These quantitative data of viral replication and transcription dynamics should be used to estimate key parameters and validate a mathematical model describing influenza virus infection of epithelial cells (Sidorenko and Reichl, 2004). This model used general information available in literature and the following parameters and modeling assumptions were supposed. In general, the present model considered a small number of viruses infecting a cell (10 viruses/cell) and an average life cycle of infected cells of about 12 h. Virus particles unable to fuse with the membrane are degraded by lysosomes, an assumption also suggested by the quantitative qPCR data. The splicing of M and NS vmRNA(+) is not considered in the model. For the overall dynamics of virus life cycle: (I) Most of the viruses attached to the cellular membrane within 2 – 5 min post infection. (II) Endocytosis is accomplished in about 10 min. (III) At about 30 min post infection the first vRNPs reach the nucleus and vmRNA(+)s are transcribed in high copy numbers. These assumptions also agree with the present experimental results. NP promotes the initiation of unprimed transcription and blocks synthesis of vmRNA(+)s. (IV) This switch from viral transcription to viral genome replication takes place at about 3 hpi and vRNA(-) is replicated and all vRNA(-) molecules are synthesized at similar rates. Data from the infection experiments supported both assumptions. For the formation of new vRNPs in the nucleus, the number of M1 proteins represents a limiting factor, which is maybe in agreement with its late transcription and degradation of vmRNA(+) molecules shown by the experimental data. (V) Approximately 5 hpi, newly produced virus particles are released into the supernatant. Until now it is not clear if each viral genome segment is selectively incorporated into progeny viruses or if packaging is a purely random process. The model assumes for simplicity, all virus particles contain eight segments. (VI) At late periods of infection (about 12 hpi) nuclear vmRNA(+) are produced at the maximum rates and the total amount of all virus proteins and viral RNAs, as well as the number of budding virus, increase linearly with times. In contrast to model

assumptions and simulation studies the measured viral RNAs concentrations achieved stationary state during late infection time points and, moreover, especially vmRNA(+)s were degraded. The overall dynamics of the model simulations agrees with the quantitative data obtained from the infection experiments. However, some parameters, estimations and the structure of the model have to be checked and adjusted eventually.

5.3.3. Determination of extracellular influenza viral RNA in cell culture supernatant by RT-qPCR

For extracellular viral RNA determination a RT-qPCR assay for vRNA(-) of segment 7 (M) was established (section 3.4.6). Validation of the extracellular viral RNA extraction showed linearity over four orders of magnitude and confirmed sensitivity (LOD) to 1.7 x 10^4 viral RNA molecules corresponding to 1.1 x 10^{-5} ng of viral RNA (Figure 4.3-11).

The assay was tested successfully on estimation of influenza virus particle concentrations in cell culture supernatants. Results were compared to conventional HA assay data, which showed a significant correlation in the results of both methods (Figure 4.3-12). Nevertheless, both quantification methods showed variations in the time courses of virus particle concentrations at the beginning (about 6 – 18 hpi) and the end (about 50 – 77 hpi) of virus infection. Variations in the beginning accounted for the low virus titers at this time of infection and the low LOD of the HA assay. Whereas, by using a RT-qPCR assay, it was possible to detect virus concentrations as low as approximately 5.0 x 10^3 virions/mL. Variations at the end of infection accounted for deterioration and lyses of virus particles due to temperature and enzymatic effects. The RT-qPCR assay monitors only the concentration of intact virions, in contrast to the HA assay, which is compromised by the presence of viral membranes or HA proteins of the cellular membrane. Accordingly, values of virus titers were determined more precisely when looking at functional and intact virus particles by using RT-qPCR quantification.

Similar RT-qPCR assay systems for quantification of influenza virus have been developed, validated and cross-checked with other conventional quantification assays (Di Trani et al., 2006; Ward et al., 2004; Youil et al., 2004). These assays showed very low detection limits of 2.1 x 10^2 virions/mL (Ward et al., 2004) or of 5 to 50 viral RNA copies (Di Trani et al., 2006). However, systems were developed for molecular diagnostic in throat swab or clinical specimens that depend for this purpose on reliable quantitative results with great sensitivity.

In conclusion, the RT-qPCR assay offers significant improvements over the conventional quantification method (HA assay) for measuring viral concentration in the cell culture supernatant of infected cells due to lower detection limits of intact virus particles. Additionally, larger numbers of samples can be rapidly tested. Resulting from that, the RT-qPCR assay

can be used for the detection, quantification and monitoring of influenza virus replication in mammalian cell culture.

6. Conclusion and Outlook

In summary, when selecting between three different human epithelial cell lines (A549, NCI-N87, HepG2) to be used as human model cell line for the proteome approach it could be seen that each human cell line supported replication of influenza A virus. MOI and trypsin addition had only slight effects on maximum HA titers of influenza virus and no influence of media composition was found. Additionally, regarding metabolism glucose and glutamine were not completely depleted and did not reach limiting levels that could induce cell death. Also, no toxic levels have been reached for cytotoxic metabolites such as lactate and ammonia ions. Finally, the A549 cell line was selected as the most promising candidate for a human cell reference model, because of its growth characteristic, best virus yield and wide use in other infection studies. With respect to proteome alteration characterization by quantitative 2-D DIGE analysis of influenza A virus infections, A549 cells have been successfully applied as a human cell infection model in comparison to canine MDCK cells (Vester et al., 2009). Furthermore, feasibility of the human cell line model has successfully been demonstrated by the use of HepG2 and A549 cells as reference models in infection experiments in recent signal transduction studies of the molecular biology subgroup of the bpt group of the MPI Magdeburg. Nevertheless, for optimal use of A549 and HepG2 cells as an infection model in further studies adaptation of the corresponding influenza viruses used is recommended (Genzel and Reichl, 2009).

Through the use of quantitative proteome-profiling, basic insights into virus-host cell interactions and into cellular pathways involved in influenza A virus replication in vaccine production cell lines and in a human cell infection model were obtained. This proteomic approach explains virus-host cell interaction behaviors at a more global level, and reveals properties of the infection process from a ‘systems level’ point of view. While additional studies are necessary to better characterize different effects of influenza virus replication on host cell response, this study is a first step towards improving our understanding of the complex cellular events and virus-host cell interactions that occur during virus replication in various vaccine production cell lines. Furthermore, it allows the investigation of mechanisms relevant for the production of different virus strain variants in their corresponding host cells. Major alterations in influenza virus infected host cells were observed for proteins involved in signal transduction, protein synthesis and degradation, cytoskeleton rearrangement, maintenance of metabolism, cellular stress response and viral defense mechanisms. Some of these proteins were also identified in gene expression studies and in proteome analysis of avian influenza virus infected cells (Baas et al., 2006; Geiss et al., 2001; Geiss et al., 2002; Liu et al., 2008) demonstrating the suitability of this proteome approach and the cell culture

model for studying virus-host cell interactions.

The total number of differentially abundant proteins was low for MDCK and A549 cell lines infected with the influenza PR/8-RKI virus variant. This low effect on proteome changes after influenza virus infection was also reported by similar proteome studies (Baas et al., 2006; Liu et al., 2008). The fact that more proteome alterations were detected in MDCK cells infected with the PR/8-NIBSC variant suggests hat virus strains have varied abilities to control the cellular machinery of their host cells and to suppress an antiviral response. Due to differences in virus spreading and replication, virus strains show a specific pattern in altering host cell response. It seems that there is a correlation between high cell specific virus yields and the induction of only minor changes in the host cell proteome patterns during infection. This suggests a lower induction of cellular antiviral and stress mechanisms by 'high yield strains'. Nevertheless, the low effect on proteome changes could also be due to limitations of the 2-D DIGE approach used in this study, which allows only for the identification of high abundant proteins (Carrette et al., 2006). Most likely, influenza virus infection involves changes in abundance levels of numerous others, low-copy number proteins. Specific optimizations on separation techniques and the use of sample prefractionation and other enrichment techniques will help to identify such equally important alterations of low abundant host cell proteins. Therefore, studies on evaluating different strategies for the enrichment of subcellular fractions and the use of solid phase hexapeptide library (ProteoMiner beads; BioRad) are in progress in the bpt group of the MPI Magdeburg. Procedures for the enrichment and isolation organelles and subcellular compartments by differential detergent fractionation (DDF) or classical sequential extraction and centrifugation techniques are tested (Michelsen and von Hagen, 2009). By using a large bead based library of combinatorial peptide ligands (ProteoMiner beads), the dynamic range of the protein concentration is compressed. With that the high abundant proteins present in the sample are reduced and the low abundant proteins are enriched, while retaining representatives of all proteins within the sample. Their application to proteomics, though, is relatively new (Thulasiraman et al., 2005). So far, this technique has been mainly applied for biomarker discovery with serum samples, urine, red blood cells and monitoring of recombinant DNA product (Boschetti and Righetti, 2009). Additionally, after influenza virus infections, PTMs of a much higher number of regulatory proteins are to be expected since this is the most common way of inactivating or activating signal transduction molecules. These PTMs should be further investigated by additional, more specific assays. For this reason, fluorescent staining or modification-specific enrichment techniques combined with advanced MS/MS methods could be tested (Hoffman et al., 2008; Zhao and Jensen, 2009).

It was shown that a Vero cell line with known deficiency in IFN production has still the ability to build-up a host cell defense state in an IFN independent manner. This virus production cell

line showed also a much higher induction of stress response compared to the MDCK cell line. The proteins identified as stress factors in this study could give useful hints concerning future cell engineering strategies to overcome virus induced apoptosis and stress mechanisms to improve cell-specific virus yields. In future studies, mechanisms of virus adaptation to new production cell lines should be further investigated, e.g. through the use of glycosylation profiling (Schwarzer et al., 2009), sequence and mutational analysis of segment HA, NA and NS1 (de Wit et al. 2010; Ma et al., 2010) and determination of viral polymerase activity (Gabriel et al., 2007).

Overall, findings provide insights concerning virus induced changes in cellular processes in vaccine production cell lines, in particular those processes related to signal transduction, cellular stress response and apoptosis. In this regard, an important aspect that has to be addressed is screening for potential target proteins for improvement of cell line performance in vaccine production among these altered proteins and pathways during influenza virus infection. For example, NDRG1 or KCIP1 in MDCK cells and hsp70 kDA or NS1/NF-κB in Vero cells might represent potential targets. These appropriate candidates should be characterized in detail for their function and influence on cell culture behavior and on virus yield. Further studies analyzing proteome and gene expression patterns are in progress to provide a more complete picture of the regulation of cellular machineries specific for different production cell lines and virus strains relevant for an increase in cell-specific virus yields (Heynisch et al., 2010) (Seitz and Frensing, personal communication). In future, these findings could be used to improve virus yields in cell culture derived influenza virus vaccine processes or to support the development of new antiviral strategies required to fight pandemics.

Besides analysis of virus-host cell interactions during the infection phase proteome profiling could also be implemented during cell culture and virus replication phase in influenza vaccine production processes. Proteomics might support at least three areas during the process: (I) analysis of cellular functions to enhance productivity or influence desired properties of biological products (cell line engineering); (II) knowledge of cell function in response to environmental condition changes, including evaluation of different cell culture media, bioreactor types and cell culture conditions such as cell density or temperature (upstream); and (III) knowledge of cell function and properties to improve product purification and characterization (downstream), e.g. monitoring of integrity (glycosylation or phosphorylation patterns) and purity (host cell protein impurities) (Gupta and Lee, 2007). Proteome studies concerning the impact of adaptation and cultivation of a new suspension MDCK cell line, MDCK.SUS2 (Lohr et al., 2010) are in progress in the bpt group of the MPI Magdeburg. They will help to gain a better understanding of the complex process of cell growth in suspension as well as the changes in the cellular proteome after adaptation to chemically defined

medium. Feasibility of the proteomic approach for profiling cell culture processes has been demonstrated by the application to a recent study of Vero cells grown under various conditions in bioreactor and static cultures and after infection with rabies virus in a cooperation project with the Pasteur Institute Tunis (Rourou et al., in preparation). Studies on the new MDCK suspension line and the rabies process led to an overwhelming amount of data generated by this approach. Therefore, it will be necessary to use a two-dimensional colored map, i.e. cluster heat maps, as a common approach to the visualization of large number of data sets (Eisen et al., 1998). Furthermore, it will be necessary to apply special statistical or mathematical tools for data analysis after protein identification, e.g. principal component analysis (PCA) (Jolliffee, 2005). PCA involves a mathematical procedure that transforms a number of possibly correlated variables into a smaller number of uncorrelated variables or hierarchical cluster analysis to detect coordinated protein regulation, functional classification or protein interactions.

Regarding the third part of the presented work it could be shown that the established, optimized and validated RT-qPCR assay showed good sensitivity, reproducibility and specificity. Moreover, the qPCR assay was shown to be important for determining essential features of intracellular events and dynamics of the life cycle of influenza virus in MDCK cell cultures. Establishment of the assays for the remaining four influenza viral segments (polymerase subunits: PB2, PB1 and PA; NP) and the corresponding viral RNA types is in progress and will allow detailed analysis and comparison of the overall virus replication dynamics of additional virus strains (e.g. PR/8-NIBSC, PR/8-delNS1 mutant strain) in MDCK cells and in other host cells (e.g. Vero, MDCK.SUS2) and under a variety of infection conditions (e.g. MOI, trypsin). Since the assay was validated for infection with the influenza PR/8 virus strain, only real-time primer needs to be adapted and optimized when using other virus subtypes. Based on the quality of the quantitative experimental data obtained, mathematical models for influenza virus replication (Sidorenko and Reichl, 2004) can be validated and key parameters of such models estimated. Therefore, this approach is a significant step towards systems biology of virus-host cell interactions. Ultimately, the fully established method could also help to understand the role of PB1, PB2 and PA in viral genome replication and transcription, the postulated switch between viral transcription and replication, the mechanism of vRNA(-) packaging, the significance of the non-coding regions in virus amplification and the different replication characteristics of virus strains. For this detailed understanding, cross-linking and integration with additional analytical methods is required, e.g. measurement of polymerase activity *in vivo* by reporter gene assays (Bussey et al., 2010), estimation of intracellular viral protein synthesis by Western blots or sequencing and mutational analysis of the non-coding regions of viral segments. Additional hints could also be obtained by the usage of plasmid based minireplicon systems for influenza A virus

(Pleschka et al., 1996). This exclusively plasmid driven system results in the efficient viral transcription and replication of the viral RNA-like reporter and allows the study of cis- and trans-acting signals involved in the transcription and replication of influenza virus RNAs, which was recently shown exemplarily for Mx proteins (Dittmann et al., 2008; Seitz et al., 2010). Especially the establishment of the qPCR assay for the polymerase subunit segments could clarify if different replication characteristics of viral strains are due to different catalytic polymerase activities (Biswas and Nayak, 1994). Recently, Bussey et al. reported characterization studies, which indicate that the high polymerase activity and enhanced viral growth of the pandemic strain in mammalian cells is, in part, dependent on AA 271 of PB2 (Bussey et al., 2010). Furthermore, this would allow to analyze the distinct operations of the polymerase complex, e.g. endonuclease cleavage, transcription, polyadenylation or replication are modulated by its interaction with vRNA(-), cRNA(+) or host cell factors. Eventually, this analytical techniques could be linked to proteomic approaches such as reported by Mayer et al. (Mayer et al., 2007).

Moreover, a slightly modified RT-qPCR assay was established and tested successfully on estimation of influenza virus particle concentrations in cell culture supernatants. Results were compared to conventional HA assay data, which showed a significant correlation in the results of both methods. Therefore, the assay can be used for the detection, quantification and monitoring of influenza virus replication in mammalian cell culture.

In conclusion, results from all parts of the presented work have elucidated the complex relationships between influenza viruses and the infected host cells, as well as the viral replication dynamics. Moreover, results have provided the basis for a more comprehensive understanding of the viral life cycle. Both approaches, proteomics and RT-qPCR, have started a new understanding of cell culture derived influenza virus vaccine production processes and can be used for studies on bioprocess engineering and systems biology of these processes.

Figures

Tables

References

Aden, D.P., Fogel, A., Plotkin, S., Damjanov, I. and Knowles, B.B., 1979. Controlled synthesis of HBsAg in a differentiated human liver carcinoma-derived cell line. Nature 282, 615-6.

Ahmed, N. and Rice, G.E., 2005. Strategies for revealing lower abundance proteins in two-dimensional protein maps. J Chromatogr B Analyt Technol Biomed Life Sci 815, 39-50.

Ahn, J., Chung, K.S., Kim, D.U., Won, M., Kim, L., Kim, K.S., Nam, M., Choi, S.J., Kim, H.C., Yoon, M., Chae, S.K. and Hoe, K.L., 2004. Systematic identification of hepatocellular proteins interacting with NS5A of the hepatitis C virus. J Biochem Mol Biol 37, 741-8.

Alban, A., David, S.O., Bjorkesten, L., Andersson, C., Sloge, E., Lewis, S. and Currie, I., 2003. A novel experimental design for comparative two-dimensional gel analysis: two-dimensional difference gel electrophoresis incorporating a pooled internal standard. Proteomics 3, 36-44.

Alfonso, P., Rivera, J., Hernaez, B., Alonso, C. and Escribano, J.M., 2004. Identification of cellular proteins modified in response to African swine fever virus infection by proteomics. Proteomics 4, 2037-46.

Amorim, M.J. and Digard, P., 2006. Influenza A virus and the cell nucleus. Vaccine 24, 6651-5.

Appel, R.D., Palagi, P.M., Walther, D., Vargas, J.R., Sanchez, J.C., Ravier, F., Pasquali, C. and Hochstrasser, D.F., 1997. Melanie II--a third-generation software package for analysis of two-dimensional electrophoresis images: I. Features and user interface. Electrophoresis 18, 2724-34.

Aragon, T., de la Luna, S., Novoa, I., Carrasco, L., Ortin, J. and Nieto, A., 2000. Eukaryotic translation initiation factor 4GI is a cellular target for NS1 protein, a translational activator of influenza virus. Mol Cell Biol 20, 6259-68.

Arcangeletti, M.C., De Conto, F., Ferraglia, F., Pinardi, F., Gatti, R., Orlandini, G., Covan, S., Motta, F., Rodighiero, I., Dettori, G. and Chezzi, C., 2008. Host-cell-dependent role of actin cytoskeleton during the replication of a human strain of influenza A virus. Arch Virol 153, 1209-21.

Arcangeletti, M.C., Pinardi, F., Missorini, S., De Conto, F., Conti, G., Portincasa, P., Scherrer, K. and Chezzi, C., 1997. Modification of cytoskeleton and prosome networks in relation to protein synthesis in influenza A virus-infected LLC-MK2 cells. Virus Res 51, 19-34.

Arya, M., Shergill, I.S., Williamson, M., Gommersall, L., Arya, N. and Patel, H.R., 2005. Basic principles of real-time quantitative PCR. Expert Rev Mol Diagn 5, 209-19.

Audsley, J.M. and Tannock, G.A., 2008. Cell-based influenza vaccines: progress to date. Drugs 68, 1483-91.

Avalos, R.T., Yu, Z. and Nayak, D.P., 1997. Association of influenza virus NP and M1 proteins with cellular cytoskeletal elements in influenza virus-infected cells. J Virol 71, 2947-58.

Baas, T., Baskin, C.R., Diamond, D.L., Garcia-Sastre, A., Bielefeldt-Ohmann, H., Tumpey, T.M., Thomas, M.J., Carter, V.S., Teal, T.H., Van Hoeven, N., Proll, S., Jacobs, J.M., Caldwell, Z.R., Gritsenko, M.A., Hukkanen, R.R., Camp, D.G., 2nd, Smith, R.D. and Katze, M.G., 2006. Integrated molecular signature of disease: analysis of influenza virus-infected macaques through functional genomics and proteomics. J Virol 80, 10813-28.

Badock, V., Steinhusen, U., Bommert, K., Wittmann-Liebold, B. and Otto, A., 2001. Apoptosis-induced cleavage of keratin 15 and keratin 17 in a human breast epithelial cell line. Cell Death Differ 8, 308-15.

Ballif, B.A., Mincek, N.V., Barratt, J.T., Wilson, M.L. and Simmons, D.L., 1996. Interaction of

cyclooxygenases with an apoptosis- and autoimmunity-associated protein. Proc Natl Acad Sci U S A 93, 5544-9.

Barnard, J.A., Snyder, P.N., Werner, M.J., Greene, H.L. and Edwards, K.M., 1988. Protein synthesis by HepG2 cells infected with influenza B virus. Pediatr Res 23, 334-7.

Basque, J.R., Chenard, M., Chailler, P. and Menard, D., 2001. Gastric cancer cell lines as models to study human digestive functions. J Cell Biochem 81, 241-51.

Bernasconi, D., Amici, C., La Frazia, S., Ianaro, A. and Santoro, M.G., 2005. The IkappaB kinase is a key factor in triggering influenza A virus-induced inflammatory cytokine production in airway epithelial cells. J Biol Chem 280, 24127-34.

Bischoff, F.R., Krebber, H., Kempf, T., Hermes, I. and Ponstingl, H., 1995. Human RanGTPase-activating protein RanGAP1 is a homologue of yeast Rna1p involved in mRNA processing and transport. Proc Natl Acad Sci U S A 92, 1749-53.

Biswas, S.K., Boutz, P.L. and Nayak, D.P., 1998. Influenza virus nucleoprotein interacts with influenza virus polymerase proteins. J Virol 72, 5493-501.

Biswas, S.K. and Nayak, D.P., 1994. Mutational analysis of the conserved motifs of influenza A virus polymerase basic protein 1. J Virol 68, 1819-26.

Bjellqvist, B., Ek, K., Righetti, P.G., Gianazza, E., Gorg, A., Westermeier, R. and Postel, W., 1982. Isoelectric focusing in immobilized pH gradients: principle, methodology and some applications. J Biochem Biophys Methods 6, 317-39.

Boschetti, E. and Righetti, P.G., 2009. The art of observing rare protein species in proteomes with peptide ligand libraries. Proteomics 9, 1492-510.

Boulo, S., Akarsu, H., Ruigrok, R.W. and Baudin, F., 2007. Nuclear traffic of influenza virus proteins and ribonucleoprotein complexes. Virus Res 124, 12-21.

Bradford, M.M., 1976. A rapid and sensitive method for the quantitation of microgram quantities of protein utilizing the principle of protein-dye binding. Anal Biochem 72, 248-54.

Brands, R., Visser, J., Medema, J., Palache, A.M. and van Scharrenburg, G.J., 1999. Influvac: a safe Madin Darby Canine Kidney (MDCK) cell culture-based influenza vaccine. Dev Biol Stand 98, 93-100; discussion 111.

Brasier, A.R., Spratt, H., Wu, Z., Boldogh, I., Zhang, Y., Garofalo, R.P., Casola, A., Pashmi, J., Haag, A., Luxon, B. and Kurosky, A., 2004. Nuclear heat shock response and novel nuclear domain 10 reorganization in respiratory syncytial virus-infected a549 cells identified by high-resolution two-dimensional gel electrophoresis. J Virol 78, 11461-76.

Burgui, I., Aragon, T., Ortin, J. and Nieto, A., 2003. PABP1 and eIF4GI associate with influenza virus NS1 protein in viral mRNA translation initiation complexes. J Gen Virol 84, 3263-74.

Bussey, K.A., Bousse, T.L., Desmet, E.A., Kim, B. and Takimoto, T., 2010, PB2 residue 271 plays a key role in enhanced polymerase activity of influenza A viruses in mammalian host cells. J Virol 84, 4395-406.

Bustin, S.A., 2000. Absolute quantification of mRNA using real-time reverse transcription polymerase chain reaction assays. J Mol Endocrinol 25, 169-93.

Bustin, S.A., Benes, V., Garson, J.A., Hellemans, J., Huggett, J., Kubista, M., Mueller, R., Nolan, T., Pfaffl, M.W., Shipley, G.L., Vandesompele, J. and Wittwer, C.T., 2009. The MIQE guidelines: minimum information for publication of quantitative real-time PCR experiments. Clin Chem 55, 611-22.

Bustin, S.A. and Nolan, T., 2004. Pitfalls of quantitative real-time reverse-transcription polymerase chain reaction. J Biomol Tech 15, 155-66.

Carrette, O., Burkhard, P.R., Sanchez, J.C. and Hochstrasser, D.F., 2006. State-of-the-art two-dimensional gel electrophoresis: a key tool of proteomics research. Nat Protoc 1, 812-23.

Carter, K., Scott, D., Salmon, J. and Zarcone, G., 1991. Confidence-limits for the abscissa of intersection of 2 least-squares lines such as linear segmented titration curves. Analytical

Chemistry 63, 1270-1278.

Chailler, P. and Menard, D., 2005. Establishment of human gastric epithelial (HGE) cell lines exhibiting barrier function, progenitor, and prezymogenic characteristics. J Cell Physiol 202, 263-74.

Chan, A.Y., Vreede, F.T., Smith, M., Engelhardt, O.G. and Fodor, E., 2006a. Influenza virus inhibits RNA polymerase II elongation. Virology 351, 210-7.

Chan, C.H., Lin, K.L., Chan, Y., Wang, Y.L., Chi, Y.T., Tu, H.L., Shieh, H.K. and Liu, W.T., 2006b. Amplification of the entire genome of influenza A virus H1N1 and H3N2 subtypes by reverse-transcription polymerase chain reaction. J Virol Methods 136, 38-43.

Chen, L.M., Davis, C.T., Zhou, H., Cox, N.J. and Donis, R.O., 2008. Genetic compatibility and virulence of reassortants derived from contemporary avian H5N1 and human H3N2 influenza A viruses. PLoS Pathog 4, e1000072.

Chen, W., Calvo, P.A., Malide, D., Gibbs, J., Schubert, U., Bacik, I., Basta, S., O'Neill, R., Schickli, J., Palese, P., Henklein, P., Bennink, J.R. and Yewdell, J.W., 2001. A novel influenza A virus mitochondrial protein that induces cell death. Nat Med 7, 1306-12.

Chen, Z. and Krug, R.M., 2000. Selective nuclear export of viral mRNAs in influenza-virus-infected cells. Trends Microbiol 8, 376-83.

Cheung, T.K. and Poon, L.L., 2007. Biology of influenza a virus. Ann N Y Acad Sci 1102, 1-25.

Chew, T., Noyce, R., Collins, S.E., Hancock, M.H. and Mossman, K.L., 2009. Characterization of the interferon regulatory factor 3-mediated antiviral response in a cell line deficient for IFN production. Mol Immunol 46, 393-9.

Chizhmakov, I.V., Geraghty, F.M., Ogden, D.C., Hayhurst, A., Antoniou, M. and Hay, A.J., 1996. Selective proton permeability and pH regulation of the influenza virus M2 channel expressed in mouse erythroleukaemia cells. J Physiol 494 (Pt 2), 329-36.

Choi, A.M., Knobil, K., Otterbein, S.L., Eastman, D.A. and Jacoby, D.B., 1996. Oxidant stress responses in influenza virus pneumonia: gene expression and transcription factor activation. Am J Physiol 271, L383-91.

Choudhary, S., De, B.P. and Banerjee, A.K., 2000. Specific phosphorylated forms of glyceraldehyde 3-phosphate dehydrogenase associate with human parainfluenza virus type 3 and inhibit viral transcription in vitro. J Virol 74, 3634-41.

Cimarelli, A. and Luban, J., 1999. Translation elongation factor 1-alpha interacts specifically with the human immunodeficiency virus type 1 Gag polyprotein. J Virol 73, 5388-401.

Ciocca, D.R., Oesterreich, S., Chamness, G.C., McGuire, W.L. and Fuqua, S.A., 1993. Biological and clinical implications of heat shock protein 27,000 (Hsp27): a review. J Natl Cancer Inst 85, 1558-70.

Connor, R.J., Kawaoka, Y., Webster, R.G. and Paulson, J.C., 1994. Receptor specificity in human, avian, and equine H2 and H3 influenza virus isolates. Virology 205, 17-23.

Corthals, G.L., Wasinger, V.C., Hochstrasser, D.F. and Sanchez, J.C., 2000. The dynamic range of protein expression: a challenge for proteomic research. Electrophoresis 21, 1104-15.

Coux, O., Tanaka, K. and Goldberg, A.L., 1996. Structure and functions of the 20S and 26S proteasomes. Annu Rev Biochem 65, 801-47.

Craggs, J.K., Ball, J.K., Thomson, B.J., Irving, W.L. and Grabowska, A.M., 2001. Development of a strand-specific RT-PCR based assay to detect the replicative form of hepatitis C virus RNA. J Virol Methods 94, 111-20.

Cros, J.F., Garcia-Sastre, A. and Palese, P., 2005. An unconventional NLS is critical for the nuclear import of the influenza A virus nucleoprotein and ribonucleoprotein. Traffic 6, 205-13.

Crow, M., Deng, T., Addley, M. and Brownlee, G.G., 2004. Mutational analysis of the influenza virus cRNA promoter and identification of nucleotides critical for replication. J

Virol 78, 6263-70.

Cruz, H.J., Ferreira, A.S., Freitas, C.M., Moreira, J.L. and Carrondo, M.J., 1999. Metabolic responses to different glucose and glutamine levels in baby hamster kidney cell culture. Appl Microbiol Biotechnol 51, 579-85.

Cudmore, S., Cossart, P., Griffiths, G. and Way, M., 1995. Actin-based motility of vaccinia virus. Nature 378, 636-8.

David, H.A., Hartley, H.O. and Pearson, E.S., 1954. The Distribution of the ratio, in a single normal sample, of range to standard deviation. Biometrika 41, 482-493.

de Wit, E., Munster, V.J., van Riel, D., Beyer, W.E., Rimmelzwaan, G.F., Kuiken, T., Osterhaus, A.D. and Fouchier, R.A., 2010, Molecular determinants of adaptation of highly pathogenic avian influenza H7N7 viruses to efficient replication in the human host. J Virol 84, 1597-606.

Deng, T., Engelhardt, O.G., Thomas, B., Akoulitchev, A.V., Brownlee, G.G. and Fodor, E., 2006a. Role of ran binding protein 5 in nuclear import and assembly of the influenza virus RNA polymerase complex. J Virol 80, 11911-9.

Deng, T., Vreede, F.T. and Brownlee, G.G., 2006b. Different de novo initiation strategies are used by influenza virus RNA polymerase on its cRNA and viral RNA promoters during viral RNA replication. J Virol 80, 2337-48.

Derry, M.C., Sutherland, M.R., Restall, C.M., Waisman, D.M. and Pryzdial, E.L., 2007. Annexin 2-mediated enhancement of cytomegalovirus infection opposes inhibition by annexin 1 or annexin 5. J Gen Virol 88, 19-27.

Di Trani, L., Bedini, B., Donatelli, I., Campitelli, L., Chiappini, B., De Marco, M.A., Delogu, M., Buonavoglia, C. and Vaccari, G., 2006. A sensitive one-step real-time PCR for detection of avian influenza viruses using a MGB probe and an internal positive control. BMC Infect Dis 6, 87.

Diaz, M.O., Ziemin, S., Le Beau, M.M., Pitha, P., Smith, S.D., Chilcote, R.R. and Rowley, J.D., 1988. Homozygous deletion of the alpha- and beta 1-interferon genes in human leukemia and derived cell lines. Proc Natl Acad Sci U S A 85, 5259-63.

Dittmann, J., Stertz, S., Grimm, D., Steel, J., Garcia-Sastre, A., Haller, O. and Kochs, G., 2008. Influenza A virus strains differ in sensitivity to the antiviral action of Mx-GTPase. J Virol 82, 3624-31.

Doms, R.W., Lamb, R.A., Rose, J.K. and Helenius, A., 1993. Folding and assembly of viral membrane proteins. Virology 193, 545-62.

Doroshenko, A. and Halperin, S.A., 2009. Trivalent MDCK cell culture-derived influenza vaccine Optaflu (Novartis Vaccines). Expert Rev Vaccines 8, 679-88.

Earnshaw, W.C., Martins, L.M. and Kaufmann, S.H., 1999. Mammalian caspases: structure, activation, substrates, and functions during apoptosis. Annu Rev Biochem 68, 383-424.

Eisen, M.B., Spellman, P.T., Brown, P.O. and Botstein, D., 1998. Cluster analysis and display of genome-wide expression patterns. Proc Natl Acad Sci U S A 95, 14863-8.

Ellen, T.P., Ke, Q., Zhang, P. and Costa, M., 2008. NDRG1, a growth and cancer related gene: regulation of gene expression and function in normal and disease states. Carcinogenesis 29, 2-8.

Ellis, J.S. and Zambon, M.C., 2002. Molecular diagnosis of influenza. Rev Med Virol 12, 375-89.

Enami, K., Sato, T.A., Nakada, S. and Enami, M., 1994. Influenza virus NS1 protein stimulates translation of the M1 protein. J Virol 68, 1432-7.

Enami, M., Sharma, G., Benham, C. and Palese, P., 1991. An influenza virus containing nine different RNA segments. Virology 185, 291-8.

Engelhardt, O.G. and Fodor, E., 2006. Functional association between viral and cellular transcription during influenza virus infection. Rev Med Virol 16, 329-45.

Espy, M.J., Uhl, J.R., Sloan, L.M., Buckwalter, S.P., Jones, M.F., Vetter, E.A., Yao, J.D.,

Wengenack, N.L., Rosenblatt, J.E., Cockerill, F.R., 3rd and Smith, T.F., 2006. Real-time PCR in clinical microbiology: applications for routine laboratory testing. Clin Microbiol Rev 19, 165-256.

Farley, A.R. and Link, A.J., 2009. Identification and quantification of protein posttranslational modifications. Methods Enzymol 463, 725-63.

Fesus, L. and Piacentini, M., 2002. Transglutaminase 2: an enigmatic enzyme with diverse functions. Trends Biochem Sci 27, 534-9.

Fields, B., Knipe, D.M. and Howley, P.M., 2001. Fields Virology, Vol. 2. Lippincott Williams & Wilkins.

Flint, J.S., Enquist, L.W., Racaniello, V.R., Krug, R.M. and Skalka, A.M., 2009. Principles of Virology: Molecular Biology, Pathogenesis, and Control. Wiley VCH, Weinheim.

Flint, J.S., Racaniello, V.R. and Krug, R.M., 2000. Principles of Virology: Molecular Biology, Pathogenesis, and Control. American Society for Microbiology, Herndon, VA.

Fodor, E., Pritlove, D.C. and Brownlee, G.G., 1994. The influenza virus panhandle is involved in the initiation of transcription. J Virol 68, 4092-6.

Fornek, J.L., Korth, M.J. and Katze, M.G., 2007. Use of functional genomics to understand influenza-host interactions. Adv Virus Res 70, 81-100.

Freeman, W.M., Walker, S.J. and Vrana, K.E., 1999. Quantitative RT-PCR: pitfalls and potential. Biotechniques 26, 112-22, 124-5.

Fronhoffs, S., Totzke, G., Stier, S., Wernert, N., Rothe, M., Bruning, T., Koch, B., Sachinidis, A., Vetter, H. and Ko, Y., 2002. A method for the rapid construction of cRNA standard curves in quantitative real-time reverse transcription polymerase chain reaction. Mol Cell Probes 16, 99-110.

Fujii, K., Ozawa, M., Iwatsuki-Horimoto, K., Horimoto, T. and Kawaoka, Y., 2009. Incorporation of influenza A virus genome segments does not absolutely require wild-type sequences. J Gen Virol 90, 1734-40.

Fullekrug, J., Shevchenko, A. and Simons, K., 2006. Identification of glycosylated marker proteins of epithelial polarity in MDCK cells by homology driven proteomics. BMC Biochem 7, 8.

Gabriel, G., Abram, M., Keiner, B., Wagner, R., Klenk, H.D. and Stech, J., 2007. Differential polymerase activity in avian and mammalian cells determines host range of influenza virus. J Virol 81, 9601-4.

Gade, D., Thiermann, J., Markowsky, D. and Rabus, R., 2003. Evaluation of two-dimensional difference gel electrophoresis for protein profiling. Soluble proteins of the marine bacterium Pirellula sp. strain 1. J Mol Microbiol Biotechnol 5, 240-51.

Gambaryan, A.S., Robertson, J.S. and Matrosovich, M.N., 1999. Effects of egg-adaptation on the receptor-binding properties of human influenza A and B viruses. Virology 258, 232-9.

Garcia-Sastre, A., 2006. Antiviral response in pandemic influenza viruses. Emerg Infect Dis 12, 44-7.

Garcia-Sastre, A., Percy, N., Barclay, W. and Palese, P., 1994. Introduction of foreign sequences into the genome of influenza A virus. Dev Biol Stand 82, 237-46.

Gaush, C.R., Hard, W.L. and Smith, T.F., 1966. Characterization of an established line of canine kidney cells (MDCK). Proc Soc Exp Biol Med 122, 931-5.

Gaush, C.R. and Smith, T.F., 1968. Replication and plaque assay of influenza virus in an established line of canine kidney cells. Appl Microbiol 16, 588-94.

Geiss, G.K., An, M.C., Bumgarner, R.E., Hammersmark, E., Cunningham, D. and Katze, M.G., 2001. Global impact of influenza virus on cellular pathways is mediated by both replication-dependent and -independent events. J Virol 75, 4321-31.

Geiss, G.K., Salvatore, M., Tumpey, T.M., Carter, V.S., Wang, X., Basler, C.F., Taubenberger, J.K., Bumgarner, R.E., Palese, P., Katze, M.G. and Garcia-Sastre, A.,

2002. Cellular transcriptional profiling in influenza A virus-infected lung epithelial cells: the role of the nonstructural NS1 protein in the evasion of the host innate defense and its potential contribution to pandemic influenza. Proc Natl Acad Sci U S A 99, 10736-41.

Genzel, Y., Behrendt, I., Konig, S., Sann, H. and Reichl, U., 2004. Metabolism of MDCK cells during cell growth and influenza virus production in large-scale microcarrier culture. Vaccine 22, 2202-8.

Genzel, Y., Fischer, M. and Reichl, U., 2006. Serum-free influenza virus production avoiding washing steps and medium exchange in large-scale microcarrier culture. Vaccine 24, 3261-72.

Genzel, Y. and Reichl, U. 2007. Vaccine production - state of the art and future needs in upstream processing. In: R. Poertner (Ed), Methods in Biotechnology: Animal Cell Biotechnolgy - Methods and Protocols, Humana Press Inc., Totowa, NJ, pp. 457-473.

Genzel, Y. and Reichl, U., 2009. Continuous cell lines as a production system for influenza vaccines. Expert Rev Vaccines 8, 1681-92.

Gerard, G.F., Fox, D.K., Nathan, M. and D'Alessio, J.M., 1997. Reverse transcriptase. The use of cloned Moloney murine leukemia virus reverse transcriptase to synthesize DNA from RNA. Mol Biotechnol 8, 61-77.

Giard, D.J., Aaronson, S.A., Todaro, G.J., Arnstein, P., Kersey, J.H., Dosik, H. and Parks, W.P., 1973. In vitro cultivation of human tumors: establishment of cell lines derived from a series of solid tumors. J Natl Cancer Inst 51, 1417-23.

Glacken, M.W., Fleischaker, R.J. and Sinskey, A.J., 1986. Reduction of waste product excretion via nutrient control: Possible strategies for maximizing product and cell yields on serum in cultures of mammalian cells. Biotechnol Bioeng 28, 1376-89.

Goerg, A., Obermaier, C., Boguth, G., Harder, A., Scheibe, B., Wildgruber, R. and Weiss, W., 2000. The current state of two-dimensional electrophoresis with immobilized pH gradients. Electrophoresis 21, 1037-53.

Goerg, A., Weiss, W. and Dunn, M.J., 2004. Current two-dimensional electrophoresis technology for proteomics. Proteomics 4, 3665-85.

Gonzalez, S. and Ortin, J., 1999. Distinct regions of influenza virus PB1 polymerase subunit recognize vRNA and cRNA templates. EMBO J 18, 3767-75.

Goodman, A.G., Smith, J.A., Balachandran, S., Perwitasari, O., Proll, S.C., Thomas, M.J., Korth, M.J., Barber, G.N., Schiff, L.A. and Katze, M.G., 2007. The cellular protein P58IPK regulates influenza virus mRNA translation and replication through a PKR-mediated mechanism. J Virol 81, 2221-30.

Govorkova, E.A., Kaverin, N.V., Gubareva, L.V., Meignier, B. and Webster, R.G., 1995. Replication of influenza A viruses in a green monkey kidney continuous cell line (Vero). J Infect Dis 172, 250-3.

Griffin, T.J., Seth, G., Xie, H., Bandhakavi, S. and Hu, W.S., 2007. Advancing mammalian cell culture engineering using genome-scale technologies. Trends Biotechnol 25, 401-8.

Gropp, F.N., Greger, D.L., Morel, C., Sauter, S. and Blum, J.W., 2006. Nuclear receptor and nuclear receptor target gene messenger ribonucleic acid levels at different sites of the gastrointestinal tract and in liver of healthy dogs. J Anim Sci 84, 2684-91.

Gupta, P. and Lee, K.H., 2007. Genomics and proteomics in process development: opportunities and challenges. Trends Biotechnol 25, 324-30.

Haegstroem, L. 2000. Cell metabolism. In: R. Stier (Ed), Encyclopedia of cell technology, Wiley VCH, New York, pp. 392-411.

Hale, B.G., Randall, R.E., Ortin, J. and Jackson, D., 2008. The multifunctional NS1 protein of influenza A viruses. J Gen Virol 89, 2359-76.

Haller, O., Kochs, G. and Weber, F., 2006. The interferon response circuit: induction and suppression by pathogenic viruses. Virology 344, 119-30.

Haller, O., Staeheli, P. and Kochs, G., 2007a. Interferon-induced Mx proteins in antiviral host

defense. Biochimie 89, 812-8.

Haller, O., Staeheli, P. and Kochs, G., 2009. Protective role of interferon-induced Mx GTPases against influenza viruses. Rev Sci Tech 28, 219-31.

Haller, O., Stertz, S. and Kochs, G., 2007b. The Mx GTPase family of interferon-induced antiviral proteins. Microbes Infect 9, 1636-43.

Hao, L., Sakurai, A., Watanabe, T., Sorensen, E., Nidom, C.A., Newton, M.A., Ahlquist, P. and Kawaoka, Y., 2008a. Drosophila RNAi screen identifies host genes important for influenza virus replication. Nature 454, 890-3.

Hao, X., Kim, T.S. and Braciale, T.J., 2008b. Differential response of respiratory dendritic cell subsets to influenza virus infection. J Virol 82, 4908-19.

Hassell, T., Gleave, S. and Butler, M., 1991. Growth inhibition in animal cell culture. The effect of lactate and ammonia. Appl Biochem Biotechnol 30, 29-41.

Hatada, E., Hasegawa, M., Mukaigawa, J., Shimizu, K. and Fukuda, R., 1989. Control of influenza virus gene expression: quantitative analysis of each viral RNA species in infected cells. J Biochem 105, 537-46.

Hay, A. 1998. The virus genome and its replication. In: K. Nickolson, R.G. Webster and A. Hay (Eds), Textbook of Influenza, Blackwell Sciences, Oxford, pp. 43-53.

Hay, A.J., Lomniczi, B., Bellamy, A.R. and Skehel, J.J., 1977. Transcription of the influenza virus genome. Virology 83, 337-55.

Hayduk, E.J. and Lee, K.H., 2005. Cytochalasin D can improve heterologous protein productivity in adherent Chinese hamster ovary cells. Biotechnol Bioeng 90, 354-64.

Hayman, A., Comely, S., Lackenby, A., Murphy, S., McCauley, J., Goodbourn, S. and Barclay, W., 2006. Variation in the ability of human influenza A viruses to induce and inhibit the IFN-beta pathway. Virology 347, 52-64.

Heynisch, B., Frensing, T., Heinze, K., Seitz, C., Genzel, Y. and Reichl, U., 2010, Differential activation of host cell signalling pathways through infection with two variants of influenza A/PR/8/34 (H1N1) in MDCK cells. Vaccine.

Higuchi, R., Dollinger, G., Walsh, P.S. and Griffith, R., 1992. Simultaneous amplification and detection of specific DNA sequences. Biotechnology (N Y) 10, 413-7.

Hoffman, M.D., Sniatynski, M.J. and Kast, J., 2008. Current approaches for global post-translational modification discovery and mass spectrometric analysis. Anal Chim Acta 627, 50-61.

Hoffmann, E., Stech, J., Guan, Y., Webster, R.G. and Perez, D.R., 2001. Universal primer set for the full-length amplification of all influenza A viruses. Arch Virol 146, 2275-89.

Hoffmann, H.H., Palese, P. and Shaw, M.L., 2008. Modulation of influenza virus replication by alteration of sodium ion transport and protein kinase C activity. Antiviral Res 80, 124-34.

Hornickova, Z., 1997. Different progress of MDCK cell death after infection by two different influenza virus isolates. Cell Biochem Funct 15, 87-93.

Iannello, A., Debbeche, O., Martin, E., Attalah, L.H., Samarani, S. and Ahmad, A., 2006. Viral strategies for evading antiviral cellular immune responses of the host. J Leukoc Biol 79, 16-35.

Jacob, R., Heine, M., Eikemeyer, J., Frerker, N., Zimmer, K.P., Rescher, U., Gerke, V. and Naim, H.Y., 2004. Annexin II is required for apical transport in polarized epithelial cells. J Biol Chem 279, 3680-4.

Jeon, J.H. and Kim, I.G., 2006. Role of protein modifications mediated by transglutaminase 2 in human viral diseases. Front Biosci 11, 221-31.

Jin, H., Leser, G.P., Zhang, J. and Lamb, R.A., 1997. Influenza virus hemagglutinin and neuraminidase cytoplasmic tails control particle shape. EMBO J 16, 1236-47.

Jolliffee, I.T., 2005. Principal Component Analysis, Vol. 3. Wiley, New York.

Julkunen, I., Sareneva, T., Pirhonen, J., Ronni, T., Melen, K. and Matikainen, S., 2001.

Molecular pathogenesis of influenza A virus infection and virus-induced regulation of cytokine gene expression. Cytokine Growth Factor Rev 12, 171-80.

Karlas, A., Machuy, N., Shin, Y., Pleissner, K.P., Artarini, A., Heuer, D., Becker, D., Khalil, H., Ogilvie, L.A., Hess, S., Maurer, A.P., Muller, E., Wolff, T., Rudel, T. and Meyer, T.F., 2010. Genome-wide RNAi screen identifies human host factors crucial for influenza virus replication. Nature 463, 818-22.

Kash, J.C., Goodman, A.G., Korth, M.J. and Katze, M.G., 2006. Hijacking of the host-cell response and translational control during influenza virus infection. Virus Res 119, 111-20.

Katze, M.G., Detjen, B.M., Safer, B. and Krug, R.M., 1986. Translational control by influenza virus: suppression of the kinase that phosphorylates the alpha subunit of initiation factor eIF-2 and selective translation of influenza viral mRNAs. Mol Cell Biol 6, 1741-50.

Kawakami E., Watanabe T., Fujii K., Goto H., Watanabe S., Noda T., Kawaoka Y., 2011. Strand-specific real-time RT-PCR for distinguishing influenza vRNA, cRNA, and mRNA. J Virol Meth 173, 1-6.

Kellam, P., 2001. Post-genomic virology: the impact of bioinformatics, microarrays and proteomics on investigating host and pathogen interactions. Rev Med Virol 11, 313-29.

Keskinen, P., Nyqvist, M., Sareneva, T., Pirhonen, J., Melen, K. and Julkunen, I., 1999. Impaired antiviral response in human hepatoma cells. Virology 263, 364-75.

Kilbourne, E.D., Schulman, J.L., Schild, G.C., Schloer, G., Swanson, J. and Bucher, D., 1971. Related studies of a recombinant influenza-virus vaccine. I. Derivation and characterization of virus and vaccine. J Infect Dis 124, 449-62.

Kistner, O., Barrett, P.N., Mundt, W., Reiter, M., Schober-Bendixen, S. and Dorner, F., 1998. Development of a mammalian cell (Vero) derived candidate influenza virus vaccine. Vaccine 16, 960-8.

Klose, J., 1975. Protein mapping by combined isoelectric focusing and electrophoresis of mouse tissues. A novel approach to testing for induced point mutations in mammals. Humangenetik 26, 231-43.

Knowles, B.B., Howe, C.C. and Aden, D.P., 1980. Human hepatocellular carcinoma cell lines secrete the major plasma proteins and hepatitis B surface antigen. Science 209, 497-9.

Kochs, G., Garcia-Sastre, A. and Martinez-Sobrido, L., 2007. Multiple anti-interferon actions of the influenza A virus NS1 protein. J Virol 81, 7011-21.

Koenig, R., Stertz, S., Zhou, Y., Inoue, A., Hoffmann, H.H., Bhattacharyya, S., Alamares, J.G., Tscherne, D.M., Ortigoza, M.B., Liang, Y., Gao, Q., Andrews, S.E., Bandyopadhyay, S., De Jesus, P., Tu, B.P., Pache, L., Shih, C., Orth, A., Bonamy, G., Miraglia, L., Ideker, T., Garcia-Sastre, A., Young, J.A., Palese, P., Shaw, M.L. and Chanda, S.K., 2010. Human host factors required for influenza virus replication. Nature 463, 813-7.

Koerner, I., Kochs, G., Kalinke, U., Weiss, S. and Staeheli, P., 2007. Protective role of beta interferon in host defense against influenza A virus. J Virol 81, 2025-30.

Komurian-Pradel, F., Perret, M., Deiman, B., Sodoyer, M., Lotteau, V., Paranhos-Baccala, G. and Andre, P., 2004. Strand specific quantitative real-time PCR to study replication of hepatitis C virus genome. J Virol Methods 116, 103-6.

Krampe, B., Swiderek, H. and Al-Rubeai, M., 2008. Transcriptome and proteome analysis of antibody-producing mouse myeloma NS0 cells cultivated at different cell densities in perfusion culture. Biotechnol Appl Biochem 50, 133-41.

Krug, R.M., St Angelo, C., Broni, B. and Shapiro, G., 1987. Transcription and replication of influenza virion RNA in the nucleus of infected cells. Cold Spring Harb Symp Quant Biol 52, 353-8.

Krug, R.M., Yuan, W., Noah, D.L. and Latham, A.G., 2003. Intracellular warfare between human influenza viruses and human cells: the roles of the viral NS1 protein. Virology 309, 181-9.

Kubista, M., Andrade, J.M., Bengtsson, M., Forootan, A., Jonak, J., Lind, K., Sindelka, R., Sjoback, R., Sjogreen, B., Strombom, L., Stahlberg, A. and Zoric, N., 2006. The real-time

polymerase chain reaction. Mol Aspects Med 27, 95-125.

Kumar, N., Gammell, P., Meleady, P., Henry, M. and Clynes, M., 2008a. Differential protein expression following low temperature culture of suspension CHO-K1 cells. BMC Biotechnol 8, 42.

Kumar, N., Xin, Z.T., Liang, Y. and Ly, H., 2008b. NF-kappaB signaling differentially regulates influenza virus RNA synthesis. J Virol 82, 9880-9.

Kuystermans, D., Krampe, B., Swiderek, H. and Al-Rubeai, M., 2007. Using cell engineering and omic tools for the improvement of cell culture processes. Cytotechnology 53, 3-22.

Laemmli, U.K., 1970. Cleavage of structural proteins during the assembly of the head of bacteriophage T4. Nature 227, 680-5.

Lafrenie, R.M. and Yamada, K.M., 1996. Integrin-dependent signal transduction. J Cell Biochem 61, 543-53.

Lamb, R.A. and Choppin, P.W., 1983. The gene structure and replication of influenza virus. Annu Rev Biochem 52, 467-506.

Lamb, R.A. and Krug, R.M. 1996. Orthomyxoviridae: The viruses and their replication. In: D.M. Knipe and P.M. Howley (Eds), Fields Virology, Lippincott -Raven, Philadelphia, pp. 1353-1395.

Lamb, R.A. and Krug, R.M. 2001. Orthomyxoviridae: The viruses and their replication. In: D.M. Knipe and P.M. Howley (Eds), Fields Virology, Lippincott Williams and Wilkins, Philadelphia, pp. 1487-1532.

Lasunskaia, E.B., Fridlianskaia, II, Darieva, Z.A., da Silva, M.S., Kanashiro, M.M. and Margulis, B.A., 2003. Transfection of NS0 myeloma fusion partner cells with HSP70 gene results in higher hybridoma yield by improving cellular resistance to apoptosis. Biotechnol Bioeng 81, 496-504.

Lau, S.C. and Scholtissek, C., 1995. Abortive infection of Vero cells by an influenza A virus (FPV). Virology 212, 225-31.

Le Ru, A., Jacob, D., Transfiguracion, J., Ansorge, S., Henry, O. and Kamen, A.A., 2010, Scalable production of influenza virus in HEK-293 cells for efficient vaccine manufacturing. Vaccine.

Li, Y., Huang, X., Xia, B. and Zheng, C., 2009. Development and validation of a duplex quantitative real-time RT-PCR assay for simultaneous detection and quantitation of foot-and-mouth disease viral positive-stranded RNAs and negative-stranded RNAs. J Virol Methods 161, 161-7.

Liang, D., Benko, Z., Agbottah, E., Bukrinsky, M. and Zhao, R.Y., 2007. Anti-vpr activities of heat shock protein 27. Mol Med 13, 229-39.

Lieber, M., Smith, B., Szakal, A., Nelson-Rees, W. and Todaro, G., 1976. A continuous tumor-cell line from a human lung carcinoma with properties of type II alveolar epithelial cells. Int J Cancer 17, 62-70.

Liu, N., Song, W., Wang, P., Lee, K., Chan, W., Chen, H. and Cai, Z., 2008. Proteomics analysis of differential expression of cellular proteins in response to avian H9N2 virus infection in human cells. Proteomics 8, 1851-8.

Livak, K.J. and Schmittgen, T.D., 2001. Analysis of relative gene expression data using real-time quantitative PCR and the 2(-Delta Delta C(T)) Method. Methods 25, 402-8.

Lohr, V., Genzel, Y., Behrendt, I., Scharfenberg, K. and Reichl, U., 2010, A new MDCK suspension line cultivated in a fully defined medium in stirred-tank and wave bioreactor. Vaccine 28, 6256-64.

Lohr, V., Rath, A., Genzel, Y., Jordan, I., Sandig, V. and Reichl, U., 2009. New avian suspension cell lines provide production of influenza virus and MVA in serum-free media: studies on growth, metabolism and virus propagation. Vaccine 27, 4975-82.

Ludwig, S., Pleschka, S., Planz, O. and Wolff, T., 2006. Ringing the alarm bells: signalling and apoptosis in influenza virus infected cells. Cell Microbiol 8, 375-86.

Lyles, D.S., 2000. Cytopathogenesis and inhibition of host gene expression by RNA viruses. Microbiology and Molecular Biology Reviews 64, 709-+.

Ma, W., Brenner, D., Wang, Z., Dauber, B., Ehrhardt, C., Hogner, K., Herold, S., Ludwig, S., Wolff, T., Yu, K., Richt, J.A., Planz, O. and Pleschka, S., 2010, The NS segment of an H5N1 highly pathogenic avian influenza virus (HPAIV) is sufficient to alter replication efficiency, cell tropism, and host range of an H7N1 HPAIV. J Virol 84, 2122-33.

Maas, F., Schaap, N., Kolen, S., Zoetbrood, A., Buno, I., Dolstra, H., de Witte, T., Schattenberg, A. and van de Wiel-van Kemenade, E., 2003. Quantification of donor and recipient hemopoietic cells by real-time PCR of single nucleotide polymorphisms. Leukemia 17, 621-9.

Mackay, I.M., Arden, K.E. and Nitsche, A., 2002. Real-time PCR in virology. Nucleic Acids Res 30, 1292-305.

Madin, S.H. and Darby, N.B., Jr., 1958. Established kidney cell lines of normal adult bovine and ovine origin. Proc Soc Exp Biol Med 98, 574-6.

Mahy, B.W.J. and Kangro, H.O., 1996. Virology Methods Manual. Academic press, London.

Marcus, P.I., Ngunjiri, J.M. and Sekellick, M.J., 2009. Dynamics of biologically active subpopulations of influenza virus: plaque-forming, noninfectious cell-killing, and defective interfering particles. J Virol 83, 8122-30.

Marouga, R., David, S. and Hawkins, E., 2005. The development of the DIGE system: 2D fluorescence difference gel analysis technology. Anal Bioanal Chem 382, 669-78.

Marsh, M. and Helenius, A., 1989. Virus entry into animal cells. Adv Virus Res 36, 107-51.

Matlin, K.S., Reggio, H., Helenius, A. and Simons, K., 1981. Infectious entry pathway of influenza virus in a canine kidney cell line. J Cell Biol 91, 601-13.

Maxwell, K.L. and Frappier, L., 2007. Viral proteomics. Microbiol Mol Biol Rev 71, 398-411.

Mayer, D., Molawi, K., Martinez-Sobrido, L., Ghanem, A., Thomas, S., Baginsky, S., Grossmann, J., Garcia-Sastre, A. and Schwemmle, M., 2007. Identification of cellular interaction partners of the influenza virus ribonucleoprotein complex and polymerase complex using proteomic-based approaches. J Proteome Res 6, 672-82.

Medcalf, L., Poole, E., Elton, D. and Digard, P., 1999. Temperature-sensitive lesions in two influenza A viruses defective for replicative transcription disrupt RNA binding by the nucleoprotein. J Virol 73, 7349-56.

Mena, I., Jambrina, E., Albo, C., Perales, B., Ortin, J., Arrese, M., Vallejo, D. and Portela, A., 1999. Mutational analysis of influenza A virus nucleoprotein: identification of mutations that affect RNA replication. J Virol 73, 1186-94.

Merten, O.W., 2002. Development of serum-free media for cell growth and production of viruses/viral vaccines--safety issues of animal products used in serum-free media. Dev Biol (Basel) 111, 233-57.

Michelsen, U. and von Hagen, J., 2009. Isolation of subcellular organelles and structures. Methods Enzymol 463, 305-28.

Mikulasova, A., Vareckova, E. and Fodor, E., 2000. Transcription and replication of the influenza a virus genome. Acta Virol 44, 273-82.

Milligan, J.F., Groebe, D.R., Witherell, G.W. and Uhlenbeck, O.C., 1987. Oligoribonucleotide synthesis using T7 RNA polymerase and synthetic DNA templates. Nucleic Acids Res 15, 8783-98.

Miralles, F. and Visa, N., 2006. Actin in transcription and transcription regulation. Curr Opin Cell Biol 18, 261-6.

Mochalova, L., Gambaryan, A., Romanova, J., Tuzikov, A., Chinarev, A., Katinger, D., Katinger, H., Egorov, A. and Bovin, N., 2003. Receptor-binding properties of modern human influenza viruses primarily isolated in Vero and MDCK cells and chicken embryonated eggs. Virology 313, 473-80.

Montagnon, B.J., Fanget, B. and Nicolas, A.J., 1981. The Large-Scale Cultivation of Vero

Cells in Micro-Carrier Culture for Virus-Vaccine Production Preliminary-Results for Killed Poliovirus-Vaccine. Developments in Biological Standardization 47, 55-64.

Montagnon, B.J. and Vincent-Falquet, J.C., 1998. Experience with the Vero cell line. Safety of Biological Products Prepared from Mammalian Cell Culture 93, 119-123.

Morris, S.J., Nightingale, K., Smith, H. and Sweet, C., 2005. Influenza A virus-induced apoptosis is a multifactorial process: exploiting reverse genetics to elucidate the role of influenza A virus proteins in virus-induced apoptosis. Virology 335, 198-211.

Morrison, T.B., Weis, J.J. and Wittwer, C.T., 1998. Quantification of low-copy transcripts by continuous SYBR Green I monitoring during amplification. Biotechniques 24, 954-8, 960, 962.

Mullin, A.E., Dalton, R.M., Amorim, M.J., Elton, D. and Digard, P., 2004. Increased amounts of the influenza virus nucleoprotein do not promote higher levels of viral genome replication. J Gen Virol 85, 3689-98.

Murakami, S., Horimoto, T., Mai le, Q., Nidom, C.A., Chen, H., Muramoto, Y., Yamada, S., Iwasa, A., Iwatsuki-Horimoto, K., Shimojima, M., Iwata, A. and Kawaoka, Y., 2008. Growth determinants for H5N1 influenza vaccine seed viruses in MDCK cells. J Virol 82, 10502-9.

Naito, T., Momose, F., Kawaguchi, A. and Nagata, K., 2007. Involvement of Hsp90 in assembly and nuclear import of influenza virus RNA polymerase subunits. J Virol 81, 1339-49.

Nayak, D.P., Hui, E.K. and Barman, S., 2004. Assembly and budding of influenza virus. Virus Res 106, 147-65.

Nemeroff, M.E., Qian, X.Y. and Krug, R.M., 1995. The influenza virus NS1 protein forms multimers in vitro and in vivo. Virology 212, 422-8.

Neumann, G., Brownlee, G.G., Fodor, E. and Kawaoka, Y., 2004. Orthomyxovirus replication, transcription, and polyadenylation. Curr Top Microbiol Immunol 283, 121-43.

Neumann, G., Hughes, M.T. and Kawaoka, Y., 2000. Influenza A virus NS2 protein mediates vRNP nuclear export through NES-independent interaction with hCRM1. EMBO J 19, 6751-8.

Ng, S.S., Li, O.T., Cheung, T.K., Malik Peiris, J.S. and Poon, L.L., 2008. Heterologous influenza vRNA segments with identical non-coding sequences stimulate viral RNA replication in trans. Virol J 5, 2.

Nickolson, K. 1998. Human Influenza. In: K. Nickolson, R.G. Webster and A. Hay (Eds), Textbook of Influenza, Blackwell Sciences, Oxford, pp. 219-264.

Nicolson, C., Major, D., Wood, J.M. and Robertson, J.S., 2005. Generation of influenza vaccine viruses on Vero cells by reverse genetics: an H5N1 candidate vaccine strain produced under a quality system. Vaccine 23, 2943-52.

Nyman, T.A., Matikainen, S., Sareneva, T., Julkunen, I. and Kalkkinen, N., 2000. Proteome analysis reveals ubiquitin-conjugating enzymes to be a new family of interferon-alpha-regulated genes. Eur J Biochem 267, 4011-9.

O'Farrell, P.H., 1975. High resolution two-dimensional electrophoresis of proteins. J Biol Chem 250, 4007-21.

O'Neill, R.E., Jaskunas, R., Blobel, G., Palese, P. and Moroianu, J., 1995. Nuclear import of influenza virus RNA can be mediated by viral nucleoprotein and transport factors required for protein import. J Biol Chem 270, 22701-4.

O'Neill, R.E., Talon, J. and Palese, P., 1998. The influenza virus NEP (NS2 protein) mediates the nuclear export of viral ribonucleoproteins. EMBO J 17, 288-96.

Ogino, T., Yamadera, T., Nonaka, T., Imajoh-Ohmi, S. and Mizumoto, K., 2001. Enolase, a cellular glycolytic enzyme, is required for efficient transcription of Sendai virus genome. Biochem Biophys Res Commun 285, 447-55.

Ollier, L., Caramella, A., Giordanengo, V. and Lefebvre, J.C., 2004. High permissivity of human HepG2 hepatoma cells for influenza viruses. J Clin Microbiol 42, 5861-5.

Olsen, J.V., Blagoev, B., Gnad, F., Macek, B., Kumar, C., Mortensen, P. and Mann, M., 2006. Global, in vivo, and site-specific phosphorylation dynamics in signaling networks. Cell 127, 635-48.

Ong, W.T., Omar, A.R., Ideris, A. and Hassan, S.S., 2007. Development of a multiplex real-time PCR assay using SYBR Green 1 chemistry for simultaneous detection and subtyping of H9N2 influenza virus type A. J Virol Methods 144, 57-64.

Ozaki, H., Govorkova, E.A., Li, C., Xiong, X., Webster, R.G. and Webby, R.J., 2004. Generation of high-yielding influenza A viruses in African green monkey kidney (Vero) cells by reverse genetics. J Virol 78, 1851-7.

Ozaki, H. and Kida, H., 2007. Extensive accumulation of influenza virus NS1 protein in the nuclei causes effective viral growth in vero cells. Microbiol Immunol 51, 577-80.

Palese, P., 1977. The genes of influenza virus. Cell 10, 1-10.

Park, J.G., Frucht, H., LaRocca, R.V., Bliss, D.P., Jr., Kurita, Y., Chen, T.R., Henslee, J.G., Trepel, J.B., Jensen, R.T., Johnson, B.E. and et al., 1990. Characteristics of cell lines established from human gastric carcinoma. Cancer Res 50, 2773-80.

Park, Y.W., Wilusz, J. and Katze, M.G., 1999. Regulation of eukaryotic protein synthesis: selective influenza viral mRNA translation is mediated by the cellular RNA-binding protein GRSF-1. Proc Natl Acad Sci U S A 96, 6694-9.

Patton, W.F., Schulenberg, B. and Steinberg, T.H., 2002. Two-dimensional gel electrophoresis; better than a poke in the ICAT? Curr Opin Biotechnol 13, 321-8.

Pau, M.G., Ophorst, C., Koldijk, M.H., Schouten, G., Mehtali, M. and Uytdehaag, F., 2001. The human cell line PER.C6 provides a new manufacturing system for the production of influenza vaccines. Vaccine 19, 2716-21.

Pearson, S., 2007. Embryonic stem cells: not just from humans. New applications promise to boost drug development and manufacturing. Gen Eng Biotech News 4, 1-3.

Perkins, D.N., Pappin, D.J., Creasy, D.M. and Cottrell, J.S., 1999. Probability-based protein identification by searching sequence databases using mass spectrometry data. Electrophoresis 20, 3551-67.

Peyrefitte, C.N., Pastorino, B., Bessaud, M., Tolou, H.J. and Couissinier-Paris, P., 2003. Evidence for in vitro falsely-primed cDNAs that prevent specific detection of virus negative strand RNAs in dengue-infected cells: improvement by tagged RT-PCR. J Virol Methods 113, 19-28.

Pleschka, S., Jaskunas, R., Engelhardt, O.G., Zurcher, T., Palese, P. and Garcia-Sastre, A., 1996. A plasmid-based reverse genetics system for influenza A virus. J Virol 70, 4188-92.

Pokrovskaya, I.D. and Gurevich, V.V., 1994. In vitro transcription: preparative RNA yields in analytical scale reactions. Anal Biochem 220, 420-3.

Poon, L.L., Fodor, E. and Brownlee, G.G., 2000. Polyuridylated mRNA synthesized by a recombinant influenza virus is defective in nuclear export. J Virol 74, 418-27.

Qian, X.Y., Chien, C.Y., Lu, Y., Montelione, G.T. and Krug, R.M., 1995. An amino-terminal polypeptide fragment of the influenza virus NS1 protein possesses specific RNA-binding activity and largely helical backbone structure. RNA 1, 948-56.

Quesney, S., Marc, A., Gerdil, C., Gimenez, C., Marvel, J., Richard, Y. and Meignier, B., 2003. Kinetics and metabolic specificities of Vero cells in bioreactor cultures with serum-free medium. Cytotechnology 42, 1-11.

Radtke, K., Dohner, K. and Sodeik, B., 2006. Viral interactions with the cytoskeleton: a hitchhiker's guide to the cell. Cell Microbiol 8, 387-400.

Ratcliff, R.M., Chang, G., Kok, T. and Sloots, T.P., 2007. Molecular diagnosis of medical viruses. Curr Issues Mol Biol 9, 87-102.

Resuehr, D. and Spiess, A.N., 2003. A real-time polymerase chain reaction-based evaluation of cDNA synthesis priming methods. Anal Biochem 322, 287-91.

Richter, M.V. and Topham, D.J., 2007. The alpha1beta1 integrin and TNF receptor II protect

airway CD8+ effector T cells from apoptosis during influenza infection. J Immunol 179, 5054-63.

Rimmelzwaan, G.F., Baars, M., Claas, E.C. and Osterhaus, A.D., 1998. Comparison of RNA hybridization, hemagglutination assay, titration of infectious virus and immunofluorescence as methods for monitoring influenza virus replication in vitro. J Virol Methods 74, 57-66.

Ririe, K.M., Rasmussen, R.P. and Wittwer, C.T., 1997. Product differentiation by analysis of DNA melting curves during the polymerase chain reaction. Anal Biochem 245, 154-60.

Robb, N.C., Smith, M., Vreede, F.T. and Fodor, E., 2009. NS2/NEP protein regulates transcription and replication of the influenza virus RNA genome. J Gen Virol 90, 1398-407.

Roberts, P.C. and Compans, R.W., 1998. Host cell dependence of viral morphology. Proc Natl Acad Sci U S A 95, 5746-51.

Rourou, S., van der Ark, A., van der Velden, T. and Kallel, H., 2009. Development of an animal-component free medium for vero cells culture. Biotechnol Prog 25, 1752-61.

Saiki, R.K., Scharf, S., Faloona, F., Mullis, K.B., Horn, G.T., Erlich, H.A. and Arnheim, N., 1985. Enzymatic amplification of beta-globin genomic sequences and restriction site analysis for diagnosis of sickle cell anemia. Science 230, 1350-4.

Santoro, M.G., 1996. Viral infection. EXS 77, 337-57.

Santoro, M.G., 2000. Heat shock factors and the control of the stress response. Biochem Pharmacol 59, 55-63.

Schauber, C., Chen, L., Tongaonkar, P., Vega, I., Lambertson, D., Potts, W. and Madura, K., 1998. Rad23 links DNA repair to the ubiquitin/proteasome pathway. Nature 391, 715-8.

Schmitt, A.P. and Lamb, R.A., 2005. Influenza virus assembly and budding at the viral budozone. Adv Virus Res 64, 383-416.

Schulze-Horsel, J., Schulze, M., Agalaridis, G., Genzel, Y. and Reichl, U., 2009. Infection dynamics and virus-induced apoptosis in cell culture-based influenza vaccine production-Flow cytometry and mathematical modeling. Vaccine 27, 2712-22.

Schwartz, L. and Gelb, R., 1984. Statistical uncertainties of end-points at intersecting straight-lines. Analytical Chemistry 56, 1487-92.

Schwarzer, J., Rapp, E., Hennig, R., Genzel, Y., Jordan, I., Sandig, V. and Reichl, U., 2009. Glycan analysis in cell culture-based influenza vaccine production: influence of host cell line and virus strain on the glycosylation pattern of viral hemagglutinin. Vaccine 27, 4325-36.

Schweiger, B., Zadow, I., Heckler, R., Timm, H. and Pauli, G., 2000. Application of a fluorogenic PCR assay for typing and subtyping of influenza viruses in respiratory samples. J Clin Microbiol 38, 1552-8.

Seitz, C., Frensing, T., Hoper, D., Kochs, G. and Reichl, U. 2010, High yields of Influenza A virus in MDCK cells are promoted by an insufficient IFN-induced antiviral state. J Gen Virol.

Shackelford, J. and Pagano, J.S., 2005. Targeting of host-cell ubiquitin pathways by viruses. Essays Biochem 41, 139-56.

Shapiro, G.I., Gurney, T., Jr. and Krug, R.M., 1987. Influenza virus gene expression: control mechanisms at early and late times of infection and nuclear-cytoplasmic transport of virus-specific RNAs. J Virol 61, 764-73.

Shapiro, G.I. and Krug, R.M., 1988. Influenza virus RNA replication in vitro: synthesis of viral template RNAs and virion RNAs in the absence of an added primer. J Virol 62, 2285-90.

Shaw, J., Rowlinson, R., Nickson, J., Stone, T., Sweet, A., Williams, K. and Tonge, R., 2003. Evaluation of saturation labelling two-dimensional difference gel electrophoresis fluorescent dyes. Proteomics 3, 1181-95.

Shaw, M.L., Stone, K.L., Colangelo, C.M., Gulcicek, E.E. and Palese, P., 2008. Cellular proteins in influenza virus particles. PLoS Pathog 4, e1000085.

Shaw, M.M. and Riederer, B.M., 2003. Sample preparation for two-dimensional gel

electrophoresis. Proteomics 3, 1408-17.

Shin, E.C., Seifert, U., Urban, S., Truong, K.T., Feinstone, S.M., Rice, C.M., Kloetzel, P.M. and Rehermann, B., 2007. Proteasome activator and antigen-processing aminopeptidases are regulated by virus-induced type I interferon in the hepatitis C virus-infected liver. J Interferon Cytokine Res 27, 985-90.

Sidorenko, Y. and Reichl, U., 2004. Structured model of influenza virus replication in MDCK cells. Biotechnol Bioeng 88, 1-14.

Sijts, A., Sun, Y., Janek, K., Kral, S., Paschen, A., Schadendorf, D. and Kloetzel, P.M., 2002. The role of the proteasome activator PA28 in MHC class I antigen processing. Mol Immunol 39, 165-9.

Simionescu, M., Gafencu, A. and Antohe, F., 2002. Transcytosis of plasma macromolecules in endothelial cells: a cell biological survey. Microsc Res Tech 57, 269-88.

Simmons, N.L., 1982. Cultured monolayers of MDCK cells: a novel model system for the study of epithelial development and function. Gen Pharmacol 13, 287-91.

Simpson-Holley, M., Ellis, D., Fisher, D., Elton, D., McCauley, J. and Digard, P., 2002. A functional link between the actin cytoskeleton and lipid rafts during budding of filamentous influenza virions. Virology 301, 212-25.

Smith, G.L. and Hay, A.J., 1982. Replication of the influenza virus genome. Virology 118, 96-108.

Stein, S., Thomas, E.K., Herzog, B., Westfall, M.D., Rocheleau, J.V., Jackson, R.S., 2nd, Wang, M. and Liang, P., 2004. NDRG1 is necessary for p53-dependent apoptosis. J Biol Chem 279, 48930-40.

Steinhauer, D.A. and Skehel, J.J., 2002. Genetics of influenza viruses. Annu Rev Genet 36, 305-32.

Subbarao, K. and Katz, J.M., 2004. Influenza vaccines generated by reverse genetics. Curr Top Microbiol Immunol 283, 313-42.

Sun, X. and Whittaker, G.R., 2007. Role of the actin cytoskeleton during influenza virus internalization into polarized epithelial cells. Cell Microbiol 9, 1672-82.

Suzuki, T., Higgins, P.J. and Crawford, D.R., 2000. Control selection for RNA quantitation. Biotechniques 29, 332-7.

Tai, H.H., Cho, H., Tong, M. and Ding, Y., 2006. NAD+-linked 15-hydroxyprostaglandin dehydrogenase: structure and biological functions. Curr Pharm Des 12, 955-62.

Takizawa, T., Ohashi, K. and Nakanishi, Y., 1996. Possible involvement of double-stranded RNA-activated protein kinase in cell death by influenza virus infection. J Virol 70, 8128-32.

Tan, S.C. and Yiap, B.C., 2009. DNA, RNA, and protein extraction: the past and the present. J Biomed Biotechnol 2009, 574398.

Tate, E.W., 2008. Recent advances in chemical proteomics: exploring the post-translational proteome. J Chem Biol 1, 17-26.

Tey, B.T. and Al-Rubeai, M., 2004. Suppression of apoptosis in perfusion culture of Myeloma NS0 cells enhances cell growth but reduces antibody productivity. Apoptosis 9, 843-52.

Thulasiraman, V., Lin, S., Gheorghiu, L., Lathrop, J., Lomas, L., Hammond, D. and Boschetti, E., 2005. Reduction of the concentration difference of proteins in biological liquids using a library of combinatorial ligands. Electrophoresis 26, 3561-71.

Tian, Q., Stepaniants, S.B., Mao, M., Weng, L., Feetham, M.C., Doyle, M.J., Yi, E.C., Dai, H., Thorsson, V., Eng, J., Goodlett, D., Berger, J.P., Gunter, B., Linseley, P.S., Stoughton, R.B., Aebersold, R., Collins, S.J., Hanlon, W.A. and Hood, L.E., 2004. Integrated genomic and proteomic analyses of gene expression in Mammalian cells. Mol Cell Proteomics 3, 960-9.

Tong, A., Wu, L., Lin, Q., Lau, Q.C., Zhao, X., Li, J., Chen, P., Chen, L., Tang, H., Huang, C. and Wei, Y.Q., 2008. Proteomic analysis of cellular protein alterations using a hepatitis B virus-producing cellular model. Proteomics 8, 2012-23.

Tree, J.A., Richardson, C., Fooks, A.R., Clegg, J.C. and Looby, D., 2001. Comparison of large-scale mammalian cell culture systems with egg culture for the production of influenza virus A vaccine strains. Vaccine 19, 3444-50.

Uchide, N., Ohyama, K., Bessho, T. and Yamakawa, T., 2002. Semi-quantitative RT-PCR-based assay, improved by Southern hybridization technique, for polarity-specific influenza virus RNAs in cultured cells. J Virol Methods 106, 125-34.

Unlu, M., Morgan, M.E. and Minden, J.S., 1997. Difference gel electrophoresis: a single gel method for detecting changes in protein extracts. Electrophoresis 18, 2071-7.

Valencia, C.A., Cotten, S.W., Duan, J. and Liu, R., 2008. Modulation of nucleobindin-1 and nucleobindin-2 by caspases. FEBS Lett 582, 286-90.

Van den Bergh, G., Clerens, S., Vandesande, F. and Arckens, L., 2003. Reversed-phase high-performance liquid chromatography prefractionation prior to two-dimensional difference gel electrophoresis and mass spectrometry identifies new differentially expressed proteins between striate cortex of kitten and adult cat. Electrophoresis 24, 1471-81.

van der Flier, A. and Sonnenberg, A., 2001. Function and interactions of integrins. Cell Tissue Res 305, 285-98.

van Elden, L.J., Nijhuis, M., Schipper, P., Schuurman, R. and van Loon, A.M., 2001. Simultaneous detection of influenza viruses A and B using real-time quantitative PCR. J Clin Microbiol 39, 196-200.

Vester, D., Lagoda, A., Hoffmann, D., Seitz, C., Heldt, S., Bettenbrock, K., Genzel, Y. and Reichl, U., 2010, Real-time RT-qPCR assay for the analysis of human influenza A virus transcription and replication dynamics. J Virol Methods.

Vester, D., Rapp, E., Gade, D., Genzel, Y. and Reichl, U., 2009. Quantitative analysis of cellular proteome alterations in human influenza A virus-infected mammalian cell lines. Proteomics 9, 3316-27.

Vester, D., Rapp, E., Kluge, S., Genzel, Y. and Reichl, U., 2010, Virus-host cell interactions in vaccine production cell lines infected with different human influenza A virus variants: A proteomic approach. J Proteomics.

Viswanathan, K. and Fruh, K., 2007. Viral proteomics: global evaluation of viruses and their interaction with the host. Expert Rev Proteomics 4, 815-29.

Vreede, F.T., Gifford, H. and Brownlee, G.G., 2008. Role of initiating nucleoside triphosphate concentrations in the regulation of influenza virus replication and transcription. J Virol 82, 6902-10.

Vreede, F.T., Jung, T.E. and Brownlee, G.G., 2004. Model suggesting that replication of influenza virus is regulated by stabilization of replicative intermediates. J Virol 78, 9568-72.

Walsh, G., 2006. Biopharmaceutical benchmarks 2006. Nat Biotechnol 24, 769-76.

Wang, C., Lamb, R.A. and Pinto, L.H., 1994. Direct measurement of the influenza A virus M2 protein ion channel activity in mammalian cells. Virology 205, 133-40.

Wang, Z. and Duke, G.M., 2007. Cloning of the canine RNA polymerase I promoter and establishment of reverse genetics for influenza A and B in MDCK cells. Virol J 4, 102.

Ward, C.L., Dempsey, M.H., Ring, C.J., Kempson, R.E., Zhang, L., Gor, D., Snowden, B.W. and Tisdale, M., 2004. Design and performance testing of quantitative real time PCR assays for influenza A and B viral load measurement. J Clin Virol 29, 179-88.

Wareing, M.D. and Tannock, G.A., 2001. Live attenuated vaccines against influenza; an historical review. Vaccine 19, 3320-30.

Watanabe, K., Fuse, T., Asano, I., Tsukahara, F., Maru, Y., Nagata, K., Kitazato, K. and Kobayashi, N., 2006. Identification of Hsc70 as an influenza virus matrix protein (M1) binding factor involved in the virus life cycle. FEBS Lett 580, 5785-90.

Webster, R.G. 1998. Section 3: Evolution and ecology of influenza viruses., Textbook of Influenza, Blackwell Science, Oxford.

WHO. 2008. Epidemic and pandemic alert response: influenza, Vol. 2008.

Wilhelm, J. and Pingoud, A., 2003. Real-time polymerase chain reaction. Chembiochem 4, 1120-8.

Wilschut, J. and McElhaney, J.E., 2005. Influenza. Mosby, London.

Wittwer, C.T., Ririe, K.M., Andrew, R.V., David, D.A., Gundry, R.A. and Balis, U.J., 1997. The LightCycler: a microvolume multisample fluorimeter with rapid temperature control. Biotechniques 22, 176-81.

Wolff, T. and Ludwig, S., 2009. Influenza viruses control the vertebrate type I interferon system: factors, mechanisms, and consequences. J Interferon Cytokine Res 29, 549-57.

Wong, D.C., Wong, K.T., Lee, Y.Y., Morin, P.N., Heng, C.K. and Yap, M.G., 2006a. Transcriptional profiling of apoptotic pathways in batch and fed-batch CHO cell cultures. Biotechnol Bioeng 94, 373-82.

Wong, D.C., Wong, K.T., Nissom, P.M., Heng, C.K. and Yap, M.G., 2006b. Targeting early apoptotic genes in batch and fed-batch CHO cell cultures. Biotechnol Bioeng 95, 350-61.

Wong, M.L. and Medrano, J.F., 2005. Real-time PCR for mRNA quantitation. Biotechniques 39, 75-85.

Wright, P.F. and Webster, R.G. 2001. Orthomyxoviruses. In: D.M. Knipe and P.M. Hawley (Eds), Fields Virology, Lippincott Williams & Wilkins, Philadelphia (PA), pp. 1564.

Wu, W.W., Wang, G., Baek, S.J. and Shen, R.F., 2006. Comparative study of three proteomic quantitative methods, DIGE, cICAT, and iTRAQ, using 2D gel- or LC-MALDI TOF/TOF. J Proteome Res 5, 651-8.

Yan, J.X., Harry, R.A., Spibey, C. and Dunn, M.J., 2000. Postelectrophoretic staining of proteins separated by two-dimensional gel electrophoresis using SYPRO dyes. Electrophoresis 21, 3657-65.

Youil, R., Su, Q., Toner, T.J., Szymkowiak, C., Kwan, W.S., Rubin, B., Petrukhin, L., Kiseleva, I., Shaw, A.R. and DiStefano, D., 2004. Comparative study of influenza virus replication in Vero and MDCK cell lines. J Virol Methods 120, 23-31.

Zhang, C.G., Chromy, B.A. and McCutchen-Maloney, S.L., 2005. Host-pathogen interactions: a proteomic view. Expert Rev Proteomics 2, 187-202.

Zhang, L., Katz, J.M., Gwinn, M., Dowling, N.F. and Khoury, M.J., 2009. Systems-based candidate genes for human response to influenza infection. Infect Genet Evol 9, 1148-57.

Zhao, Y. and Jensen, O.N., 2009. Modification-specific proteomics: strategies for characterization of post-translational modifications using enrichment techniques. Proteomics 9, 4632-41.

Zheng, H., Palese, P. and Garcia-Sastre, A., 1996. Nonconserved nucleotides at the 3' and 5' ends of an influenza A virus RNA play an important role in viral RNA replication. Virology 217, 242-51.

Zhirnov, O.P., Konakova, T.E., Wolff, T. and Klenk, H.D., 2002. NS1 protein of influenza A virus down-regulates apoptosis. J Virol 76, 1617-25.

Zhou, G., Li, H., DeCamp, D., Chen, S., Shu, H., Gong, Y., Flaig, M., Gillespie, J.W., Hu, N., Taylor, P.R., Emmert-Buck, M.R., Liotta, L.A., Petricoin, E.F., 3rd and Zhao, Y., 2002. 2D differential in-gel electrophoresis for the identification of esophageal scans cell cancer-specific protein markers. Mol Cell Proteomics 1, 117-24.

Appendix

A. Chemicals, equipment and consumables

Table A-1: List of applied chemicals

Name	Supplier
Acetic acid, glacial (CH_3COOH), 99.8%	Merck, Darmstadt, Germany
Acetonitrile (CH_3CN), LC-MS grade	Riedel-de-Haën, Taufkirchen, Germany
Acrylamide 30%	AppliChem, Darmstadt, Germany
Agarose NEEO Ultra	Roth, Karlsruhe, Germany
Ammonium persulfate (APS) ($(NH_4)_2S_2O_8$)	GE Healthcare, München, Germany
Ampicillin	Merck, Darmstadt, Germany
BactoTM Tryptone	BD, Heidelberg, Germany
BactoTM Yeast Extract	BD, Heidelberg, Germany
Bromophenole blue	GE Healthcare, München, Germany
BSA	BioRad, München, Germany
Bind-Silane	Sigma-Aldrich, Taufkirchen, Germany
Caso-Bouillon	Fluka, Taufkirchen, Germany
CHAPS	AppliChem, Darmstadt, Germany
Coomassie brilliant blue G-250	Merck, Darmstadt, Germany
DeStreak rehydration solution	GE Healthcare, München, Germany
Digitonin	Sigma-Aldrich, Taufkirchen, Germany
Dimethylformamide ($(CH_3)_2NC(O)H$)	Sigma-Aldrich, Taufkirchen, Germany
Dipotassium hydrogenphosphate (K_2HPO_4)	Merck, Darmstadt, Germany
dNTP Set pH7	Roth, Karlsruhe, Germany
DTT	GE Healthcare, München, Germany
EDTA	Merck, Darmstadt, Germany
Ethanol (C_2H_5OH), 99.8%, undenatured	Roth, Karlsruhe, Germany
FCS (Cat.-Nr. 3302-P250922)	PAN, Aidenbach, Germany
F12-Kaighns, nutrient mixture 1x (Cat-Nr. 21127022)	Gibco, Karlsruhe, Germany
Formamide (CH_3NO)	Roth, Karlsruhe, Germany
Formic acid (HCOOH)	Fluka, Taufkirchen, Germany
Gentamycin	Merck, Darmstadt, Germany
GMEM without glutamine (Cat.-Nr. 22100-093)	Sigma-Aldrich, Taufkirchen, Germany
Glucose (Cat.-Nr. X997.3)	Roth, Karlsruhe, Germany
Glutamine (Cat.-Nr. G-3126)	Sigma-Aldrich, Taufkirchen, Germany
Glycerol ($C_3H_5(OH)$), 87%	AppliChem, Darmstadt, Germany
Glycine (NH_2CH_2COOH)	AppliChem, Darmstadt, Germany
HEPES (Cat.-Nr. HN77)	Roth, Karlsruhe, Germany
Hydrochloric acid (HCl) 1M	Roth, Karlsruhe, Germany
Immobiline dry cover fluid	GE Healthcare, München, Germany
IPTG	Roth, Karlsruhe, Germany
Iodacetamide (C_2H_4INO)	AppliChem, Darmstadt, Germany
Lab-M peptone (Cat.-Nr. MC001)	Lab-M, Lancs, UK
L-Lysin	Sigma-Aldrich, Taufkirchen, Germany
Magnesium chloride ($MgCl_2$)	Roth, Karlsruhe, Germany
Magnesium sulfate ($MgSO_4$)	Fluka, Taufkirchen, Germany
MEM eagle basal medium (Cat.-Nr. M2279)	Sigma-Aldrich, Taufkirchen, Germany
MEM-non-essential amino acids (Cat.-Nr.11140050)	Gibco, Karlsruhe, Germany
Methanol (CH_3OH), 99.9%	Roth, Karlsruhe, Germany
MOPS, minimal medium	Merck, Darmstadt, Germany
O`GeneRuler DNA Ladder Mix	Fermentas, St. Leon-Rot, Germany

Ortho-Phosphoric acid (H_3PO_4), 85%	AppliChem, Darmstadt, Germany
Pharmalyte, broad range pH 3-10	GE Healthcare, München, Germany
Potassium chloride (KCl)	Merck, Darmstadt, Germany
Potassium hydrogen phosphate (K_2HPO_4)	Riedel-de-Haën, Taufkirchen, Germany
Porcine trypsin, sequencing grade	Promega, Madison, WI, USA
Propidium iodide	Sigma-Aldrich, Taufkirchen, Germany
Random hexamer primer	Promega, Madison, WI, USA
RiboRuler High Range RNA Ladder	Fermentas, St. Leon-Rot, Germany
RNAse A	Sigma-Aldrich, Taufkirchen, Germany
RPMI basal medium (Cat.-Nr. 11875-093)	Sigma-Aldrich, Taufkirchen, Germany
SDS	AppliChem, Darmstadt, Germany
Sodium acetate (NaOAc)	J.T. Baker, Deventer, Netherlands
Sodium hydroxide (NaOH)	Roth, Karlsruhe, Germany
Sodium chloride (NaCl)	Roth, Karlsruhe, Germany
Sodium citrate ($C_6H_7NaO_7$)	Neolab Migge, Heidelberg, Germany
Sodium dihydrogenphosphate (NaH_2PO_4)	Fluka, Taufkirchen, Germany
Sodium hydrogenphosphate (Na_2HPO_4)	Merck, Darmstadt, Germany
Sodium pyruvate ($C_3H_3NaO_3$) (Cat.-Nr. P2256)	Sigma-Aldrich, Taufkirchen, Germany
Super Signal West Dura Extended Duration Substrate	Thermo scientific, Waltham, MA, USA
Sypro Ruby	Genomic Solutions, Ann Arbor, USA
TEMED	GE Healthcare, München, Germany
Thiourea (CH_4N_2S)	Sigma-Aldrich, Taufkirchen, Germany
Trifluoroacetic acid (CF_3CO_2H)	Fluka, Taufkirchen, Germany
TRIS-HCl	AppliChem, Darmstadt, Germany
TRIS	AppliChem, Darmstadt, Germany
Trypan blue	Merck, Darmstadt, Germany
Trypsin (2.5%, porcine) 0.5 mg/mL (Nr. 27250-018)	Gibco, Karlsruhe, Germany
Ultrapure water, LC-MS grade	Riedel-de-Haën, Taufkirchen, Germany
Urea (CH_4N_2O)	GE Healthcare, München, Germany
Water, DEPC-treated	Roth, Karlsruhe, Germany
X-Gal	Roth, Karlsruhe, Germany
Xylencyanol	Sigma-Aldrich, Taufkirchen, Germany

Table A-2: List of equipment

Name	Supplier
Analyst QS software version 1.1	Applied Biosystems, Carlsbad, USA
Balance PG5002-S, PG12001-S, AG204, PR9620-3	Mettler-Toledo, Giessen, Germany
Biofuge Fresco, Strato, Nano, Primo	Heraeus Instruments, Waltham, USA
Bioprofile 100 plus Analyzer	Nova biomedical, Rödermark, G.
Camera Easy 429K	Herolab, Wiesloch, Germany
Ceramic strip holders	GE Healthcare, München, Germany
Chemolumineszenz Imager CHEMOCAM	INTAS, Göttingen, Germany
Clean bench Herasafe	Heraeus Instruments, Waltham, USA
DeCyder software package (version 6.04.11)	GE Healthcare, München, Germany
Digital camera	Nikon, Düsseldorf, Germany
Electrophoresis chamber Midi-B, Mini-D	BioRad, München, Germany
Ettan Dalt II system	GE Healthcare, München, Germany
Ettan spot picker	GE Healthcare, München, Germany
Gel analysis software EasyWin 32 V.3.01	Herolab, Wiesloch, Germany
Gel Pro Analyzer Software	Media Cybernetics, Bethesda, USA
Incubator T6060	Heraeus Instruments, Waltham, USA
IPGphor system	GE Healthcare, München, Germany
Laser Scanning Microscope 510	Carl Zeiss AG
Magnetic stirrer VarioMag	Biosystem
MASCOT version 2.2	Matrix Science

Micro pipettes (1, 10, 100, 200 µL and 1, 5 mL)	Eppendorf, Hamburg, Germany
Micro pipettes (2, 10, 20, 100, 1000, 5000 µL)	Gilson, Middleton, WI, USA
Microtiter plate photometer Rainbow Spectro	Tecan, Crailsheim, Germany
Mini-Protean electrophoresis system	BioRad, München, Germany
nanoHPLC instrument of the 1100 Series	Agilent, Waldbronn, Germany
pH meter Inolab	WTW, Kleinmachnow, Germany
Pipettor Pipetus	Hirschmann, Eberstadt, Germany
PowerPac 300, Basic	BioRad, München, Germany
QSTAR XL (QqTOF) mass spectrometer	Applied Biosystems, Carlsbad, USA
Realtime-PCR-Cycler, iCycler iQ V.3.1.7050	BioRad, München, Germany
Shaker KS-15	Edmund Bühler GmbH, Hechingen, G
Shaker Polymax 1040	Heidolph, Schwabach, Germany
Sonotrode SonoPuls	Bandelin electronic, Berlin, Germany
SpeedVac SPD121P	Thermo Electron, Dreieich, Germany
T3 Thermocycler	Biometra, Goettingen, Germany
Thermomixer	Eppendorf, Hamburg, Germany
Typhoon Variable Mode Imager 9400	GE Healthcare, München, Germany
Ultracentrifuge Optima CE-80K	Beckman Coulter, Krefeld, Germany
Ultrapure Water Purification System Milli-Q	Millipore, Billerica, MA, USA
UV Transluminator	Gibco, Karlsruhe, Germany
UV/VIS spectrometer photometer NanoDrop ND 1000	NanoDrop, Wilmington, USA
Varioclav	Certoclav, Traun, Germany
Vi-Cell TM XR Cell Viability Analyzer	Beckman Coulter, Krefeld, Germany
Vortexer Reax Top	Heidolph, Schwabach, Germany
Wet-blot blotting system	BioRad, München, Germany

Table A-3: List of consumables

Name	Supplier
Culture dish 50x20mm	Greiner bio-one, Solingen, Germany
Culture dish with vent 60, 94x16 mm	Greiner bio-one, Solingen, Germany
Falcon tubes (10 mL, 50 mL)	Greiner bio-one, Solingen, Germany
Microfuge tubes 1.5 mL	Beckman Coulter, Krefeld, Germany
Microtiter plates with 96-well format, Flat bottom	Greiner bio-one, Solingen, Germany
Microtiter plates with 96-well format, U bottom	Greiner bio-one, Solingen, Germany
Micropipettes tips (2, 10, 100, 200 µL)(1 mL, 5 mL), Art 10 reach low Retention, Safeguard, SR-L200F	VWR, Darmstadt /PeqLab, Erlangen /Eppendorf, Hamburg/Rainin, Giessen; Germany
Paper wicks	GE Healthcare, München, Germany
PCR thermo tubes 0.2 mL	Peqlab, Erlangen, Germany
PCR plates ThermoFast 96 Semiscired	Abgene, Epsom, UK
PCR ultra clear cap strips 0.2 mL	Abgene, Epsom, UK
Pipettes Cellstar 1,2, 5, 10, 25, 50 mL	Greiner bio-one, Solingen, Germany
Porous Cellophane	GE Healthcare, München, Germany
PVDF membranes	Millipore, Billerica, MA, USA
Reaction tubes 0.5 mL, 1.5 mL, 2 mL	Eppendorf, Hamburg/Corning, Wiesbaden/VWR, Darmstadt; Germany
Sample application pieces	Serva, Heidelberg, Germany
Sterile filter Minisart 0.22 µm	Sartorius BBI, Göttingen, Germany
Sterile membrane filter 0.22 µm	Nalgene nunc, Rochester, USA
Syringe disposable 2 mL, 5 mL, 10 mL, 50 mL	Greiner bio-one, Solingen, Germany
T-flasks Cellstar 25, 75, 175 cm^2	Greiner bio-one, Solingen, Germany
PET roller bottles	Greiner bio-one, Solingen, Germany

B. Cell culture material

Cell culture media

Table B-1: Media composition for cell growth or virus infection experiments of MDCK and Vero cells

	GMEM	
Compound	**Cell growth**	**Infection**
GMEM powder	12.5 g/L	12.5 g/L
Glucose	5.5 g/L	5.5 g/L
$NaHCO_3$	4.0 g/L	4.0 g/L
Peptone	2 g/L	2 g/L
FCS	10%	-
$H_2O_{ultrapure}$	ad 1 L	

pH adjusted to 6.8 with HCl; sterile filtered (0.22 µm); storage at 4°C

Table B-2: Media composition for cell growth or virus infection experiments of A549 cells

	F12K		MEM	
Compound	**Cell growth**	**Infection**	**Cell growth**	**Infection**
Glutamine	2 mM	2 mM	2 mM	2 mM
FCS	10%	-	10%	-
Peptone	-	2 g/L	-	2 g/L
Basal medium	ad 1 L			

Compounds sterile filtered (0.22 µm); storage at 4°C

Table B-3: Media composition for cell growth or virus infection experiments of NCI-N87 cells

	RPMI-1640		MEM	
Compound	**Cell growth**	**Infection**	**Cell growth**	**Infection**
Glutamine	2 mM	2 mM	2 mM	2 mM
HEPES	10 mM	10 mM	-	-
Sodium pyruvate	1.0 mM	1.0 mM	-	-
Glucose	4.5 g/L	4.5 g/L	4.5 g/L	4.5 g/L
FCS	10%	-	10%	-
Peptone	-	2 g/L	-	2 g/L
Basal medium	ad 1 L			

Compounds sterile filtered (0.22 µm); storage at 4°C

Table B-4: Media composition for cell growth or virus infection experiments of HepG2 cells

	MEM		RPMI-1640	
Compound	**Cell growth**	**Infection**	**Cell growth**	**Infection**
Glutamine	2 mM	2 mM	2 mM	2 mM
Non-essential amino acids	10 mM	10 mM	-	-
Sodium pyruvate	1.0 mM	1.0 mM	-	-
Glucose	4.5 g/L	4.5 g/L	4.5 g/L	4.5 g/L
FCS	10%	-	10%	-
Peptone	-	2 g/L	-	2 g/L
Basal medium	ad 1 L			

Compounds sterile filtered (0.22 µm); storage at 4°C

Cell lines

Name	***Origin***	***Supplier***	***Cat.- Nr.***
A549	human, lung epithelial	ATCC, Middlesex, UK	CRL-185
NCI-N87	human, gastric epithelial	ATCC, Middlesex, UK	CCC-185
HepG2	human, hepatocellular epithelial	DSMZ, Braunschweig, Germany	ACC 180
MDCK	canine, kidney epithelial	ECACC, Salisbury, UK	84121903
Vero	monkey, kidney epithelial WHO seed	ECACC, Salisbury, UK	88020401

Virus Strains

Name	***Abbreviation***	***Supplier***
Human influenza virus A/PR/8/34 (H1N1); NIBSC Code: 06/114	PR/8-NIBSC	NIBSC, Hertfordshire, UK
Human influenza virus A/ PR /8/34 (H1N1); RKI Code: 3138	PR/8-RKI	RKI, Berlin, Germany
Human influenza virus A/ PR /8/34; RKI Code: 3138; adapted to Vero cells; (H1N1)	PR/8-RKI-Vero	RKI, Berlin, Germany

C. Material for nucleic acid quantification

Enzymes

Name	*Supplier*
Sph I	NEB, Ipswich, MA, USA
BamH I	NEB, Ipswich, MA, USA
Nde I	NEB, Ipswich, MA, USA
GoTaq Flexi DNA-Polymerase (Cat.-Nr. M8301)	Promega, Madison, WI, USA
Phusion High Fidelity DNA-Polymerase (Cat.-Nr. F-530S)	Finnzyme, Espoo, Finland
RNAse A (Cat.-Nr. 7156.1)	Roth, Karlsruhe, Germany
SuperScript II reverse transcriptase (Cat.-Nr. 18064022)	Invitogen, Carlsbad, CA, USA
ThermoScript reverse transcriptase (Cat.-Nr. 12236-022)	Invitrogen, Carlsbad, CA, USA

Kits

Name	*Supplier*
Eurogentec qPCR Core Kit for SYBR Green I (Cat.-Nr. RT-SN10-05NR)	Eurogentec, Köln, Germany
NucleoSpin Plasmid Kit (Cat.-Nr.)	Macherey-Nagel, Düren, Germany
NucleoSpin RNA II (Cat.-Nr.)	Macherey-Nagel, Düren, Germany
pGEM-T-easy Vector Systems (Cat.-Nr. TM042)	Promega, Madison, WI, USA
QiaAmp Viral RNA Mini Kit (Cat.-Nr. 124116026)	Qiagen, Hilden, Germany
RiboMax Large Scale RNA Production System (Cat.-Nr. 224313)	Promega, Madison, WI, USA
TranscriptAid T7 High Yield Transcription Kit (Cat.-Nr. K0441)	Fermentas, St. Leon-Rot, Germany
Wizard SV Gel and PCR Clean Up System (Cat.-Nr. A9281)	Promega, Madison, WI, USA

Plasmids

pGEM-T Easy Vector System, Promega, Madison, WI, USA (Cat.-Nr. TM042)

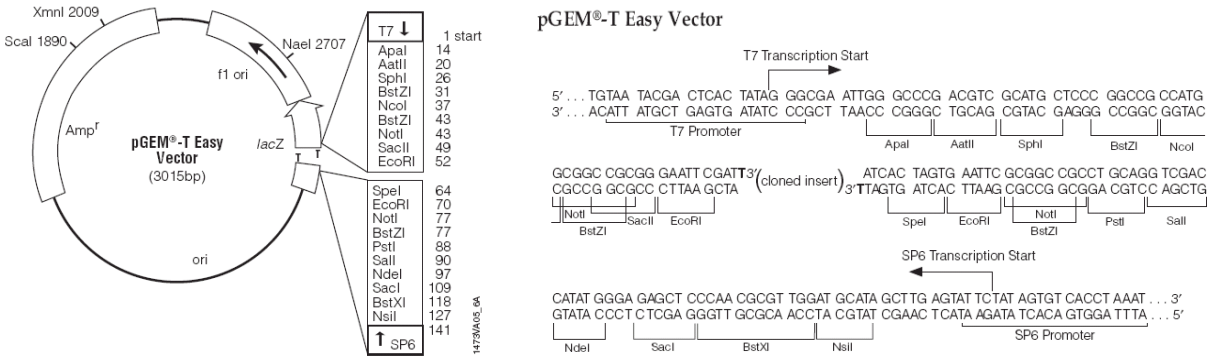

Figure C-1: Vector map pGEM-T Easy (Promega; Technical manual#TM042)

Primer

Modified primer from sequences described previously (Chan et al., 2006) were used for the production of synthetic viral RNA reference standards used during uniRT or full length PCR steps. Primer sets for qPCR were designed using the Lasergene Primer Select v7.0 software (DNASTAR, Madison, WI, USA). Primer sequences are shown in the following tables.

Table C-1: Characteristics of primer sets for MDCK reference genes (Gropp et al.*, 2006)*

Target	Name	Sequence (5'-3')
ß-Actin	ß-Actin_for	TCCCTGGAGAAGAGCTACGA
	ß-Actin_rev	CTTCTGCATCCTGTCAGCAA
GAPDH	GAPDH_for	AACATCATCCCTGCTTCCAC
	GAPDH_rev	GACCACCTGGTCCTCAGTGT

Table C-2: Characteristics of primer sets for universal reverse transcription (uniRT) or full length PCR steps (PCR) used for production of synthetic viral RNA reference standards of vRNA(-), cRNA(+), vmRNA(+) of viral segments 4 (HA), 6 (NA), 7 (M) and 8 (NS)

Target	Purpose	Name	Sense	Sequence (5'-3')	Position (nt)	Product length (bp)
All	Full length uniRT primer	Uni12(M)		AGCAAAAGCAGG	1-12	
Seg 4 (HA)	Standard PCR cRNA(+)	S4-Stdfor	+	TAATAGCACTCACTATAGGGAGCAAAAGCAGGGGAA	1-16	1798
		S4-Stdrev		AGTAGAAACAAGGGTGTTTT	1758-1778	
	Standard PCR vRNA(-)	S4+Stdfor	-	AGCAAAAGCAGGGGAA	1-16	1798
		S4+Stdrev		TAATAGCACTCACTATAGGGAGTAGAAACAAGGGTGTTTT	1758-1778	
	Standard PCR vmRNA(+)	S4mStdfor	+	TAATAGCACTCACTATAGGGAGCAAAAGCAGGGGAA	1-16	872
		S4mStdrev		TTTTTTTCCGGACCCAAAGCCTCTAC	853-872	
Seg 6 (NA)	Standard PCR cRNA(+)	S6-Stdfor	+	TAATAGCACTCACTATAGGGAGCGAAAGCAGGAGT	1-15	1433
		S6-Stdrev		AGTAGAAACAAGGAGTTTTTT	1393-1413	
	Standard PCR vRNA(-)	S6+Stdfor	-	AGCGAAAGCAGGAGT	1-15	1433
		S6+Stdrev		TAATAGCACTCACTATAGGGAGTAGAAACAAGGAGTTTTTT	1393-1413	
	Standard PCR vmRNA(+)	S6mStdfor	+	TAATAGCACTCACTATAGGGAGCGAAAGCAGGAGT	1-15	1327
		S6mStdrev		TTTTTTTTCACTATTCACGCCACAAAAAG	1305-1327	
Seg 7 (M)	Standard PCR cRNA(+)	S7-Stdfor	+	TAATAGCACTCACTATAGGGAGCGAAAGCAGGTAG	1-15	1047
		S7-Stdrev		AGTAGAAACAAGGTAGTTTTT	1007-1027	
	Standard PCR vRNA(-)	S7+Stdfor	-	AGCGAAAGCAGGTAG	1-15	1047
		S7+Stdrev		TAATAGCACTCACTATAGGGAGTAGAAACAAGGTAGTTTTT	1007-1027	
	Standard PCR vmRNA(+)	S7mStdfor	+	TAATAGCACTCACTATAGGGAGCGAAAGCAGGTAG	1-15	779
		S7mStdrev		TTTTTTTTGCGGCAATAGCGAGAGGAT	759-779	
Seg 8 (NS)	Standard PCR cRNA(+)	S8-Stdfor	+	TAATAGCACTCACTATAGGGAGAAAAAGCAGGGTGACAAA	1-20	910
		S8-Stdrev		AGTAGAAACAAGGGTGTTTT	871-890	
	Standard PCR vRNA(-)	S8+Stdfor	-	AGAAAAAGCAGGGTGACAAA	1-20	910
		S8+Stdrev		TAATAGCACTCACTATAGGGAGTAGAAACAAGGGTGTTTT	871-890	
	Standard PCR vmRNA(+)	S8mStdfor	+	TAATAGCACTCACTATAGGGAGAAAAAGCAGGGTGACAAA	1-20	698
		S8mStdrev		TTTTTTTCCCGCCATTTCTCGTTTCTG	678-698	

Table C-3: Characteristics of primer sets for polarity-specific priming reverse transcription (pspRT) or quantitative real-time PCR steps (qPCR) used for quantification of vRNA(-), cRNA(+), vmRNA(+) of viral segments 4 (HA), 6 (NA), 7 (M) and 8 (NS)

Target	Purpose	Name	Sense	Sequence (5'-3')	Position (nt)	Product length (bp)
All	pspRT primer vmRNA(+)	Oligo-dT		$TTTTTT_{12-18}$	1-6	
Seg 4 (HA)	pspRT primer cRNA(+)	S4+RTrev	+	CCGGACCCAAAGCCTCTAC	853-872	872
	pspRT primer vRNA(-)	S4-RTfor	-	ACAGCCACAACGGAAAACTATG	187-209	1591
	qPCR primer	S4qPCRfor		GGCCCAACCACAACACAACC	451-471	99
		S4qPCRrev		AGCCCTCCTTCTCCGTCAGC	530-550	
Seg 6 (NA)	pspRT primer cRNA(+)	S6+ RTrev	+	TCACTATTCACGCCACAAAAAG	1305-1327	1327
	pspRT primer vRNA(-)	S6- RTfor	-	TGCAACCAAAACATCATTACCT	165-186	1248
	qPCR primer	S6qPCRfor		CCGCCATGGGTGTCTTTC	855-874	144
		S6qPCRrev		TCCCTTTACTCCGTTTGCTCCATC	975-999	
Seg 7 (M)	pspRT primer cRNA(+)	S7+ RTrev	+	TGCGGCAATAGCGAGAGGAT	759-779	779
	pspRT primer vRNA(-)	S7- RTfor	-	AGCCGAGATCGCACAGAGACTT	63-85	964
	qPCR primer	S7qPCRfor		ATTTGCCTATGAGACCGATGCT	363-381	98
		S7qPCRrev		AGGATGGGGGCTGTGACC	439-461	
Seg 8 (NS)	pspRT primer cRNA(+)	S8+ RTrev	+	CCCGCCATTTCTCGTTTCTG	678-698	698
	pspRT primer vRNA(-)	S8- RTfor	-	GATAGTGGAGCGGATTCTGA	215-234	675
	qPCR primer	S8qPCRfor		GATAGTGGAGCGGATTCTGA	215-234	154
		S8qPCRrev		GAGGGCCTGCCACTTTCT	352-369	

Table C-4: Characteristics of primer sets for determination of extracellular viral RNA in cell culture supernatant by RT-qPCR

Target	Name	Sequence (5'-3')	Position (nt)	Product length (bp)
All	Random hexamer	NNNNNN		
Seg 7 (M)	S7qPCRexfor	CTTCTAACCGAGGTCGAAACG	32-54	147
	S7qPCRexrev	GGATTGGTCTTGTCTTTAGCCA	159-179	

D. Material for protein analysis

Antibodies

Antibody	*Antigen*	*Supplier*
Anti-NS1 (Cat.-Nr. sc-17596)	NS1	Santa Cruz Biotechnology, Santa Cruz, USA
Anti-Mx1	Mx1	Georg Kochs (Uni Freiburg, Germany)
Anti-actin (Cat.-Nr. sc-1616)	Actin (I-29)	Santa Cruz Biotechnology, Santa Cruz, USA
Anti-ERK2 (Cat.-Nr. sc-153)	ERK2	Santa Cruz Biotechnology, Santa Cruz, USA
Peroxidase-conjugated donkey anti-rabbit (Cat.-Nr. 711-001-003)		Jackson ImmunoResearch, Suffolk, UK
Peroxidase-conjugated donkey anti-goat (Cat.-Nr. 705-001-003)		Jackson ImmunoResearch, Suffolk, UK

Fluorescent dyes

Name	*Supplier*
CyDye DIGE Fluor, Cy2 minimal dye (Cat.-Nr. 25-8008-60)	GE Healthcare, München, Germany
CyDye DIGE Fluor, Cy3 minimal dye (Cat.-Nr. 25-8008-61)	GE Healthcare, München, Germany
CyDye DIGE Fluor, Cy5 minimal dye (Cat.-Nr. 25-8008-62)	GE Healthcare, München, Germany

IPG Strips

Name	*Supplier*
Immobiline DryStrip pH 3-7, 24 cm (Cat.-Nr. 17-6002-46)	GE Healthcare, München, Germany
Immobiline DryStrip pH 3-11 NL, 24 cm (Cat.-Nr. 17-6002-45)	GE Healthcare, München, Germany

E. Detailed protocol for the identification of proteins

In-gel digestion for nanoHPLC-nanoESI-MS/MS

After separation, protein spots were picked from 2-D DIGE gels utilizing an Ettan spot picker (GE-Healthcare). The proteins were digested enzymatically in-gel and identified by nanoHPLC-nanoESI-MS/MS. Therefore, the picked protein spots were washed by alternating incubation (i.e.: shaking at room temperature for 10 min) in 200 µL 25 mM NH_4HCO_3(aq) (Fluka Ultra-grade, Sigma-Aldrich, Taufkirchen, Germany) and 200 µL 50 mM NH_4HCO_3(aq) – acetonitrile (1:1), respectively. Water and acetonitrile used for protein identification were high-quality (Riedel-de-Haën Chromasolv LC-MS grade, Sigma-Aldrich, Taufkirchen, Germany). Both steps were repeated twice. A final washing step with 400 µL pure acetonitrile led to dehydration and shrinking of the protein spots. The washed protein spots were dried by centrifugal vacuum evaporation in a SpeedVac SPD121P (Thermo Electron, Dreieich, Germany) for 10 min at RT. The protein spots were pre-incubated each with 5-10 µL ice-cold protease solution (modified porcine trypsin: Sequencing Grade, Promega, Mannheim, Germany, at 0.02 µg/µL in 25 mM NH_4HCO_3(aq)) and stored at 4°C until they were re-swollen. Digestion was performed overnight at 37°C.

Sample preparation for nanoHPLC-nanoESI-MS/MS

Digestion was stopped by adding 30 µL 1% v/v trifluoracetic acid (TFA; Fluka puriss p.a. eluent additive for LC-MS, Sigma-Aldrich) in water (TFA(aq)) and incubating the protein spots for 30 min by shaking at 37°C. The supernatant of this first extraction was removed and stored at 4°C. For a second peptide extraction step 30 µL 1% v/v TFA in 75% v/v H_2O / 25% v/v acetonitrile was added, a third extraction step was performed adding 30 µL 1% v/v TFA in 50% v/v H_2O / 50% v/v acetonitrile. For both steps, the protein spots were incubated as described before and the corresponding supernatants were removed and pooled with the previous extract. In a next step, the peptide extraction pools were shock-frozen at -180°C (by dipping the microcentrifuge tubes into liquid nitrogen) and dried below 5 µL (not to dryness) by centrifugal lyophilization (SpeedVac SPD121P). The final sample volume of 10 µL was obtained by adding the appropriate amount of 0.1% v/v TFA(aq). These samples were used directly for nanoHPLC-nanoESI-MS/MS analysis or stored at -80°C until analysis.

Online pre-concentration and separation of peptides

A set of capillary- and nanoHPLC instruments of the 1100 Series (Agilent, Waldbronn, Germany) connected in series, did allow fully automated online pre-concentration and separation of the tryptic digested samples. 8 µL of each sample were drawn by the cooled micro-HPLC autosampler (1100 Series microWPS; G1377A) and injected onto a C18-

precolumn (300 µm ID * 5 mm packed with C18-PepMap, 100 Å pore size, 5 µm particle size, Dionex, Idstein, Germany, adapted to the Agilent 1100 System) for concentration to a 350 nL sample volume. This was done by stacking and desalting the peptides onto the pre-column at a flow rate of 10 µL/min 0.05% v/v TFA(aq), generated by the capillary-HPLC pump (1100 Series CapPump; G1376A). These pre-concentrated digestion mixtures were eluted directly from the pre-column and separated onto a nano-column by switching the pre-column from capillary-HPLC flow into nanoHPLC flow (using the MicroValve 2/10; G1163A). A nanoHPLC pump (1100 Series NanoPump; G2226A), running at a column flow-rate of 300 nL/min, was used for gradient elution of the sample. NanoHPLC was performed on a C18-nano-column (75 µm ID * 150 mm packed with C18-PepMap, 100 Å pore size, 3 µm particle size, Dionex, adapted to the Agilent 1100 System). An elution gradient (solvent A: 0.1% v/v formic acid (FA; Fluka puriss p.a. eluent additive for LC-MS, Sigma-Aldrich) in 98% v/v H_2O / 2% v/v acetonitrile versus solvent B: 0.1% v/v FA in 20% v/v H_2O / 80% v/v acetonitrile) started at 0% solvent B and increased to 50% solvent B within 30 min.

Online acquisition of ESI-MS/MS peptide spectra

Detection was carried out by online coupling nanoHPLC with nanoESI-MS/MS via start/stop trigger signals. MS and MS/MS spectra were recorded on a QSTAR XL (QqTOF) mass spectrometer (Applied Biosystems/MDS/Sciex, Darmstadt, Germany) equipped with an online nano-electrospray ion source (NanoSpray II Source) and upgraded with a heated interface. Peptides eluting from the nano-column were electrosprayed via an online electrospray needle (uncoated SilicaTips (OD 360 µm / ID 20 µm/Tip ID 10 µm), New Objective, Woburn, MA, USA) and were focused into the mass spectrometer. The following ESI parameters were used: Needle voltage 2.6 kV, ion source gas 12 psi, curtain gas 12 psi, interface temperature 140°C, declustering potential 60 V, focusing potential 220 V, declustering potential 15 V, collision gas 4 (dimensionless parameter setting). Utilizing Analyst QS software (version 1.1, Applied Biosystems/MDS/Sciex) full scan and product ion spectra were collected in an information dependent acquisition mode. IDA-mode settings included continuous cycles of one full TOF-MS scan from 385-1610 m/z (1s) plus three product ion scans from 150-1610 m/z (enhance all, 1s each). Precursor m/z values were selected from a peak list (ion charge state 2-4, ion cut-off >10 counts, exclusion of isotopes), generated automatically by Analyst QS from the previous TOF-MS scan during acquisition, starting with the most intense ion. The collision energy was set to rolling collision energies, dependent on the m/z value of the precursor ion. Furthermore, the data was collected in profile mode and dynamic exclusion was used for data acquisition with an exclusion duration of 90 s for former target ions and an exclusion mass width of ± 0.05 mmu.

Data processing and interpretation of ESI-MS/MS spectra

For automatic database search of product-ion spectra of HPLC-ESI-MS/MS analysis, MASCOT (version 2.2, Matrix Science) was used to identify corresponding peptides. For all searches, algorithm screened actual NCBI non-redundant database were used. Search parameters: Species, mammals; tryptic digest with a max. of one missed cleavage; no fixed modification; variable modifications, oxidation of methionine (M) and carbamidomethylation (C) of cysteine; peptide masses were assumed to be monoisotopic; mass tolerance of 0.1 Da for the precursor ion and 0.07 Da for product ions. For final confirmation at least two product-ion spectra of different peptides of each identified protein were verified.

F. Standard operating procedures (SOPs)

Nr. Z/ 01: determination of the cell count

1.0 Intention

Determination of the total cell count and of the living cell count in a trypsinize cell culture or in a suspension culture (to calculate the density of the follow- up culture for example). The colourant trypan- blue can only penetrate in death cells. Living cells are uncoloured and are silhouetted against the blue- grey background.

2.0 Materials

- aliquot of a trypsinize culture or suspension culture
- 1.5 mL- reaction tube, sterile
- 15 mL Falcon, unsterile
- microliter pipette (100 and 1000 µL) and tips
- PBS
- Trypan- blue solution 0,5%, filtrated; firm: Merck; order.Nr.: 1.11732.0025 attention toxic! Wear protection gloves!
- Fuchs-Rosenthal-counting chamber (chamber depth 0.2 mm, 16 big quadrates per 1 mm^2, 16 small quadrates for each big quadrate
- Microscope with objective x10 (phase contrast)

3.0 Methods

3.1 Preperation of the trypan- blue solution

- 18 g NaCl; firm: Merck; order.Nr.: 1.06400.5000 and 10 g trypan- blue; fill up with Milli-Q-water up to 1000mL and use a big fluted filter to filter the solution
- working solution: 1:2- dilution of the stock solution with de- ionise water
- trypan- blue is durable at 5-30°C; leftovers are hazardous waste and will be dispose by the chemical commissioner
- trypan- blue is durable for ~6 month
- the concentration of the colourant will be reduced after the creation of aggregates; in this case don't use the solution anymore

3.2 Preparation of the cells

- stop the cells with FCS after trypsinization
- take one sterile aliquot from the trypsinized culture or from the suspension culture (for example 1mL) and transfer it into a 15mL- Falcon tube

3.3 Determination of the cell count

- clear the surface of the counting chamber and the cover glass with 70% ethanol
- breath on the counting chamber and apply the cover glass; maybe move the cover glass until you see (so called) Newton rings ('rainbow')
- dilute the cell aliquot 1:10 with trypan blue solution (1 mL cell suspension + 9 mL trypan blue solution), mix it carefully
- fill the counting chamber by using a 100 µL microliter pipette (put the pipette at the edge of the counting chamber; the capillary force suck the solution into the gap between chamber and cover glass
- place the chamber under the microscope
- count 5 quadrates of 16 (do not count cells on lines twice; cell cluster comply with 2 cells) and built the sum
  → example: see figure

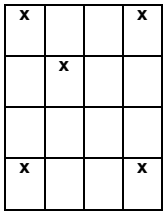

- the determination is more exactly by using both counting chambers (over and under the stay) and build the arithmetic mean
- cell concentration/mL = arithmetic mean of the sum x 10^4
- total cell count = cell concentration/mL x volume of the cell suspension
- % living cells = uncoloured (living) cells : (uncoloured cells + coloured cells) x 100
- if cell count is too high use a dilution 1:100 (mix 100µL cell suspension, 900µL PBS, 9mL trypan blue solution in a 15mL Falcon- tube) and count the cells like description above
- calculation: cell concentration/mL = arithmetic mean of the sum x 10^5
- if you have to repeat the cell counting use a new sample preparation because trypan blue affect toxic and with rising incubation time the count of living cells will be reduced
- dilution of the culture with growth medium until reaching the required density and volume (see work instruction Z/04) - if its necessary to freeze the cells (see work instruction Z/06)

3.4. Example for determination of the cell count

- 40 mL cell volume
- mix 1mL of the cells with 9mL of the trypan blue solution
- total cell count = 8.5 x 10^5 x 40 mL = 3.4 x 10^7 (cells in 40 mL volume)

4.0 Storage

- filtrated 0.5% trypan blue solution is durable ca. 6 month at room temperature; the solution could aggregate by overrun the durability

Nr. G/ 21: ViCell XR counting device

The Vi-Cell XR Cell Viability Analyzer is a video imaging system used to automatically analyze mammalian cells. It automates the trypan blue exclusion protocol, in which dead cells take up the dye while live cells do not, and provides data on % viability & cell counts. The Vi-Cell takes up the sample and delivers it to a flow cell and camera for imaging where differences in the grey scale between live & dead cells are determined by the software.

1. Attention should be paid for:

- Each person who will be using the Vi-Cell system must be trained by a briefed person
- Do not use unfiltrated microcarrier suspension
- Validated working range (cell type ‚MDCK 100': 9.6*10^4-1.0*10^7 cells/mL, total cell count)

2. Material:

Original products from Beckman Coulter:

Nr. 383260	Single Pack	250 measurements, reagents/ sample cups (~240 Euro)
Nr. 383194	Quad Pack	1000 measurements (4x Single Pack; ~845 Euro)
Nr.		sample cups (ViCell cups)

Wash sample cups and use it several times. Reagent packs contain the different components or should be made by oneself:

- Trypan blue solution: 0.4 w/v Trypan blue + 0.15 mol/L NaCl (use VE-Water)
- Filtrate with paper filter followed by 0.45 µm filtration

- Desinfection solution: Isopropanol (2-Propanol), 90%
- Wash solution: Beckman Coulter Clenz (Nr. 8448222, 5 L)
- Buffer solution: dH_20

Used reagent volume for 250 measurements:
Trypan blue: about 110 mL; other reagents: about 220 mL

Refill of reagents:
If the reagent pack is empty, choose under menu 'instrument', 'Replace reagent pack' follow-up the instructions steps.
Do not use a new reagent pack, refill the old one with corresponding volume (110, 220 mL).
Decant the waste bottle in a schott-flask, autoclave and dispose it into the trypan blue waste.

3. Switch on and off:

Switch on:
- For switching on ViCell press power button at the back
- Switch on computer and start Software 'ViCELL XR 2.03'

Switch off:
- Switch off software, afterwards switch off computer
- Switch off ViCell

4. Running a sample:

Preparation of the cell suspension:
- Sample volume: min. 0.5 mL, max. 1.5 mL per sample cup
- Concentration range (manufacturer specifications): $1.0 * 10^4 – 1.0 * 10^7$ cells/mL
- Dilute samples with > $1.0 * 10^7$ cells/mL
- Samples with carrier must be filtrated (<100µm)(e.g. Partec Celltrics 100 µm, Nr. 04-0042-2318); Becton Dickinson Bioscience Discovery Labware, Cell strainer, 70 µm, Nr. 352235)

1. Put sample only in original sample cup.
2. Place sample cup in next available carousel position.
3. Log in sample on the computer by clicking on the Log in sample button:
   a. Select cup position on carousel
   b. Enter your Sample ID (the software is smart and will increment multiple samples)
   c. Choose a Cell type (*first time choose default)
   d. Select a dilution factor
   e. Click OK or Next sample to enter additional sample data (*once start the continue to enter samples, so it saves time to start the queue first)
4. From the navigation menu, choose Autosampler queue to see samples in queue.
5. From this screen, you can also edit/remove samples in queue while a run is in progress.
6. Click on Start queue to begin sample analysis. Once the run begins, sample will disappear from the queue and you will only see it on the main screen. The bottom of the screen will tell exactly what the instrument is doing (i.e. mixing trypan blue, loading flow cell, etc) and right side displays the run data (i.e. image #,% viable, cell count). Measuring time about 3 min.
7. storage location (excel sheet): local or at the network
   c:\daten\ViCell\Excell\
   h:\bio\daten\vicellxr\Excell\

5. Measurement of infectious samples:

Pay attention to the following specifics:
- Before measuring, frame and waste bottle
- Fill virus sample in sample cups only under the hood
- After measurement: put sample cups of the frame and waste bottle in virus waste and desinfect the frame

Nr. A/02 Bioprofile

Version: 1.0 (07.04.2010) Author: Verena Lohr

Determination of basic extracellular metabolites

1.0 Intention

With the help of the Bioprofile concentrations of extracellular metabolites, e.g. ammonia, glucose, lactate, glutamine or glutamate could be measured in cell culture supernatants.

2.0 Materials

- Centrifuge Multi-spin PCV-3000, Grant Instruments (N1.07)
- Centrifuge Biofuge primo R, Heraeus (N1.06)
- Heating block (N1.06) Vortex (N1.07)
- BioProfile lOOPlus (N1.07)
- 1000 JlL- pipette
- Standards for dilution series for BioProfile (-80°C Freezer)
  - Glucose in PBS
  - Glu, Gln, Lac, Amm in GMEM (GMEM without Glc, Sigma #G5154)

3.0 Methods

3.1 Sample preperation

1.6 mL sample volume is needed; microcarrier, cell impurities should be removed via centrifugation.

Adherend cells
Supernatants of adherend cells cultered in microtiter plates, t-flasks or rollerbottles could be directly used. Adherend cells on micro carrier: supernatants should be centrifuged (5000xg, 5 min) before use.

Suspension cells
Centrifuge cell supsension 1000 x *g* 1min and use the supernatant for measurement. Heat sample from infection experiments (mock, growth and infection phase for comparability) at 80°C for 3 min (accounting for virus inactivation & glutamate degradation). In case of infection series samples should be stored at -80°C and measured in parallel.

3.2 Sample measurement

The instruction manual G_22 for BioProfile lOOPlus should be read before usage and persons should trained by a briefed person.

Before measurment
Check under „Status“ the fill level of reagent pack (full = 350 samples, 2 weeks usability after insertion). Check under „Status“ the flow rate (flow rate < 3.5 sec).
“C” behind the respective metabolite means calibrated and “NC” not calibrated. If “NC” occurs than contact a responsible person (Clandia Best, Ilona Behrendt and Verena Lohr).

Measurement
Thaw the samples and standard dilution series of all metabolites on ice for 6h or at RT for 1-2h. Vortex the samples and standards. Fill the auosampler in following order:

1. Glucose standards, randomized
2. Other standards, randomized
3. Samples randomized

Randomization is necessary due to systemic errors and drift in measurements. Only single assay run is needed, due validation of single run. Per sample 3€ and 3 min is needed.
After sample measurement the 6 standards should be measured another time per hand.

After measurement
Order of the sample should be noted carefully and validated concentration range should be compared. Higher concentrations should be diluted 1:2 or 1:3 with PBS, vortexed and measured again.

3.3 Analysis

Raw data should be writen in excel file due to fading of the thermo paper print outs. The respective BioProfile files are archived in BPT-folder under H:/bpt/usp/Labor/ Bioprofile_calibration_curves/201O/Quartal_1 (respective year and quarter).
Enter the two values of the standards. A mean value is builded and automatically put in a diagram. The equation of the calibration curve is directly transmitted. Only parameters of square function should be transfered by hand.
Measured values could be writen in other tabs. Under "Documentation" the date, person parameters of the service pack (expiry date, Lot number).

4.0 Explanatory notes

Effect of pH on measurement

Even pH have an influence on measurements. Therefore, thawed samples should not be allowed to stand in the auto sampler to long due to CO_2 gasing. Critical samples should be measured by hand or in shorter sequences or the pH must be checked afterwards (significant changes of >1).

Repeated measurements
Samples of one experiment should be measured in parallel and re-measuring should be avoided.

Effect of salts on measurement
Effects of salt concentration on measurements were till now only tested in GMEM. Other media were not tested and could have other effects than GMEM which should be taken into account when used.
The following table should give hints on effects of different salts and concentrations on measurements with the bioprofile.
Notice that with addition of 20mM NaHC03 in PBS glutamate could be detetected (increasing glutamate concentration with increasing NaHC03 concentration till 200 rnM) neither no glutamate is added in PBS.

Salt	Conc. [mM]	Influence on	Influence with increasing salt conc.?
NaCl	50-250 mM	Glucose	Decrease clearly
NaCl	50-250 mM	Osmolality	Decrease clearly
NaHC03	20-200 mM	Glucose	Decrease clearly
NaHC03	20-200 mM	Glutamate	Increase clearly
NaHC03	20-200 mM	pH	Increase
NaHC03	20-200 mM	Osmolality	Increase clearly
Mg2S04	0.5-I0 mM	Glucose	Decease
CaCl2	0.5-I0 mM	Glucose	Decease
CaCl2	0.5-10 mM	Glutamate	Decease
KCl	0.5-I0 mM	Glucose	Decease
KCl	0.5-10 mM	Ammonia	Increase

Nr. V/05 HA-Assay

Version: 2.2 (20.01.2011) Author: Verena Lohr

Hemagglutination assay (HA assay)

This SOP is based on the SOP written by Bernd Kalbfuß, Version 2.1 (04.12.2006)

1. Introduction

The HA assay is used to detect influenza virus particles (infectious and non-infectious). Influenza viruses carry the protein hemagglutinin (HA) on their surface which binds to specific glycosylation patterns on proteins which are located on the outer membrane of a cell. Thus, virus particles bin to cells and by using erythrocytes as cell system, influenza virus particles can cross-link erythrocytes with each other. This agglutination of erythrocytes can be observed in wells of a round bottom well plate as agglutinated erythrocytes sediment like a carpet at the bottom of the well instead of a point-like sedimentation.

By titrating the virus containing sample, one can determine a critical concentration of the sample at which this switch in sedimentation behaviour occurs. The negative logarithm of this dilution has been defined as the logarithmic HA titer (or simply log-titer) and is a measure for the concentration of influenza virus particles in the sample. The inverse of the dilution has been termed HA activity with units HAU/100 µL and is also supposed to be proportional to the number of virions in the sample.

There are two ways in which one can analyze the HA assay (procedure of pipetting is the same for both methods):

i) a classical analysis in which the experimenter visually evaluates the HA titer
ii) a photometric analysis which uses an automated procedure in order to minimize subjectivity and which includes an additional dilution step that increases sensitivity and reduces the error of the method

2. Material

- Protective clothing: lab coat, protective gloves (Nitrile)
- Centrifuge (e.g. Primo R, Hera, N1.06)
- Sterile kryotubes
- Influenza virus samples (active or chemically inactivated)
- Internal HA standard (= control which is an chemically inactivated influenza virus sample with defined HA titer, stored at -80°C in N1.11, produced as described in SOP HA assay from Bernd Kalbfuß, Version 2.1 (04.12.2006))
- Erythrocyte suspension (conc. approximately 2.0×10^7 erythrocytes/mL, stored at 4 °C in N1.06, produced as described in SOP V/07 from Claudia Best (07.06.2007))
- Unsterile phosphate buffered saline, PBS (stored in N1.06, produced as described in SOP M/01 from Claudia Best (26.09.2007))
- Unsterile transparent 96well round bottom microtiter plates (stored in N1.06, e.g. Greiner Bio-One, Cat.No. 650101) + transparent disposable lids (stored in N1.06, e.g. Greiner Bio-One, Cat.No. 656101)
- 100 µL micropipette + disposable tips
- 8x100 µL or 8x300 µL multichannel micropipette + disposable tips
- Electronic 8x1200 µL multichannel pipette + 1250 µL disposable tips
- 2 reservoirs for multichannel micropipette (PBS, erythrocyte suspension)
- Plate photometer (e.g. Tecan spectra, Tecan Instruments, N1.07)

3. Sample preparation

Infected cell culture with cells and without microcarrier should be filled directly into sterile kryotubes or other sterile tubes and centrifuged at 300 x *g* for 5 min at 4 °C. If cells can not be settled at this g force, choose an appropriate centrifugation setting. After the centrifugation step transfer the supernatant into a new sterile kryotube and freeze at -80 °C.

4. Assay procedure

It is absolutely necessary to pipet exactly in this assay!!

Active samples have to be handled under S2 work bench! For handling outside the safety hood (e.g. when scanning the microtiter plate with the spectrometer), keep disinfectant or citric acid ready in case of accidental spillage!

4.1 Classical method

The titration of influenza virus by the classical method is based on the method described by Mahy and Kangro [1].

1. Pre-dilute samples which are known to be highly concentrated in PBS (all samples which have a HA activity above 3.0 log HA units/100 µL should be diluted). Typically, a 1:10 pre-dilution is sufficient. Samples from cell culture normally do not require this pre-dilution. However, this has to be decided from the assay performer.
2. Fill the wells of column 2-12 with 100 µL PBS each. Wells B, D, F and H of column 1and 2 are filled with 29.3 µL PBS.
3. Perform the following steps with a 100 µL pipette under S2 work bench! Don't spray disinfectant onto reservoirs and microtiter plates.
   The wells 1 and 2 of row A are filled with 100 µL of internal HA standard. Beneath these, a pre-dilution of internal HA standard is prepared by adding 70.7 µL of HA standard to wells 1 and 2 of row B. These 4 wells are prepared accordingly for the samples in rows 3 to 8. This means that on each plate 3 samples can be prepared. If there are more samples, an additional plate is necessary. Standard is necessary on every second plate.

Pipetting scheme for pipetting internal HA standard and samples onto microtiter plate

	1	2	3
A	100 µL HA standard	100 µL HA standard	…
B	70.7 µL HA standard 29.3 µL PBS	70.7 µL HA standard 29.3 µL PBS	...
C	100 µL sample 1	100 µL sample 1	…
D	70.7 µL sample 1 29.3 µL PBS	70.7 µL sample 1 29.3 µL PBS	…
E	...	...	…

4. Mix column 2 three times with a multichannel pipette and transfer 100 µL of column 2 to column 3. Empty the pipette tips completely once before the transfer. Mix again three times and continue the serial dilution until the end of the plate (column 12). The remaining 100 µL should be disposed. Each well has to be filled with 100 µL after finishing these steps. Add 100 µL of erythrocyte suspension into each well by using an electronic multichannel pipette. Mix the suspension well before you start! Start pipetting

at the column with the highest dilution (column 12. *For each plate new tips have to be used!*

5. Each well which has been pipetted faulty should be marked as the values from these wells need to be eliminated during assay evaluation!
6. Incubate the plates for at least 3 hours under the work bench. If the assay is not analyzable, incubation must be prolonged (over night if necessary).
7. Evaluate the results visually. Therefore, mark every well which shows a perfect erythrocyte dot with a (●) and each imperfect dot with a (○). Record your findings by taking the document "AB-HA_Testauswertung_3.pdf". The last dilution with an imperfect dot is the end point of the titration and is expressed as log HA units per test volume (100 µL). The inverse of this dilution gives the HA activity [HAU/100 µL].
8. Compare the measured titer of the internal standard with its nominal titer. The difference (*nominal-measured*) has to be added to the titer of each sample. If two or more standards were analyzed (e.g. because 3 plates were assayed) use the mean difference. If the measured titer of internal standard is more than 0.3 log HAU/100 µL different from its nominal titer, re-do the whole assay!
9. After evaluation of the titer microtiter plates scan them (see section 4.1) or dispose them into S2 waste!!

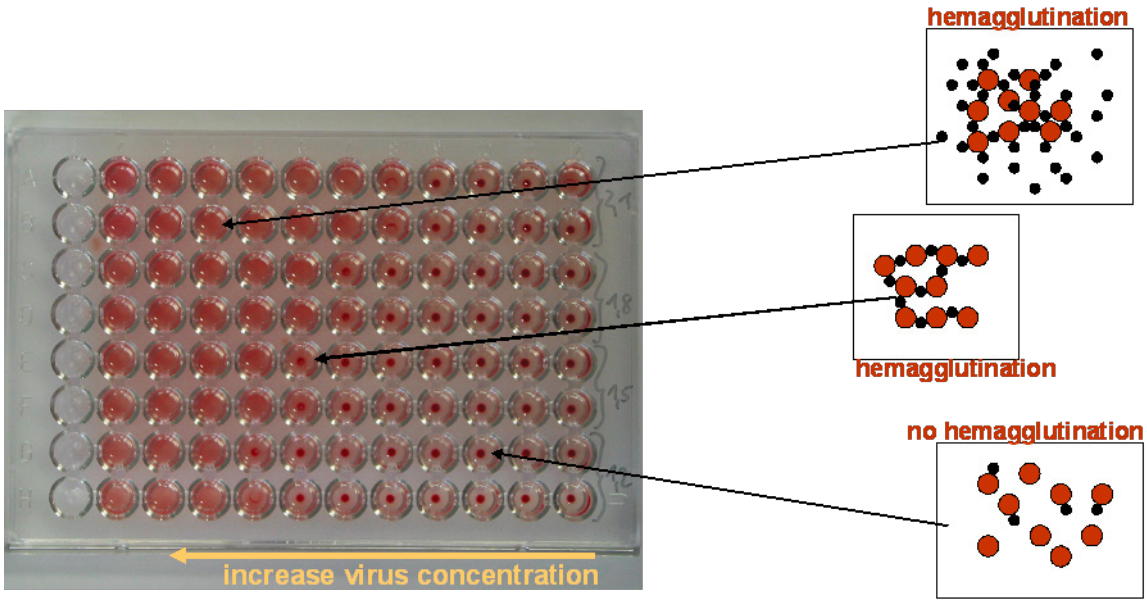

Scheme for determination of HA titers in micro titer plate (example shows HA titers from 1.2-2.1 log HA units/100 µL in double determination)

Overview on dilutions and resulting HA titers (log HA units/100 µL)

	1	2	3	4	5	6	7	8	9	10	11	12
Dilution	1:1	1:2	1:4	1:8	1:16	1:32	1:64	1:128	1:256	1:512	1:1024	1:2048
HA titer (100 µL sample)	0	0.3	0.6	0.9	1.2	1.5	1.8	2.1	2.4	2.7	3.0	3.3
HA titer (70.7 µL sample)	0.15	0.45	0.75	1.05	1.35	1.65	1.95	2.25	2.55	2.85	3.15	3.45

4.1.1 Points to consider

- The detection limit of this assay is 0.15 log HAU/100 µL. This corresponds to approximately $2.0x10^7$ virions/mL; assuming that the number of erythrocytes is proportional to the number of virus particles (each virus particle binds to one erythrocyte).
- The assay has been validated with a standard deviation of +- 0.03 log HAU/100 µL which is the dilution error.
- The confidence interval for HA activity was determined to be +15/-13 % (with a confidence level of 95 %).
- The validation has been made for the assay procedure which is described here. If you change singular steps in your procedure, be aware that validation is not valid then.
- Before you start with serious analyses, train yourself in pipetting accurately and precisely, e.g. by measuring standard samples several times.
- HA activity may suffer depending on sample treatment and storage conditions. Thus, do not freeze a measured sample and re-thaw it. Probably, HA titer has then been changed.

4.2 Photometric analysis

In order to minimize subjectivity (dependence on the experimenter), the titration result is evaluated photometrically using an automated procedure. However, this evaluation is restricted to samples with titer >1.0 log HAU/100 µL. Otherwise, sample titers have to be evaluated with the classical method.

4.2.1 Measurement of extinction

1. Perform all steps which are described for the classical method.
2. Cover microtiter plates containing active virus samples with an appropriate lid.
3. Make sure that Tecan photometer is switched on. Open the software “iControl” and choose “HA protocol” from the list of used protocols. The settings should be defined as follows: Messfilter 700 nm, Referenzfilter none, 10 Blitze, Temperatur 0.0 °C, Schüttelmodus none. (Changes can be made by clicking on button “Messparameter definieren”, but should not be done for standard HA protocol.)
4. After having inserted the plate into the reader, click the button “Messung starten”. You will be asked for a file name first and to put your plate onto the tray afterwards. The measurement will be carried out immediately afterwards.
   It is of utmost importance to remove either the lid before scanning and to remove any condensed water from the bottom of a microtiter plate before scanning!!
5. Save extinction data as Excel-file in the folder “/bpt/data/Tecan/HA_assay/2010/…” using the file name pattern “<Number>-<Date>_<Experimenter>.xls (e.g. 145_10-03-31_CB). If more than one plate will be measured, let the excel file from the first plate open. Then, the results from the following plate will be saved as a new sheet in this file. You have to rename the sheets after your measurement in order to document which sheet belongs to which plate.
6. Repeat step 4 and 5 for each plate of the assay run.

4.2.2 Evaluation of HA titers

A data evaluation template (Excel-file) has been prepared. The evaluation procedure is described in the following. You have to enable macros for the sheet to work properly!

7. Open the data evaluation template (“/bpt//Labor/HA_neu/Data_Evaluation_ Template.xls”) and save a copy in the appropriate folder (/bpt/usp/Labor/HA_neu/data/2010/...).

8. Import your extinction data. Therefore, copy all values and paste them into data-sheet. Delete extinction values of all wells that suffered from erroneous pipetting! As long as affected wells are not within the zone of transition, the assay result may be unaffected.
9. Adjust the sample names and dilutions in the “Report” sheet. Fill all empty header fields and transfer the remarks from the run protocol. Specify the internal standard used and the position of the internal standard (normally, position 1 and 9). If only one standard was measured, specify the same position twice.
10. Click “Evaluate” to start HA titer evaluation.
11. Check difference between nominal titer of the standard and the evaluated titer. Re-do the assay if both values differ more than 0.3 log HAU/100 µL.
12. Check all fitted curves in the “Evaluation” sheet. If fitting of extinction values has not been made by a sigmoidal curve, then re-analyze the sample. Be careful, if this maybe is due to a low titer of the sample. Then take titers evaluated by the classical method.

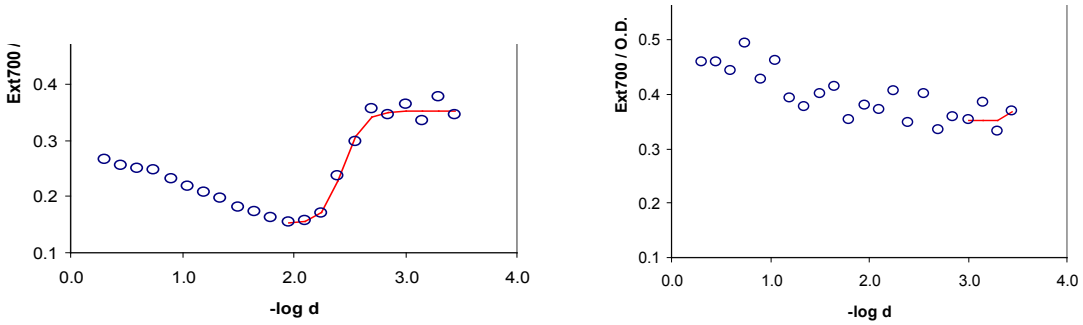

Evaluation of the transition point by a Boltzmann function. Left: correct fitting, right: erroneous fitting which would lead to high titer evaluation if curve is not checked and rejected

13. Compare the evaluated titers with the results obtained by the classical method. The discrepancy should be less than 0.3 log HAU/100 µL.
14. Save the document and make at least one hardcopy of the “Report” and “Evaluation” sheets. Documents are collected in a folder located in N1.07 and N0.13.

5. Sample storage

If samples are kept at below -70 °C, they can be stored up to five years without loss of HA activity. Anyway, this holds true for samples which have been prepared as described in this document (see sample preparation). After this period, it cannot be guaranteed that measured HA activities resemble the original values.

[1] Mahy B.W.J., Kangro H.O. "Virology Methods Manual": Academic Press Limited, 1996.

Nr. V/08 $TCID_{50}$-Assay

Version: 2.0 (23.03.2010) Author: Verena Lohr

Active virus titration- $TCID_{50}$ assay

1. Introduction

Determination of virus concentration of which 50% of adherent cells are infected.

2. Material

2.1. Cell culture and virus propagation

- 4-8 days old confluent MDCK cells in cell culture flasks (T175 or RB)
- Sterile PBS (SOP Nr. M/01)
- Trypsin 10000BAEE/mL in Milli-Q water, filtrated (trypsin, sigma, T-7409), store at -70°C
- Cell culture media (GMEM + 1% Lab-M-Pepton + 10% FCS) SOP Nr. M/04
- VVM (GMEM + 1% Lab-M-Pepton) SOP Nr. M/04
- Gentamycin 10 mg / mL (Invitrogen, 11130-036) store at room temperature
- 96-well plate 400µl volume with flat bottom and cap (Cellstar, Greiner bio-one, 655180)
- Reaction tubes 1.5 mL, sterile for dilution series
- Sterile pipettes, pippetor, 100µl pipette
- Electronic one-chanel pipette, 10 0µl (Eppendorf)
- Electronic multichannel pipette, 1mL (Eppendorf)
- Pipette tips, 100µl (Plastibrand, sterile); Pipette tips, 1250µl (Eppendorf, sterile)
- Multipette with combitips 10mL (Eppendorf, combitips plus biopure)
- 1 sterile Schott-flasks (250, 500mL); 4 pipette trays, sterile; 2 small lab trays, sterile
- Security advcice labels, biohazard

2.2. Fixation and staining

- 80% acetone solution in water (acetone, p.a.)
- primary antibody according to the virus tested
  e.g. Equine Influenza A anti-goat, final bleed, goat 613, nano Tools (1:100 diluted PBS)
  Influenza Anti A/Wisconsin/67/2005 H_3N_2 (HA Serum sheep) (NIBSC)
  Influenza Anti A/Wisconsin/67/2005 H_3N_2 (HA Serum sheep) (NIBSC)
  Influenza Anti A/PR/8/34 H_1N_1 (HA Serum sheep) (NIBSC)
- PBS sterile (SOP Nr. M/01)
- Confluent grown cell culture (T75, RB)
- Secondary antibody (Invitrogen, A-11015)
- 100 µL 8-Chanel-Pipette. Pipette tips
- Lab tray, 3 pipette trays, aceton waste vessel

3. Assay procedure

3.1 Cell culture and virus propagation

A) Cell culture

- wash three-times confluent grown MDCK cells in cell culture flasks with PBS, trypsinize with corresponding amount of trypsin (1 mg/mL) 20 min 37°C, stop with cell culture media (SOP Nr. Z/04)
- Mix cell culture media with gentamycin (100 mL with 1 mL gentamycin)
- Dilute trypsinized cells with cell culture media to 4-5* 10^5 Zellen / mL (SOP Nr. Z/01, G/21)
- For one cell culture plate 10 mL cell suspension is needed
- Pipette with 8-channel pipette 100 µl cell suspension to each well
- Incubate cells 1-2 d at 37°C, 5% CO_2 (after microscopical evaluation the cells should be confluent at this stage, otherwise the experiment has to be stopped)

B) Preperation of virus dilution

- Add trypsin and gentamycin to VMM (100 mL + 20 µl Trypsin + 1mL gentamycin) (100 mL is needed for about 10 dilution series)
- Pipette 900 µl VMM in 8-9 reaction tubes (corresponding to dilution step)
- Set up virus dilution to the following scheme in reaction tubes: pipette 100 µl of sample or standard in reaction tube, pipette up an down five-times for mixing, pipette 100 µl with a new tip in the next reaction tube, continue till the end

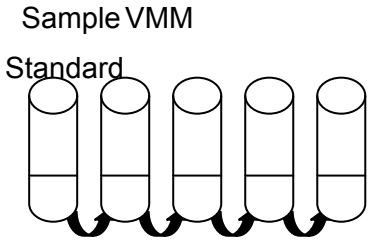

10^0	10^1	10^2	10^3	10^4	10^5	10^6	10^7	10^8

C) Virus propagation

- Wash cell culture plates two-times with 100 µl PBS with 8-channel pipette (emptying wash solution in lab tray)
- Pipette 100 µl virus solution to the 8 wells of the cell culture plate with highest dilution step
- Pipette only 100 µl VMM (with trypsin and gentamycin)per well to row 1, 2, 11 and 12 (Negativ control, boundary effects could be avoided)
- Dilution steps: HA above 2.7: $10^3 – 10^{10}$
  HA between 2.1-2.7 (standard seed virus for fermentation): $10^1 – 10^8$
  HA under 2.1: $10^0 – 10^7$

	1	2	3	4	5	6	7	8	9	10	11	12
A	VVM	VVM	**10^1**	**10^2**	**10^3**	**10^4**	**10^5**	**10^6**	**10^7**	**10^8**	VMM	VMM
B	VMM	VMM	**10^1**	**10^2**	**10^3**	**10^4**	**10^5**	**10^6**	**10^7**	**10^8**	VMM	VMM
C	VMM	VMM	**10^1**	**10^2**	**10^3**	**10^4**	**10^5**	**10^6**	**10^7**	**10^8**	VMM	VMM
D	VMM	VMM	**10^1**	**10^2**	**10^3**	**10^4**	**10^5**	**10^6**	**10^7**	**10^8**	VMM	VMM
E	VMM	VMM	**10^1**	**10^2**	**10^3**	**10^4**	**10^5**	**10^6**	**10^7**	**10^8**	VMM	VMM
F	VMM	VMM	**10^1**	**10^2**	**10^3**	**10^4**	**10^5**	**10^6**	**10^7**	**10^8**	VMM	VMM
G	VMM	VMM	**10^1**	**10^2**	**10^3**	**10^4**	**10^5**	**10^6**	**10^7**	**10^8**	VMM	VMM
H	VMM	VMM	**10^1**	**10^2**	**10^3**	**10^4**	**10^5**	**10^6**	**10^7**	**10^8**	VMM	VMM

- incubate plates with a security advice 1d 37°C, 5% CO_2

D) Trypsin addition

- Put trypsin and genatmycin to the virus (100 ml + 40 µl trypsin + 1 mL genatymcin)
- Pipette 100 µl to each well (to avoid contamination: pipett from right to left, starting with lowest dilution step)
- Incubate virus plate additionally 1d 37°C, 5% CO_2

3.2 Fixation and staining

A) Preperation of primary antibody

- Primary antibody of equine influenza A goat serum is a polyclonal antibody against equine influenza but also against cell components, therefore antibodies against cell components has to be absorpt otherwise they overlap fluorescence of virus antibody
- wash three-times 1-2 d old confluent cell culture flasks with PBS
- Put 1 mL of diluted primary antibody to T25 and 3 mL to T75-flask incubate 30 min 37°C
- Cleaned primary antibody should be stored at -20°C

B) Fixation

- Decant virus supernatant into a lab tray with 2% glacial acid under the hood and clean it up S2 and virus-compatible
- Pipette 100 µl cold acetone to each well (acetone had to be cooled on not in a fridge)
- Incubate cell culture plates 30 min on Eis for fixation → virus is now inactivated → additional steps could be done outside the hood
- Wash cell culture plates two-times with PBS (collect and clean it seperately)

C) Staining

- Dilute cleaned primary antibody of equine influenza A goat serum 1:100 with PBS
- Dilute the rest of the primary antibody 1:200
- Pipette 50 µl of primary antibody to each well (with 8-chanel pipette) and incubate 60 min 37°C
- Afterwards wash two-times with PBS
- Dilute secondary-antibody 1:500 with PBS
- Pipett 5 0µl of secondary-antibody dilution to each well and incubate 60 min 37°C
- Wash two-times with PBS, afterwards put 100µl PBS to each well

4.0 Anaylsis and calculation

- Analysis is done with a fluorescence microscope
- Each well with fluorescent cells (this means with virus) is positive counted (1), each well without fluorescent cells is negaitv (0) and noted in the worksheet
- Calculation is done with the equation of Spearmann and Kärber :

$$(\log \text{virions } 100\%) + (0.5) - \frac{\text{cumulativ } 100\ \%}{\text{Number of tests (per diltion)}} = \log \text{virions / } 100\ \mu L$$

Example:

	1	2	3	4	5	6	7	8	9	10	11	12
A	0	0	1	1	1	1	1	1	1	0	0	0
B	0	0	1	1	1	1	1	1	1	0	0	0
C	0	0	1	1	1	1	1	1	0	0	0	0
D	0	0	1	1	1	1	1	1	0	0	0	0
E	0	0	1	1	1	1	1	1	0	0	0	0
F	0	0	1	1	1	1	1	1	1	0	0	0
G	0	0	1	1	1	1	1	0	0	0	0	0
H	0	0	1	1	1	1	1	1	1	0	0	0

0	**0**	**10^{-1}**	**10^{-2}**	**10^{-3}**	**10^{-4}**	**10^{-5}**	**10^{-6}**	**10^{-7}**	**10^{-8}**	**0**	**0**

0: no virus, negative well; 1: virus, positive well

Dilution step	Number positive wells / total amount wells	Number positive wells cumulativ
10^{-5}	8 / 8	19
10^{-6}	7 / 8	11
10^{-7}	4 / 8	4
10^{-8}	0 / 8	0

Model calculation:
(-5) + 0.5 - 19/8 = - 6.875 = y ; $10^{6,875+1}$ virions / mL = 7.58 x 10^{7} virions/mL

5.0 Determination of reference value

For each prepared standard a two-time six-fold determination by two persons have to be done. By this procedure the mean value of the standard is determined, which acts as a reference value.

G. Statistical analysis – normal distribution test after David

Table G-1: Normal distribution critical values after David (David et al.*, 1954)*

Sample size n	Lower bound					Upper bound				
	Level of significance α									
	0.005	**0.01**	**0.025**	**0.05**	**0.10**	**0.10**	**0.05**	**0.025**	**0.01**	**0.005**
3	1.735	1.737	1.745	1.758	1.782	1.997	1.999	2.000	2.000	2.000
4	1.83	1.87	1.93	1.98	2.04	2.409	2.429	2.439	2.445	2.447
5	1.98	2.02	2.09	2.15	2.22	2.712	2.753	2.782	2.803	2.813
6	2.11	2.15	2.22	2.28	2.37	2.949	3.012	3.056	3.095	3.115
7	2.22	2.26	2.33	2.40	2.49	3.143	3.222	3.282	3.338	3.369
8	2.31	2.35	2.43	2.50	2.59	3.308	3.399	3.471	3.543	3.585
9	2.39	2.44	2.51	2.59	2.68	3.449	3.552	3.634	3.720	3.772
10	2.46	2.51	2.59	2.67	2.76	3.57	3.685	3.777	3.875	3.935
11	2.53	2.58	2.66	2.74	2.84	3.68	3.80	3.903	4.012	4.079
12	2.59	2.64	2.72	2.80	2.90	3.78	3.91	4.02	4.134	4.208
13	2.64	2.70	2.78	2.86	2.96	3.87	4.00	4.12	4.244	4.325
14	2.70	2.75	2.83	2.92	3.02	.95	4.09	4.21	4.34	4.431
15	2.74	2.80	2.88	2.97	3.07	4.02	4.17	4.29	4.44	4.53
16	2.79	2.84	2.93	3.01	3.12	4.09	4.24	4.37	4.52	4.62
17	2.83	2.88	2.97	3.06	3.17	4.15	4.31	4.44	4.60	4.70
18	2.87	2.92	3.01	3.10	3.21	4.21	4.37	4.51	4.67	4.78
19	2.90	2.96	3.05	3.14	3.25	4.27	4.43	4.57	4.74	4.85
20	2.94	2.99	3.09	3.18	3.29	4.32	4.49	4.63	4.80	4.91
25	3.09	3.15	3.24	3.34	3.45	4.53	4.71	4.87	5.06	5.19
30	3.21	3.27	3.37	3.47	3.59	4.70	4.89	5.06	5.26	5.40
35	3.32	3.38	3.48	3.58	3.70	4.84	5.04	5.21	5.42	5.57
40	3.41	3.47	3.57	3.67	3.79	4.96	5.16	5.34	5.56	5.71
45	3.49	3.55	3.66	3.75	3.88	5.06	5.26	5.45	5.67	5.83
50	3.56	3.62	3.73	3.83	3.95	5.14	5.35	5.54	5.77	5.93
55	3.62	3.69	3.80	3.90	4.02	5.22	5.43	5.63	5.86	6.02
60	3.68	3.75	3.86	3.96	4.08	5.29	5.51	5.70	5.94	6.10
65	3.74	3.80	3.91	4.01	4.14	5.35	5.57	5.77	6.01	6.17
70	3.79	3.85	3.96	4.06	4.19	5.41	5.63	5.83	6.07	6.24
75	3.83	3.90	4.01	4.11	4.24	5.46	5.68	5.88	6.13	6.30
80	3.88	3.94	4.05	4.16	4.28	5.51	5.73	5.93	6.18	6.35
85	3.92	3.99	4.09	4.20	4.33	5.56	5.78	5.98	6.23	6.40
90	3.96	4.02	4.13	4.24	4.36	5.60	5.82	6.03	6.27	6.45
95	3.99	4.06	4.17	4.27	4.40	5.64	5.86	6.07	6.32	6.49
100	4.03	4.10	4.21	4.31	4.44	5.68	5.90	6.11	6.36	6.53
150	4.32	4.38	4.48	4.59	4.72	5.96	6.18	6.39	6.64	6.82
200	4.53	4.59	4.68	4.78	4.90	6.15	6.39	6.60	6.84	7.01
500	5.06	5.13	5.25	5.37	5.49	6.72	6.94	7.15	7.42	7.60
1000	5.50	5.57	5.68	5.79	5.92	7.11	7.33	7.54	7.80	7.99

H. Detailed raw-data of viral RNA time course experiments

Table H-1: Raw data of C_q, viral RNA molecule number and HA titer of segment 4 (HA)

hpi	vRNA(-)		cRNA(+)		vmRNA(+)		Log HA
[h]	C_q	Molecule/cell	C_q	Molecule/cell	C_q	Molecule/cell	[Units/100 µL]
0	20.12	86.8	31.23	0.1	28.81	0.2	0.0
0.5	20.92	50.5	30.53	0.2	28.35	0.3	0.0
1	22.25	20.56	29.32	0.2	26.51	1.0	0.0
1.5	22.83	13.9	27.55	0.2	24.98	2.8	0.0
2	22.31	19.7	24.59	0.4	21.76	22.9	0.0
2.5	22.15	22.0	22.99	14.6	20.28	60.7	0.0
3	21.32	38.5	21.70	9.2	19.10	132.3	0.0
3.5	20.84	53.3	20.79	53.5	18.18	241.9	0.0
4	18.07	347.0	18.05	102.8	15.21	1715.0	0.0
5	15.84	1567.3	16.34	3963.0	14.78	2266.5	0.0
6	16.35	1110.2	16.77	2385.9	15.52	1395.2	0.0
7	14.11	5048.7	15.66	4142.8	14.08	3602.2	0.6
8	16.79	824.5	17.83	1144.0	15.98	1028.2	0.6
9	14.37	4234.7	16.57	2568.1	14.68	2431.5	1.2
10	14.31	4410.1	16.06	3336.2	14.84	2183.5	1.2
11	14.68	3433.9	16.56	3164.7	15.15	1780.2	1.8
12	14.14	4947.3	16.15	3250.7	14.32	3075.4	2.1
24	14.90	2959.3	18.89	293.7	16.62	677.5	2.7

Table H-2: Raw data of C_q, viral RNA molecule number and HA titer of segment 6 (NA)

hpi	vRNA(-)		cRNA(+)		mRNA(+)		Log HA
[h]	C_q	Molecule/cell	C_q	Molecule/cell	C_q	Molecule/cell	[Units/100 µL]
0	16.63	59.0	22.80	0.7	23.40	1.3	0.0
0.5	17.20	40.6	22.83	0	22.17	2.8	0.0
1	18.77	14.4	22.03	0	21.53	4.3	0.0
1.5	19.03	12.1	21.63	0	20.93	6.3	0.0
2	19.37	9.7	20.33	0.5	20.07	11.1	0.0
2.5	18.03	23.4	18.90	0	18.27	35.7	0.0
3	17.43	34.8	17.33	13.0	16.90	86.8	0.0
3.5	16.70	56.4	16.50	25.6	16.00	155.8	0.0
4	14.37	263.1	14.00	440.6	13.80	651.7	0.0
5	11.67	1562.1	12.17	1680.9	11.80	2393.3	0.0
6	12.20	1098.7	12.90	1073.6	12.70	1332.8	0.0
7	10.17	4202.5	11.57	3230.4	11.43	3037.9	0.6
8	12.40	962.9	13.60	628.5	13.43	827.2	0.6
9	9.90	5010.9	11.80	2747.2	11.70	2554.1	1.2
10	9.87	5122.3	11.87	1667.8	11.27	3385.7	1.2
11	10.23	4021.7	12.30	1600.9	12.00	2101.3	1.8
12	9.80	5352.7	12.13	1830.9	11.83	2341.9	2.1
24	9.87	5122.3	12.77	1343.9	12.73	1304.2	2.7

Table H-3: Raw data of C_q, viral RNA molecule number and HA titer of segment 7 (M)

hpi	vRNA(-)		cRNA(+)		vmRNA(+)		Log HA
[h]	C_q	Molecule/cell	C_q	Molecule/cell	C_q	Molecule/cell	[Units/100 µL]
0	20.03	53.5	28.68	0.1	29.20	0.1	0.0
0.5	20.30	45.0	27.76	0.1	28.46	0.2	0.0
1	21.49	20.8	26.92	0.4	28.53	0.2	0.0
1.5	21.28	23.8	24.6	1.7	26.62	0.8	0.0
2	21.67	18.4	24.27	1.1	25.35	2.0	0.0
2.5	21.99	15.0	21.83	8.9	23.95	5.3	0.0
3	21.25	24.3	21.00	12.6	22.89	11.0	0.0
3.5	20.46	40.6	19.36	39.3	21.68	25.2	0.0
4	17.83	225.4	16.99	111.3	18.94	164.9	0.0
5	15.28	1186.9	12.16	1815.1	14.48	3533.0	0.0
6	15.58	978.1	12.90	1111.7	15.11	2291.7	0.0
7	13.33	4253.6	11.54	2098.1	13.78	5741.5	0.6
8	14.74	1691.8	13.23	640.1	15.21	2139.5	0.6
9	14.60	1857.6	11.76	1374.9	13.85	5446.9	1.2
10	13.88	2964.8	11.47	2153.4	13.71	5996.9	1.2
11	13.52	3757.8	11.84	2011.7	14.14	4483.3	1.8
12	13.61	3535.8	11.56	1333.0	13.62	6379.4	2.1
24	13.61	3535.8	12.33	855.9	14.32	3952.7	2.7

Table H-4: Raw data of C_q, viral RNA molecule number and HA titer of segment 8 (NS)

hpi	vRNA(-)		cRNA(+)		vmRNA(+)		Log HA
[h]	C_q	Molecule/cell	C_q	Molecule/cell	C_q	Molecule/cell	[Units/100 µL]
0	18.07	63.1	26.70	0.16	27.73	0.1	0.0
0.5	18.43	49.7	22.83	1.10	22.73	1.7	0.0
1	19.70	21.7	21.80	1.95	21.63	3.6	0.0
1.5	20.60	12.1	20.87	3.83	20.77	6.6	0.0
2	19.80	20.4	19.27	10.08	19.13	20.2	0.0
2.5	18.40	50.8	16.70	55.46	16.63	113.1	0.0
3	17.53	89.3	15.70	25.49	15.20	303.4	0.0
3.5	17.10	118.5	14.47	199.19	14.33	551.1	0.0
4	15.00	466.4	12.37	27.47	11.83	3083.1	0.0
5	13.17	1542.0	10.97	747.15	10.63	7045.6	0.0
6	13.70	1089.0	11.77	1025.66	11.63	3538.5	0.0
7	11.67	4102.3	10.93	1238.99	10.70	6729.4	0.6
8	13.77	1042.6	13.37	17.21	12.83	1548.4	0.6
9	11.70	4014.1	11.33	624.98	11.00	5473.3	1.2
10	11.63	4192.5	11.37	1194.83	11.20	4769.0	1.2
11	12.07	3160.2	12.07	431.53	11.73	3303.0	1.8
12	11.70	4014.1	11.97	202.02	11.53	3790.7	2.1
24	12.00	3300.6	14.20	187.33	13.97	709.4	2.7

Curriculum vitae Diana Vester

ANSCHRIFT Georg-Heidler Strasse 17, 39114 Magdeburg

GEBURTSDATUM 14. April 1981

GEBURTSORT Haldensleben (Deutschland)

SCHULISCHER WERDEGANG

1987-1999	Grundschule, Sekundarschule und Gymnasium Haldensleben
	Abschluss: Abitur (Note: 1,8)

STUDIUM

1999-2005	Technische Universität Braunschweig, Studium Biologie mit Vertiefung Mikrobiologie, Biochemie/Biotechnologie und Genetik
	Abschluss: Dipl.-Biol. (Note: sehr gut)
2003-2004	Laborpraktika: „Hefegenetik“, Prof. N. Käufer, Genetisches Institut, TU Braunschweig; „Klinische Biofilme“, Prof. Dr. K. Timmis, Abteilung Umweltmikrobiologie, GBF Braunschweig
	Studentische Hilfskraft: Zellbiologisches Praktikum “Zelle I, II“, Dr. F. Vauti, Zellbiologisches Institut, TU Braunschweig
2004-2005	Diplomarbeit, Gesellschaft für Biotechnologische Forschung (GBF), Abteilung Umweltmikrobiologie, Braunschweig, Prof. Dr. K. Timmis
	Titel: „Evaluierung von drei molekularbiologischen Methoden zur Bestimmung der Bakteriendiversität in verschiedenen mikrobiellen Habitaten“

WISSENSCHAFTLICHER WERDEGANG

2005 – 2010	Wissenschaftliche Mitarbeiterin (Promotion), Otto-von-Guericke-Universität Magdeburg des Lehrstuhls Bioprozesstechnik am Max-Planck-Institut für Dynamik komplexer technischer Systeme, Magdeburg, Prof. Dr.-Ing. U. Reichl
	Titel: „Molekularbiologische Untersuchungen der dynamischen Interaktionen zwischen Influenza-Viren und deren Wirtszellen – Wirtszell-Proteom und virale Replikations-Dynamik“
2010 – dato	Wissenschaftliche Mitarbeiterin, Deutsches Krebsforschungszentrum (DKFZ) Heidelberg, Abteilung Tumorvirus-Charakterisierung, Prof. Dr. Ethel-Michele de Villiers und Prof. Dr. Harald zur Hausen

Magdeburg, 31.07.2011

Publications

D. Vester, E. Rapp, S. Kluge, Y. Genzel, U. Reichl: 'Virus-host cell interactions in vaccine production cell lines infected with different human influenza A virus variants: a proteomic approach', Journal of Proteomics, 2010, 73, 1656-1669

D. Vester, A. Lagoda, D. Hoffmann, C. Seitz, S. Heldt, K. Bettenbrock, Y. Genzel, U. Reichl: 'Quantitative real-time RT-qPCR assay for the analysis of human influenza A virus transcription and replication dynamics', Journal of Virological Methods, 2010, 168, 63-71

D. Vester, E. Rapp, D. Gade, Y. Genzel, U. Reichl: 'Quantitative analysis of cellular proteome alterations in human influenza A virus infected mammalian cell lines', Proteomics, 2009, 9, 3316–3327

D. Vester, E. Rapp, D. Gade, Y. Genzel, U. Reichl: 'Proteomic analysis of influenza A virus infected mammalian cells by 2D-DIGE', Proceedings from the 20th ESACT Meeting: Cells and Culture, Noll, T. (ed.), Springer, 2007

Poster/talks

D. Vester, E. Rapp, Y. Genzel, U. Reichl: 'Virus-host cell interactions in a vaccine manufacturing process: Proteomics of production cell lines in response to human influenza A virus infection', (Poster Contribution) at the 21th ESACT meeting, June 07-10, 2009, Dublin/Ireland

D. Vester, E. Rapp, D. Gade, Y. Genzel, U. Reichl: 'Virus-host cell interactions in a vaccine production process : Proteomic analysis of influenza A virus infected mammalian cells by 2D-DIGE', (Talk at event) at the Proteomics Europe congress, October 16-17, 2008, Lisboa/Portugal

D. Vester, E. Rapp, D. Gade, Y. Genzel, U. Reichl: 'Dynamics of the proteomes of mammalian cell lines during influenza A virus infection', (Poster Contribution) at the HuPo congress, August 18-20, 2008, Amsterdam/The Netherlands

D. Vester, E. Rapp, D. Gade, Y. Genzel, U. Reichl: 'Virus-host cell interactions in a vaccine production process: Proteomic analysis of influenza A virus infected mammalian cells by 2D-DIGE', (Poster Contribution) at the 2th Vaccine congress, December 09-12, 2007, Amsterdam/The Netherlands

D. Vester, E. Rapp, D. Gade, Y. Genzel, U. Reichl: 'Proteomic analysis of influenza A virus infected mammalian cells by 2D-DIGE', (Poster Contribution) at the 20th ESACT meeting, June 17-20, 2007, Dresden/Germany

D. Vester, C. Seitz, K. Bettenbrock, D. Gade, Y. Genzel, U. Reichl: 'Development of a real-time PCR assay for quantitative analysis of human influenza A virus replication', (Poster Contribution) at the qPCR 2007 Event, March 26-30, 2007, Freising-Weihenstephan/Germany

D. Vester, K. Bettenbrock, N. Schlawin, Y. Genzel, U. Reichl: 'Real-Time PCR for quantitative analysis of human influenza A virus in infected mammalian cells', (Poster Contribution) at the GVC/DECHEMA-Jahrestagungen, September 26-28, 2006, Wiesbaden/Germany

D. Vester, C. Best, D. Gade, Y. Genzel, U. Reichl: 'Analysis of cellular metabolism and influenza viral replication of three human cell lines as candidates for proteomics', (Poster Contribution) at the 6th ESBES meeting, August 27-30, 2006, Salzburg/Austria